Molecular and functional analyses of mutant Idh1 in murine neural stem and progenitor cells

Inaugural-Dissertation

zur Erlangung des Doktorgrades
der Mathematisch-Naturwissenschaftlichen Fakultät
der Heinrich-Heine-Universität Düsseldorf

vorgelegt von

Miriam Knühmann
aus Kamp-Lintfort

Düsseldorf, April 2019

aus dem Institut für Neuropathologie
der Heinrich-Heine-Universität Düsseldorf

Gedruckt mit der Genehmigung der
Mathematisch-Naturwissenschaftlichen Fakultät der
Heinrich-Heine-Universität Düsseldorf

Referent: Prof. Dr. med. Guido Reifenberger

Koreferent: Prof. Dr. Andreas Weber

Tag der mündlichen Prüfung: 05.Juli 2019

• FOR MY FAMILY •

“IT DOESN’T MATTER IF YOU FALL DOWN AS LONG AS YOU PICK SOMETHING UP FROM THE FLOOR WHEN YOU GET UP.”

EFRAIM RACKER

I. CONTENTS

I. Contents **1**

II. Abbreviations **5**

III. SI units **10**

IV. Zusammenfassung **11**

V. Summary **12**

1.0 Introduction **13**

1.1 Classification of diffuse gliomas and glioblastomas 13

1.2 Implications of wildtype and mutant IDH 15

1.3 2-HG in health and disease 18

1.4 ROS and oxidative stress-responsive signaling 19

1.4.1 The oxidative stress response by NF-κB, NRF2, HSF1 and AP-1 21

1.4.2 The oxidative stress response by MAPKs 22

1.4.3 The integrated stress response 23

1.5 Cytoprotective signaling and programmed cell death 24

1.6 Cell cycle regulation 26

1.7 The conditional CreER^{tam}/*loxP* mouse model 27

1.8 4-OHT and its effects on the cell 29

1.9 Neural stem cells as a model for the characterization of *IDH1* mutation 30

1.10 Aims 32

2.0 Materials and methods **33**

2.1 Materials 33

2.1.1 Chemicals and kits 33

2.1.2 Materials and technical devices 36

2.1.3 Software 38

2.1.4 Solutions and buffer 39

2.1.5 Primers 41

2.1.6 Antibodies 43

2.1.7 Inhibitors 44
2.2 Methods 46
2.2.1 Cell culture 46
2.2.1.1 Conditional knock-in mouse model 46
2.2.1.2 Isolation and culturing of murine NSC/NPCs 47
2.2.2 Genotyping 48
2.2.2.1 Extraction of genomic DNA from mice tails 48
2.2.2.2 Genotyping PCR reaction 48
2.2.3 Quantitative real-time PCR 49
2.2.3.1 RNA extraction with Trizol® 49
2.2.3.2 cDNA synthesis 49
2.2.3.3 qRT-PCR 50
2.2.4 Transcriptome profiling 50
2.2.4.1 RNA extraction using the QIAGEN RNeasy Mini Kit 50
2.2.4.2 RNA sequencing analyses 51
2.2.4.3 Microarray analyses 51
2.2.5 Western Blotting 52
2.2.5.1 Cell lysis 52
2.2.5.2 BCA assay for protein quantification 52
2.2.5.3 SDS-PAGE 52
2.2.5.4 Transfer of proteins onto nitrocellulose membranes 53
2.2.5.5 Immunostaining of blotted proteins 53
2.2.6 Metabolome profiling 54
2.2.7 Flow cytometric analyses 55
2.2.7.1 FITC Annexin V / 7-AAD apoptosis staining 55
2.2.7.2 Cell cycle analysis using BrdU incorporation 56
2.2.7.3 ROS detection with the DHE/DCF assay 57
2.2.8 Viability assay (MTT assay) 57
2.2.9 Kinase inhibitor screening 57
2.2.10 Caspase-Glo® 3/7 assay 59

2.2.11 Proteome profiling 59

3.0 Results.....61

3.1 Validation of the conditional knock-in mouse model 61

3.1.1 Expression of recombinant DNA decreases over time after 4-OHT treatment .62

3.1.2 Concentrations of the oncometabolite 2-HG decrease over time after 4-OHT treatment.....63

3.2 The effect of 4-OHT on NSC/NPCs.....64

3.2.1 4-OHT mediates ER-independent cytotoxic effects on NSC/NPCs.....64

3.2.2 4-OHT induces autophagic cell death in NSC/NPCs 66

3.2.3 4-OHT induces apoptotic cell death in NSC/NPCs 68

3.2.4 4-OHT treatment affects Jak2/Stat3 signaling in NSC/NPCs 71

3.2.5 4-OHT-mediated cytotoxicity on NSC/NPCs is attenuated by Jak2 inhibition and amplified by IKK inhibition 74

3.2.6 4-OHT-treated NSC/NPCs arrest in G0/G1- and in G2/M-phase 78

3.3 Characterization of *Idh1*-mutant NSC/NPCs using a conditional knock-in model....80

3.3.1 Mutant Idh1 induces Hmox1 expression in NSC/NPCs 80

3.3.2 Idh1-mutant NSC/NPCs show increased 2-HG and decreased glycolate metabolite levels 83

3.4 Validation of Idh1 mutation-mediated effects in 2-HG-treated *Idh1*$^{wt/wt}$ *Cre*$^{-/-}$ NSC/NPCs.....87

3.4.1 NSC/NPCs are highly sensitive to 2-HG treatment.....87

3.4.2 2-HG treatment results in stress-responsive gene expression in NSC/NPCs...88

3.4.3 2-HG causes elevated ROS levels and induces an antioxidative response in NSC/NPCs.....89

3.4.4 2-HG treatment of NSC/NPCs results in p38 phosphorylation 92

3.4.5 2-HG treatment of NSC/NPCs induces the integrated stress response 94

3.4.6 2-HG treatment of NSC/NPCs mediates apoptotic cell death 96

3.4.7 2-HG treatment of NSC/NPCs induces cell cycle arrest and *Cdkn1a* expression 99

3.4.8 2-HG-mediated apoptotic cell death in NSC/NPCs is attenuated by antioxidant treatment.....101

3.5 Comparison of 2-HG-mediated effects on NSC/NPCs to RNA sequencing and proteomic data of NSC/NPCs from conditional *Idh1*-mutant knock-in mice 103

4.0 Discussion.....107

4.1 Limitations of the use of NSC/NPCs from conditional *Idh1*-mutant knock-in mice 107

4.2 Cytotoxic effect of 4-OHT on NSC/NPCs 109

4.2.1 4-OHT-mediated cytotoxicity on NSC/NPCs is ER-independent.....109

4.2.2 4-OHT treatment induces autophagic and apoptotic cell death in NSC/NPCs110

4.2.3 4-OHT treatment affects Jak/Stat signaling and NF-κB signaling in NSC/NPCs 111

4.2.4 4-OHT-mediated apoptotic and autophagic cell death might result from NF-κB signaling inhibition.....112

4.3 Characterization of *Idh1* mutation using NSC/NPCs from a conditional knock-in mouse model 113

4.3.1 *Idh1*-mutant NSC/NPCs show induced stress-responsive *Hmox1* expression 114

4.3.2 *Idh1*-mutant NSC/NPCs show increased 2-HG and decreased glycolate metabolite levels 116

4.4 Validation of *Idh1* mutation-dependent effects by 2-HG treatment of NSC/NPCs .117

4.4.1 *Hmox1* overexpression was validated in 2-HG-treated NSC/NPCs 118

4.4.2 2-HG treatment of NSC/NPCs results in elevated ROS levels.....118

4.4.3 p38 signaling is induced in 2-HG-treated NSC/NPCs 119

4.4.4 2-HG treatment activates the integrated stress response in NSC/NPCs.....120

4.4.5 2-HG treatment results in cell cycle arrest and apoptotic cell death in NSC/NPCs.....122

4.4.6 2-HG-induced apoptotic cell death in NSC/NPCs is mediated by ROS.....124

5.0 Summary and outlook 125

6.0 Literature 129

VI. Danksagung.....162

VII. Eidesstattliche Erklärung.....163

II. ABBREVIATIONS

2-HG	2-Hydroxyglutarate / (2R)-Octyl-α-hydroxyglutarate
2-HGA	2-HG aciduria
2-HGDA	2-HG dehydrogenase
3-MA	3-Methyladenine
4E-BP1 / **Eif4ebp1**	Eukaryotic translation initiation factor 4E-binding protein 1
4-OHT	4-Hydroxytamoxifen
7-AAD	7-Amino-actinomycin D
α-KG	alpha-Ketoglutarate
β-ES	beta-Estradiol
AKT	Protein kinase B
AML	Acute myeloid leukemia
AP-1	Activator protein 1
ARE	Antioxidative response element
ARF1	ADP-ribosylation factor
ARSB	Arylsulfatase B precursor
ASK1	Apoptosis signal-regulating kinase 1
ATF4	Activating transcription factor 4
ATG	Autophagy related gene
ATRX	Alpha thalassemia/mental retardation syndrome X-linked
BCA	Bicinchoninic acid
BCL-2	B-cell lymphoma 2
BMFZ	Biological and Medical Research Center
BNIP3	BCL2-interacting protein 3
BrdU	Bromodeoxyuridine
Cat	Catalase
CDK	Cyclin dependent kinase
CDKN	Cyclin dependent kinase inhibitor
cDNA	Complementary deoxyribonucleic acid
C/EBP	CCAAT/enhancer-binding proteins
CEPLAS	Cluster of Excellence on Plant Sciences

CHOP	C/EBP homologous protein
CIMP	CpG island methylator phenotype
CIP/KIP	CDK interacting proteins / kinase inhibitor proteins
CKI	Cyclin-dependent kinase inhibitor
CNS	Central nervous system
Cre	Cre recombinase
COL	Collagen
DCF	Dichlorodihydrofluorescein
dH_2O	Deionized water
DHE	Dihydroethidium
DMEM	Dulbecco's modified eagle medium
DMF	Dimethylformamid
DMSO	Dimethyl sulfoxide
DNA	Deoxyribonucleic acid
dNTP	Deoxynucleotide
DPBS	Dulbecco's phosphate-buffered saline
EDTA	Ethylenediaminetetraacetic acid
EGF	Epidermal growth factor
EGFR	Epidermal growth factor receptor
EGLN	Egl nine homolog
eIF2α	Eukaryotic translation initiation factor 2A
eIF4F	Eukaryotic initiation factor 4F
ER	Estrogen receptor
ERK	Extracellular-signal regulated kinase
FACS	Fluorescence activated cell sorting
FC	Fold change
FCS	Fetale calf serum
FGF	Fibroblast growth factor
FITC	Fluorescein isothiocyanate
FMK	Fluoromethyl ketone
FSC	Forward scatter
GADD34	Growth arrest and DNA damage-inducible protein 34
GC	Gas chromatography

GCLC	Glutamate--cysteine ligase catalytic subunit
GCLM	Gamma-glutamylcysteine synthetase regulatory subunit
GCN2	Glutamate dehydrogenase
GDH	Growth hormone
GLS	Glutaminase
GPx	Glutathione peroxidase
GRP78 / ***Hspa5***	78 kDa glucose-regulated protein
GSH / **GSSG**	Glutathione (reduced / oxidized)
H_2O_2	Hydrogen peroxide
HEATR7A	HEAT repeat containing 7A
HEPES	4-(2-Hydroxyethyl)-1-piperazineethanesulfonic acid
HIF1α	Hypoxia inducible factor 1 alpha
HMOX1	Heme oxygenase 1
HPLC	High performance liquid chromatography
HRI	Heme-regulated initiation factor 2 alpha kinase
HSF1	Heat shock factor protein 1
IC_{50}	Half maximal inhibitory concentration
IDH	Isocitrate dehydrogenase
IκB	Inhibitor of NF-κB
IKK	IκB kinase
INK4	Inhibitors of CDK4
JAK	Janus kinase
JNK	c-jun N-terminal kinase
KCTD12	Potassium channel tetramerization domain containing 12
KDM	Histone lysine demethylase
Keap1	Kelch like ECH associated protein 1
KEGG	Kyoto Encyclopedia of Genes and Genomes
LC3 / **Map1LC3A**	Microtubule-associated proteins 1A/1B light chain 3A
loxP	Locus of X(cross)-over in P1
LSL	Lox Stop Lox
MAPK	Mitogen-activated protein kinase
MDM2	Mouse double minute 2
ME	Malic enzyme

MES	2-(N-morpholino)ethanesulfonic acid
Mm	*Mus musculus*
MPL	Molecular b oratory
mRNA	Messenger ribonucleic acid
mTORC1	Mammalian target of rapamycin complex 1
MTT	3-(4,5-Dimethylthiazol-2-yl)-2,5-diphenyltetrazolium bromide
Mut	Mutant
NAC	N-acetyl-cysteine
NADPH / NADP	Nicotinamide adenine dinucleotide phosphate (hydrogen)
NF-κB	Nuclear factor of kappa light polypeptide gene enhancer in B-cells 2
NOS	Not otherwise specified
NOX	NADPH oxygenase
NP-40	Nonidet P-40
NPC	Neural progenitor cells
NQO1	NADPH quinone dehydrogenase 1
NRF2	Nuclear factor erythroid 2-related factor 2
NSC	Neural stem cell
OD	Optical density
P4HA	Prolyl 4-hydroxylase
p53	Tumor protein 53
p70S6 / RPS6BK1	Ribosomal protein S6 kinase beta-1
PCR	Polymerase chain reaction
PE	Phycoerythrin
PERK	PKR-like endoplasmic reticulum kinase
PI3K	Phosphatidylinositol-3-kinase
PKC	Protein kinase C
PKR	Protein kinase R
PLOD	Procollagen-lysine 2-oxoglutarate 5-dioxygenase
PPP	Pentose phosphate pathway
PTEN	Phosphatase and tensin homolog
qRT-PCR	Quantitative real-time polymerase chain reaction
QTOF	Quadrupole time-of-flight

Rb	Retinoblastoma
rcf	Relative centrifugal force
RIPA	Radioimmunoprecipitation assay
RNA	Ribonucleic acid
ROS	Reactive oxygen species
rpm	Rounds per minute
SAPK	Stress-activated protein kinase
SB	SB203580
SDS	Sodium dodecyl sulfate
SDS-PAGE	SDS polyacrylamide gel electrophoresis
SEM	Standard error of the mean
SERM	Selective estrogen receptor modulator
SERPINA3N	Serine (or cysteine) proteinase inhibitor, clade A, member 3
SOCS2	Suppressor of cytokine signaling 2
SOD	Superoxide dismutase
SQSTM1	Sequestosome-1
SSC	Side scatter
STAT	Signal transducer and activator of transcription
TBS	Tris-buffered saline
TBST	TBS with Tween 20
TCA	Tricarboxylic acid
TE	Tris-ethylenediaminetetraacetic acid
TERT	Telomerase reverse transcriptase
TET	Ten-eleven translocation
TNFα	Tumor necrosis factor α
TRAIL	TNF-related apoptosis inducing ligand
WHO	World Health Organization
Wt	Wildtype

III. SI UNITS

°C	Degree Celsius
A	Ampere
cm	Centimeter
d	Days
g	Gram
h	Hours
l	Liter
M	Molar
µ	Micro
m	Milli
min	Minutes
n	Nano
s	Seconds
V	Volt
W	Watt

IV. ZUSAMMENFASSUNG

Mutationen des *Isozitratdehydrogenase 1* (*IDH1*)-Gens finden sich in etwa 70 % der diffusen und anaplastischen Gliome der World Health Organization (WHO)-Grade II und III. Die eingehende Charakterisierung der funktionellen Bedeutung dieser Mutationen ist durch die eingeschränkte Verfügbarkeit geeigneter Zellmodelle, welche die Pathophysiologie IDH1-mutanter Gliomzellen widerspiegeln, erschwert. In dieser Doktorarbeit wurde ein konditionelles knock-in Mausmodell untersucht, welches auf der heterozygoten Expression eines mutanten *Idh1*-Allels unter dem endogenen Promotor in nicht-immortalisierten neuralen Stamm- und Progenitorzellen (NSZ/NPZ) basiert. Im Gegensatz zu transfizierten und überexprimierenden IDH1-mutanten menschlichen Glioblastomzelllinien weisen induzierbare Idh1-mutante murine NSZ/NPZ keinen neoplastischen Mutationshintergrund auf, wodurch die alleinige Charakterisierung der Idh1-Mutation möglich ist und eine frühe Phase der Gliomentstehung modelliert werden kann.

In den eigenen Untersuchungen stellte sich allerdings heraus, dass einige Faktoren die Verwendung des auf einem durch 4-Hydroxytamoxifen (4-OHT)-induzierbaren $CreER^{tam}$/*loxp* Rekombinase-System basierenden knock-in Modells limitierten. Neben 4-OHT-vermittelter Zytotoxizität für NSZ/NPZ wurden eine geringe Rekombinationseffizienz sowie ein Proliferationsnachteil rekombinanter Zellen und damit das Verschwinden der Idh1-mutanten Zellen aus der kultivierten Zellpopulation über die Zeit festgestellt. Potentielle Mechanismen der Zytotoxizität von 4-OHT wurden in der vorliegenden Arbeit untersucht, jedoch gelang es nicht diese vollständig zu umgehen. Aufgrund des Verschwindens Idh1-mutanter Zellen aus den kultivierten NSZ/NPZ-Populationen über die Zeit konnten weiterhin nur akute Effekte der Idh1-Mutation erfasst werden. Ausgeprägte Unterschiede zwischen einzelnen NSZ/NPZ-Kulturen und Experimenten können auf interindividuelle Unterschiede sowie unterschiedliche Anteile rekombinanter Zellen in den jeweilig untersuchten Populationen zurückgehen.

Trotz dieser experimentellen Limitationen konnten durch RNA-Sequenzierung der konditionellen Idh1-mutanten knock-in NSZ/NPZ im Vergleich zu Idh1-Wildtyp NSZ/NPZ Unterschiede auf Transkriptebene identifiziert werden. Unter anderem wurde in Idh1-mutanten Zellen die Expression von *Hmox1* induziert. Eine vestärkte Expression von HMOX1 wurde bereits für humane Gliome beschrieben und mit vermindertem Ansprechen auf eine Chemotherapie in Verbindung gebracht. Die von der Idh1-Mutation abhängige Induktion der Hmox1-Expression wurde auf Transkript- und Proteinebene in 2-HG behandelten NSZ/NPZ verifiziert, um Nebeneffekte des konditionellen knock-in Modells als Auslöser auszuschließen. Als potenzielle Ursachen der Hmox1-Induktion in NSZ/NPZ durch 2-HG wurden erhöhte ROS-Level, eine induzierte integrierte Stressantwort, die Aktivierung des p38-Signalweges und eine Induktion der *Cdkn1a*-Transkription nachgewiesen.

Das konditionelle knock-in Mausmodell für mutantes Idh1 konnte somit in dieser Arbeit trotz verschiedener Limitationen erfolgreich für die molekulare und funktionelle Charakterisierung möglicher Effekte einer Idh1-Mutation in murinen NSZ/NPZ-Kurzzeitkulturen eingesetzt werden. Weitergehende Untersuchungen sind notwendig, um die Mechanismen der Idh1-abhängigen Gliomentstehung und der möglichen Rolle von Hmox1 bei diesem bislang erst ansatzweise verstandenen Prozess besser zu verstehen.

V. SUMMARY

Mutations of the *isocitrate dehydrogenase 1* (*IDH1*) gene are found in approximately 70 % of the diffuse and anaplastic gliomas of World Health Organization (WHO) grades II and III. The in-depth characterization of the functional importance of these mutations is hampered by the limited availability of suitable cell models reflecting the pathophysiology of IDH1-mutant glioma cells. In this doctoral thesis, a conditional knock-in mouse model was investigated that is based on the heterozygous expression of a mutant *Idh1*-allele under the endogenous promoter in non-immortalized neural stem and progenitor cells (NSC/NPCs). In contrast to transfected and overexpressing IDH1-mutant human glioblastoma cell lines, inducible Idh1-mutant murine NSC/NPCs have no neoplastic mutation background, allowing for the specific characterization of the Idh1 mutation and thus modeling an early phase of glioma formation.

Own investigations, however, revealed that several factors limited the use of the knock-in model based on a 4-hydroxytamoxifen (4-OHT)-inducible CreER^{tam}/*loxP* recombinase system. In addition to 4-OHT-mediated cytotoxicity for NSC/NPCs, a low recombination efficiency was found. Moreover, recombinant cells demonstrated a proliferation disadvantage and hence vanished from the cultured cell population over time. Potential mechanisms of cytotoxicity of 4-OHT were investigated in the present work and attempts were made to circumvent them experimentally. However, this was not completely successful. Due to the disappearance of Idh1-mutant cells from the cultured NSC/NPC populations over time, only acute effects of the Idh1 mutation could be experimentally assessed. Variabilities of experimental findings detected between individual NSC/NPC cultures were likely due to interindividual differences of the investigated cultures as well as differences in the proportion of recombinant cells in the cell populations studied.

Despite these experimental limitations, RNA sequencing of conditional Idh1-mutant knock-in NSC/NPC cultures succeeded in identifying differences at the transcript level compared to their Idh1-wildtype counterparts. For example, expression of *Hmox1* was found to be induced in Idh1-mutant cells. Enhanced expression of HMOX1 has been previously reported for human gliomas and associated with decreased response to chemotherapy. The Idh1 mutation-dependent induction of Hmox1 expression was verified by targeted analyses at the transcript and protein levels in 2-hydroxyglutarate (2-HG)-treated NSC/NPC cultures to exclude unspecific effects of the conditional knock-in model. As potential causes of Hmox1 induction in NSC/NPC by 2-HG, increased ROS levels, an induced integrated stress response, activation of the p38 signaling pathway, and induction of *Cdkn1a* transcription were observed.

In spite of several limitations, the conditional knock-in mouse model for mutant Idh1 was successfully employed for the molecular and functional characterization of possible effects of Idh1 mutation in murine NSC/NPC short-term cultures. Further investigations are needed to better understand the mechanisms of Idh1-dependent glioma formation and the possible role of Hmox1 in this complex process, which remains only been partially understood to date.

1.0 INTRODUCTION

1.1 Classification of diffuse gliomas and glioblastomas

Among primary tumors of the central nervous system (CNS) glioma is the most common primary human brain tumor entity[1-3]. Gliomas are supposed to arise from neural stem or progenitor cells and may show astrocytic, oligodendroglial or ependymal differentiation[4-6]. Gliomas are classified according to the World Health Organization (WHO) guidelines for tumors of the CNS from 2016, depending on the histology of the tumors as well as on molecular parameters **(Fig. 1.1)**[1]. In addition, these tumors are divided into four malignancy grades, i.e. WHO grades I-IV[1].

Well circumscribed, slowly growing gliomas are classified as WHO grade I tumors[7]. Since these tumors occur clearly separated from the surrounding tissues, they can usually be cured by surgical resection. Diffuse gliomas on the other hand are characterized by an infiltrative growth behavior and are graded according to the WHO classification as WHO grade II, III or IV, depending on the histology and to some extent on their molecular characteristics[1,7]. As they are not clearly delimited from the surrounding tissue, the resection of these tumors is challenging and has to be accompanied by further treatment like chemotherapy and radiotherapy[8]. WHO grade II and III diffuse gliomas include astrocytic and oligodendroglial tumors[1,9]. The median survival of patients with tumors of WHO grade II, mostly rather slow-growing diffuse gliomas, is within a range of 7-15 years after diagnosis[9]. WHO grade III anaplastic gliomas and WHO grade IV glioblastomas are characterized by a more rapid growth[9]. Therefore, patients require surgical resection as well as aggressive adjuvant treatments with radio- or chemotherapy[8]. For WHO grade IV tumors, the median survival of the patients is in general not longer than 15 months after diagnosis[9]. Glioblastomas are divided into primary and secondary glioblastoma[1,7]. Primary glioblastoma occurs without any clinically known precursor lesion, whereas secondary glioblastoma arises from WHO grade II or III astrocytomas, showing the characteristic molecular markers of their precursor lesions[1,7,8,10-12].

The most important molecular marker for the classification of glioma entities is a tumor-specific hotspot mutation within the *isocitrate dehydrogenase 1* or *2* (*IDH1* or *IDH2*) genes[13-17] **(Fig. 1.1)**. A heterozygous mutation in either *IDH1* or *IDH2* (collectively referred to as IDH from here on) is found in more than 70% of WHO grade II and III gliomas as well as in approximately 5-15% of glioblastomas, including most secondary

glioblastomas[13,17]. Furthermore, IDH mutations have been detected in other tumors like acute myeloid leukemia (AML), chondrosarcoma and cholangiocarcinoma and contribute to tumor formation in several tissues in *in vivo* studies[18-23]. In the CNS, the mutation affects the number of stem cells and impairs the differentiation of the same[24-29]. Thus, it is believed to be the first mutation to occur during gliomagenesis and to be the driver mutation leading to the generation of IDH-mutant diffuse gliomas and later on often to the formation of secondary glioblastomas[1,16,17,30,31]. The *IDH1* mutation alone is not sufficient for tumor formation[28,32] but strongly supportive, since it was crucial for gliomagenesis in combination with other glioma-associated genetic alterations in *in vivo* experiments using immortalized astrocytes[33]. These results stress the significance of the *IDH1* mutation in glioma formation. As glioblastoma patients with IDH-mutant tumors have a better prognosis than glioblastoma patients with IDH-wildtype tumors, IDH mutation is an important prognostic marker[17,34]. However, the median overall survival is still poor, pointing to the urgency of understanding the biology behind IDH mutations and their influence on gliomagenesis[13].

Additional lesions, like mutations in the *alpha-thalassemia/mental retardation syndrome X-linked* (*ATRX)* gene, mutations of the *tumor protein 53* (*P53)* gene or a co-deletion of the chromosome arm 1p and 19q (1p/19q co-deletion) are relevant tumor entity-defining additional mutations in IDH-mutant astrocytomas and oligodendrogliomas[1,11,12] **(Fig 1.1)**.

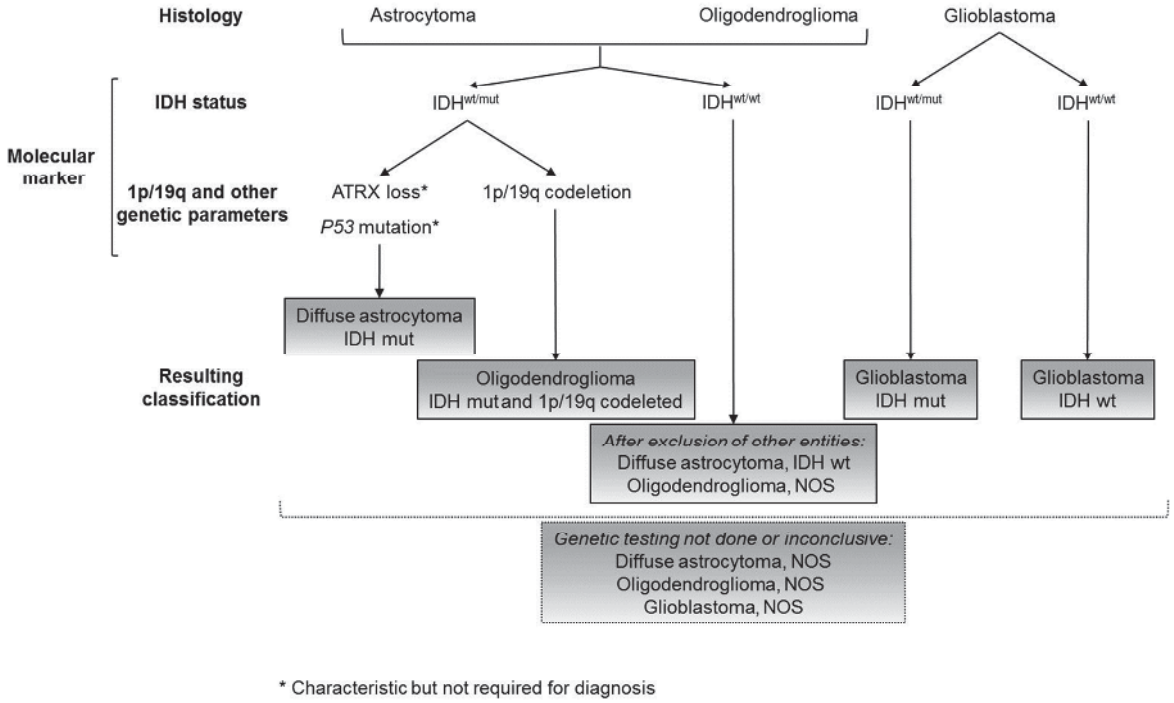

Fig 1.1: WHO classification of diffuse astrocytic and oligodendroglial gliomas (modified from [1]). (IDH: isocitrate dehydrogenase, wt: wildtype, mut: mutant, NOS: not otherwise specified)

1.2 Implications of wildtype and mutant IDH

The *IDH1* and *IDH2* genes encode for similar metabolic enzymes, which form homodimers and catabolize the oxidative decarboxylation of isocitrate to α-ketoglutarate (α-KG) in a reversible reaction **(Fig.1.2)**[35,36]. During this enzymatic step, nicotinamide adenine dinucleotide phosphate hydrogen (NADPH) is generated by the reduction of $NADP^+$[35,36]. NADPH is an essential reducing factor, important for the maintenance of the homeostasis of antioxidants and reactive oxygen species (ROS) in the cells[37-39]. Hence, it acts for instance as a co-factor for the recycling of oxidized glutathione (GSSG) to reduced glutathione (GSH)[40,41]. The tripeptide GSH is in turn a crucial co-factor for the antioxidative enzyme glutathione peroxidase (GPx) that detoxifies H_2O_2 and lipid peroxides[40,41].

IDH1 and IDH2 catalyze the same reaction in different compartments of the cell. While IDH1 exerts its function in the cytosol and in the peroxisomes, IDH2 is located in the mitochondria[15,35,42]. IDH3 is a third isozyme of IDH also located in the mitochondria, where it is involved in the tricarboxylic acid (TCA) cycle[43]. It likewise converts isocitrate to α-KG but acts as a tetrameric enzyme and generates NADH instead of NADPH[43,44]. In contrast to the IDH1- and IDH2-catalyzed reaction, the reaction catalyzed by IDH3 is irreversible. *IDH3* mutations have not been described as glioma-associated mutations so far[43-47].

Glioma-associated heterozygous *IDH1* mutations were first described in 2008 in a genome-wide mutational analysis of glioblastomas[17]. Thereby, the amino acid residue R132 was altered in five of six secondary glioblastomas and in over 70 % of WHO grade II and III gliomas[17]. *IDH1*-wildtype diffuse gliomas rarely show a heterozygous mutation at the analogous amino acid residue R172 within the *IDH2* gene[17,48]. In both instances, the replaced amino acid is an arginine located in the active site of the respective enzyme, where it forms hydrogen bonds with the substrate isocitrate[17,48]. All detected mutations at these residues lead to a gain of function, resulting from structural changes and a consequent loss of binding affinity for isocitrate[49]. Thereby, the ability to decarboxylate isocitrate to α-KG decreases by 1000-fold[49,50]. Instead, the affinity for the co-factor NADPH as well as for the substrate α-KG increases in mutant IDH1/2, favoring the NADPH-dependent reduction of α-KG to (D)-2-hydroxyglutarate ((D)-2-HG)[17,23,49,51]. By forming heterodimers with wildtype IDH1 or 2, the mutant enzyme is furthermore directly connected to a source of the new substrate α-KG and to the co-factor NADPH[52].

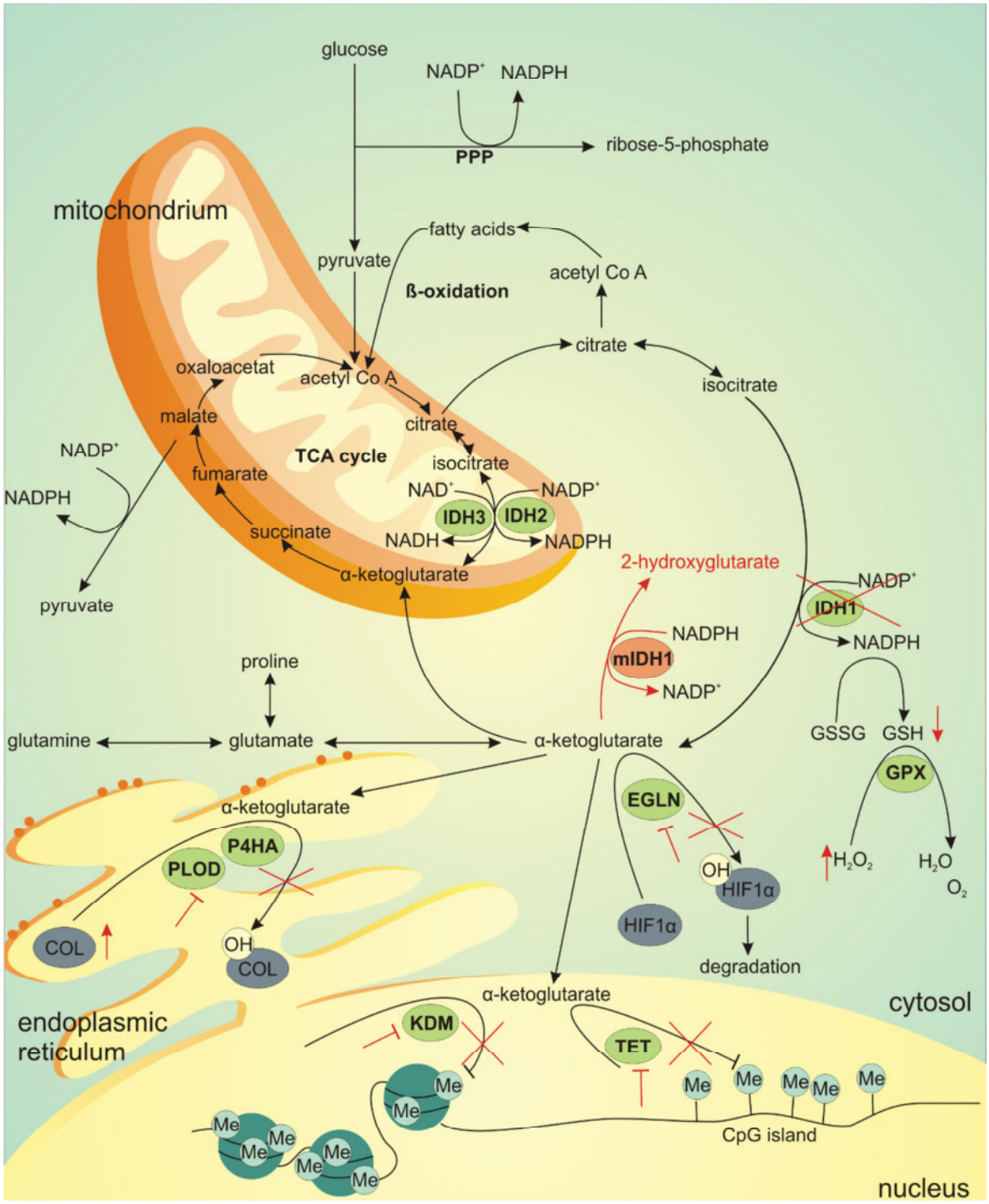

Fig. 1.2: Implications of wildtype and mutant IDH proteins (modified from [53-55]).
(**IDH**: isocitrate dehydrogenase, **NADP(H)**: nicotinamide adenine dinucleotide phosphate (hydrogen), **GSSG/GSH**: oxidized/reduced glutathione, **GPX**: glutathione peroxidase, **PPP**: pentose phosphate pathway, **TCA cycle**: tricarboxylic acid cycle, **HIF1α**: hypoxia-induced factor 1α, **COL**: collagen, **EGLN**: Egl nine homolog, **P4HA**: prolyl-4-hydroxylases, **PLOD**: procollagen-lysine 2-oxoglutarate 5-dioxygenases, **KDM**: lysine demethylases, **TET**: Ten-eleven translocation, **Me**: methylation, **OH**: hydroxylation; red signs mark the implication of 2-HG)

Since an IDH mutation might entail reduced NADPH and α-KG levels as well as increased 2-HG levels, consequences for the cells ROS homeostasis, metabolism and epigenetics are implied **(Fig. 1.2)**.

NADPH is not solely generated by wildtype IDH activity but also by enzymes of the pentose phosphate pathway (PPP) and by malic enzyme (ME), catalyzing the conversion from malate to pyruvate[56,57]. By shifting the metabolism to NADPH-generating pathways, IDH mutation-dependent elevated $NADP^+$/NADPH ratios might be compensated. Gelman and colleagues showed for instance an increased PPP flux in an *IDH1*-mutant human colon carcinoma cell line[58]. The induction of the PPP flux, however, was not sufficient to compensate for the *IDH1* mutation-dependent reduction of NADPH. Increased $NADP^+$/NADPH ratios were moreover observed in further studies with *IDH1*-mutant cells, resulting in an increased sensitivity to oxidative stress and DNA-damaging agents[33,58-63]. *IDH1*-mutant glioblastomas also show increased ROS levels. However, in *Idh1*-mutant mouse models ROS levels were attenuated, pointing again to potential compensatory mechanisms[27,63,64].

Besides NADPH, also α-KG is consumed by generating 2-HG. α-KG levels were shown to be reduced in *in vivo* approaches with *Idh1*-mutant mice compared to α-KG levels in *Idh1*-wildtype mice[28,64]. However, α-KG levels were unaltered in a transfected *IDH1*-mutant glioblastoma cell line as well as in transformed astrocytes[65]. The compensation for reduced α-KG metabolite levels was herein achieved by glutamine dependency. The reconstitution of α-KG occurred via the two-step conversion of glutamine by the enzymes glutaminase (GLS) and glutamate dehydrogenase (GDH)[66,67] **(Fig. 1.2)**. The latter was found to be overexpressed in *IDH1*-mutant gliomas[31,49,68,69]. Since the inhibition of glutamine metabolism resulted in elevated levels of glycolytic intermediates, *IDH1*-mutant glioblastomas seem to rely mainly on oxidative phosphorylation, whereby glutamine-derived α-KG shuttles from the cytosol into the mitochondria. Accordingly, enhanced glycolysis results from reduced α-KG levels as a compensatory mechanism, certainly showing reduced proliferation capacity[65]. Besides replenishing the TCA cycle, α-KG serves as a precursor for several amino acids such as proline[70]. Since proline is a crucial substrate for collagen synthesis, α-KG is moreover important for collagen metabolism, wherefore alterations of α-KG levels in *IDH1*-mutant cells further effect the composition of the extracellular matrix[64,71-73].

Besides effects on ROS homeostasis and metabolism resulting from NADPH and α-KG consumption, most of the effects detected in IDH-mutant cells are directly mediated by the newly formed metabolite 2-HG.

1.3 2-HG in health and disease

2-HG is a five-carbon dicarboxylic acid with a hydroxyl group at the α-carbon[74,75]. Thereby, 2-HG is an enantiomer existing in the D- or L-configuration[75]. Under physiological conditions, these two enantiomers of 2-HG are mainly generated in side reactions of the TCA cycle[76-78]. Two dehydrogenases, named D-2-HG dehydrogenase (D-2-HGDH) and L-2-HG dehydrogenase (L-2-HGDH), maintain endogenous levels of 2-HG under 100 µM by oxidizing it to α-KG[79-83]. Neither physiological levels of (D)-2-HG nor (L)-2-HG were shown to have an impact on mammalian cells so far. However, elevated levels of 2-HG are associated with the diseases (D)-2-HG aciduria ((D)-2-HGA) and (L)-2-HG aciduria ((L)-2-HGA)[76,84]. The accumulation of (D)-2-HG in (D)-2-HGA is caused by loss of function mutations within the *2-HGDH* genes or by a dominant genetic R140Q gain of function mutation within the *IDH2* gene[84-87]. (D)-2-HGA patients reach plasma (D)-2-HG concentrations of 26-757 µM[75]. (D)-2-HGA is known as a neurometabolic disorder encompassing, among others, phenotypes like epilepsy, hypotonia and psychomotor retardation as well as shorter lifespans[88,89]. To the current knowledge, (D)-2-HGA does not lead to a higher incidence for brain tumor malignancies[75]. (L)-2-HGA results from a disorder in (L)-2-HGDH and is also characterized by mental and motor developmental delay and epilepsy[79,81,90]. In 1993, the first association of (L)-2-HGA and brain malignancy was described by Wilcken and colleagues but also in other cases the occurrence of brain tumors in (L)-2-HGA patients was delineated[91-96].

The IDH mutations found in gliomas lead to strongly increased (D)-2-HG (further on referred to as 2-HG) levels between 5 - 35 mM within the tumor tissue[49,97]. Since patients with (D)-2-HGA do not develop malignancies, a multifactorial pathogenesis of *IDH1/IDH2*-mutant gliomas appears likely. In addition, differences in overall 2-HG concentrations could be responsible for the diverse outcome on gliomagenesis in (D)-2-HGA patients, as the high (D)-2-HG plasma concentrations measured in (D)-2-HGA patients might not predict tissue (D)-2-HG concentrations. 2-HG plasma levels are not elevated in patients with IDH-mutant glioma[98,99].

Numerous mechanisms of 2-HG favoring tumor formation are already known. Most of these mechanisms are based on the structural and chemical similarity to α-KG, wherefore 2-HG is able to bind with a very high affinity to around 60 α-KG-dependent dioxygenases, leading to a competitive inhibition of these enzymes[100-102] **(Fig. 1.2)**. One family of α-KG-dependent enzymes comprises the Ten-eleven translocation (TET) enzymes, important for the demethylation of DNA and thereby for the epigenetic regulation of gene expression[103-107]. 2-HG inhibits the catalytic activity of TET2, resulting in DNA

hypermethylation and epigenetic dysregulation in IDH-mutant tumors[101,108]. This DNA hypermethylation is known as the CpG island methylator phenotype (CIMP)[109-111]. Another family of α-KG-dependent enzymes is the Jumonji-C family of histone lysine demethylases (KDM) involved in the packaging of DNA in the nucleus[100,112]. By defining the structure of chromatin and thereby the accessibility of the DNA to the transcription machinery, these enzymes are also involved in epigenetic regulation of gene expression[112,113]. 2-HG inhibits the activity of the JmjC histone demethylases KDM2A, KDM4A, KDM4C and KDM7A[26,100,101] subsequently leading, for instance, to increased histone methylation marks in immortalized astrocytes[26]. The third important group of α-KG-dependent enzymes is the family of Egl nine homolog (EglN) prolyl-4-hydroxylases (P4HAs)[101]. Under aerobic conditions, these enzymes hydroxylate specific proline residues on hypoxia-induced factor 1 α (HIF1α), resulting in its proteosomal degradation[114,115]. Under hypoxic conditions the hydroxylation by EglN is blocked and HIF1α accumulates, dimerizes with HIF1β and acts as a transcription factor that mediates the cellular response to hypoxia[114,115]. Among other functions, it promotes angiogenesis and induces a metabolic switch from oxidative phosphorylation to anaerobic glycolysis[114-116]. Therefore, it is often oxygen-independently activated in many cancers[114-116]. It has been shown that 2-HG might either inhibit EglN enzymes or enhance the activity of EglN[64,117]. The group of P4HAs comprises furthermore P4HA1, 2 and 3. Together with pro-collagen-lysine 2-oxoglutarate 5-dioxygenases 1, 2 and 3 (PLOD1/2/3), they hydroxylate prolines and lysines, crucial for the maturation and stability of collagens[118]. Since these enzymes are also α-KG-dependent, they are bound and inhibited by 2-HG, leading to the accumulation of unfolded proteins and a resulting stress response of the endoplasmic reticulum[64].

As 2-HG leads to altered epigenetic modifications through the inhibition of DNA- and histone-demethylases as well as to the stabilization of HIF1α and the manifestation of a hypoxic phenotype, the metabolite is considered to be an oncometabolite promoting gliomagenesis. An additional oncogenic effect of 2-HG, not attributable to its structural and chemical similarity with α-KG, might be mediated by an increase of ROS levels in several tissues[119-121].

1.4 ROS and oxidative stress-responsive signaling

ROS describe reactive derivatives of molecular oxygen, generated during numerous cellular reactions in aerobic organisms[122,123]. These derivatives comprise free radicals, like the hydroxyl radical or the superoxide anion, characterized by unpaired electrons in the

outer valence orbitals[124]. Furthermore, also non-radical compounds, like hydrogen peroxide (H_2O_2), are regarded as ROS[124,125]. All ROS are characterized by inherent chemical properties, providing them with a high reactivity against different cellular structures and macromolecules, like DNA, lipids and proteins[126,127]. Under physiological conditions, ROS are mainly formed in the mitochondria during oxidative phosphorylation as a result of one-electron reductions, whereby superoxide anions are generated[124,128]. Other sources, generating superoxide anions as a byproduct, are several enzymatic reactions, for instance by cytochrome P450 monooxygenases or NAD(P)H oxidases (NOX)[127,129-131]. H_2O_2 is generated during the alleged detoxification of superoxide anions but can also be formed by NOX[132]. Unphysiologically elevated ROS levels result in oxidative stress characterized by the consequent oxidation of macromolecules[133]. These alterations can be prevented by stress-responsive signaling and by certain antioxidants, being oxidized instead[134]. Besides several non-enzymatic antioxidants like vitamins, carotinoids or GSH, cells express several antioxidative enzymes[135]. The detoxification of superoxide anions occurs enzymatically by three isoforms of superoxide dismutases (SODs) with distinct subcellular localizations, resulting in the generation of H_2O_2[136]. While SOD1 is mainly located in the cytosol, SOD2 is found in the mitochondrial matrix[137]. Due to the localization, SOD2 directly converts superoxide anions, produced during the oxidative phosphorylation, to H_2O_2[138]. The third isoform SOD3 is secreted into the extracellular matrix[139,140]. Since the conversion of superoxide anions to H_2O_2 occurs rapidly, an accumulation of superoxide anions is highly associated with oxidative stress[141]. Produced H_2O_2 is further on detoxified to H_2O and O_2 by several antioxidative enzymes, comprising catalase and several GPx[142-144]. Catalase is mainly located in the peroxisomes, where H_2O_2 is produced in high concentrations during the β-oxidation of fatty acids, but it can also be found in other compartments of the cell like in the cytosol[145,146]. In contrary to catalase, GPx are dependent on a co-factor[146,147]. Two molecules of the electron donor GSH are oxidized to the disulfide-linked GSSG molecule, thereby reducing H_2O_2 to molecular oxygen and dH_2O. GSSG is in turn reduced to two GSH again by the GSSG reductase under NADPH consumption[146,147]. In mammals, the four isoforms GPx1, GPx2, GPx3 and GPx4 exist. While the expression of GPx2 occurs solely in specific organs like in the gallbladder and liver, and GPx3 mRNA expression is rather low in the brain, GPx1 and GPx4 are ubiquitously expressed[148,149].

Although ROS like the superoxide anions and H_2O_2 show a high reactivity against cellular macromolecules, it became apparent in the last decades that those radicals and reactive molecules also have a physiological function as signal mediators[137]. Especially H_2O_2 is an important signaling molecule and involved in many cellular processes, like the regulation of protein-phosphorylations or certain transcription factors[127,150-154]. The role of ROS as

signal modulators allows the cells to adapt to stressful conditions, making them more resistant to elevated ROS levels. Thereby, a balanced homeostasis between ROS and antioxidants, crucial for a physiological phenotype, should be maintained[141,152]. Consequently, only a heterostasis in favor of ROS describes oxidative stress, resulting in unphysiological changes like extensive mutations within the genome or in cell death[126,152]. Therefore, oxidative stress is a known trigger for numerous diseases, including neurodegenerative diseases and cancer[152,155,156].

1.4.1 The oxidative stress response by NF-κB, NRF2, HSF1 and AP-1

In order to cope with elevated ROS levels, H_2O_2 or superoxide anions induce an oxidative stress-responsive gene expression. This response is mainly mediated by the four transcription factors nuclear factor kappa-light-chain-enhancer of activated B-cells (NF-κB), nuclear factor erythroid-2 related factor 2 (NRF2), activator protein 1 (AP-1) and heat shock factor 1 (HSF1)[157-159].

The transcription factor NF-κB is activated by H_2O_2. Thereby, H_2O_2 affects the phosphorylation of the inhibitor of NF-κB α (IκBα), with its subsequent inhibition and degradation[160,161]. The active transcription factor, consisting of Rel protein family members, translocates into the nucleus and leads to the expression of genes encoding antioxidative enzymes like GPx1, catalase, or SOD1 and SOD2[162-165]. Furthermore, genes encoding enzymes involved in GSH synthesis, like the glutamate-cysteine ligase catalytic subunit (GCLC), as well as the cell cycle regulator P53 are downstream targets of active NF-κB[166,167]. An additional pathway responsive to ROS, like superoxide anions or H_2O_2, involves the transcription factor NRF2, its inhibitor kelch-like ECH-associated protein 1 (KEAP1) and antioxidant response elements (AREs)[168,169]. NRF2 signaling works similar to NF-κB signaling. Under unstressed conditions, NRF2 is bound to KEAP1 resulting in the degradation of the transcription factor[169,170]. Upon the oxidation of cysteine residues of KEAP1, NRF2 is released and can translocate into the nucleus[171]. NRF2 induces, amongst others, also the expression of genes encoding proteins involved in the antioxidative defense like GPx4 and GCLC[172]. Furthermore, the expression of genes encoding NADPH-generating enzymes like ME1, NADPH quinone dehydrogenase 1 (NQO1) and IDH1 is induced by NRF2. Additional NRF2 target genes are P53 and the autophagy receptor sequestosome 1 (SQSTM1/p62)[169,172-177]. The third transcription factor responsive to oxidative stress is HSF1[178]. The transcription factor senses oxidative stress via two redox-sensitive cysteine residues within its DNA-binding domain, resulting in the

formation of disulfide bonds[178,179]. These structural changes allow the formation of homotrimers, building the active transcription factor[178]. As a heat shock factor, HSF1 promotes the proteolytic degradation or the repair of misfolded and stress-damaged proteins[157,159]. Besides the expression of genes encoding heat shock proteins or chaperones, the expression of genes encoding SQSTM1/p62 and the first NADPH-generating enzyme of the PPP, glucose-6-phosphate-dehydrogenase (G6PD), is induced by HSF1[180-182]. The fourth major transcription factor activated by oxidative stress is AP-1, consisting of jun and fos members[183,184]. Unlike the other three transcription factors, AP-1 is a constitutive nuclear transcription factor. Amongst others, antioxidative enzymes like GPx1 belong to AP-1-responsive genes[163].

Although an overlap in gene expression exists for the activation by NF-κB, NRF2, HSF1 and AP-1, solely one gene is expressed by all four transcription factors, making its expression an important marker for cellular stress conditions and for the expression of cytoprotective genes[157]. It encodes the protein heme oxygenase 1 (HMOX1), a heat shock protein named after its function of degrading heme to biliverdin, CO and ferrous iron. Its overexpression is observed in numerous tumors[185]. Amongst other cancers, HMOX1 is overexpressed in gliomas and glioblastomas compared to normal brain and is furthermore described to characterize glioma stem cells[186,187]. Since HMOX1 refers to the expression of cytoprotective genes, high HMOX1 expression levels in brain tumors indicate a worse therapy response to the chemotherapeutic agent temozolomide[188]. In *in vitro* experiments, an additional inhibition of the HMOX1 expression-inducing transcription factor NRF2 increases the sensitivity of cells to temozolomide treatment[189,190].

1.4.2 The oxidative stress response by MAPKs

Another response to oxidative stress comprises the mitogen-activated protein kinases (MAPKs)[191,192]. MAPKs are part of a serine/threonine kinase cascade-mediating signal transduction from the cell surface to the nucleus, ending with the phosphorylation and activation of transcription factors followed by induction of target gene expression[193]. The three major MAPK signaling pathways involve the MAPKs p42/44 or extracellular signal regulated kinase 1/2 (ERK1/2), p38 (p38α/β/γ/δ) and the c-Jun N-terminal kinases 1/2/3 (JNK1/2/3)[191,193]. p42/44 is mainly activated by mitogens via receptor tyrosine kinases regulating cell growth and proliferation. Its activity is mainly associated with survival and anti-apoptotic function[194]. p38 and JNK2/3 are mainly activated under stress conditions, like in response to inflammatory cytokines and heat shock, wherefore they are also named

stress-activated protein kinases (SAPKs)[195,196]. Both pathways decide about survival and cell death by inducing stress response pathways and regulating autophagy and apoptosis, for instance via the induced expression of genes coding for pro-apoptotic p53 or CCAAT/enhancer-binding protein (C/EBP) homologous protein (CHOP) as well as for jun and fos[197,198]. All three MAPKs are activated by oxidative stress[191,199-201]. Several potential mechanisms leading to the ROS-dependent MAPK activation were described so far. One mechanism relies on the oxidation of catalytic cysteine residues in MAPK phosphatases, resulting in their consequent inhibition and thus stabilization of active MAPKs[202]. Another mechanism is the activation of apoptosis signal-regulating kinase 1 (ASK1), an upstream kinase of JNK and p38, by the oxidation of its inhibitor thioredoxin[201,203].

Besides the potential initiation of cell cycle arrest and apoptosis in response to severe oxidative stress, all three MAPKs were furthermore shown to activate the four transcription factors NF-κB, NRF2, HSF1 and AP-1, strengthening the cytoprotective stress response[157,204-210].

1.4.3 The integrated stress response

The so-called integrated stress response represents a cytoprotective mechanism in eukaryotic cells that is induced by a variety of cellular stresses[211,212]. This pathway involves four serine/threonine kinases activated by distinct stress stimuli[213]. The kinase general control nonderepressible 2 (GCN2) mainly responds to amino acid starvation, the protein kinase R (PKR) senses double stranded RNA and viral infections, the heme-regulated initiation factor (HRI) is essentially activated by heme deprivation and oxidative stress and the PKR-like endoplasmic reticulum kinase (PERK) especially signals in response to endoplasmic reticulum stress like unfolded proteins[213]. The common target and thereby key-mediator of the integrated stress response is the eukaryotic translation initiation factor 2 alpha (eIF2α)[213,214]. As a part of a ternary complex, unphosphorylated eIF2α is involved in the transport of the initiator methionyl-tRNAi^{Met} to the translation initiation side[215]. Its phosphorylation and inactivation in response to cellular stress consequently results in the repression of global cap-dependent translation, in favor of the selectively increased cap-independent translation of specific mRNAs by open reading frames[211,216]. Thereby, the specific translation of the activating transcription factor 4 (ATF4) is induced, which in turn mediates the transcription of cytoprotective genes, encoding for instance antioxidative enzymes such as HMOX1, chaperones such as the glucose-regulated protein 78 (GRP78) and autophagy-related proteins like LC3, helping

the cell to cope with its stress conditions[211,217,218]. However, under prolonged or severe stress conditions, ATF4 favors the expression of cell cycle arrest-inducing genes as well as pro-apoptotic genes like *CHOP* or *growth arrest and DNA damage-inducible* (*GADD34*), to exclude heavily impaired cells from the tissue[219-222].

1.5 Cytoprotective signaling and programmed cell death

Cell death is a crucial event maintaining tissue homeostasis and leading to the disposal of harmfully altered cells, which includes cells with disturbed genome integrity or cells that cannot compensate severe stress conditions via stress response signaling[223,224]. Thereby, several distinct forms of cell death are distinguished, including apoptosis, autophagic cell death and necrosis[224]. Apoptosis as well as autophagic cell death refer to modes of programmed cell death, while necrosis depicts an uncontrolled and pathological type of cell death comprising the loss of membrane integrity[223,225]. The latter describes an autolysis that also affects the surrounding tissue by inducing inflammation[226].

Apoptosis is a molecularly regulated type of cell death[227,228]. Diverse stimuli lead to pro-apoptotic signaling and the consequent “self-killing” of the cell[229]. This process involves the outflow of electrolytes from the cell, resulting in cell shrinkage and the detachment from the tissue[230]. Further on, chromatin condensation and DNA fragmentation by endonucleases occur[231]. The cell membrane blebs and incorporates degraded cell debris[232]. Built apoptotic bodies are recognized by macrophages, based on a loss of membrane symmetry by the shift of the membrane component phosphatidylserine to the outer side of the membrane[233]. The apoptotic bodies are digested and eliminated by macrophages without an effect on the surrounding tissue[229,234-236]. A hallmark of apoptosis is the activation of **c**ysteinyl-**asp**artate specific nucle**ases** (caspases) that are expressed as inactive pro-caspases and are activated by proteolysis[237]. Caspases are divided into initiator caspases, comprising amongst others the caspases 8, 9, and 10, and effector caspases, that contain the caspases 3 and 7[238-240]. They belong to an activation cascade, starting with the activation of initiator caspases via protein-protein interactions in apoptosomes[241]. In order, activated initiator caspases activate the effector caspases, decomposing proteins and activating endonucleases responsible for DNA fragmentation[242-244]. Although the executive downstream signaling comprises common parts, the activation of apoptosis occurs via two different main mechanisms – the extrinsic pathway and the intrinsic pathway[224,245,246]. Extrinsic apoptosis is activated by ligands that bind to membrane-bound death receptors. Known ligands are among others the Fas

ligand, tumor necrosis factor α (TNFα) or the TNF-related apoptosis inducing ligand (TRAIL)[247,248]. The intrinsic pathway responds to various intracellular stresses like DNA damages, oxidative stress or endoplasmic reticulum stress[249]. It is also referred to as mitochondrial-dependent apoptosis pathway, since the release of cytochrome c from the mitochondria is crucial for the apoptosome formation and the consequent activation of initiator caspases[224,250].

Like apoptosis, autophagy is a self-degrading process that may eventually lead to programmed cell death[224,251]. Upon the initiation of autophagy, organelles and cytoplasmic materials are engulfed in vesicles, called autophagosomes, which in turn fuse to lysosomes[252]. In the resulting autolysosomes, enclosed cell components are degraded by lysosomal acidic hydrolases[252]. These steps are regulated by autophagy-related proteins (ATGs) downstream of the negative regulator of autophagy mammalian target of rapamycin complex 1 (mTORC1)[253,254]. mTORC1 senses the abundance of nutrients, growth factors and energy in the cell and is inactivated by the lack of at least one of the latter, resulting in autophagy[253]. Although autophagy describes a possible way of programmed cell death, its mechanism mainly refers to a cytoprotective signaling pathway, increasing the threshold of stress sufficient for cell death induction[255]. Under nutrient starvation, it provides recycled building blocks for the ongoing synthesis of macromolecules[254,256-258]. Moreover, autophagy prevents, comparable to the ubiquitin–proteasome system, the accumulation of damaged cell organelles or unfolded proteins by the directed degradation and recycling of these components[259]. Selective autophagy involves adaptors like SQSTM1/p62, delivering ubiquitinated proteins to lipidated LC3, an ubiquitin-like protein tightly associated with the autophagosomal membrane[259,260].

Autophagy and apoptosis inhibit each other by involving pathways like p53, phosphatidylinositol-3-kinase and protein kinase B (PI3K/AKT) and JNK signaling[261-264]. On the contrary, characteristic events of both pathways are found in the same cells and many players are shared between the pathways or influenced by each other[265]. Two transcription factors decisively involved in apoptosis and autophagy are NF-κB and the signal transducer and activator of transcription 3 (STAT3)[266-269]. NF-κB is frequently activated by the IκB kinase (IKK) complex, phosphorylating IκBs, wherefore the active transcription factor translocates into the nucleus and induces the target gene expression of, for instance, anti-apoptotic genes[270,271]. STAT3 is activated upon its phosphorylation by active Janus kinase (JAK) receptors, leading to dimerization and target gene expression[272-274]. Like NF-κB, active STAT3 induces the expression of anti-apoptotic genes like *B-cell lymphoma 2* (*Bcl-2*) and represses the expression of the tumor suppressor *p53*[266,275,276]. Both signaling pathways are therefore frequently constitutively

active in tumor cells, supporting tumor initiation and progression as pathologically altered cells keep on proliferating without being eliminated from the tissue[266,277-279]. The inhibition of both transcription factors is not only associated with the induction of apoptosis but also with autophagy initiation[267,280,281]. Although autophagy describes a rather tumor-suppressive process, due to the induced degradation of damaged organelles and harmful proteins, it might also protect cancer cells from apoptosis and mediate resistance to therapy[282]. Autophagy as well as apoptosis are therefore often modulated by therapeutic agents[283].

1.6 Cell cycle regulation

The cell cycle with its various checkpoints is a highly conserved mechanism of the cell[284]. It ensures the cell-doubling and the accurate segregation into two daughter cells. By checking for cell size, correct replication and the integrity of the chromosomes, the cell cycle sorts for physiologically healthy cells[285,286]. Cells showing, for example, genomic alterations, arrest and are repaired or discarded, depending on the severity of the alteration.

The cell cycle divides into the phase of DNA synthesis (S-phase), where the DNA replication takes place, and the phase of mitosis (M-phase), where the chromosome separation occurs. These phases are separated by the gap phases G1 and G2, in which the cells prepare for mitosis and synthesis, respectively[287-291]. The several phases are tightly controlled by the fast synthesis and the ubiquitin-dependent proteolysis of the main regulators of the cell cycle called cyclins[292,293]. They drive the transition of the cell from one phase to the other by binding to specific cyclin-dependent kinases (CDKs) leading to active confirmations of the enzymes[294]. Activated enzymes are able to regulate cellular processes important for the cell cycle progression, like the condensation of chromosomes or the entry into mitosis by nuclear envelope breakdown[294,295]. Additionally, transcription is regulated by CDKs via the phosphorylation and inactivation of the transcriptional repressor retinoblastoma protein (RB), binding and inactivating the transcription factor E2F[296-298]. The phosphorylation of RB leads to the release of E2F and the transcription of cell cycle-related genes[296-304]. Furthermore, transcription is induced by the activation of RNA polymerase II by CDK-mediated phosphorylation[305-307]. Besides the activation of CDKs by cyclins, a negative regulation of CDKs exists. Hence, CDKs are inhibited under unfavorable conditions by the binding of small cyclin-dependent kinase inhibitors (CKIs) as well as by phosphorylation[308,309]. Two classes of CKIs are known - the inhibitors of

CDK4 (INK4), specific for the inhibition of CDK4 and CDK6, as well as the CDK-interacting proteins / kinase inhibitor proteins (CIP/KIPs), inhibiting a broad spectrum of cyclin-CDK complexes. The class of INK4 comprises the proteins p16, p15, p18 and p19, encoded by *CDKN2A*, *CDKN2B*, *CDKN2C* and *CDKN2D* respectively. The small inhibitory proteins p21, p27 and p57 belong to the class of CIP/KIPs and are encoded by *CDKN1A*, *CDKN1B* and *CDKN1C* respectively[310-320].

Depending on cues like growth factor abundance, genome integrity or several stresses, many signaling pathways are involved in the regulation of the cell cycle progression. Besides others, JAK/STAT signaling, MAPK signaling and PI3K/AKT signaling are involved in cell cycle regulation[321-331]. All of these pathways regulate the expression of cell cycle regulators like CDKs, CKIs and cyclins and are thereby able to rather support cell cycle progression or to induce either G0/G1-phase arrests or G2/M-phase arrests[323,325,326]. However, the most important and most intensively studied player of cell cycle regulation is p53[332,333]. Under unstressed conditions p53 is inactive and bound by the ubiquitin protein ligase mouse double minute 2 homolog (MDM2) mediating the proteosomal degradation of p53[334]. In case of cell damages like DNA alterations, p53 is phosphorylated and thereby released from MDM2, resulting in its accumulation in the nucleus, where it controls, for instance, the expression of cell cycle arrest-inducing regulators like p21 as well as DNA repair enzymes in order to reconstitute genome integrity[316,335-338]. However, if the damage is too severe, the induction of apoptosis by the expression of pro-apoptotic proteins is mediated by p53[339-341]. Thereby, p53 ensures, that genome alterations cannot be passed on to daughter cells and thus do not accumulate in the tissue. p53 mutations are found in over 50 % of all human cancers, resulting in accumulating mutations, ongoing proliferation and apoptosis resistance[342,343]. After many years suggesting a simple inactivation of p53, it was found, that mutations of p53 result in gain of function by allowing the binding to mutant p53-specific binding partners and the regulation of diverse downstream target genes[344-348].

1.7 The conditional CreER^{tam}/*loxP* mouse model

Transgenic mouse models and gene knock-out technology have been used for decades to study the effects of disease-related mutations pushing the knowledge of genetic disorders and thereby the generation of novel treatments. Nevertheless, these approaches show several limitations[349]. Some mutations or knockouts of genes are embryonic lethal, excluding the analysis of the mutation in somatic tissues. Additionally, only early effects of

the mutation or knockout are depicted, whereas the expression of some genes might have diverse functions at different time points in processes like development or differentiation. Besides that, knockout systems are not feasible to distinguish between a direct effect of the mutation or the knockout and pleiotropic effects[350]. To circumvent these issues, a new system has been developed, which does not only allow silencing of particular genes in particular tissues, but also a temporal regulation – the CreER^{tam}/*loxP* recombinase system, which evolved from a simple tool for site-specific recombination in bacteria to an inducible tool for genome tailoring in mammals[349,351].

The Cre recombinase (**c**auses **re**combination), a 38 kDa protein, derives from the bacteriophage P1 and belongs to the integrase family of site-specific recombinases[349]. Its action of catalyzing the intra- or intermolecular recombination between two of its recombination sites *loxP* (**l**ocus **o**f **X** (cross)-over in **P**1) without any additional co-factors, makes it suitable for easy genome tailoring. The *loxP* site is a 34 bp consensus sequence, consisting of a core spacer sequence of 8 bp, flanked by two palindromic sequences of 13 bp each[352,353]. It is restricted to the P1 phage genome and is long enough, that it is highly unlikely to occur randomly in other genomes. One recombinase binds to one palindromic sequence of the *loxP* site each, thereby forming a dimer, before a tetramer is formed by the recombinases of two *loxP* sites[354]. The Cre recombinases cause DNA double-strand breaks resulting in recombination between the two spacer regions[354,355]. The asymmetric core sequence defines the orientation of the *loxP* site and thereby the result of the recombination, resulting in excision, inversion, insertion or translocation between two molecules[349,356-359] **(Fig. 1.3)**.

The CreER^{tam} recombinase is a fusion protein consisting of the Cre recombinase and a linked mutated ligand-binding domain of the human estrogen receptor (ER)[349]. The receptor lost its ability to bind endogenous estrogen but binds the estrogen receptor modulator 4-hydroxytamoxifen (4-OHT)[349]. This is followed by the translocation of the Cre fusion protein into the nucleus, where the Cre recombinase executes its function. By activating Cre recombinase with 4-OHT tight temporal regulation is possible[349,360,361].

The CreER^{tam}/*loxP* recombinase system is not only used for the knockout or translocation of genes, but also for controlled gene expression[355]. Placing a so-called *lox-stop-lox* (*LSL*) cassette in between a promoter and the affiliated gene the expression is prevented, if Cre recombinase is absent or not active. The stop sequence is excised when Cre recombinase is abundant as well as activated, and then gene expression proceeds[355,362] **(Fig. 1.3)**.

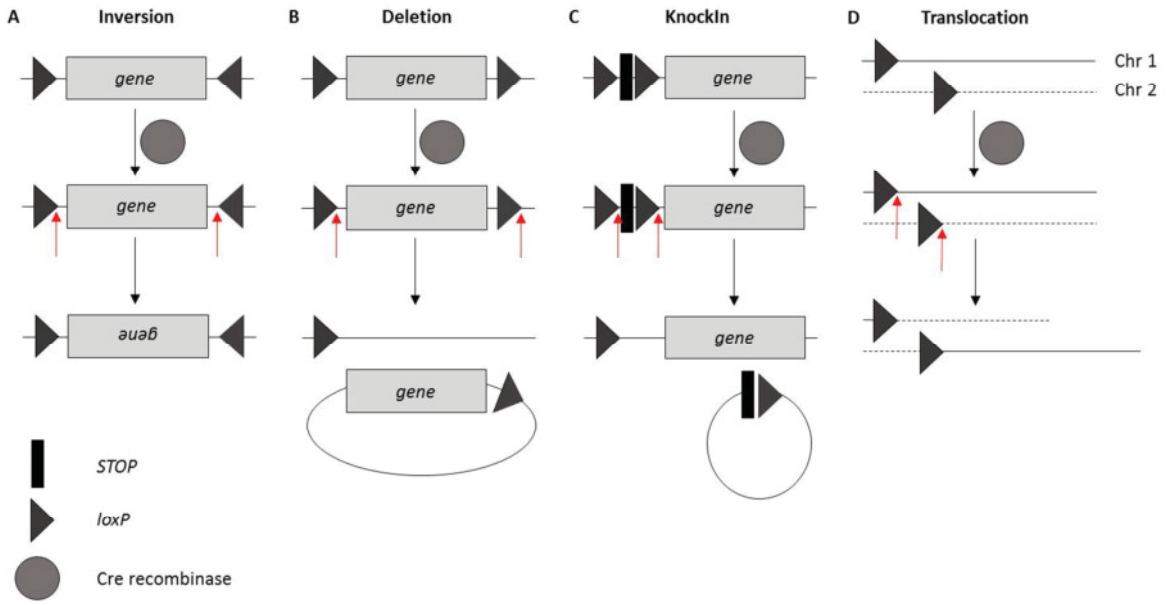

Fig. 1.3: Cre/*loxP* system and possible implications
(Chr: chromosome)

1.8 4-OHT and its effects on the cell

4-OHT is a potent metabolite of the triphenylethylene tamoxifen in humans and mammals[363-371]. Tamoxifen and 4-OHT are non-steroidal substances exhaustively tested according to their ability of competitively inhibiting ERα and ERβ in breast tissue[363,372-376]. Tamoxifen is commonly used for chemotherapy of breast cancer, leading to cell cycle arrest of the tumor cells in the G0/G1-phase by inducing levels of the cell cycle regulators p21 and p27 as well as to the induction of regulated cell death[364,365,367,370,375,377-387]. The ER-dependent effect of 4-OHT on breast cancer cells relies furthermore on the inhibition of a positive cross-talk between the activated ER, itself serving as a transcription factor, and NF-κB in gene expression, resulting in the consecutive induction of apoptotic cell death[388-391]. Moreover, the activation of PI3K/AKT and p42/44 signaling is repressed, thereby reducing the ER-mediated effects of proliferation and migration[390,392,393]. Although the anti-estrogenic effect of tamoxifen and its metabolites is the first choice in breast cancer treatment, also agonistic effects were observed at ERs in distinct tissues like endometrium, liver and bone tissue, favoring malignancies[375,394-397]. Therefore, tamoxifen is called a selective estrogen receptor modulator (SERM)[378,398,399]. Besides distinct ER-dependent effects in different tissues, 4-OHT also exerts ER-independent effects, which are also manifold and tissue-dependent. They comprise, for instance, the inhibition of the Ca^{2+}-dependent protein kinase C (PKC) in rat brain cells and neutrophils or the activation of stress-signaling pathways like JNK signaling and NF-κB signaling by elevated ROS

levels, resulting in apoptosis in Jurkat and ovarian or breast cancer cells[400-406]. Contrary results were obtained by Wei and colleagues who reported an inhibitory effect of tamoxifen on NF-κB signaling in neural cells[407]. Ongoing studies additionally revealed the ER-independent inhibition of mTORC1 signaling and induction of autophagy of breast cancer cells after tamoxifen treatment[408]. 4-OHT-mediated autophagic cell death is moreover induced in apoptosis-resistant glioblastoma cell lines[409,410], accompanied by a decrease of epidermal growth factor receptor (EGFR) protein levels, a mitogen-responsive receptor frequently overexpressed and constitutively active in around 60 % of primary glioblastomas[409,411,412]. Since tamoxifen is lipophilic and thereby able to cross the blood brain barrier, the compound was considered for glioblastoma treatment, resulting in phase I and II clinical trials of tamoxifen in adult patients with glioblastomas[413-419]. However, the adjuvant therapy with tamoxifen combined with radiotherapy did not improve treatment results or survival of glioblastoma patients[420-422].

1.9 Neural stem cells as a model for the characterization of *IDH1* mutation

In order to functionally characterize glioma-associated mutations, established glioma cell lines are typically used that were derived from IDH-wildtype glioblastomas. To study effects of IDH mutation, mutant IDH1 has been transiently or stably transfected into such IDH-wildtype cell lines[63,423-425]. As the IDH mutations naturally found in IDH-mutant gliomas and glioblastomas are typically heterozygous and since mutant IDH proteins form heterodimers with their wildtype counterparts, these models are not necessarily appropriate to characterize the mutation[17,426]. Furthermore, established IDH-wildtype glioblastoma cell lines carry numerous other mutations that are usually absent in IDH-mutant gliomas, making it difficult to draw conclusions about IDH mutation-mediated effects and about its possible role as a gliomagenesis-initiating mutation[426].

In recent years, the theory of cancer stem cells as tumor-initiating cells has been proposed. Indeed, cancer stem cells have been found to constitute a small subpopulation of tumor cells in brain tumor tissue and share characteristics with neural stem cells (NSCs), including maintained proliferation and self-renewal capacities[427-429]. Like NSCs that occupy distinct niches like the subventricular zone within the adult brain, also glioblastoma stem cells rely on the interaction with a specific microenvironment to maintain their stem cell characteristics[430-434]. The concept of using glioma stem cells as a prioritized model for the functional characterization of glioma biology has been promoted over the last decade[4,5,435-438], and it has been suggested that glioma stem cells most likely

originate from NSCs or neural progenitor cells (NPCs), albeit some studies also suggested possible glioma origins from oligodendroglial progenitor cells or astrocytes[3,439,440]. By performing a global expression profiling Lee and colleagues demonstrated in 2006 that resected gliomas cultured in serum-free medium with EGF and FGF clustered according to their expression profiles with the parental tumor as well as with NSCs, while the same cells cultured in serum clustered with commonly used glioblastoma cell lines away from the parental tumor[441]. Besides alterations of the genome and transcriptome in glioblastoma cell lines cultured in serum-containing medium, tumors formed by these cells in xenografts refused to show characteristics of glioblastomas like the characteristic diffusely infiltrative growth[441,442]. In contrast, an injection of glioma stem cells cultured under conditions normally used for NSC-culturing into mouse brains led to the development of tumors with the characteristics of the original tumor[443-446]. First *in vivo* experiments of Sasaki and colleagues using an NSC-specific knock-in of mutant *Idh1* in mice resulted in brain hemorrhages and perinatal lethality[64]. Similar results were obtained by Bardella and co-workers in 2016, using a conditional knock-in model relying on 4-OHT and Cre recombinase[28]. Conditional *in vitro* models using NSCs represent feasible models to study the effects of mutant *Idh1* on NSCs and at the same time avoiding the negative side effects of the expression of mutant *Idh1* in developing mice.[29,447,448].

1.10 Aims

Since a heterozygous mutation of *IDH1* is the most common alteration in diffuse astrocytic and oligodendroglial gliomas of WHO grades II or III and a subset of glioblastomas, a functional characterization of cellular and molecular effects of this mutation is necessary to improve mechanistic understanding of glioma development and reveal new therapeutic strategies against this deadly disease. The gain of function mutations in *IDH1* or *IDH2* inhibit the physiological NADPH-generating conversion of isocitrate to α-KG and favor the NADPH-consuming conversion of α-KG to the oncometabolite 2-HG, affecting among others the cells' ROS homeostasis, metabolism as well as epigenetics. However, a multifactorial pathogenesis of IDH-mutant tumors is suggested, as patients with (D)-2-HGA, also characterized by elevated 2-HG levels, do not develop brain tumors. Although an IDH mutation is believed to be the first mutation to occur in gliomagenesis, mutation of *IDH1* or *IDH2* by itself is not sufficient for gliomagenesis. This stresses the necessity of understanding the cellular implications of these mutations for finding possible therapeutics against the potential tumor-initiating events in IDH-mutant cells. However, most investigations addressing the role of mutant IDH1 in glioma so far resulted from experiments with mutant IDH1-overexpressing glioblastoma cell lines carrying a background of mutations not typically present in IDH-mutant gliomas or their putative cells of origin, thereby preventing the characterization of IDH mutation-mediated effects in a disease-specific model system. The overexpression of mutant IDH1 in glioma cells derived from IDH-wildtype tumors thus reflects neither physiological nor pathological conditions, as the formation of heterodimers of mutant and wildtype IDH1 is not taken into account. Furthermore, isolated glioma cells cultured in stem cell medium were shown to be more similar to the initial tumor tissue when compared to glioma cells cultured in FCS-containing medium, raising the concept of glioma stem cells as drivers of gliomagenesis and arguing against established long-term cultured glioblastoma cell lines for characterizing glioma biology.

By using a conditional knock-in mouse model relying on the 4-OHT-inducible CreER^{tam}/*loxP* recombinase system, the functional and molecular analyses of the effects of heterozygous *Idh1* mutation under the endogenous promoter are possible. Therefore, NSC/NPCs derived from P0/P1 mice carrying an inducible knock-in of mutant *Idh1* were cultured in stem cell medium. The implications of the *Idh1* mutation on ROS homeostasis, metabolism and signaling in these putative cells of origin for gliomas should be evaluated. The validation of the conditional *Idh1*-mutant knock-in mouse model, as well as the search for possible effects on cell biology and gene expression mediated by induced Idh1 mutation in murine NSC/NPCs were the major aims of this thesis.

2.0 MATERIALS AND METHODS

2.1 Materials

2.1.1 Chemicals and kits

All chemicals and kits used for the experiments performed for this thesis were obtained from commercial sources. **Tab. 2.1** provides an overview of the individual chemicals and kits and their respective sources.

Tab. 2.1: Summary of used chemicals and kits

Chemical/Kit	Order Number	Company
(2R)-Octyl-α-hydroxyglutarate	16366	Cayman Chemical, Ann Arbor, Michigan, USA
7-AAD	559925	BD Pharmingen™, San Jose, California, USA
α-Ketoglutarate	11970	Cayman Chemical, Ann Arbor, Michigan, USA
β-Estradiol	E8875	Sigma-Aldrich®, St. Louis, Missouri, USA
2- Mercaptoethanol	M3148-100ML	Sigma-Aldrich®, St. Louis, Missouri, USA
AccuPrime™ Taq DNA Polymerase High Fidelity Kit	12346086	Invitrogen, Carlsbad, California, USA
Adonitol / Ribitol	A5502	Sigma-Aldrich®, St. Louis, Missouri, USA
Agarose standard	3810.3	ROTH®, Karlsruhe, Germany
Albumin Fraction V	8076.3	ROTH®, Karlsruhe, Germany
Annexin V Binding Buffer (10x)	556454	BD Pharmingen™, San Jose, California, USA
Annexin V, FITC	556419	BD Pharmingen™, San Jose, California, USA
Benzonase® Nuclease	E1014-25KU	Sigma-Aldrich®, St. Louis, Missouri, USA
BrdU Flow Kit, FITC – Part A	51-2354AK	BD Pharmingen™, San Jose, California, USA
Bromphenol blue	B-8026	Sigma-Aldrich®, St. Louis, Missouri, USA

Caspase-Glo® 3/7 Assay	G8093	Promega, Madison, Wisconsin, USA
CellTiter-Glo® Luminescent Cell Viablility Assay	G7571	Promega, Madison, Wisconsin, USA
$CHCl_3$	1.02431.2500	Merck Millipore, Burlington, Massachusetts, USA
CM-H2DCFDA	C6827	Invitrogen, Carlsbad, California, USA
cOmplete Mini, EDTA-free	11836170001	Roche, Basel, Switzerland
Dihydroethidium	D11347	Invitrogen, Carlsbad, California, USA
DMEM/F-12	31330-038	Thermo Scientific™, Waltham, Massachusetts, USA
DMEM, high glucose	41965-039	Thermo Scientific™, Waltham, Massachusetts, USA
DMF	270547-1L	Merck Millipore, Burlington, Massachusetts, USA
Dimethyl sulfoxide	D5879-500ML	Sigma-Aldrich®, St. Louis, Missouri, USA
DPBS, no calcium, no magnesium	14190-094	Thermo Scientific™, Waltham, Massachusetts, USA
EGF, recombinant human	AF-100-15-1000	PEPROTECH, Rocky Hill, New Jersey, USA
EtOH	20821.330	VWR®, Darmstadt, Germany
Fetal Bovine Serum	26400044	Thermo Scientific™, Waltham, Massachusetts, USA
FGF, recombinant human	AF-100-18B-1000	PEPROTECH, Rocky Hill, New Jersey, USA
Geltrex™	A14132-02	Thermo Scientific™, Waltham, Massachusetts, USA
Glycerol	818709.1000	Merck Millipore, Burlington, Massachusetts, USA
Heparin Sodium Cell Culture	H-3149	Sigma-Aldrich®, St. Louis, Missouri, USA
HotStar HiFidelity Polymerase Kit	202602	Qiagen, Hilden, Germany
Isopropanol	6752.5	ROTH®, Karlsruhe, Germany
Laminin from Engelbreth-Holm-Swarm murine sarcoma basement membrane	L2020	Sigma-Aldrich®, St. Louis, Missouri, USA
Laminin, Mouse, 1mg	354232	Thermo Scientific™, Waltham, Massachusetts, USA

MeOH	CP43,4	ROTH®, Karlsruhe, Germany
Midori Green Advance	MG04	NIPPON Genetics Europe, Dueren, Germany
MTT (Thiazolyl Blue Tetrazolium Bromide)	M5655	Sigma-Aldrich®, St. Louis, Missouri, USA
my-Budget 100 bp + 1.5 DNA ladder	85-2150-050	Bio-Budget, Krefeld, Germany
N-2 Supplement	17502-048	Thermo Scientific™, Waltham, Massachusetts, USA
N-Acetyl-L-Cysteine	A7250-5G	Sigma-Aldrich®, St. Louis, Missouri, USA
NaCl	P029.3	ROTH®, Karlsruhe, Germany
Neural Tissue Dissociation Kit	130092628	Miltenyi Biotech, Bergisch Gladbach, Germany
Nonidet™ P 40 Substitute	74385-1L	Sigma-Aldrich®, St. Louis, Missouri, USA
PageRuler™ Prestained Protein Ladder, 10 to 180 kDa	26616	Thermo Scientific™, Waltham, Massachusetts, USA
Pen Strep	15140-122	Thermo Scientific™, Waltham, Massachusetts, USA
PhosSTOP EASY pack	04906837001	Roche, Basel, Switzerland
Pierce™ BCA Protein Assay Kit	23225	Thermo Scientific™, Waltham, Massachusetts, USA
Platinum SyBr™ Green qPCR SuperMix™-UDG w/ROX	11744100	Thermo Scientific™, Waltham, Massachusetts, USA
Powdered milk	T145.3	ROTH®, Karlsruhe, Germany
Proteinase K, lyophilized	70663	Merck Millipore, Burlington, Massachusetts, USA
RevertAid First Strand cDNA Synthesis Kit	K1621	Thermo Scientific™, Waltham, Massachusetts, USA
RNaseZAP™	R2020-250ML	Sigma-Aldrich®, St. Louis, Missouri, USA
RNeasy Mini Kit	74104	Qiagen, Hilden, Germany
SDS	D6750-100G	Sigma-Aldrich®, St. Louis, Missouri, USA
Sodium deoxycholate	D6750-100G	Sigma-Aldrich®, St. Louis, Missouri, USA
Soybean Trypsin Inhibitor, powder	17075029	Thermo Scientific™, Waltham, Massachusetts, USA
Staurosporine	9953	Cell Signaling Technology®, Danvers, Massachusetts, USA

TRIS	9090.3	ROTH®, Karlsruhe, Germany
TRIzol™ Reagent	15596018	Invitrogen, Carlsbad, California, USA
Trypan Blue Stain (0.4 %)	15250-061	Thermo Scientific™, Waltham, Massachusetts, USA
Trypsin-EDTA (0.05 %), phenol red	25300054	Thermo Scientific™, Waltham, Massachusetts, USA
Tween® 20	9127.2	ROTH®, Karlsruhe, Germany
(Z)-4-Hydroxytamoxifen	H7904-5MG	Sigma-Aldrich®, St. Louis, Missouri, USA

2.1.2 Materials and technical devices

All materials and technical devices used for the experiments performed for this thesis were obtained from commercial sources. **Tab. 2.2** provides an overview of used materials and their respective sources. **Tab. 2.3** shows the used technical devices and their commercial suppliers.

Tab. 2.2: Summary of used materials

Material	Order Number	Company
6 cm cell culture dishes, Nunclon™ Delta Surface	150288	Thermo Scientific™, Waltham, Massachusetts, USA
6-well plates, Nunclon™ Delta Surface	140685	Thermo Scientific™, Waltham, Massachusetts, USA
10 cm cell culture dishes, Nunclon™ Delta Surface	172931	Thermo Scientific™, Waltham, Massachusetts, USA
96-well plates, Nunclon™ Delta Surface	161093	Thermo Scientific™, Waltham, Massachusetts, USA
96-well plates, white	3610	Corning, New York, USA
384-well assay plates	3701	Corning, New York, USA
384-well plates, white	3570	Corning, New York, USA
Amersham™ Protan™ 0.2 µM NC	10600001	GE healthcare, Little Chalfont, United Kingdom
Cell Lifter	3008	Corning, New York, USA
Combitips advanced® 1 ml / 5 ml	0030089.430 0030089.456	Eppendorf, Hamburg, Germany
MicroAMP® Fast Optical 96-Well Reaction Plate	4346906	Applied Biosystems®, Foster City, California, USA

Multipette® stream	4987000010	Eppendorf, Hamburg, Germany
my-Budget 8er Strips Caps	30-SP-0075	Bio-Budget, Krefeld, Germany
my-Budget “96-well” PCR plates	30-SP-9600	Bio-Budget, Krefeld, Germany
Nunc™ EasYFlask™ 75 cm	156499	Thermo Scientific™, Waltham, Massachusetts, USA
NuPAGE™ Novex™ 4-12 % Bis-Tris Protein Gels	NP0322 NP0335 NP0336	Thermo Scientific™, Waltham, Massachusetts, USA
Pipette tips	S1120-3810 S1120-1810 S1120-1840 S1120-8810 S1120-1830	STARLAB, Hamburg, Germany
Polypropylene Round-Bottom Tube, 5 ml	352053	Corning, New York, USA
Safe-Lock Tubes, 1.5 ml	0030120086	Eppendorf, Hamburg, Germany
Safe-Lock Tubes, 2.0 ml	0030120094	Eppendorf, Hamburg, Germany
StarSeal Advanced Polyolefin Film	E2796-9795	STARLAB, Hamburg, Germany
Stripettes, 25 ml / 10 ml / 5 ml	4489 4488 4487	Corning, New York, USA
CELLSTAR® Centrifuge Tubes, 15 ml	188271	VWR®, Darmstadt, Germany
CELLSTAR® Centrifuge Tubes, 50 ml	227261	VWR®, Darmstadt, Germany
Vi-CELL™ 4 ml Sample Vials	383721	BECKMAN COULTER®, Brea, California, USA
Whatman™ Chromatography Paper, 3 mm Chr	3030-861	GE healthcare, Little Chalfont, United Kingdom

Tab. 2.3: Summary of used technical devices

Device	**Company**
ALC-3100.2 (Scale)	ACCULAB, New York, USA
BD FACSCanto™ II (Cell analyzer)	BD Pharmingen™, San Jose, California, USA
Biometra OV 5 (Hybridization oven)	Analytik Jena, Jena, Germany
Biometra TRIO (PCR thermal cycler)	Analytik Jena, Jena, Germany

CyAn ADP (Cell analyzer)	BECKMAN COULTER®, Brea, California, USA
Fusion FX (Gel documentary system)	Vilber Lourmat Deutschland GmbH, Eberhardzell, Deutschland
Incubator	BINDER, Tuttlingen, Germany
KERN 430-33 (Scale)	ACCULAB, New York, USA
KS 250 basic (Shaker)	IKA®, Staufen, Germany
MilliQ Integral 5 (Water treatment unit)	Merck Millipore, Burlington, Massachusetts, USA
MSC-ADVANTAGE (Safety cabinet)	Thermo Scientific™, Waltham, Massachusetts, USA
NanoDrop® ND-1000 Spectrophotometer	VWR®, Darmstadt, Germany
Odyssey® CLx Image System	LI-COR®, Lincoln, Nebraska, USA
OLYMPUS IX50 (Microscope)	OLYMPUS, Center Valley, USA
PARADIGM™ (Platereader)	BECKMAN COULTER®, Brea, California, USA
PerfectSpin 24R Refrigerated microcentrifuge	VWR®, Darmstadt, Germany
Phblot-1010E	Biotec-Fischer GmbH, Reiskirchen, Deutschland
PowerPac™ 300 (Power supply)	BIO-RAD, Hercules, California, USA
PowerPac™ Basic (Power supply)	BIO-RAD, Hercules, California, USA
Rotina 46 R (Centrifuge)	Hettich, Tuttlingen, Germany
ROTOFIX 32 (Centrifuge)	Hettich, Tuttlingen, Germany
StepOnePlus Real-Time PCR System	Applied Biosystems®, Foster City, California, USA
Systec VX-150 (Autoclave)	Systec, Linden, Germany
ThermoMixerC	Eppendorf, Hamburg, Germany
Vi-CELL™ XR (Cell counter)	BECKMAN COULTER®, Brea, California, USA
X Cell SureLock™ Electrophoresis Cell	Thermo Scientific™, Waltham, Massachusetts, USA

2.1.3 Software

The distinct software programs that were used for this thesis, as well as their suppliers and usages are listed in **Tab. 2.4.**

Tab. 2.4: Overview of used software

Software	Application	Company
CorelDraw X3 Graphics Suite	Graphing software **(Fig. 1.2)**	Corel Corporation, Ottawa, Canada
Endnote X7	Citation program	Clarivate Analytics, Philadelphia, Pennsylvania, USA
FlowJo™	Flow analysis software	FlowJo LLC, Ashland, Oregon, USA
GIMP 2	Image editor	Open source: https://www.gimp24.de/
GraphPad Prism 5 / 7	Analysis and graphing software	GraphPad, San Diego, California, USA
Image J	Image processing software	Open source: https://imagej.nih.gov/ij/
Image Studio Lite v2.1	Densitometric protein quantification software	LI-COR Biosciences, Lincoln, Nebraska, USA
IrfanView	Image view software	Open source: https://www.irfanview.com/
Microsoft Office 2016	Writing and graphing softwares	Microsoft Corporation, Redmond, Washington, USA
Multimode Analysis Software	Platereader software	PerkinElmer, Waltham, Massachusetts, USA
ND-1000 v3.7.1	DNA / RNA Quantification	VWR®, Darmstadt, Germany
Quantum-Capt-1	Gel documentation imaging system	Vilber Lourmat Deutschland GmbH, Eberhardzell, Deutschland
StepOne™ Software v2.0.1	qRT-PCR analysis software	Thermo Scientific™, Waltham, Massachusetts, USA
Summit™	Flow cytometry analysis	DakoCytomation, Santa Clara, California, USA
ViCELLXR 2.03	Cell counting	BECKMAN COULTER®, Brea, California, USA

2.1.4 Solutions and buffer

Tab. 2.5 shows the protocols for the preparation of solutions and buffers used in this thesis.

Tab. 2.5: Protocols for used solutions and buffers

Solution/buffer	Protocol
2-HG	20 mg/ml in EtOH
3-MA	50 mM in DMEM/F-12
4-OHT	2 mg/ml in EtOH 7,75 mg/ml in DMSO
α-KG	20 mg/ml in EtOH
β-Estradiol	25 mM in EtOH
AG 490	100 mM in DMSO
Agarosegel loadingbuffer	30 % [v/v] glycerin, 0.5 % [w/v] bromphenolblue xylencyanol, ad dH_2O
Bafilomycin A1	0.1 mg/ml in DMSO
EGF	10 µg/ml in 0.5 % [v/v] 10 mM acetic acid with 0.1 % BSA in DMEM/F-12 with
FGF	10 µg/ml in DPBS with 0.1 % BSA
Heparin	2 mg / ml in DPBS
IKK 16	50 mM in DMSO
Laemmli buffer, 4x	100 mM TRIS, 6 % [v/v] SDS, 40 % [v/v] glycerol, 4 % [v/v] β-mercaptoethanol, spatula tip bromphenol blue, ad dH_2O
MES buffer, 20x	1 M MES, 1 M TRIS, 70 mM SDS, 20 mM EDTA, ad dH_2O, pH 7.3
MTT reagent	5 mg/ml in DPBS
MTT solubilization solution	40 % [v/v] DMF, 2 % [v/v] glacial acetic acid, 16 % [w/v] SDS, ad dH_2O, pH 4
NAC	0,5 M in dH_2O
Proteinase K (10 mg/ml)	50 % [v/v] DPBS, 50 % [v/v] Glycerol
RIPA buffer	50 mM TRIS-HCl (pH 8), 150 mM NaCl, 1 % [v/v] NP-40, 0.5 % [v/v] sodium deoxycholate, 0.1 % [w/v] SDS
SB203580	20 mg/ml in DMSO
Soybean Trypsin Inhibitor	2 mg/ml in DPBS
Staurosporine	1 mM in DMSO
Tail digest buffer	100 mM TRIS-HCl (pH 8), 200 mM NaCl, 5 mM EDTA (pH 8), 0,4 % [v/v] SDS
TBS buffer, 10x	10 mM TRIS, 150 mM NaCl, ad dH_2O
TBST buffer	1:10 TBS buffer (10x), 1:1000 Tween® 20, ad dH_2O
TE buffer	10 mM TRIS, 100 mM EDTA, ad dH_2O

Transfer buffer, 1x	1:10 transfer buffer (10x), 20 % [v/v] methanol, ad dH_2O
Transfer buffer, 10x	250 mM TRIS, 2 M glycerine, ad dH_2O
Z-DEVD-FMK	20 mM in DMSO
Z-VAD-FMK	20 mM in DMSO

2.1.5 Primers

Tab. 2.6 provides an overview of the primer sequences used in this thesis. All oligonucleotide primers were purchased from Sigma-Aldrich®. The respective oligonucleotides arrived in dried form and were reconstituted with 5 mM Tris HCl (pH 7.0) to 100 mM stock solutions. They were stored at -20°C until further use.

Tab. 2.6: Used primers and their sequences

Primer name	Gene	Primersequence
Atf4-Mm-F1	*Atf4*	5'-gaatggccggctatggatgat-3'
Atf4-Mm-R1	*Atf4*	5'-cattcgaaacagagcatcgaagtc-3'
Cat-Mm-F1	*Cat*	5'-ggagaggcagtctattgcaagt-3'
Cat-Mm-R1	*Cat*	5'-gatctcggaggccataatcc-3'
Chop-Mm-F1	*Ddit3*	5'-gaggtcctgtcctcagatgaa-3'
Chop-Mm-R1	*Ddit3*	5'-gatgtgcgtgtgacctctgttg-3'
Gadd34-Mm-F1	*Ppp1r15a*	5'-ctgcagaggcggctcagatt-3'
Gadd34-Mm-R1	*Ppp1r15a*	5'-cagcaaggaaatggactgtgact-3'
Gclc-Mm-F1	*Gclc*	5'-ctcagccagaccatatctaca-3'
Gclc-Mm-R1	*Gclc*	5'-gatagtggccagctgatcata-3'
Gclm-Mm-F1	*Gclm*	5'-gctataggcacctctgatcta-3'
Gclm-Mm-R1	*Gclm*	5'-gaggccaggttaacttggtta-3'
Gpx1-Mm-F1	*Gpx1*	5'-ctacaccgagatgaacgatctg-3'
Gpx1-Mm-R1	*Gpx1*	5'-ccaccaggtcggacgtactt-3'
Gpx4-Mm-F1	*Gpx4*	5'-ctacactcagctagtcgatct-3'
Gpx4-Mm-F1	*Gpx4*	5'-cacagatcttgctgtacatgtc-3'
Heatr7a-Mm-F1	*Heatr7a*	5'-ggctaccagcgagatgacaa-3'
Heatr7a-Mm-R1	*Heatr7a*	5'-ccatcacctggttggtgaat-3'
Hmox1-Mm-F1	*Hmox1*	5'-cacagatggcgtcacttcgt-3'
Hmox1-Mm-R1	*Hmox1*	5'-gatgagctagtgctgatctg-3'

Mdm2-Mm-F1	*Mdm2*	5‘-gcgtggaatttgaagttgagtct-3‘
Mdm2-Mm-R1	*Mdm2*	5‘-ggaaatctcaggatctccttcaa-3‘
Nes-Mm-F1	*Nes*	5‘-gaggcgctggaacagagattg-3‘
Nes-Mm-R1	*Nes*	5‘-ctgagcgatctgactctgtag-3‘
p15-Mm-F1	*Cdkn2b*	5‘-ccaatccaggtcatgatgatg-3‘
p15-Mm-R1	*Cdkn2b*	5‘-ccaggcgtcacacacatc-3‘
p16-Mm-F1	*Cdkn2a*	5‘-ggctagagaggatcttgagaag-3‘
p16-Mm-R1	*Cdkn2a*	5‘-gtcctcgcagttcgaatctg-3‘
p18-Mm-F1	*Cdkn2c*	5‘-ggacctagagcaacttactagtt-3‘
p18-Mm-R1	*Cdkn2c*	5‘-gattagcacctctgaggagaag-3‘
p19-Mm-F1	*Cdkn2d*	5‘-cgtggcgacgtgcaagag-3‘
p19-Mm-R1	*Cdkn2d*	5‘-ccttgcttcaggagctccaa-3‘
p21-Mm-F1	*Cdkn1a*	5‘-ccacagcgatatccagacattc-3‘
p21-Mm-R1	*Cdkn1a*	5‘-cgcaatcacggcgcaactg-3‘
p27-Mm-F1	*Cdkn1b*	5‘-gccttcgacgccagacgta-3‘
p27-Mm-R1	*Cdkn1b*	5‘-gtgcttatacaggatgtccattc-3‘
p57-Mm-F1	*Cdkn1c*	5‘-gaactgcgcaggagaacaag-3‘
p57-Mm-R1	*Cdkn1c*	5‘-ctctctggccgttagcctcta-3‘
Serpina3n-Mm-F1	*Serpina3n*	5‘-gaactggtctcagacctggat-3‘
Serpina3n-Mm-R1	*Serpina3n*	5‘-ctcagacttgaacgtgtcaaga-3‘
Socs2-Mm-F1	*Socs2*	5‘-ctgggacgtgttgactcatct-3‘
Socs2-Mm-R1	*Socs2*	5‘-ggcttcattaacagtcatacttc-3‘
Sod1-Mm-F1	*Sod1*	5‘-ccatccacttcgagcagaag-3‘
Sod1-Mm-R1	*Sod1*	5‘-ccatgctggccttcagttaatc-3‘
Sod2-Mm-F1	*Sod2*	5‘-cagcctgcactgaagttcaat-3‘
Sod2-Mm-R1	*Sod2*	5‘-cttgatagcctccagcaact-3‘
Sod3-Mm-F1	*Sod3*	5‘-ggctcttcctccggcctcta-3‘
Sod3-Mm-R1	*Sod3*	5‘-ggccaacatggctgaggttct-3‘

2.1.6 Antibodies

Tab. 2.7 and **Tab. 2.8** provide an overview of used primary and secondary antibodies and their respective sources. All antibodies were diluted according to the manufacturer's protocol (shown in **Tab. 2.14**).

Tab. 2.7: Summary of used primary antibodies

1st Antibody	Order Number	Company
4E-BP1	9644S	Cell Signaling Technology®, Danvers, Massachusetts, USA
α-Tubulin	2144S	Cell Signaling Technology®, Danvers, Massachusetts, USA
Akt	9272S	Cell Signaling Technology®, Danvers, Massachusetts, USA
Atf4	11815S	Cell Signaling Technology®, Danvers, Massachusetts, USA
Catalase	14097S	Cell Signaling Technology®, Danvers, Massachusetts, USA
eIF2α	5324S	Cell Signaling Technology®, Danvers, Massachusetts, USA
Grp78	3177S	Cell Signaling Technology®, Danvers, Massachusetts, USA
Hmox1	MA1-112	invitrogen, Carlsbad, California, USA
Jnk	9252S	Cell Signaling Technology®, Danvers, Massachusetts, USA
LC3A/B	12741S	Cell Signaling Technology®, Danvers, Massachusetts, USA
Stat3	9139S	Cell Signaling Technology®, Danvers, Massachusetts, USA
Socs2	2779S	Cell Signaling Technology®, Danvers, Massachusetts, USA
p38	9212S	Cell Signaling Technology®, Danvers, Massachusetts, USA
p42/44	9102S	Cell Signaling Technology®, Danvers, Massachusetts, USA
p4E-BP1 (Thr37/46)	2855S	Cell Signaling Technology®, Danvers, Massachusetts, USA
p53	MA1-7629	invitrogen, Carlsbad, California, USA
p70S6	2708S	Cell Signaling Technology®, Danvers, Massachusetts, USA

pAkt (Ser473)	9271S	Cell Signaling Technology®, Danvers, Massachusetts, USA
peIF2α (Ser51)	3398S	Cell Signaling Technology®, Danvers, Massachusetts, USA
Perk	3192S	Cell Signaling Technology®, Danvers, Massachusetts, USA
pJnk (Thr183/Tyr185)	9251S	Cell Signaling Technology®, Danvers, Massachusetts, USA
pStat3 (Tyr705)	9145S	Cell Signaling Technology®, Danvers, Massachusetts, USA
pp38 (Thr180/Tyr182)	9211S	Cell Signaling Technology®, Danvers, Massachusetts, USA
pp42/44 (Thr202/Tyr204)	9101S	Cell Signaling Technology®, Danvers, Massachusetts, USA
pp53 (Ser15)	12571S	Cell Signaling Technology®, Danvers, Massachusetts, USA
pp70S6 (Thr389)	9234S	Cell Signaling Technology®, Danvers, Massachusetts, USA
pPerk (Thr980)	3179S	Cell Signaling Technology®, Danvers, Massachusetts, USA
Vinculin	129002	Abcam®, Cambridge, United Kingdom

Tab. 2.8: Summary of used secondary antibodies

2nd Antibody	Order Number	Company
IRDye® 800CW anti mouse	926-32210	LI-COR®, Lincoln, Nebraska, USA
IRDye® 800CW anti rabbit	926-32211	LI-COR®, Lincoln, Nebraska, USA

2.1.7 Inhibitors

Tab. 2.9 shows the inhibitors that were used in this thesis and their respective suppliers. The inhibitors were diluted as shown in **Tab. 2.5**.

Tab. 2.9: Summary of used inhibitors

Inhibitor	Order Number	Company
3-MA	sc-205596	Santa Cruz Biotechnology®, Dallas, Texas, USA
AG 490	0414	Tocris bioscience, Bristol, United Kingdom
Bafilomycin A1	sc-201550	Santa Cruz Biotechnology®, Dallas,

		Texas, USA
GW5074	G 6416	Sigma-Aldrich®, St. Louis, Missouri, USA
IKK 116	2539	Tocris bioscience, Bristol, United Kingdom
SB203580	S8307-1MG	Sigma-Aldrich®, St. Louis, Missouri, USA
U0126	9903	Cell Signaling Technology®, Danvers, Massachusetts, USA
Z-DEVD-FMK	sc-311558	Santa Cruz Biotechnology®, Dallas, Texas, USA
Z-VAD-FMK	sc-3067	Santa Cruz Biotechnology®, Dallas, Texas, USA

2.2 Methods

2.2.1 Cell culture

2.2.1.1 Conditional knock-in mouse model

For the characterization of mutant *Idh1* in NSC/NPCs, a conditional knock-in mouse model relying on the CreER^{tam}/*loxP* recombinase system was used. The CreER^{tam} is further on referred to as Cre or Cre recombinase. *LSL-Idh1* mice were generated as described by Sasaki and colleagues in 2012[64]. The mice were crossed into C57BL/6NTac-*Gt(ROSA)26-Sor*$^{tm9(cre/ESR1)Arte}$ mice from Taconic, generated as described by Seibler and colleagues[449], for more than ten generations. Mice with the following four genotypes were generated: *Idh1*$^{wt/wt}$ *Cre*$^{-/-}$, *Idh1*$^{wt/wt}$ *Cre*$^{-/+}$, *Idh1*$^{wt/LSL}$ *Cre*$^{-/-}$ and *Idh1*$^{wt/LSL}$ *Cre*$^{-/+}$ **(Fig. 2.1)**. The mice were maintained according to standard animal care protocols and sacrificed under protocol 039/12.

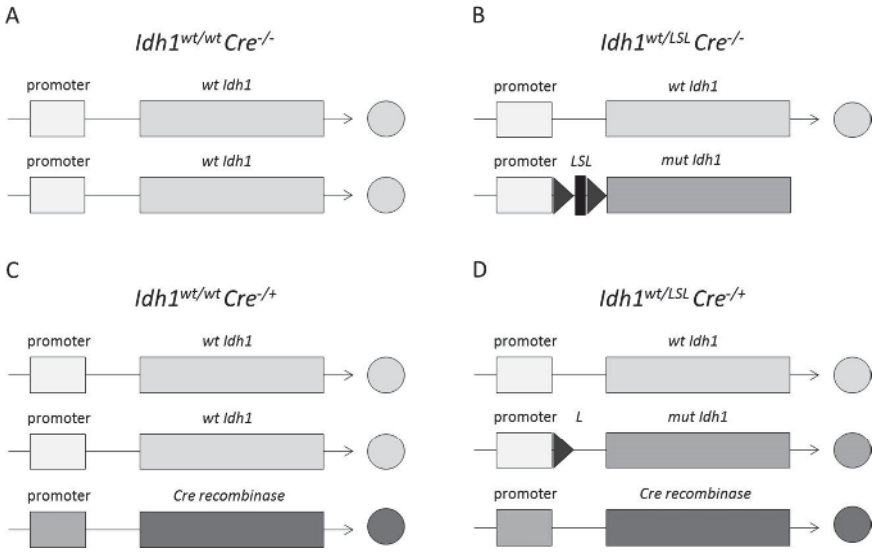

Fig. 2.1: Genotypes of the NSC/NPCs
(A) *Idh1*$^{wt/wt}$ *Cre*$^{-/-}$ NSC/NPCs with two alleles expressing wildtype *Idh1* (*wt Idh1*). **(B)** *Idh1*$^{wt/LSL}$ *Cre*$^{-/-}$ NSC/NPCs with one allele encoding wildtype *Idh1*, which is expressed under normal conditions. The second allele codes for mutant *Idh1* (*mut Idh1*) under the endogenous promoter. However, since no Cre recombinase is expressed, the *loxP-stop-loxP* (*LSL*) sequence remains between the promoter and the gene and prevents the expression of the mutant protein. **(C)** *Idh1*$^{wt/wt}$ *Cre*$^{-/+}$ NSC/NPCs with two alleles expressing wildtype *Idh1*. Additionally, Cre recombinase is expressed in these NSC/NPCs. As there are no *loxP* sequences naturally occurring, an expression and activation of Cre recombinase should not have an effect. **(D)** *Idh1*$^{wt/LSL}$ *Cre*$^{-/+}$ NSC/NPCs with a knock-in of mutant *Idh1* upon the activation of Cre recombinase by 4-OHT. These cells express wildtype *Idh1* and mutant *Idh1* under the endogenous promoter.

The gene encoding Cre recombinase was heterozygously integrated into the *Rosa26* locus, resulting in constitutive and ubiquitous expression of the protein. The activation of Cre recombinase by 4-OHT treatment allowed the recombination between two *loxP* sites. By successful recombination, the stop sequence between the two *loxP* sites was eliminated and mutant *Idh1* was expressed under the endogenous *Idh1* promoter.

2.2.1.2 Isolation and culturing of murine NSC/NPCs

P0-P2 mice were decapitated and the entire brain was dissociated using the Neural Tissue Dissociation Kit from Miltenyi Biotech according to the manufacturer's protocol. Early passages were cryopreserved in 10 % [v/v] DMSO in DMEM/F-12 and thawn when needed. NSC/NPCs were cultured in cell culture dishes and well plates coated with 1:250 [v/v] Laminin from Engelbreth-Holm-Swarm murine sarcoma basement membrane in DPBS **(3.1, 3.2)** or 1:200 [v/v] Geltrex™ in DMEM/F-12 without any supplements **(3.3, 3.4)** as an adherent monolayer. For the stem cell medium, DMEM/F-12 (Thermo Scientific™) was supplemented with 1:100 [v/v] Penicillin-Streptomycin (10,000 U/ml; Thermo Scientific™), 1:100 [v/v] CTS™ N-2 Supplement (Thermo Scientific™), 4 µg/ml Heparin (Sigma-Aldrich®), 20 ng/ml recombinant human EGF (PEPROTECH) and 10 ng/ml recombinant human FGF (PEPROTECH). After every 72-96 h the cells were passaged. Therefore, the NCS/NPCs were detached with Trypsin-EDTA (0.05 %) (Thermo Scientific™). This reaction was stopped by adding Soybean Trypsin Inhibitor (Thermo Scientific™) in a 1:1 molar ratio. The NSC/NPCs were seeded after cell counting with the Vi-CELL™ XR from BECKMAN COULTER®. For the preservation of the cultures 1 million to 1.2 million cells where seeded onto coated 10 cm dishes, depending on the proliferation of the respective NSC/NPC culture. For experiments, NSC/NPCs were seeded into coated cell culture dishes as described in **Fig. 3.1** – **Fig. 3.30**. The cells were cultured in an incubator with 37°C, 5 % CO_2 levels and 95 % relative humidity. The mouse-derived NSC/NPC cultures were sequentially numbered, wherefore one number stands for NSC/NPCs from one mouse. The NSC/NPC cultures were used for experiments until passage twenty-five, however, early passages until passage ten were preferred. Quantitative real-time polymerase chain reaction (qRT-PCR) for nestin was used for the characterization of the cells as NSC/NPC. Cultures were discarded in case of morphological changes or changes in growth behavior.

2.2.2 Genotyping

2.2.2.1 Extraction of genomic DNA from mice tails

After isolation and culturing of the NSC/NPCs **(2.2.1.2)**, the tails of the sacrificed mice were incubated with 500 µl Tail digest buffer and 1:100 proteinase K (10 mg/ml) over night at 56°C while shaking. Afterwards, 500 µl isopropanol was added, followed by at least 2 h of incubation at -20°C. The samples were centrifuged for 30 min at 4°C and 14,000 rpm and the supernatant was discarded. The DNA pellets were dissolved in 500 µl TE buffer and used for genotyping PCRs.

2.2.2.2 Genotyping PCR reaction

For the genotyping PCR reaction, the following mixtures were prepared **(Tab. 2.10)**. Used primers are listed in **Tab. 2.11**.

Tab. 2.10: Genotyping PCR reactions for *Idh1* and *Cre recombinase* (1x)

Substance	*Cre recombinase* [µl]	*Idh1* [µl]
10x buffer	2	2
dNTP	0.5	0.4
Primer I	0.5	0.4
Primer II	0.5	0.4
Primer III	-	0.4
$MgCl_2$	0.5	0.8
dH_2O	14.9	14.4
DNA	1	1
Taq	0.1	0.2

Tab. 2.11: Primer sequences for genotyping PCR reaction

Primername	Primersequence
Idh1-genotyping-1	5‘-accagcacctcccaacttgtat-3‘
Idh1-genotyping-2	5‘-aggttagctcttgccgatccgt-3‘
Idh1-genotyping-3	5‘-cagcagcctctgttccacatac-3‘
*Cre*1	5‘-gctcgaccagtttagttaccc-3‘
*Cre*2	5‘-tcgcgattatcttctatatcttcag-3‘

The PCR reaction took place using the PCR protocol as listed in **Tab. 2.12**. Afterwards, the PCR products were supplemented with agarose loading buffer and separated on a 2 % [w/v] agarose gel with Midori Green Advance from Biozym® at 180 V for 20 min in 1x TAE buffer. The PCR products were detected by using the Fusion FX gel documentary system from Vilber Lourmat Deutschland GmbH.

Tab. 2.12: PCR protocol for the genotyping PCR reaction (*40x)

Time [min]	Temperature [°C]
-	95
15	95
30*	95*
20*	56*
30*	72*
10	72
∞	4

2.2.3 Quantitative real-time PCR

2.2.3.1 RNA extraction with Trizol®

Cells were centrifuged and the pellet was resuspended in 1 ml Trizol® (Thermo Scientific™). After 5 min of incubation at RT, 200 µl chloroform was added followed by vigorous shaking and 10 min of incubation at RT. The samples were centrifuged for 10 min with 12,000 rcf at 4°C. The aqueous phase was transferred into a new tube and 500 µl isopropanol was added. After invertation and 10 min incubation at RT, the samples were again centrifuged with the stated settings. Afterwards, the pellets were washed with 500 µl 75 % ethanol and centrifuged for 5 min and 2000 rcf at 4°C. After removing the supernatant, the pellets were dried and resolved in 50 µl dH_2O before they were quantified using the NanoDrop® ND-1000 Spectrophotometer from PEQLAB. The samples were stored at -80°C until further processing.

2.2.3.2 cDNA synthesis

For cDNA synthesis, 1 µg of RNA from each sample was used. RevertAid First Strand cDNA Synthesis Kit from Thermo Scientific™ was used according to the manufacturer's

protocol using random hexamer primers. The synthesized cDNA was diluted 1:20 with dH_2O and was stored at 4°C.

2.2.3.3 qRT-PCR

The Platinum® SYBR® Green Kit (Thermo Scientific™) was used for qRT-PCR analyses with 0.65 µl of each primer. For each sample, duplets were measured with the StepOnePlus Real-Time PCR System (Thermo Scientific™) according to the protocol in **Tab. 2.13**. 3 µl cDNA was used for each measurement. ROX was used as the passive reference. For relative quantification through comparative C_T values ($\Delta\Delta C_T$) *Arf1* was detected as an endogenous control and mouse universal reference cDNA was used as reference sample. dH_2O served as negative control. Used primers are shown in **Tab. 2.6**.

Tab. 2.13: PCR protocol for the qRT-PCR reaction (*40x)

Time	Temperature [°C]
10 min	95
15 s*	95*
1 min*	60*
15 s	95
1 min	60
15 s	95

2.2.4 Transcriptome profiling

2.2.4.1 RNA extraction using the QIAGEN RNeasy Mini Kit

RNA for RNA sequencing and microarray analyses was isolated using the RNeasy Mini Kit from QIAGEN. The treated cells were scraped off the 10 cm dishes with 600 µl RLT buffer each and stored at -80°C until further processing. After thawing, 1 % [v/v] β-mercaptoethanol was added to the samples. Further steps are explained in the manufacturer's protocol. An additional DNase digest took place (Appendix D, QIAGEN manual). The RNA was eluted in 60 µl RNase-free water during two centrifugation steps, followed by quantification using the NanoDrop® ND-1000 Spectrophotometer from PEQLAB. The samples were stored at -80°C until further usage.

2.2.4.2 RNA sequencing analyses

The RNA sequencing analyses were performed as described in the publication of Forget and colleagues[450] at the Department of Pediatric Oncology, Hematology and Clinical Immunology in collaboration with Dr. Marc Remke and Daniel Picard. After assessing RNA quality with RNA 6000 Nano chips (Agilent Technologies) on a bioanalyzer, the TruSeq Stranded RNA LT Kit (low-throughput protocol, Illumina®) was used to prepare barcoded libraries from 500 ng total RNA. The validation and quantification of the libraries were performed with the Agilent DNA 1000 Kit (Agilent Technologies) and high sensitivity chips on a bioanalyzer (Agilent Technologies). 7.5 pM of the denaturated libraries were used as the input for cBot (Illumina®), before deep sequencing took place on a HiSeq 2500 (Illumina®) for 101 cycles with additional seven cycles for index reading. For data analysis, Partek® Flow® was used. Log2 intensity was normalized to counts per million. The reads were aligned against the reference *Mus musculus* chromosome 10 (mmu10) using the STAR v2.4.1d aligner. Gene expression was quantified using the mm10 ENSEMBL (Transcripts release 84) database by the Partek® Expectation-Maximization algorithm.

2.2.4.3 Microarray analyses

The microarray analyses were carried out at the Genomics and Transcriptomics Laboratory (GTL) of the Center for Biological and Medical Research (BMFZ) in collaboration with René Deenen. Synthesis of biotin-labeled cDNA was performed with 100 ng of total RNA according to the manufacturer's protocol (WT Plus Reagent Kit, Affymetrix, Inc.). End labeled cDNA was hybridized to Affymetrix Mouse Gene 2.0 ST Gene Expression Microarrays for 16 h at 45°C, stained by strepatavidin / phycoerythrin conjugate, and scanned as described in the manufacturer's protocol. Data analyses on Affymetrix CEL files were conducted with GeneSpring GX software (vers. 12.5; Agilent Technologies). Probes within each probe set were summarized by GeneSprings´ ExonRMA16 algorithm after quantile normalization of probe level signal intensities across all samples to reduce inter-array variability[451]. Input data pre-processing was concluded by baseline transformation to the median of all samples. After grouping of replicated samples according to their respective experimental condition a given probe set had to be expressed above background (i.e. fluorescence signal of a probe set was detected within the 20th and 100th percentiles of the raw signal distribution of a given array) in at least

three of four NSC/NPC cultures in at least one or both conditions to be further analyzed in pairwise comparisons.

2.2.5 Western Blotting

2.2.5.1 Cell lysis

RIPA buffer was freshly supplied with PhosSTOP Phosphatase Inhibitor Cocktail Tablets (Roche), cOmplete Protease Inhibitor Cocktail Tablets (Roche) and 1:1000 Benzonase® Nuclease (Novagen®). The cells were washed with pre-chilled DPBS before they were scraped off the 6 cm dishes with 70-100 µl completed RIPA buffer followed by 5-10 min incubation on a rotating wheel at 4°C. Afterwards, the samples were centrifuged for 10 min with 13,000 rcf at 4°C, after which the cell lysates were transferred into new tubes and were stored at -20°C until further processing.

2.2.5.2 BCA assay for protein quantification

For protein quantification, the Pierce™ BCA Protein Assay Kit by Thermo Scientific™ was used. BSA concentrations of 0, 0.5, 1, 1.5 and 2 mg/ml in completed RIPA buffer were used as a concentration standard. For each reaction, 5 µl of cell lysate or concentration standard was pipetted into 96-well plates and covered with 200 µl of the freshly prepared master mix consisting of 50 parts of BCA Reagent A and 1 part of BCA Reagent B. The concentration standard was measured in triplets, for the cell lysates each sample was measured twice. The formation of the detectable BCA-copper-complex took place during 30 min of incubation at 37°C followed by the colorimetric measurement at 570 nm using the PARADIGM™ platereader from BECKMAN COULTER™.

2.2.5.3 SDS-PAGE

The electrophoretic separation of the proteins in the cell lysate was accomplished by an SDS polyacrylamide gel electrophoresis (SDS-PAGE). For each sample, 20 µg of protein was mixed with 1:4 Laemmli buffer, followed by denaturation at 95°C for 5 min.

Afterwards, the samples were loaded onto NuPAGE™ Novex™ 4-12 % Bis-Tris Protein Gels (Thermo Scientific™) and ran for approximately 80 min with a current of 130 V in 1x MES buffer.

2.2.5.4 Transfer of proteins onto nitrocellulose membranes

The electrophoretically separated proteins were transferred onto Amersham™ Protan™ 0.2 µM NC membranes (GE healthcare) using a tank blotting system. The transfer took place in 1x transfer buffer for 150 min using a constant current of 250 mA. Afterwards, the membranes were blocked with 5 % MP in TBST for 1 h at RT while shaking.

2.2.5.5 Immunostaining of blotted proteins

The membranes were incubated with the primary antibody at 4°C overnight while shaking. The antibodies were diluted as stated in **Tab. 2.14**. Afterwards, the membranes were washed with TBST three times for 10 min before they were incubated with the secondary antibody in a 1:10,000 dilution in TBST for 1 h at RT. The membranes were again washed with TBST three times for 10 min before the fluorescent signal of the secondary antibody was detected using the Odyssey® CLx Imaging System from LI-COR®. The densitometric analyses were performed using Image Studio Lite Software. Data for the protein of interest were normalized to data for the control proteins vinculin or α-tubulin (tubulin), respectively.

Tab. 2.14: Used antibody dilutions

1st Antibody	Dilution
4E-BP1	1:1000 in 5 % BSA in TBST
α-Tubulin	1:1000 in 5 % BSA in TBST
Akt	1:1000 in 5 % BSA in TBST
Atf4	1:1000 in 5 % BSA in TBST
Catalase	1:1000 in 5 % MP in TBST
eIF2α	1:1000 in 5 % BSA in TBST
Grp78	1:1000 in 5 % BSA in TBST
Hmox1	1:1000 in 5 % MP in TBST

Jnk	1:1000 in 5 % BSA in TBST
LC3A/B	1:1000 in 5 % BSA in TBST
Stat3	1:1000 in 5 % MP in TBST
Socs2	1:250 in 5 % MP in TBST
p38	1:1000 in 5 % BSA in TBST
p42/44	1:1000 in 5 % BSA in TBST
p4E-BP1	1:1000 in 5 % BSA in TBST
p53	1:1000 in 5 % BSA in TBST
p70S6	1:1000 in 5 % BSA in TBST
pAkt	1:1000 in 5 % BSA in TBST
peIF2α	1:1000 in 5 % BSA in TBST
Perk	1:1000 in 5 % BSA in TBST
pJnk	1:500 in 5 % BSA in TBST
pStat3	1:250 in 5 % BSA in TBST
pp38	1:500 in 5 % BSA in TBST
pp42/44	1:1000 in 5 % BSA in TBST
pp53	1:1000 in 5 % MP in TBST
pp70S6	1:1000 in 5 % BSA in TBST
pPerk	1:1000 in 5 % BSA in TBST
Vinculin	1:1000 in 5 % MP in TBST

2.2.6 Metabolome profiling

The cells were centrifuged, cell pellets were washed with pre-chilled DPBS and cells were centrifuged again. The pellets were then resuspended in 2.5 ml DPBS and cell numbers were determined by using the Vi-CELL™ XR from BECKMAN COULTER®. Equal numbers of cells of each condition were centrifuged for 5 min with 2000 rpm at 4°C. The supernatant was collected as a negative control. DPBS, used medium and an empty tube were used as further controls. The cell pellets were lyzed in 100 µl per 100,000 cells dH_2O : MeOH : $CHCl_3$ at a ratio of 1 : 2.5 : 1 containing 50 µM ribitol. For the controls, 1 ml of the mix was added. The samples were incubated for 10 min at 4°C on a rotating wheel and centrifuged for 5 min at 10,000 rpm at 4°C. The supernatants were collected in new tubes and stored at -80°C until the metabolite measurements were performed at the Cluster of Excellence on Plant Sciences (CEPLAS) Plant Metabolism and Metabolomics

Labor in collaboration with Dr. Tabea Mettler-Altmann. The metabolite analysis was performed with the 7200 gas chromatography (GC)-coupled quadrupole time-of-flight (QTOF) mass spectrometer from Agilent Technologies. The results were analyzed with the Agilent Technologies software MassHunter as described by Fiehn and Kind[452]. For relative quantification, the area response measured for the metabolites was normalized to the measured area response of the internal standard ribitol.

2.2.7 Flow cytometric analyses

2.2.7.1 FITC Annexin V / 7-AAD apoptosis staining

For apoptosis staining, FITC-coupled Annexin V from BD Pharmingen™ was used. The corresponding protocol was adjusted. The supernatant from the cells was collected into Polypropylene Round-Bottom Tubes. The cells were washed, taken up with DPBS and also collected. Trypsin-EDTA was used to detach the cells from the dish, followed by Trypsin-EDTA inactivation by adding Soybean Trypsin Inhibitor in a 1:1 molar ratio. The cells were centrifuged with 1300 rpm for 5 min at 4°C followed by resuspension of the cell pellets in 1 ml freshly prepared Annexin V Binding Buffer and another centrifugation step with the stated settings. After the centrifugation, cell pellets were resuspended in 100 µl master mix **(Tab. 2.15)** and incubated for 15 min at RT in the dark. Then, 1 ml 1x Annexin V Binding Buffer was added to each sample and the samples were centrifuged with the stated settings. The pellets were resuspended in 200 µl 1x Annexin V Binding Buffer and 20 µl 7-AAD and stored at 4°C until the flow cytometry measurement was performed. An unstained control as well as samples solely stained with either 7-AAD or Annexin V were used for compensation purposes. Analyses of the data were performed using the FlowJo™ software. After gating for the cell population in a side scatter (SSC) to forward scatter (FSC) plot, included cells were gated corresponding their staining for unstained NSC/NPCs, Annexin V- or 7-AAD-stained NSC/NPCs and double-stained NSC/NPCs.

Tab. 2.15: Annexin V / 7-AAD apoptosis staining (1x)

Substance	Amount [µl]
(10x) Annexin V Binding Buffer	10
FITC Annexin V	4
7-AAD	4
dH_2O	82

2.2.7.2 Cell cycle analysis using BrdU incorporation

The BrdU Flow Kit from BD Pharmingen™ was used for cell cycle analysis. Cultured cells were treated with BrdU according to the manufacturer's instructions for 4 h at 37°C. Following treatment, the medium was collected and cells were washed with DPBS before being detached with 200 µl Trypsin-EDTA per well. Soybean Trypsin Inhibitor was added afterwards in a 1:1 molar relationship. The cells were taken up with DPBS. The samples were centrifuged for 5 min and 1300 rpm at 4°C. The supernatants were discarded and the pellets were resuspended in 100 µl BD Cytofix/Cytoperm each, followed by 30 min incubation at 4°C. In the meantime, BD staining buffer was prepared using 30 µl heat-inactivated FCS and 970 µl DPBS per sample. After the incubation, 1 ml BD staining buffer was added and the samples were centrifuged again with the stated settings. The supernatant was discarded and the pellets were frozen with 1:10 [v/v] DMSO in FCS at -80°C until further processing.

After thawing, the pellets were washed with the BD staining buffer and centrifuged again with the stated settings. The supernatant was discarded and the pellets were resuspended in 100 µl BD Cytofix/Cytoperm, followed by an incubation for 5 min at RT. Afterwards, 1 ml 1x washing buffer was added and samples were centrifuged again with the stated settings. The pellets were resuspended in 100 µl DNase solution, which contained 300 µg / ml DNase in DPBS. This attempt was incubated for 1 h at 37°C, before 1 ml 1x washing buffer was added and the samples were centrifuged with the stated parameters. Afterwards, the pellets were resuspended in 50 µl BrdU staining solution, which contained 1:50 anti BrdU fluorescence antibody in 1x washing buffer. The samples were incubated for 20 min at RT until 1 ml 1x washing buffer was added. The cells were pelleted again by centrifugation with the stated settings, followed by resuspension of the cells in 20 µl 7-AAD. Furthermore, 200 µl staining buffer was added per sample. The samples were kept on ice until measurement via flow cytometry was performed. An unstained control as well as samples solely stained with either 7-AAD or BrdU staining solution were used for compensation. Analyses of the data were performed with FlowJo™ software. After gating for the cell population in a SSC to FSC plot, included cells were gated corresponding their staining for unstained NSC/NPCs, BrdU- or 7-AAD-stained NSC/NPCs and double-stained NSC/NPCs.

2.2.7.3 ROS detection with the DHE/DCF assay

Dihydroethidium (DHE) and CM-H2DCFDA (DCF) from Invitrogen™ were used for ROS measurements. After collecting the supernatant from the cells in polypropylene round-bottom tubes, the cells were washed and taken up in DPBS and also collected. Trypsin-EDTA was used to detach the cells from the dish, followed by Trypsin-EDTA inactivation by adding Soybean Trypsin Inhibitor in an 1:1 molar relationship. The cells were pelleted by centrifugation at 1000 rpm for 5 min at RT followed by the resuspension of the pellets in 500 µl medium supplemented with 10 µM DHE or DCF. The unstained control was solely resuspended in 500 µl medium. The cells were incubated for 20 min at 37°C, until adding 4 ml DPBS. The cells were centrifuged again with the above-mentioned settings and the pellet resuspended in 1 ml DPBS. The samples were stored in the dark at 4°C until the flow cytometry measurement was performed. Analyses of the data were performed using FlowJo™ software. Fluorescence was depicted in histograms.

2.2.8 Viability assay (MTT assay)

To determine the cytotoxic effects of several substances, an MTT assay from Sigma-Aldrich® was performed. The cells were seeded and treated in 96-well plates using triplets for each measurement. At the end of each treatment period, 1:10 [v/v] MTT agent (5 mg/ml in DPBS) was added for 1 h at 37°C. Afterwards, 1:1 [v/v] MTT solubilization solution was added directly into the wells. Following at least 2 h of mixing and incubating at RT, the OD was measured at 570 nm and 650 nm as a reference wavelength with the PARADIGM™ platereader. Values measured at the reference wavelength were substracted from values measured at 570 nm for each well. Additionally, the mean background value from empty, coated wells was substracted. Mean values for treated NSC/NPCs were normalized to the mean values of untreated NSC/NPCs and depicted in concentration-dependency curves.

2.2.9 Kinase inhibitor screening

First, cell numbers for sub-confluently grown monolayer cultures were determined for each culture by seeding dilution series in triplets in 384-well plates as follows. The wells were coated for 30 min at 37°C with 10 µl of 1:250 laminin diluted in stem cell medium

calculated to an endvolume of 30 µl. After the 30 minutes, 20 µl of the dilution series were added to each well followed by an incubation for 72 h at 37°C. After these 72 h the cell density in each well was assessed by light microscopy and the number of cells for each cell line which resulted in subconfluency was identified. For the next step, the determined cell numbers were seeded on laminin-coated white 384-well plates and incubated with a dilution series of 4-OHT in triplets. After 72 h of 4-OHT treatment, the CellTiter-Glo® Luminescent Cell Viability assay from Promega was performed according to the manufacturer's protocol. The IC_{50} of 4-OHT for each cell line was determined.

Tab. 2.16: Kinase inhibitor library of the Department of Pediatric Oncology, Hematology and Clinical Immunology

Kinase inhibitor library		
(-)-Terreic acid	GW 843682X	Ro 31-8220 mesylate
1,2,3,4,5,6-Hexabromocyclohexane	H 89 dihydrochloride	Ryuvidine
10-DEBC hydrochloride	HA 1100 hydrochloride	SB 202190
1-Naphthyl PP1	IKK 16	SB 203580 hydrochloride
AG 490	IMD 0354	SB 216763
Aminopurvalanol A	Iressa	SB 218078
API-2	Ki 8751	SB 239063
Arctigenin	KU 55933	SB 415286
Arcyriaflavin A	LFM-A13	SB 431542
BI 78D3	LY 294002 hydrochloride	SC 514
BIBX 1382 dihydrochloride	LY 364947	SD 208
BIO	ML 9 hydrochloride	SL 327
CGK 733	NH 125	SP 600125
CGP 53353	NSC 693868	Staurosporine
CGP 57380	NU 7026	SU 4312
Compound 401	Olomoucine	SU 5416
D 4476	PD 198306	TBB
EO 1428	PD 407824	TCS 359
ER 27319 maleate	PD 98059	TPCA-1
Fasudil hydrochloride	PHA 665752	U0126
FPA 124	PI 828	Y-27632 dihydrochloride
Genistein	PP 1	ZM 306416 hydrochloride
GF 109203X	PP 2	ZM 323881 hydrochloride
GSK 650394	PQ 401	ZM 336372
GW 441756	Purvalanol A	ZM 39923 hydrochloride
GW 5074	Purvalanol B	ZM 447439
GW 583340 dihydrochloride	Ro 08-2750	ZM 449829

The kinase inhibitor screen was performed at the Department of Pediatric Oncology, Hematology and Clinical Immunology in collaboration with David Pauck. The determined cell numbers in a solution with 1:250 [v/v] laminin were directly seeded into 384-well plates with imprinted kinase inhibitors **(Tab. 2.16)** in single wells of eleven concentrations ranging from 0.0043 -25 µM with and without the IC_{50} of 4-OHT, respectively. After 72 h, the CellTiter-Glo® Luminescent Cell Viability assay from Promega was performed according to the manufacturer's protocol. The data for NSC/NPCs treated with or without the respective IC_{50} of 4-OHT and with different concentrations of each kinase inhibitor were normalized to the data of the respective solvent control. For comparison, concentration-dependency curves were modeled and overlayed for each kinase inhibitor using a non-linear regression (Four Parameter Logistic Regression). Interesting candidates were selected according to consistent and distinct effects on the modulation of the curves for each kinase inhibitor by 4-OHT in all three tested NSC/NPC cultures.

2.2.10 Caspase-Glo® 3/7 assay

For measuring the activity of the effector caspases 3 and 7, the Caspase-Glo® 3/7 Assay from Promega was used. The reconstituted Caspase-Glo® 3/7 reagent was given to the cells in a 1:1 ratio [v/v]. After 1 h of incubation at RT in the dark, the luminescence was measured for 1000 ms using the PARADIGM™ plate reader. For each condition, triplets were measured. The mean background luminescence of empty coated wells was substracted for each well. As the NSC/NPCs were highly sensitive to treatment and cell death could not be excluded, luminescence values were normalized to the actual number of cells per well as assessed by an MTT assay. The MTT assay was performed as described in **2.2.8**. Resulting data of treated NSC/NPCs were combined to mean values and normalized to the mean value of untreated cells.

2.2.11 Proteome profiling

The proteome analyses were performed in collaboration with Dr. Nina Overbeck at the Molecular Proteomics Laboratory (MPL) of the BMFZ as a part of her PhD studies ('Charakterisierung der Isocitrat-Dehydrogenase 1 im Zusammenhang der Tumorgenese von Gliomen mithilfe der Proteomanalyse'). Mass spectrometry was performed with a high performance liquid chromatography (HPLC)-coupled quadrupole-orbitrap mass

spectrometer (Thermo Scientific™). Therefore, the complex samples were separated in a chromatography gradient for 2 h, before they were ionized and transferred to the mass spectrometer. Proteome Discoverer™ software (Thermo Scientific™) was used for the identification of proteins and peptides. The proteomic data analysis software Progenesis® QI (Nonlinear Dynamics) was used for quantifications. Signal intensities for detected peptides and proteins were normalized to the total intensity.

3.0 RESULTS

The present thesis employs NSC/NPCs derived from conditional knock-in mice to study functional and molecular effects of Idh1 mutation. NSC/NPCs expressing a 4-OHT-responsive Cre recombinase were treated with 4-OHT to induce the Cre recombinase-mediated recombination between two *loxP* sites, resulting in the expression of mutant Idh1.

3.1 Validation of the conditional knock-in mouse model

After isolation and culturing of the NSC/NPCs the following workflow was designed **(Fig. 3.1)**.

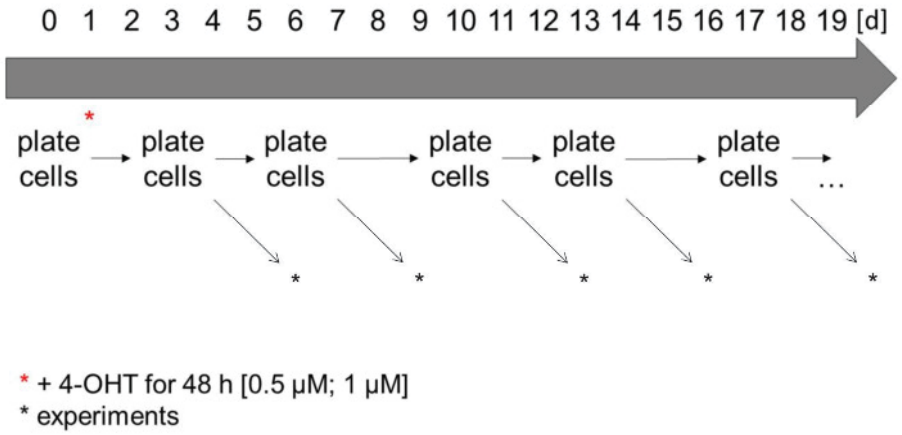

Fig. 3.1: Workflow for NSC/NPC culturing
Idh1$^{wt/wt}$ *Cre*$^{-/-}$, *Idh1*$^{wt/wt}$ *Cre*$^{-/+}$, *Idh1*$^{wt/LSL}$ *Cre*$^{-/-}$ and *Idh1*$^{wt/LSL}$ *Cre*$^{-/+}$ NSC/NPCs were cultured in 10 cm dishes for 24 h. The cells were treated with 0.5 µM or 1 µM 4-OHT for 48 h, passaged and seeded for experiments afterwards twice a week. The experiments were performed 72 h after seeding.

The NSC/NPCs of all four genotypes (*Idh1*$^{wt/wt}$ *Cre*$^{-/-}$, *Idh1*$^{wt/wt}$ *Cre*$^{-/+}$, *Idh1*$^{wt/LSL}$ *Cre*$^{-/-}$ and *Idh1*$^{wt/LSL}$ *Cre*$^{-/+}$) were incubated with 4-OHT. In *Cre*$^{-/+}$ cell lines, 4-OHT treatment results in the activation of Cre recombinase, followed by the knock-in of mutant *Idh1* in *Idh1*$^{wt/LSL}$ *Cre*$^{-/+}$ NSC/NPCs. *Idh1*$^{wt/wt}$ *Cre*$^{-/-}$, *Idh1*$^{wt/wt}$ *Cre*$^{-/+}$ and *Idh1*$^{wt/LSL}$ *Cre*$^{-/-}$ served as controls. The cells were treated with 0.5 µM 4-OHT once for 48 h. The recombination was supposed to be present afterwards. However, since the experiments showed no differences comparing the NSC/NPCs of the different genotypes, it was necessary to confirm the recombination.

3.1.1 Expression of recombinant DNA decreases over time after 4-OHT treatment

For validation of Cre recombinase-mediated recombination after 4-OHT treatment in *Idh1*$^{wt/LSL}$ *Cre*$^{-/+}$ NSC/NPCs DNA sequences specific for wildtype *Idh1* (*wt Idh1*), mutant *Idh1 (mut Idh1)* and the non-recombinant mutant *Idh1* (*LSL mut Idh1*) were amplified by PCR. The PCR products were visualized by agarose gel electrophoresis **(Fig. 3.2)**. Pellets for the isolation of genomic DNA were collected 3 d, 6 d, 10 d and 13 d after 4-OHT treatment and processed as described in **2.2.2**. *Idh1*$^{wt/LSL}$ *Cre*$^{-/-}$ NSC/NPCs served as a control.

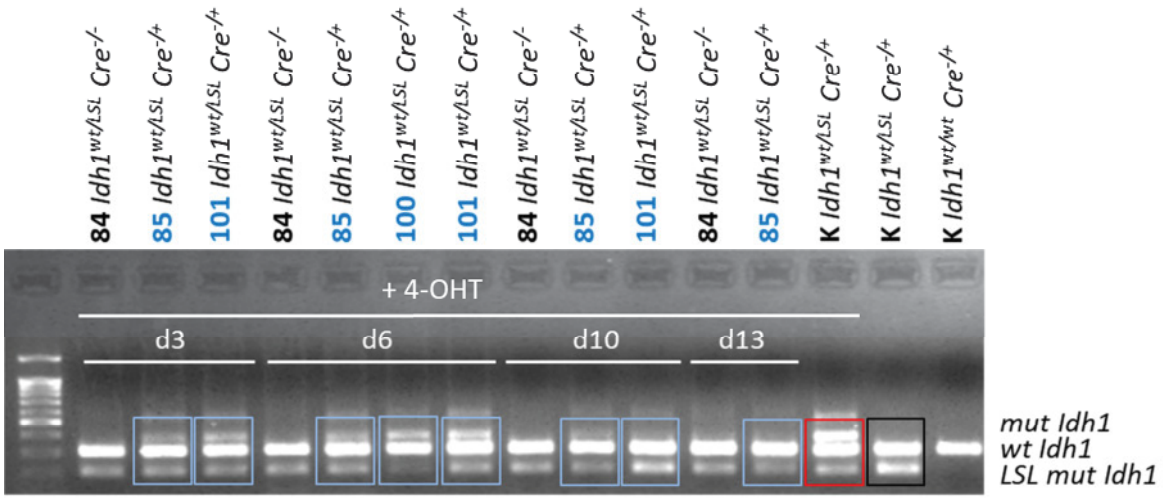

Fig. 3.2: Validation of Cre recombinase-mediated recombination
Idh1$^{wt/LSL}$ *Cre*$^{-/-}$ and *Idh1*$^{wt/LSL}$ *Cre*$^{-/+}$ NSC/NPCs were cultured in 10 cm dishes with 1,000,000 cells per dish for 24 h. Afterwards, the cells were treated with 0.5 µM of 4-OHT. 3 d, 6 d, 10 d and 13 d after 4-OHT treatment, samples were collected and genomic DNA was isolated. Sequences of the wildtype *Idh1* allele *(wt Idh1)*, the non-recombinant LSL mutant *Idh1* allele *(LSL mut Idh1)*, as well as the knock-in mutant *Idh1* allele *(mut Idh1)* were amplified by a PCR reaction and visualized by electrophoresis. Blue boxes indicate results for *Idh1*$^{wt/LSL}$ *Cre*$^{-/+}$ NSC/NPCs, the red box marks the positive control for recombination and the black box marks the amplified DNA of untreated *Idh1*$^{wt/LSL}$ *Cre*$^{-/+}$ NSC/NPCs. *Idh1*$^{wt/LSL}$ *Cre*$^{-/-}$ NSC/NPCs were used as control.

For 4-OHT-treated *Idh1*$^{wt/LSL}$ *Cre*$^{-/-}$ NSC/NPCs no recombinant mutant *Idh1* allele was detected due to the lack of Cre recombinase. The PCR amplification only detected wildtype *Idh1* and non-recombinant LSL mutant *Idh1* alleles at any time point after 4-OHT treatment **(Fig. 3.2)**. In contrast, the recombinant mutant *Idh1* allele was detected in *Idh1*$^{wt/LSL}$ *Cre*$^{-/+}$ NSC/NPCs after 4-OHT treatment. However, the recombination efficiency did not reach 100 % as LSL mutant *Idh1* alleles were still detectable after 4-OHT treatment. Furthermore, recombinant alleles showed a time-dependent decrease after

Cre-mediated recombination, with virtually no detection of recombinant mutant *Idh1* at 13 d after 4-OHT treatment **(Fig. 3.2)**.

3.1.2 Concentrations of the oncometabolite 2-HG decrease over time after 4-OHT treatment

To prove the abundance of functional active mutant Idh1 in 4-OHT-treated *Idh1*$^{wt/LSL}$ *Cre*$^{-/+}$ NSC/NPCs, the product of the mutant Idh1 enzyme – the oncometabolite 2-HG – was evaluated by mass spectrometry **(Fig. 3.3)**. The samples for mass spectrometry were collected 6 d, 9 d, 12 d and 15 d after activation of Cre recombinase and were processed as described in **2.2.6**. Besides *Idh1*$^{wt/LSL}$ *Cre*$^{-/+}$ NSC/NPCs, also *Idh1*$^{wt/wt}$ *Cre*$^{-/-}$ and *Idh1*$^{wt/LSL}$ *Cre*$^{-/-}$ NSC/NPCs were treated with 4-OHT and served as controls.

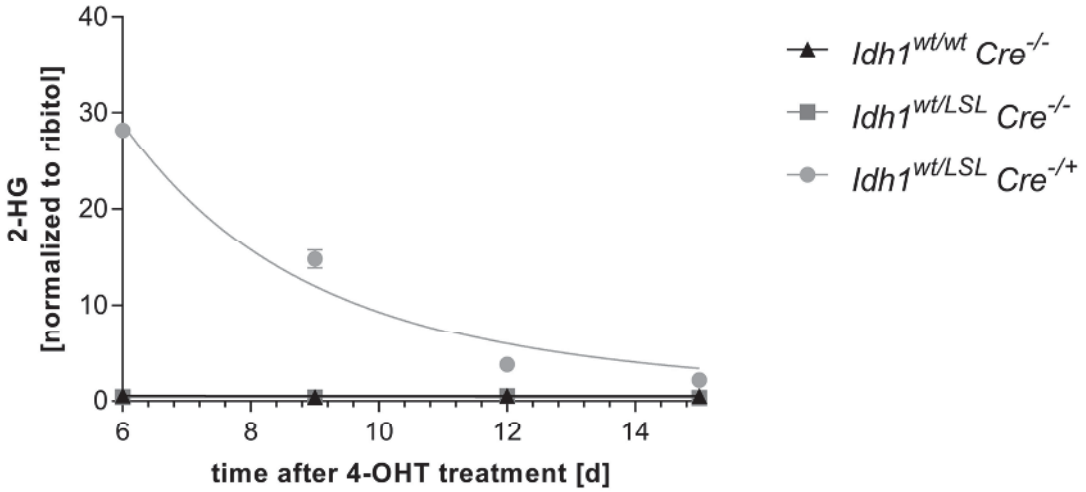

Fig. 3.3: Validation of mutant Idh1 activity by measuring the metabolite levels of 2-HG
Idh1$^{wt/wt}$ *Cre*$^{-/-}$, *Idh1*$^{wt/LSL}$ *Cre*$^{-/-}$ and *Idh1*$^{wt/LSL}$ *Cre*$^{-/+}$ NSC/NPCs were cultured in 10 cm dishes with 1,000,000 cells per dish for 24 h. Afterwards, cells were treated with 0.5 µM 4-OHT for 48 h. After 6 d, 9 d, 12 d and 15 d of treatment, samples were collected and mass spectrometry was performed. The results are based on data of one cell culture per genotype. Metabolite levels are normalized to the reference metabolite ribitol.

In *Idh1*$^{wt/wt}$ *Cre*$^{-/-}$ or *Idh1*$^{wt/LSL}$ *Cre*$^{-/-}$ NSC/NPCs, low levels of the oncometabolite 2-HG were detected after 4-OHT treatment at any time point. In contrast, *Idh1*$^{wt/LSL}$ *Cre*$^{-/+}$ NSC/NPCs showed about 55-fold higher 2-HG metabolite levels 6 d after 4-OHT treatment. The loss of recombinant DNA over time **(Fig. 3.2)** was accompanied by decreasing levels of 2-HG. After 15 d of 4-OHT treatment, the 2-HG metabolite levels in *Idh1*$^{wt/LSL}$ *Cre*$^{-/+}$ NSC/NPCs were nearly reduced to the metabolite levels of the control NSC/NPCs.

3.2 The effect of 4-OHT on NSC/NPCs

Since the recombinant gene and consequently also the metabolite levels of 2-HG vanished in *Idh1*$^{wt/LSL}$ *Cre*$^{-/+}$ NSC/NPCs after several days of Cre recombinase-activation by 4-OHT, the following experiments were performed for time periods of not longer than 72 h following 4-OHT treatment **(Fig. 3.4)**.

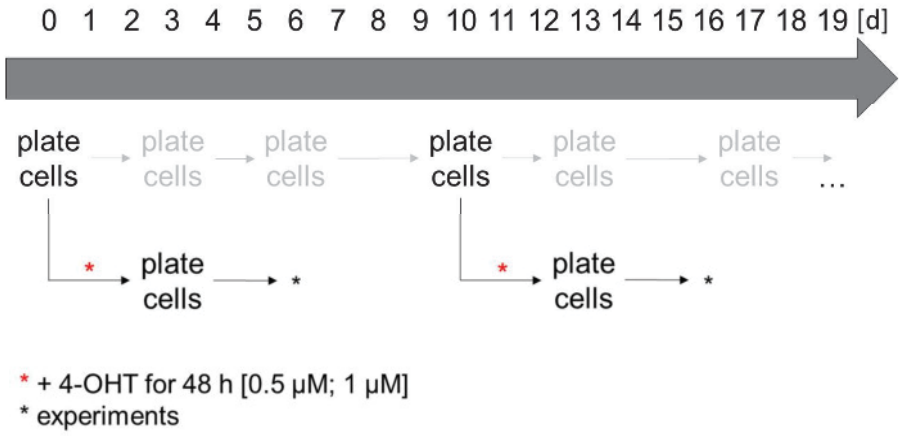

Fig. 3.4: Adapted workflow for NSC/NPC culturing
Idh1$^{wt/wt}$ *Cre*$^{-/-}$, *Idh1*$^{wt/wt}$ *Cre*$^{-/+}$, *Idh1*$^{wt/LSL}$ *Cre*$^{-/-}$ and *Idh1*$^{wt/LSL}$ *Cre*$^{-/+}$ NSC/NPCs were cultured in 10 cm dishes for 24 h. NSC/NPCs for experiments were seeded into additional 10 cm dishes for 4-OHT treatment with 0.5 µM or 1 µM 4-OHT for 48 h. After passaging, the cells were seeded for experiments once. The experiments were performed at 72 h after seeding and 4-OHT treatment.

4-OHT treatment resulted in reduced cell numbers compared to untreated NSC/NPCs. To elucidate, whether 4-OHT exerts a cytotoxic effect on NSC/NPCs while excluding possible effects of the *Idh1* mutation or the Cre recombinase, *Idh1*$^{wt/wt}$ *Cre*$^{-/-}$ NSC/NPCs were incubated with 4-OHT for 24 h for the following experiments. Biological replicates were used to exclude cell culture-specific effects.

3.2.1 4-OHT mediates ER-independent cytotoxic effects on NSC/NPCs

A potential cytotoxic effect of 4-OHT on *Idh1*$^{wt/wt}$ *Cre*$^{-/-}$ NSC/NPCs was elucidated by MTT assays that were performed as described in **2.2.9 (Fig. 3.5)**. Three independent cultures of *Idh1*$^{wt/wt}$ *Cre*$^{-/-}$ NSC/NPCs were used.

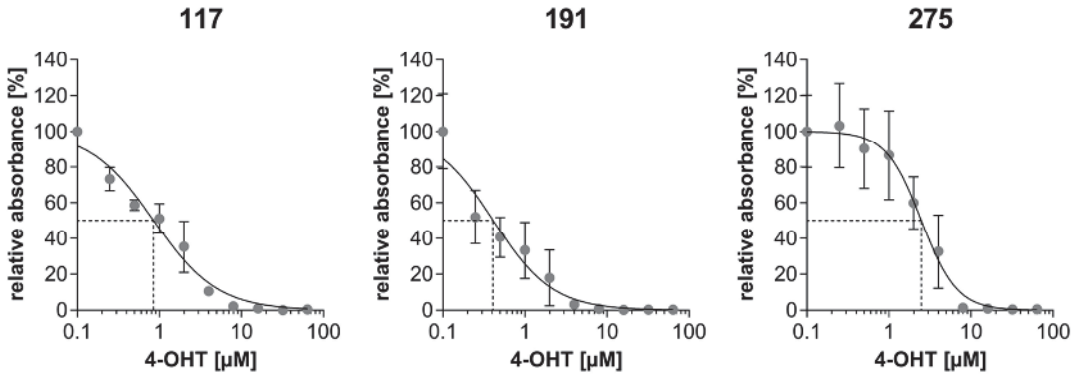

Fig. 3.5: Cytotoxicity of 4-OHT on NSC/NPCs
Idh1$^{wt/wt}$ *Cre*$^{-/-}$ NSC/NPCs were cultured in 96-well plates with 10,000 cells per well for 24 h. The cells were treated with 4-OHT for additional 24 h before the MTT assay was performed. The $OD_{570\text{-}650\ nm}$ was measured. Results are composed of three technical replicates from three independent cultures (117, 191, 275). The values were normalized to the solvent control (x = 0.1). The graphs show a nonlinear fit of the data, with mean values ± SEM being indicated for each concentration.

4-OHT treatment of *Idh1*$^{wt/wt}$ *Cre*$^{-/-}$ NSC/NPCs resulted in strongly reduced cell numbers after 24 h of treatment compared to the solvent control in all tested cultures. The viability was reduced to 50 % by concentrations of 0.9 µM 4-OHT for NSC/NPC 117 cells, 0.4 µM 4-OHT for NSC/NPC 191 cells and 2.5 µM 4-OHT for NSC/NPC 275 cells. Commonly used 4-OHT concentrations for the Cre recombinase activation in LSL systems ranging between 0.5 µM to 1 µM, reduced the cell numbers to around 90 % in the least sensitive NSC/NPC culture (275) and to around 35 % in the most sensitive NSC/NPC culture (191). Depending on the individual culture, even the lowest tested concentration of 0.25 µM 4-OHT resulted in diminished cell numbers to 73 % (117) and 52 % (191). The treatment with 8 µM 4-OHT for 24 h reduced the viability to less than 5 % compared to the solvent control in all three tested NSC/NPC cultures.

4-OHT is a known SERM with either antagonistic or agonistic effects at estrogen receptors[373,453]. As the co-incubation of tamoxifen and the endogenous ER ligand 17-β-estradiol (β-ES) reduced the cytotoxicity of 4-OHT on CNS glial progenitor cells[454], a possible ER-mediated cytotoxic effect of 4-OHT on NSC/NPCs was elucidated. Therefore, three independent NSC/NPC cultures were co-incubated with several concentrations of 4-OHT and 1 µM β-ES **(Fig. 3.6)**. MTT assays were performed as described in **2.2.9**.

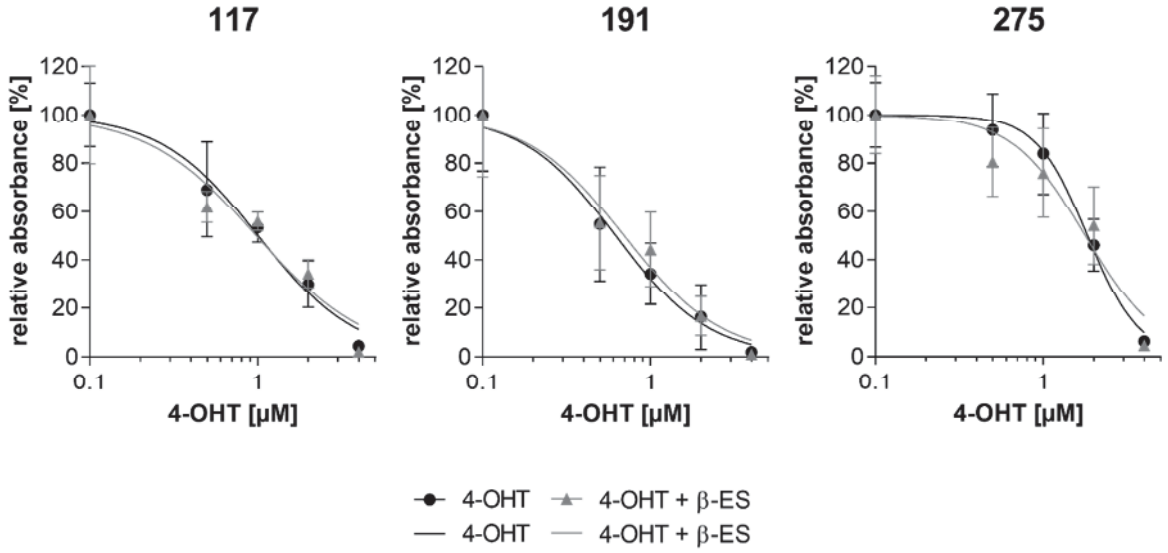

Fig. 3.6: Effect of β-ES on 4-OHT-mediated cytotoxicity on NSC/NPCs
Idh1$^{wt/wt}$ *Cre*$^{-/-}$ NSC/NPCs were cultured in 96-well-plates with 10,000 cells per well for 24 h. The cells were treated with 4-OHT and with and without 1 µM β-ES for additional 24 h before the MTT assay was performed. The $OD_{570\text{-}650\ nm}$ was measured. Results are composed of three technical replicates from each NSC/NPC culture (117, 191, 275). Data were normalized to the solvent control (x = 0.1). The graphs show a nonlinear fit of the transformed data with mean values ± SEM being indicated for each concentration.

The cytotoxic effect of 4-OHT on *Idh1*$^{wt/wt}$ *Cre*$^{-/-}$ NSC/NPCs was not affected by the co-incubation with 1 µM β-ES. Cell numbers of 4-OHT-treated NSC/NPCs were unaltered at any time point.

3.2.2 4-OHT induces autophagic cell death in NSC/NPCs

4-OHT was shown to induce autophagic cell death in glioma cell lines[409]. To answer the question whether 4-OHT treatment results in autophagic cell death in *Idh1*$^{wt/wt}$ *Cre*$^{-/-}$ NSC/NPCs, Western blot analyses **(2.2.5)** of the autophagy marker LC3II were performed **(Fig. 3.7 A, B)**.

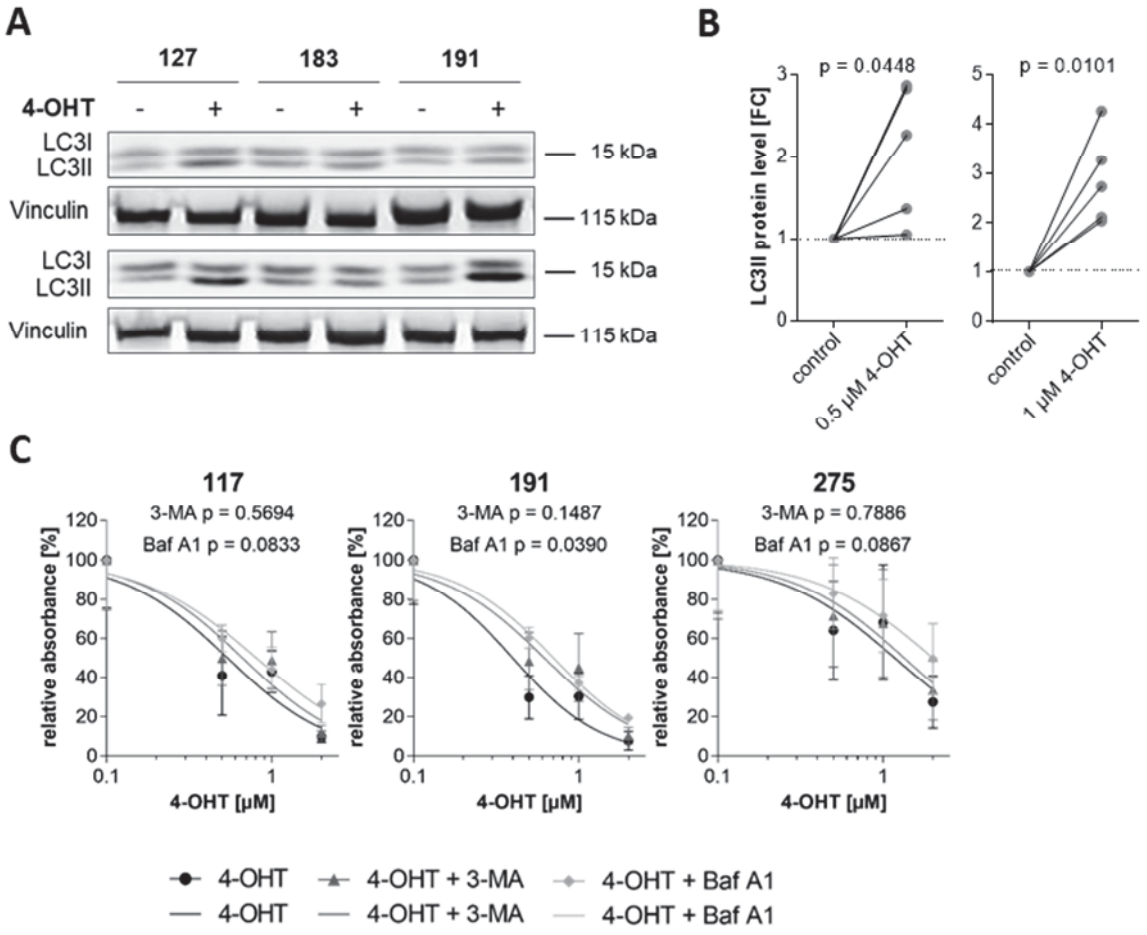

Fig. 3.7: Autophagy in 4-OHT-treated NSC/NPCs

(A, B) Idh1$^{wt/wt}$ *Cre*$^{-/-}$ NSC/NPCs were cultured in 6 cm dishes with 150,000 cells per dish for 24 h. The cells were treated with 0.5 µM or 1 µM 4-OHT for 24 h. Proteins were isolated and used for Western blotting of LC3II. Vinculin was detected for normalization. Detected bands were analyzed densitometrically. The resulting values were normalized to the solvent control. **(A)** A representative blot is shown for three individual NSC/NPC cultures. **(B)** The data of the graphs are composed of one (126), two (127, 183, 191) or three (117) technical replicates from five independent NSC/NPC cultures. The mean values are indicated for each NSC/NPC culture. Significances were examined by paired two-tailed t-test analyses. **(C)** *Idh1*$^{wt/wt}$ *Cre*$^{-/-}$ NSC/NPCs were cultured on 96-well plates with 10,000 cells per well for 24 h. The cells were treated with 4-OHT in presence or absence of 1 mM 3-MA or 0.5 nM Bafilomycin A1 (Baf A1) for additional 24 h before the MTT assay was performed. The $OD_{570\text{-}650\ nm}$ was measured. Results are composed of three technical replicates from three independent NSC/NPC cultures (117, 191, 275). Data were normalized to solvent control (x = 0.1). The graphs show a nonlinear fit of the transformed data with mean values ± SEM being indicated for each condition. Significances between the concentration-dependency curves for different treatments were examined by Two-way ANOVA analyses of variance with Tukey's Multiple Comparison Test.

4-OHT treatment resulted in increased LC3II protein levels in NSC/NPCs after 24 h. The effect was concentration-dependent. LC3II protein levels were already significantly elevated after the treatment with 0.5 µM 4-OHT in nearly all NSC/NPC cultures compared

to the solvent control (p = 0.0448) showing up 1.4- to 2.9-fold higher protein levels. Only one culture showed 1.05-fold and thereby unaltered LC3II protein levels after 4-OHT treatment compared to the untreated controls. After the treatment with 1 µM 4-OHT, 2.0- to 4.3-fold increased protein levels were detected for LC3II (p = 0.0101).

To further investigate whether induced LC3II levels were accompanied by autophagic cell death, MTT assays with 4-OHT in co-incubation with two autophagy inhibitors were performed **(Fig. 3.7 C)**. Baf A1 inhibits vacuolar acidification and thereby autophagosome maturation and late autophagy[455]. 3-MA inhibits type III PI3K and thereby early autophagosome formation and autophagy[456].

The co-incubation with 1 mM 3-MA or 0.5 nM Baf A1 attenuated the cytotoxic effect of 4-OHT on *Idh1*$^{wt/wt}$ *Cre*$^{-/-}$ NSC/NPCs in all three tested cultures. While this effect was significant for the co-incubation of 4-OHT with Baf A1 in the 191 cells (p = 0.0390), the co-incubation of 4-OHT with 3-MA did not have any significant effect (p = 0.5694, p = 0.1487, p = 7886).

3.2.3 4-OHT induces apoptotic cell death in NSC/NPCs

4-OHT treatment was shown to induce apoptosis in glioma cell lines via PKC inhibition[457]. To elucidate, whether 4-OHT induces apoptosis in NSC/NPCs, an Annexin V / 7-AAD staining **(Fig. 3.8 A, B)** was performed according to **2.2.8.1**.

The treatment of NSC/NPCs with 0.5 µM 4-OHT reduced the percentage of living and therefore double negative cells from 58 % to 44 % in NSC/NPC 117 cells, from 45 % to 21 % in NSC/NPC 127 cells and from 26 % to 23 % in NSC/NPC 191 cells compared to the solvent controls (p = 0.3226, p = 0.8503, p > 0.9999). The treatment with 2 µM 4-OHT for 24 h provoked an even higher decrease in the number of double negative cells. This effect was significant for NSC/NPC 117 cells, where the treatment with 2 µM 4-OHT resulted in a reduction of double negative cells from 58 % to 28 % of all gated cells (p = 0.0019). For NSC/NPC 127 cells, the fraction of unstained cells decreased to 18 % (p = 0.5704) and for NSC/NPC 191 cells a reduction to 16 % of all gated cells was observed compared to the untreated control after the treatment of 2 µM 4-OHT (p > 0.9999). The fraction of NSC/NPCs merely stained with Annexin V increased after the treatment with 0.5 µM 4-OHT in 117 and 127 cells from 5 % to 12 % (p > 0.9999) and from 24 % to 29 % (p > 0.9999), respectively, but showed lower increases after the treatment with 2 µM 4-OHT to 17 % (p = 0.7199) and 24 % (p > 0.9999). For the

NSC/NPC 191 cells, the fraction of Annexin V-stained cells decreased for both concentrations of 4-OHT from 48 % to 34 % and 42 % of all gated cells ($p > 0.9999$, $p > 0.9999$). However, these effects were not significant. The percentage of 7-AAD-stained cells did not change after the treatment with 0.5 µM and 2 µM 4-OHT for NSC/NPC culture 117. For 127 cells, the fraction slightly decreased from 17 % to 14 % after the treatment with 0.5 µM 4-OHT, but increased to 27 % after the treatment with 2 µM 4-OHT ($p > 0.9999$). For NSC/NPC culture 191, the fraction of 7-AAD-stained cells slightly increased from 8 % to 9 % after the treatment with 0.5 µM 4-OHT and to 12 % after the treatment with 2 µM 4-OHT (both $p > 0.9999$). Cell fractions of NSC/NPCs stained for Annexin V and 7-AAD were increased in all three tested NSC/NPC cultures for both tested concentrations of 4-OHT. Double positive cells increased in percentage from 3 % to 12 % and 25 % for NSC/NPC 117 cells ($p > 0.9999$, $p = 0.0309$), from 15 % to 37 % and 32 % for NSC/NPC 127 cells (both $p > 0.9999$) and for NSC/NPC 191 cells, the fraction of double positive cells increased from 19 % to 36 % and 33 % after 4-OHT treatment ($p = 0.9641$, $p > 0.9999$).

To elucidate, whether the 4-OHT-induced cytotoxicity on *Idh1*$^{wt/wt}$ *Cre*$^{-/-}$ NSC/NPCs is at least in part mediated by apoptosis, additional MTT assays were performed for 4-OHT in co-incubation with two apoptosis inhibitors for 24 h **(Fig. 3.8 C)**. Therefore, the *pan*-caspase inhibitor Z-VAD-FMK and the caspase-3-inhibitor Z-DEVD-FMK were used.

Both apoptosis inhibitors reduced the cytotoxic effect of 4-OHT on *Idh1*$^{wt/wt}$ *Cre*$^{-/-}$ NSC/NPCs independently of the used concentration. However, these effects were not significant for the *pan*-caspase inhibitor Z-VAD-FMK ($p = 0.1302$, $p = 0.8718$, $p = 0.4005$). The rescuing effect of Z-DEVD-FMK on 4-OHT-mediated cytotoxicity was moreover not significant for the NSC/NPC 117 and 275 cells ($p = 0.0505$, $p = 0.0969$), however, a significant increase in viability was observed for NSC/NPC 191 cells after the co-incubation of 4-OHT and Z-DEVD-FMK compared to 4-OHT-treated cells ($p = 0.0207$).

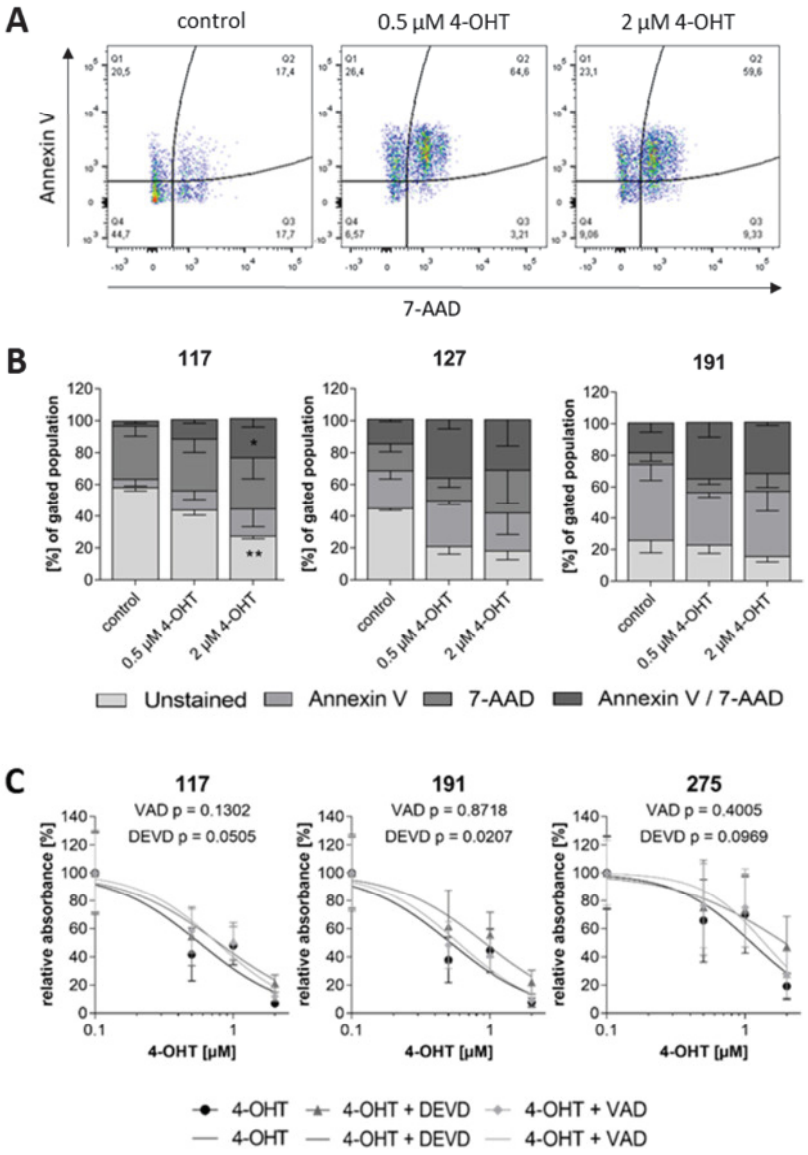

Fig. 3.8: Apoptosis in 4-OHT-treated NSC/NPCs

(A, B) *Idh1*$^{wt/wt}$ *Cre*$^{-/-}$ NSC/NPCs were cultured in 6-well plates with 500,000 cells per well for 24 h. The cells were treated with 0.5 µM or 2 µM 4-OHT for 24 h. Annexin V and 7-AAD staining was performed. **(A)** After SSC-FSC gating, the included cells were gated corresponding to their staining. A representative gating is shown for one individual NSC/NPC culture. **(B)** The results are composed of three technical replicates from three individual NSC/NPC cultures (117, 127, 191). The mean values and SEM are indicated for each NSC/NPC culture and each condition. Significances between the fractions of untreated and treated NSC/NPCs were examined by Two-way ANOVA analyses of variance with Bonferroni's Multiple Comparison Test (** p =0.0019, * p = 0.0309). **(C)** *Idh1*$^{wt/wt}$ *Cre*$^{-/-}$ NSC/NPCs were cultured on 96-well plates with 10,000 cells per well for 24 h. Afterwards the cells were treated with 4-OHT in the presence or absence of 50 µM Z-VAD-FMK (VAD) or 5 µM Z-DEVD-FMK (DEVD) for additional 24 h before MTT assay was performed. The $OD_{570\text{-}650\ nm}$ was measured. Results are composed of three technical replicates from each investigated NSC/NPC culture (117, 191, 275). Data were normalized to solvent control (x = 0.1). The graphs show a nonlinear fit of the transformed data with mean values ± SEM being indicated for each condition. Significances between the concentration-dependency curves for different treatments were examined by Two-way ANOVA analyses of variance with Tukey's Multiple Comparison Post-Test.

3.2.4 4-OHT treatment affects Jak2/Stat3 signaling in NSC/NPCs

In order to further investigate transcriptional changes associated with the cytotoxic effect of 4-OHT on NSC/NPCs, whole-transcript microarray analyses **(2.2.4.3)** were performed **(Fig. 3.9)**. Therefore, *Idh1*$^{wt/wt}$ *Cre*$^{-/-}$ NSC/NPCs of four independent NSC/NPC cultures were treated with 1 µM 4-OHT for 24 h, followed by RNA extraction and Affymetrix chip-based transcriptome profiling as described above **(2.2.4.3)**. The microarray analysis and data analyses were performed at the Genomics and Transcriptomics Core Facility of the BMFZ (head: Prof. Karl Köhrer) in collaboration with René Deenen.

Evaluation of the microarray data sets revealed transcriptome differences between each of the NSC/NPC cultures that were more pronounced as the effects of 4-OHT treatment, as indicated by the fact that 4-OHT-treated and untreated *Idh1*$^{wt/wt}$ *Cre*$^{-/-}$ NSC/NPCs of each culture clustered together, instead of all untreated cells vs all 4-OHT-treated cells. Overall, 2144 transcripts were significantly altered with $p \leq 0.05$ in all four tested NSC/NPC cultures after 4-OHT treatment. However, by further filtering the results for candidates with FC ± 1.5 and $p \leq 0.01$, *Socs2*, *Serpina3n* and *Heatr7a* were the only three transcripts found ($p = 0.0005$, $p = 0.0023$, $p = 0.0095$). The mRNA expression of the housekeeping genes *Actg1*, *Actb* and *Vcl* was unaffected by 4-OHT treatment. The upregulation of *Socs2*, *Serpina3n* and *Heatr7a* after 4-OHT treatment was validated by qRT-PCR in the same NSC/NPC cultures. The mRNA levels were upregulated 3.4-, 1.8-, 2.0- and 1.5-fold for *Socs2*. For *Serpina3n,* increased transcript levels of 2.3-, 1.3-, 2.1- and 1.8-fold were detected, and for *Heatr7a* 2.4-, 2.3-, 2.2- and 1.8-times higher transcript levels were observed after 4-OHT treatment compared to the solvent controls ($p = 0.0684$, $p = 0.0280$, $p = 0.0024$).

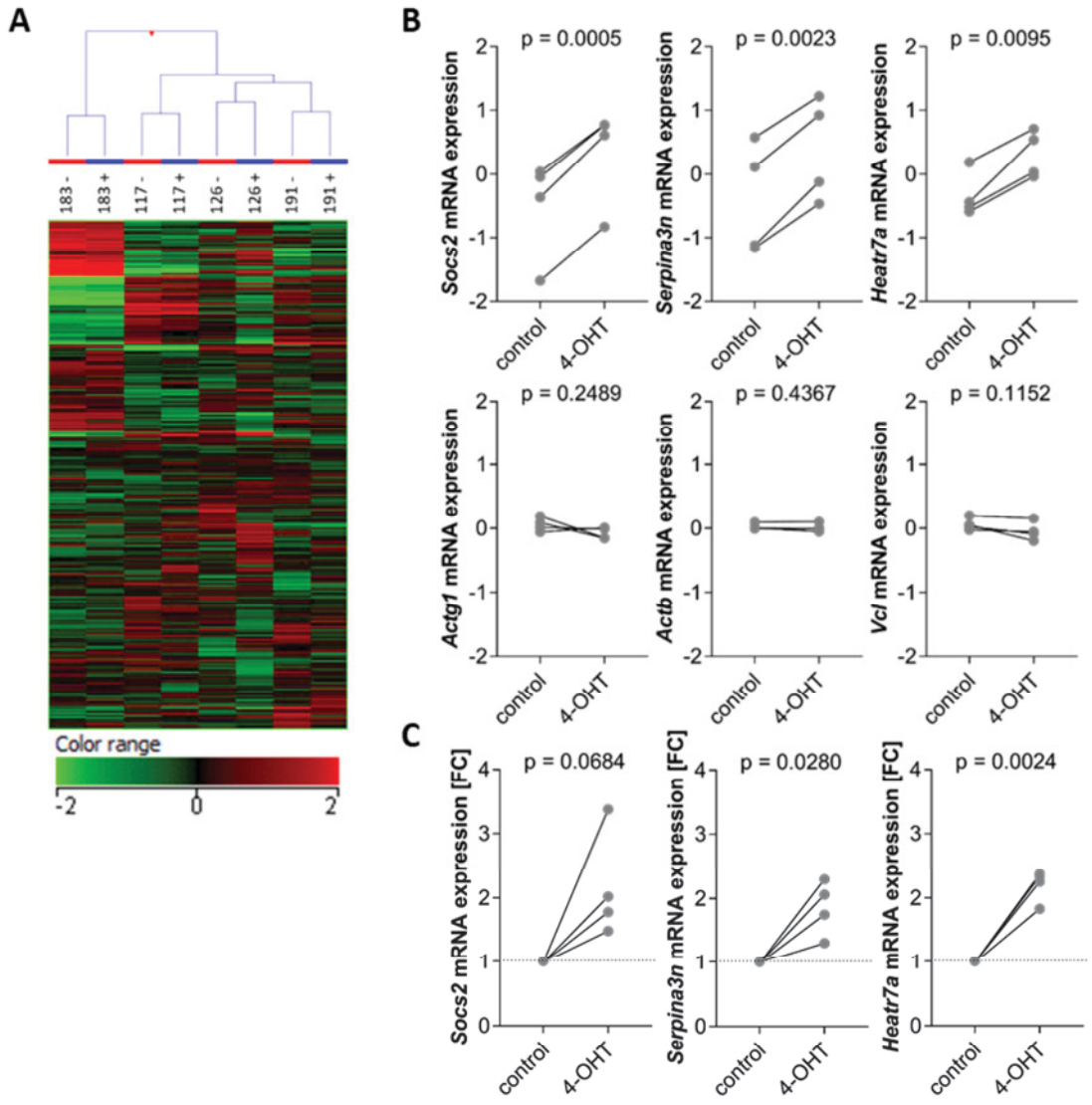

Fig. 3.9: Transcriptome analyses of 4-OHT-treated NSC/NPCs

Idh1$^{wt/wt}$ *Cre*$^{-/-}$ NSC/NPCs were cultured in 6 cm dishes with 500,000 cells per dish for 24 h. The cells were treated with 1 µM 4-OHT or solvent control for additional 24 h. Cells were harvested and RNA was isolated. Microarray analysis was performed with amplified biotin-labeled cDNA being hybridized to Affymetrix Mouse Gene 2.0 ST Gene Expression Microarrays for 16 h at 45°C. Four independent NSC/NPC cultures were tested (117, 126, 183, 191). **(A)** Transcript level heat map showing the results of unsupervised cluster analysis of transcripts found in the untreated and 4-OHT-treated *Idh1*$^{wt/wt}$ *Cre*$^{-/-}$ NSC/NPCs. **(B)** Significantly regulated candidate transcripts with a FC ≥ 1.5 and p ≤ 0.01 upon microarray analysis (paired two-tailed t-test). For comparison, transcript levels of selected housekeeping genes are shown (*Actg1*, *Actb*, *Vcl*). The graphs show the deviation from the mean signal intensity for the respective transcript. **(C)** Validation of selected microarray results by qRT-PCR. Results are composed of four individual NSC/NPC cultures. Values were normalized to solvent control. Significances between untreated and treated NSC/NPCs were examined by paired two-tailed t-test analyses.

Since available data on *Heatr7a* and *Serpina3n* are limited, *Socs2* and the affiliated signaling pathways were of interest for the following experiments. As Socs2 is involved in

Jak/Stat signaling pathways[458], the phosphorylation status of Stat3 in 4-OHT-treated *Idh1*$^{wt/wt}$ *Cre*$^{-/-}$ NSC/NPCs was checked by Western blotting **(2.2.5) (Fig. 3.10)**.

Stat3 protein levels were not altered after the treatment with 0.5 µM 4-OHT in NSC/NPCs ($p = 0.7886$) nor after the treatment with 1 µM 4-OHT ($p = 0.9811$). Phosphorylated Stat3 levels were not affected by treatment with 0.5 µM 4-OHT ($p > 0.9999$), while the treatment with 1 µM 4-OHT elevated the levels of phosphorylated Stat3 ($p = 0.1263$) by 1.2-fold on average.

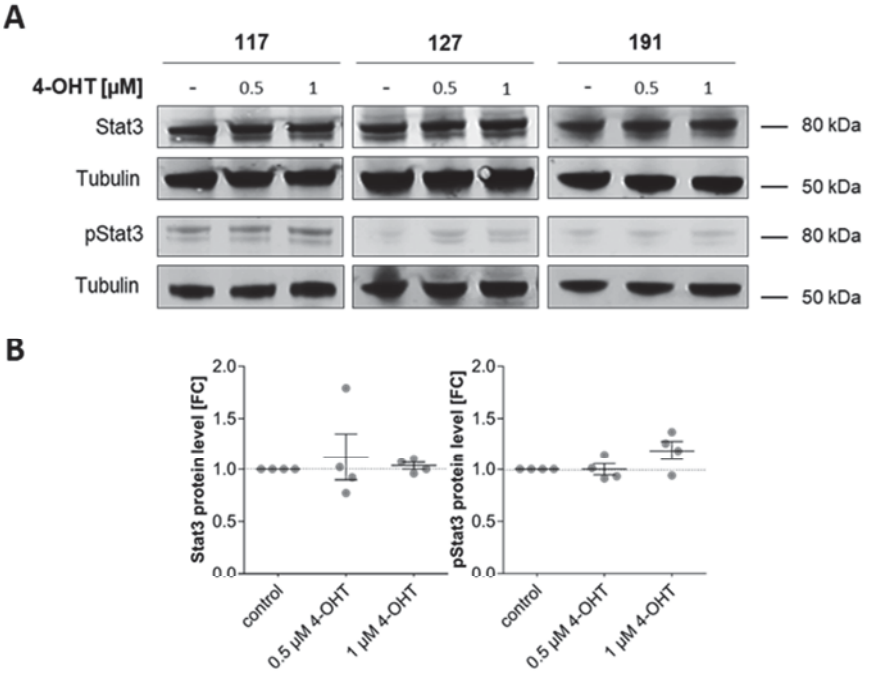

Fig 3.10: Phosphorylation of Stat3 in 4-OHT-treated NSC/NPCs

Idh1$^{wt/wt}$ *Cre*$^{-/-}$ NSC/NPCs were cultured in 6 cm dishes with 150,000 cells per dish for 24 h. The cells were treated with 0.5 µM or 1 µM 4-OHT for additional 24 h. Afterwards, proteins were isolated and used for Western blotting of Stat3 and phosphorylated Stat3 (pStat3). Values were normalized to the solvent control. Tubulin was detected for normalization. **(A)** Representative blots are shown for three individual NSC/NPC cultures. **(B)** Data of the graphs are composed of one (127, 183), two (191) and three (117) technical replicates from four different NSC/NPC cultures. Individual data points and mean values ± SEM are indicated. Significances between untreated and treated NSC/NPCs were examined by One-way ANOVA analyses of variance with Tukey's Multiple Comparison Test.

3.2.5 4-OHT-mediated cytotoxicity on NSC/NPCs is attenuated by Jak2 inhibition and amplified by IKK inhibition

4-OHT, the commonly used activation agent of CreERT recombinase, led to autophagic and apoptotic cell death of NSC/NPCs **(Fig. 3.5 – Fig. 3.8)**. However, microarray analysis failed to reveal unequivocal signaling pathways involved in 4-OHT-mediated cytotoxicity **(Fig. 3.9)**. To gain further information about interfering signaling pathways in 4-OHT-mediated cytotoxicity on NSC/NPCs and to determine potential inhibitors of the latter, an *in vitro* kinase inhibitor screen **(2.2.9)** was performed in co-operation with the group of Dr. Marc Remke at the Department of Pediatric Oncology, Hematology and Clinical Immunology **(Fig. 3.11 A, B)**. Therefore, 81 kinase inhibitors were printed into 384-well plates in random distribution at 12 different concentrations. In addition to these inhibitors, half of the plates were also printed with the IC_{50} of 4-OHT for the tested cell lines, respectively. $Idh1^{wt/wt}$ $Cre^{-/-}$ NSC/NPCs were plated into the wells according to previously determined cell numbers **(2.2.9)**. After 72 h, a CellTiter-Glo® assay from Promega was performed. The results of the single-agent-treated NSC/NPCs (kinase inhibitor only) were compared to the corresponding NSC/NPCs treated with both kinase inhibitor and 4-OHT regarding the potential modulation of the effect of each kinase inhibitor by 4-OHT. Kinase inhibitors whose cytotoxic effect was altered by 4-OHT, were *vice versa* tested with respect to their effect on 4-OHT-mediated cytotoxicity in MTT assays **(Fig. 3.11 C)**.

The cytotoxic effect of two kinase inhibitors was modulated consistently in all three tested NSC/NPC cultures by 4-OHT treatment. The cytotoxic effect of AG 490 was decreased by 4-OHT treatment in all three tested NSC/NPC cultures. The IC_{50} for AG490 increased from 1668 nM to 2457 nM in the 117 cells. For the 183 and 191 cells, the IC_{50} increased by the co-incubation of AG490 and 4-OHT from 925 nM to 10029 nM and from 333.8 nM to 4360 nM. In co-incubation with IKK 16, 4-OHT amplified the cytotoxic effect in all tested NSC/NPC cultures. Measured IC_{50} values for IKK 16 decreased from 688.3 nM to 159 nM in the cell line 117, from 1652 nM to 391.7 nM in 183 cells and from 1726 nM to 128.7 nM in 191 cells after 4-OHT treatment.

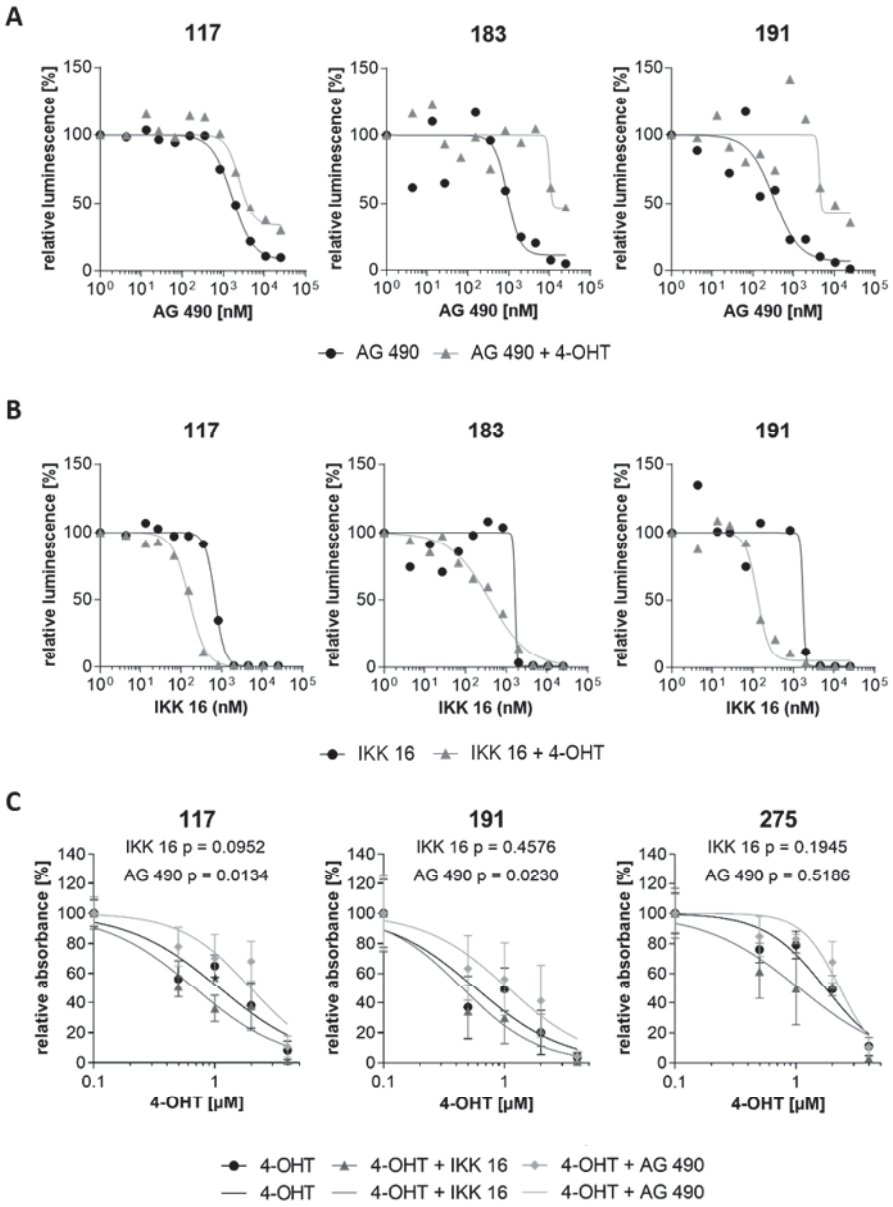

Fig. 3.11: Effects of AG 490 and IKK 16 on 4-OHT-mediated cytotoxicity

(A, B) *Idh1*$^{wt/wt}$ *Cre*$^{-/-}$ NSC/NPCs were cultured in preprinted 384-well plates. Eleven different concentrations of 81 kinase inhibitors (0.0043 - 25 µM) were tested. CellTiter-Glo® assay was performed after 72 h. The luminescence was measured for 1000 ms. Individual data points are shown for three NSC/NPC cultures (117, 183, 191). Values were normalized to the solvent control ($x = 10^0$). **(A)** The graphs show the transformed data of the kinase inhibitor AG 490 in the presence and absence of additional 4-OHT treatment. **(B)** The graphs show the transformed data of the kinase inhibitor IKK 16 in presence or absence of additional 4-OHT treatment. **(C)** *Idh1*$^{wt/wt}$ *Cre*$^{-/-}$ NSC/NPCs were cultured in 96-well plates with 10,000 cells per well for 24 h. The cells were treated 4-OHT in presence or absence of 1 µM AG 490 or 0.2 µM IKK 16 for additional 24 h before MTT assay was performed. The $OD_{570\text{-}650\ nm}$ was measured. Results are composed of three technical replicates from three individual NSC/NPC cultures (117, 191, 275). Values were normalized to the corresponding 4-OHT-untreated controls ($x = 0.1$). The graphs show a nonlinear fit of the transformed data with mean values ± SEM being indicated for each NSC/NPC culture and each condition. Significances between the concentration-dependency curves for different treatments were examined by Two-way ANOVA analyses of variance with Tukey's Post-Test.

The attenuating effect of 4-OHT on AG 490-mediated cytotoxicity as well as the amplifying effect of 4-OHT on IKK 16-mediated cytotoxicity were *vice versa* validated in MTT assays **(Fig. 3.11 C)**. In each NSC/NPC culture, the co-incubation of 4-OHT and AG 490 resulted in a diminished cytotoxicity at all tested concentrations of 4-OHT in relation to AG 490 treatment alone. This effect was significant for the 117 and 191 NSC/NPCs ($p = 0.0134$, $p = 0.0230$). In the less sensitive 275 cells, the AG 490-mediated decrease of the 4-OHT-mediated cytotoxic effect was not significant ($p = 0.5186$). The co-incubation of 4-OHT and IKK 16 led in all three tested cultures of *Idh1*$^{wt/wt}$ *Cre*$^{-/-}$ NSC/NPCs to an increased cytotoxic effect at all used concentrations of 4-OHT in relation to treatment with IKK 16 alone. However, this effect was not statistically significant in any of the three NSC/NPC cultures ($p = 0.0952$, $p = 0.4576$, $p = 0.1945$).

AG 490 is an inhibitor of Egfr, Jak2 and Jak3[459-461]. IKK 16 is a selective inhibitor of IKK and thereby an inhibitor of NF-κB signaling[462]. Since AG 490 attenuated the cytotoxic effect of 4-OHT significantly in two cell lines, its effect on the protein levels of lipidated LC3 as well as of Socs2 and the phosphorylation status of Stat3 was investigated after the co-incubation of 0.5 µM 4-OHT and 1 µM AG 490 for 24 h **(Fig. 3.12)**.

4-OHT treatment led to 2.2-fold (NSC/NPC 117 cells), 1.6-fold (NSC/NPC 183 cells) and 1.4-fold (NSC/NPC 275 cells) increased LC3II protein levels ($p = 0.2474$). After the co-incubation of 4-OHT and AG 490 even higher protein levels of lipidated LC3 were detected. LC3II protein levels were 2.7-fold (NSC/NPC 117 cells), 2.6-fold (NSC/NPC 183 cells) and 1.5-fold (NSC/NPC 275 cells) higher than in the untreated cells. This effect was significant ($p = 0.0243$). The co-incubation with AG 490 resulted in an on average 1.3-fold increase of LC3II protein levels compared to LC3II protein levels in NSC/NPCs solely treated with 4-OHT ($p = 0.3961$).

Socs2 protein levels were increased 1.7-fold and 1.8-fold in the NSC/NPC 117 and 183 cells after 4-OHT treatment. However, unaltered protein levels were detected for NSC/NPC 275 cells ($p = 0.1614$). In the 117 cells, Socs2 protein levels rose 1.3-fold after the co-incubation of 4-OHT and AG490 compared to the controls and for 183 cells, Socs2 protein levels were decreased to 0.8-fold. For NSC/NPC 275 cells, an increase of Socs2 protein levels was observed after the co-incubation of 4-OHT and AG 490. Socs2 protein levels were 1.3-fold elevated ($p = 0.9651$). The co-incubation of 4-OHT with AG 490 attenuated the increase of Socs2 in two NSC/NPC cultures. Compared to the 4-OHT-treated NSC/NPCs, Socs2 protein levels were attenuated to 0.8- and 0.4-fold in 117 and 183 cells after the co-incubation of 4-OHT and AG 490, whereas Socs2 protein levels increased by 1.3-fold in 275 cells ($p = 0.2983$).

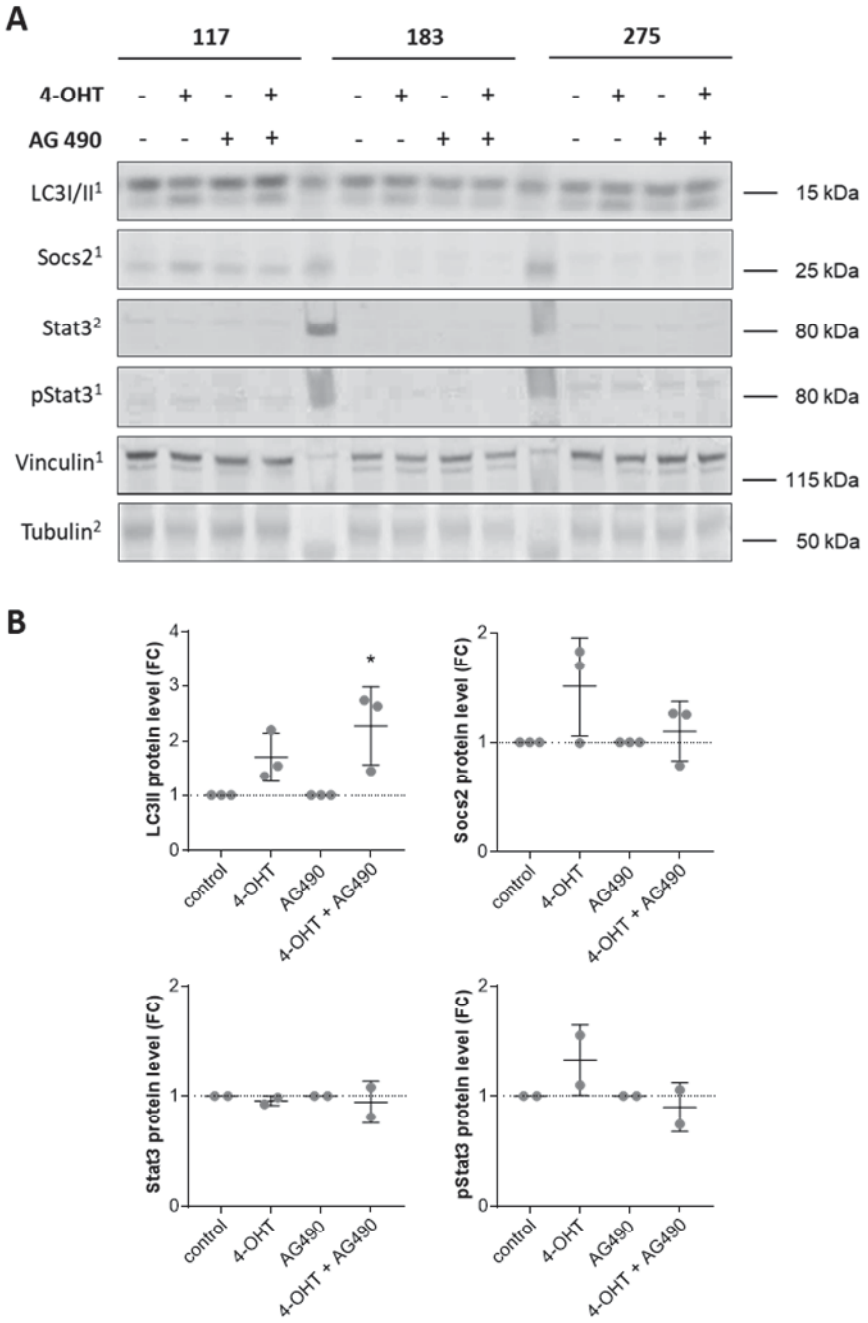

Fig. 3.12: Modulation of 4-OHT-mediated effects by AG 490

Idh1$^{wt/wt}$ *Cre*$^{-/-}$ NSC/NPCs were cultured in 6 cm dishes with 500,000 cells per dish for 24 h. The cells were treated with 0.5 µM 4-OHT in presence or absence of 1 µM AG 490 for additional 24 h. Then, Proteins were isolated and used for Western blotting of Stat3 and phosphorylated Stat3 (pStat3) as well as for LC3 and Socs2. Values were normalized to the solvent control. Tubulin or vinculin were detected for normalization. **(A)** Representative blots are shown for three individual NSC/NPC cultures (117, 183, 275). **(B)** Data of the graphs are composed of one to three technical replicates from two (Stat3, pStat3) or three (LC3, Socs2) tested NSC/NPC cultures and represented as mean values ± SEM. Significances between untreated and treated NSC/NPCs were examined by One-way ANOVA analyses of variance with Tukey's Post-Test (* p = 0.0243).

Total Stat3 protein levels were unaltered upon 4-OHT treatment in NSC/NPC 117 cells, whereas a slight decrease was detected in NSC/NPC 275 cells with Stat3 protein levels of 0.9-fold compared to the untreated control (p = 0.9668). The co-incubation of 4-OHT and AG 490 resulted in 1.1-fold increased Stat3 protein levels in NSC/NPC 117 cells and to slightly decreased Stat3 protein levels to 0.8-fold in NSC/NPC 275 cells (p = 0.9315). The co-incubation did not result in a significant change of Stat3 protein expression compared to 4-OHT-treated NSC/NPCs (p = 0.9989). For phosphorylated Stat3, 1.1-fold (NSC/NPC 117 cells) and 1.6-fold (NSC/NPC 275 cells) increased protein levels were detected after 4-OHT treatment (p = 0.4418). The co-incubation of 4-OHT and AG 490 resulted in 1.1-fold (NSC/NPC 117 cells) increased and 0.8 fold (NSC/NPC 275 cells) decreased pStat3 protein levels compared to the protein levels in the controls (p = 0.9469). Thus, the co-incubation did not alter pStat3 levels in the 117 cells and led to an attenuated increase of phosphorylated Stat3 in the 275 cells compared to the protein levels in 4-OHT-treated NSC/NPCs (p = 0.2662).

3.2.6 4-OHT-treated NSC/NPCs arrest in G0/G1- and in G2/M-phase

The Stat3 signaling pathway is involved in cell cycle regulation by modulating the transcription of genes like *Cdkn2b*, *Cdkn2d* and *Ccnd1*[463,464]. BrdU assays **(2.2.7.2)** were performed after 4-OHT treatment for 24 h in NSC/NPCs **(Fig. 3.13)**.

4-OHT-treated NSC/NPCs showed an increased fraction of cells in the G0/G1-phase as well as in the G2/M-phase. This was consistent in all three tested NSC/NPC lines. In the untreated controls, most of the cells were in the S-phase of the cell cycle with 68 %, 70 % and 58 % of all gated cells (NSC/NPCs 117, 127, 183). After 4-OHT treatment, the percentage of cells in the S-phase decreased to 29 % in NSC/NPC 117 cells (p = 0.0758), to 42 % in 127 cells and to 35 % in 183 cells (p = 0.0435). In contrast, the fraction of cells found in the G0/G1-phase increased after 4-OHT treatment from 29 % to 54 % in 117 cells (p = 0.1698), from 27 % to 46 % in 127 cells and from 40 % to 59 % in 183 cells (p = 0.0636). Also in the G2/M-phase of the cell cycle an increased fraction of cells was detected after 4-OHT treatment. For the NSC/NPC line 117, cell numbers in G2/M-phase rose from 4 % to 17 % (p = 0.4935), for 127 cells an increase from 3 % to 12 % was detected, and in the 183 NSC/NPC line, 6 % of the gated cells were found in the G2/M-phase compared to 2 % for the untreated cells (p = 0.8463).

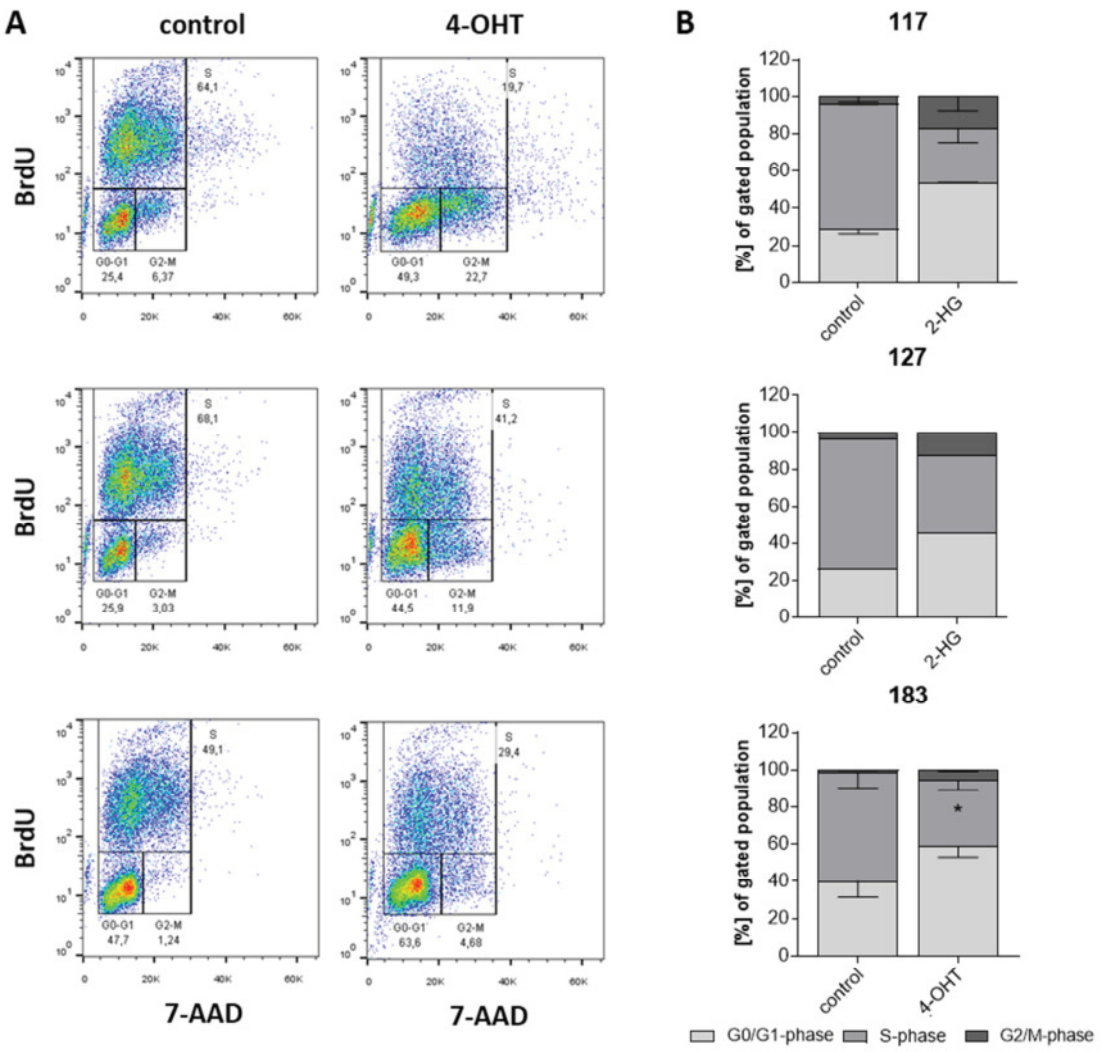

Fig. 3.13: Cell cycle distribution of 4-OHT-treated NSC/NPCs

Idh1$^{wt/wt}$ *Cre*$^{-/-}$ NSC/NPCs were cultured in 6-well plates with 500,000 cells per well for 24 h. The cells were treated with 0.5 µM 4-OHT for additional 24 h and incubated with BrdU 4 h prior proceeding. The BrdU Flow Kit from BD Pharmingen™ was used. Antibodies against incorporated BrdU as well as total DNA-binding 7-AAD were detected by flow cytometry. **(A)** Representative figure of gated cells in G0/G1-, S- or G2/M-phase of the cell cycle is shown for three independent NSC/NPC cultures (top to bottom: 117, 127, 183; left: control, right: 4-OHT-treated). **(B)** The results of the graphs are composed of one (127) to two (117, 183) technical replicates from three NSC/NPC cultures. Mean fractions and SEM of the individual NSC/NPC cultures in different cell cycle phases are shown. Significances in cell cycle distribution between untreated and treated NSC/NPCs were examined by Two-way ANOVA analyses with Bonferroni's Multiple Comparison Test (* p = 0.0435).

3.3 Characterization of *Idh1*-mutant NSC/NPCs using a conditional knock-in model

4-OHT treatment for the activation of Cre recombinase led to significantly reduced cell numbers **(Fig. 3.5)** and the recombination was neither stable nor efficient in all NSC/NPCs **(Fig. 3.2, Fig. 3.3)**. Furthermore, NSC/NPCs from different animals showed marked interindividual differences that might impair detection of potential effects during the 4-OHT treatment **(Fig. 3.9)**. Therefore, the use of the conditional knock-in model was limited. Nevertheless, screening experiments were performed for detecting Idh1 mutation-mediated effects. For this approach, 4-OHT-treated *Idh1*$^{wt/LSL}$ *Cre*$^{-/+}$ NSC/NPCs were compared to controls consisting of 4-OHT-treated *Idh1*$^{wt/wt}$ *Cre*$^{-/-}$, *Idh1*$^{wt/wt}$ *Cre*$^{-/+}$ and *Idh1*$^{wt/LSL}$ *Cre*$^{-/-}$ NSC/NPCs.

3.3.1 Mutant Idh1 induces Hmox1 expression in NSC/NPCs

For the characterization of altered expression profiles in *Idh1*-mutant compared to *Idh1*-wildtype NSC/NPCs, RNA sequencing was performed **(Fig. 3.14)**. Therefore, NSC/NPCs of different genotypes were treated with 0.5 µM 4-OHT for 48 h. After additional 72 h, RNA was extracted and subjected to RNA sequencing at the Department for Pedriatic Oncology, Hematology and Clinical Immunology in cooperation with the group of Dr. Marc Remke.

All *Idh1*$^{wt/LSL}$ *Cre*$^{-/+}$ NSC/NPCs RNA expression profiles clustered together, while for NSC/NPCs of the other three genotypes, i.e. *Idh1*$^{wt/wt}$ *Cre*$^{-/-}$, *Idh1*$^{wt/wt}$ *Cre*$^{-/+}$ and *Idh1*$^{wt/LSL}$ *Cre*$^{-/-}$, no genotype-specific profiles were detectable. The Venn diagram reflects the heterogeneity of the RNA profile among the genotypes (**Fig. 3.14 B).** As there was no conclusive clustering perceivable, the control groups were combined and analyzed against *Idh1*$^{wt/LSL}$ *Cre*$^{-/+}$ NSC/NPCs. Besides 17,983 commonly expressed genes, more than 2,000 genes were exclusively expressed in *Idh1*$^{wt/LSL}$ *Cre*$^{-/+}$ NSC/NPCs. Around 200 exclusively transcribed genes characterized the control group. The exclusively expressed genes in *Idh1*$^{wt/LSL}$ *Cre*$^{-/+}$ NSC/NPCs or control NSC/NPCs were compared to a proteomic data set (experiments performed by Dr. Nina Overbeck at the MPL of the BMFZ Düsseldorf) consisting of data from *Idh1*$^{wt/LSL}$ *Cre*$^{-/-}$ NSC/NPCs and *Idh1*$^{wt/LSL}$ *Cre*$^{-/+}$ NSC/NPCs. None of the proteins encoded by the genes showing exclusive expression in

the controls or in *Idh1*$^{wt/LSL}$ *Cre*$^{-/+}$ NSC/NPCs by RNA sequencing, demonstrated altered expression when compared to *Idh1*$^{wt/LSL}$ *Cre*$^{-/-}$ NSC/NPCs in the proteomic data sets.

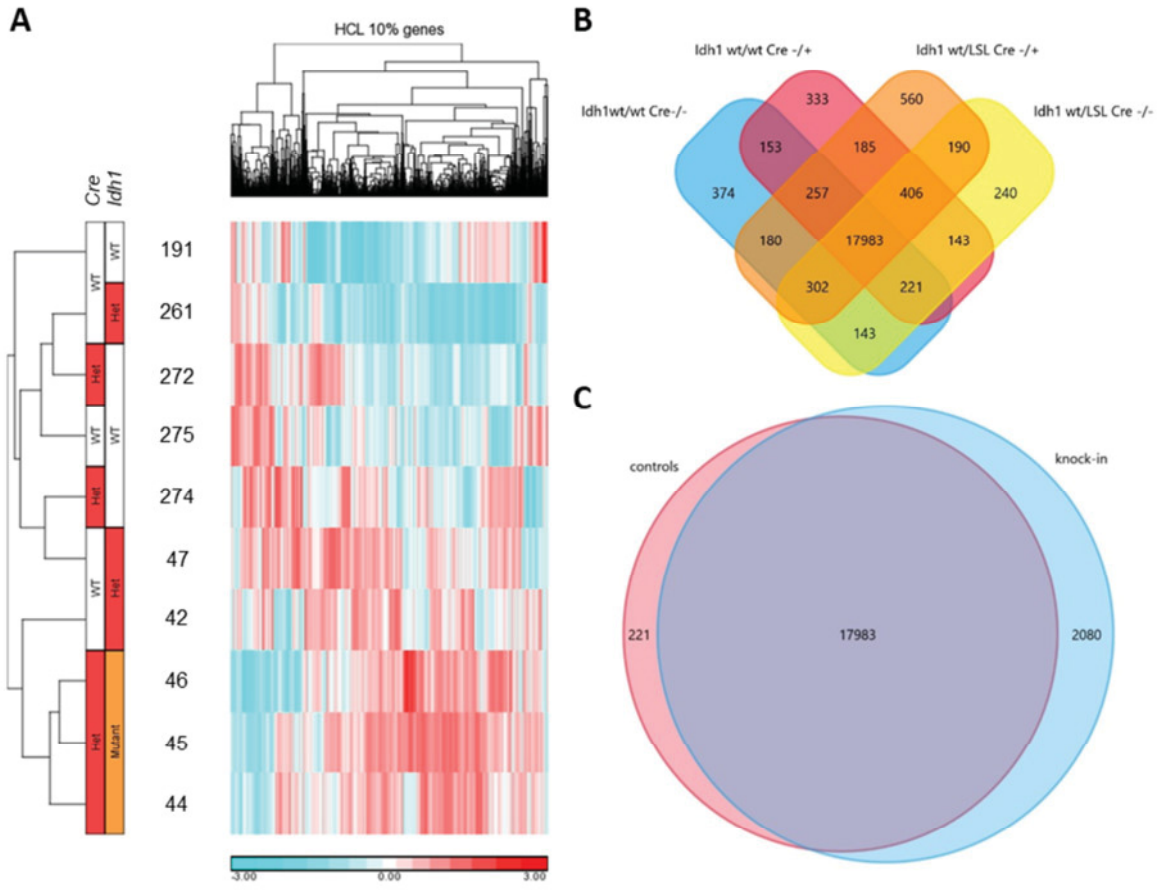

Fig. 3.14: Differentially expressed RNA in *Idh1*$^{wt/LSL}$ *Cre*$^{-/+}$ NSC/NPCs vs control NSC/NPCs
Idh1$^{wt/wt}$ *Cre*$^{-/-}$, *Idh1*$^{wt/wt}$ *Cre*$^{-/+}$, *Idh1*$^{wt/LSL}$ *Cre*$^{-/-}$ and *Idh1*$^{wt/LSL}$ *Cre*$^{-/+}$ NSC/NPCs were cultured in 6 cm dishes with 500,000 cells per dish for 24 h. The cells were treated with 0.5 µM 4-OHT for additional 48 h, before cells were harvested and RNA was isolated. RNA sequencing was performed. NSC/NPC cultures from two distinct mice each were tested among the *Idh1*$^{wt/wt}$ *Cre*$^{-/-}$ and *Idh1*$^{wt/wt}$ *Cre*$^{-/+}$ NSC/NPCs (191, 275; 272, 274). Three distinct NSC/NPC cultures each were tested among the *Idh1*$^{wt/LSL}$ *Cre*$^{-/-}$ and *Idh1*$^{wt/LSL}$ *Cre*$^{-/+}$ NSC/NPCs (42, 47, 261; 44, 45, 46). Significant differences were examined by paired two-tailed t-test analyses. **(A)** Heat map showing results of unsupervised cluster analysis of 4-OHT-treated NSC/NPCs. **(B)** Venn diagram of expressed genes found in the individual NSC/NPC cultures of the different genotypes. Genes not detectable in each cell culture of a given genotype were excluded. **(C)** Venn diagram of expressed genes found in all control NSC/NPCs against expressed genes found in *Idh1*$^{wt/LSL}$ *Cre*$^{-/+}$ NSC/NPCs (Wt: wildtype, Het: heterozygous).

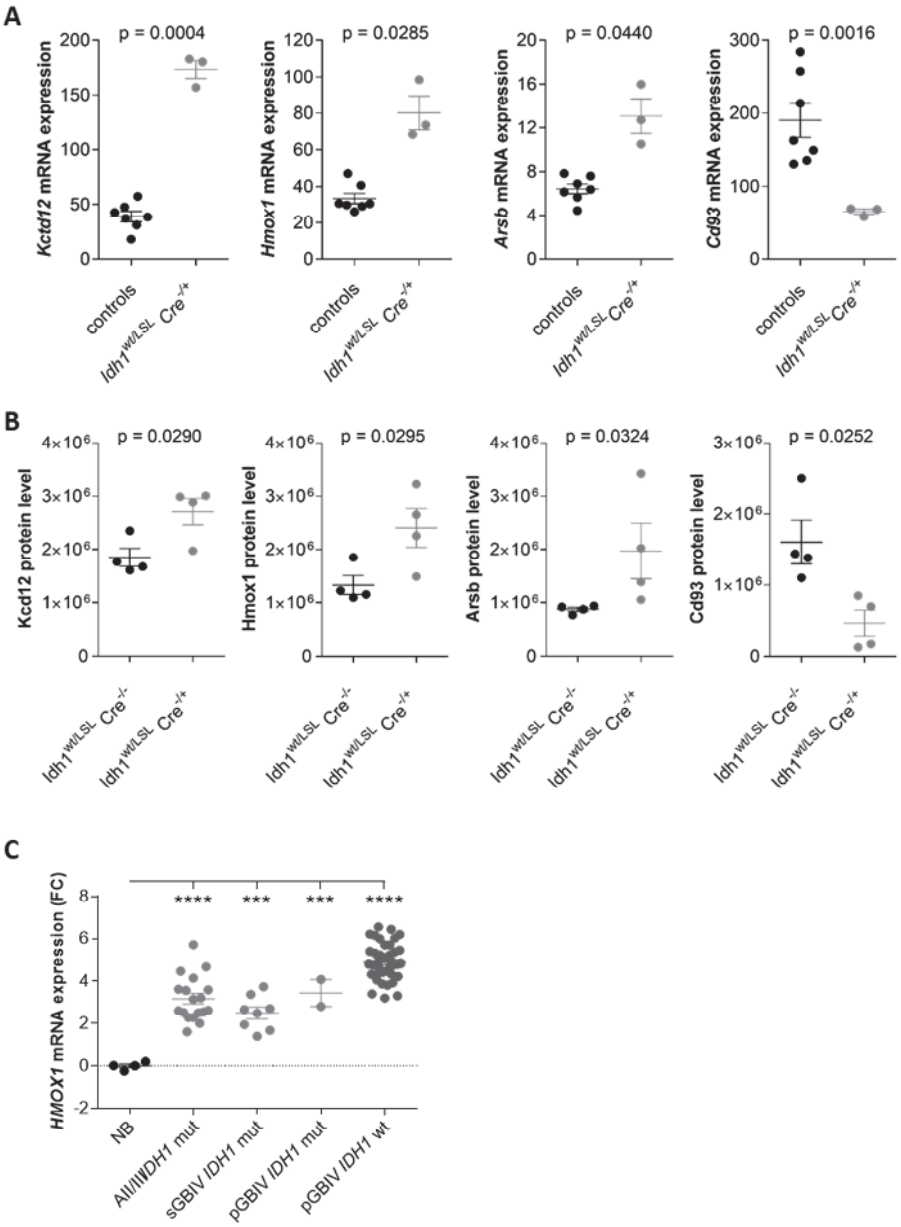

Fig. 3.15: Idh1 mutation-dependent alterations at the RNA and protein levels

(A) The mRNA expression data were obtained as described in **Fig.3.14 A**. The graphs show significantly up- or downregulated transcript levels in *Idh1*-mutant NSC/NPCs. Individual data points and mean values ± SEM are indicated for the controls or *Idh1*-mutant NSC/NPCs. Significances were determined by paired two-tailed t-test analyses. **(B)** The protein expression data were obtained from Dr. Nina Overbeck (MPL, BMFZ). HPLC-coupled mass spectrometry was performed. For this purpose, *Idh1*$^{wt/LSL}$ *Cre*$^{-/-}$ and *Idh1*$^{wt/LSL}$ *Cre*$^{-/+}$ NSC/NPCs were cultured in 10 cm dishes with 1,000,000 cells per dish for 24 h. After the treatment with 1 µM 4-OHT for additional 48 h, the cells were replated. After 72 h, the medium was changed for 24 h, and the cells were prepared for the proteome analysis. Relative intensities were measured. The graphs show significantly altered protein levels in *Idh1*$^{wt/LSL}$ *Cre*$^{-/+}$ NSC/NPCs compared to *Idh1*$^{wt/LSL}$ *Cre*$^{-/-}$ NSC/NPCs with individual data points and mean values ± SEM being indicated for the NSC/NPC cultures of the respective genotypes. Significant differences were examined by the proteomic data analysis software Progenesis® QI, which uses ANOVA for statistical testing. **(C)** The graph shows results obtained by microarray analysis of different types of IDH-mutant or IDH-wildtype astrocytic

gliomas as reported by Toedt and colleagues[465] with individual data points and mean values ± SEM being indicated for the different entities. Significant differences between normal brain (NB) and tumors were examined by One-way ANOVA analysis of variance with Tukey's Post Test (*** $p \leq 0.001$, **** $p \leq 0.0001$). (AII/III: diffuse and anaplastic astrocytomas, WHO grade II and III, s/pGBIV: secondary/primary glioblastomas, WHO grade IV).

Hence, the RNA sequencing data were re-analyzed. From the 17,983 commonly expressed genes, all significantly overexpressed (FC ≥ 2, $p \leq 0.05$) or repressed (FC ≤ 0.5, $p \leq 0.05$) transcripts in *Idh1*$^{wt/LSL}$ *Cre*$^{-/+}$ NSC/NPCs were filtered out (unpaired two-tailed t-test with Welch's correction). In *Idh1*$^{wt/LSL}$ *Cre*$^{-/+}$ NSC/NPCs, 482 genes were significantly upregulated compared to the controls, while 287 genes were significantly downregulated. Significantly up- or downregulated candidates were again compared to the proteomic data sets **(Fig. 3.15)**. With Kctd12, Hmox1, Arsb and Cd93, four candidates were consistently and significantly altered at the RNA and protein levels in *Idh1*$^{wt/LSL}$ *Cre*$^{-/+}$ NSC/NPCs. The increase of *Kctd12* RNA expression levels was 4.5-fold compared to the controls ($p = 0.0004$). *Hmox1* was 2.4-fold overexpressed and the *Arsb* RNA expression levels were elevated 2-fold compared to the controls ($p = 0.0285$, $p = 0.0440$). *Cd93* expression was 2.9-fold downregulated in *Idh1*$^{wt/LSL}$ *Cre*$^{-/+}$ NSC/NPCs compared to the controls ($p = 0.0016$). At the protein level, Kctd12 was induced 1.5-fold, Hmox1 was induced 1.8-fold and Arsb was upregulated 2.3-fold ($p = 0.0290$, $p = 0.0295$, $p = 0.0324$). Cd93 protein level increased 3.5-fold in *Idh1*$^{wt/LSL}$ *Cre*$^{-/+}$ NSC/NPCs compared to *Idh1*$^{wt/LSL}$ *Cre*$^{-/-}$ NSC/NPCs ($p = 0.0252$). Analyzing the data of a microarray-based analysis of IDH-mutant astrocytomas and IDH-wildtype and -mutant glioblastomas generated by Toedt and colleagues[465], a significantly elevated *HMOX1* mRNA expression was found for IDH-mutant astrocytomas (**** $p \leq 0.0001$), IDH-mutant glioblastomas (*** $p \leq 0.001$), as well as IDH-wildtype glioblastomas (**** $p \leq 0.0001$) (**Fig. 3.15 C**).

3.3.2 Idh1-mutant NSC/NPCs show increased 2-HG and decreased glycolate metabolite levels

Since Idh1 is a metabolic enzyme and the production of 2-HG is accompanied by the consumption of NADPH and α-KG[23,52], changes within the metabolism of *Idh1*$^{wt/LSL}$ *Cre*$^{-/+}$ NSC/NPCs are to be expected. To investigate the influence of the Idh1 mutation on NSC/NPCs metabolism, metabolome profiling was performed **(Fig. 3.16)**. Therefore, NSC/NPCs of different genotypes were treated with 4-OHT for 48 h. Samples were then prepared according to **(2.2.6)** and subjected to metabolome measurements via mass

spectrometry performed in collaboration with Dr. Tabea Mettler-Altmann, Institute of Plant Biochemistry, Heinrich-Heine-University Düsseldorf

A significant increase of 2-HG metabolite levels was observed in the *Idh1*-mutant knock-in NSC/NPCs ($p = 0.0032$) **(Fig. 3.16 A)**. The three tested cell cultures of *Idh1*$^{wt/LSL}$ *Cre*$^{-/+}$ NSC/NPCs differed markedly concerning 2-HG metabolite levels with fold changes of 15.3, 62.9 and 29.8 compared to the mean metabolite levels of 2-HG in the controls. Amino acid levels were mostly unaltered comparing *Idh1*$^{wt/LSL}$ *Cre*$^{-/+}$ NSC/NPCs with the controls **(Fig. 3.16 B)**. For most amino acids, highly variable metabolite levels were measured throughout the comparing groups. The mean metabolite levels were nearly unaltered for β-alanine, glycine, isoleucine, leucine, serine, threonine, tyrosine and valine ($p \geq 0.6473$). For aspartate a slightly increased mean metabolite level was detected ($p = 0.2423$). Glutamate mean metabolite level was slightly decreased ($p = 0.4376$). However, for both metabolites marked differences were observed among the metabolite levels in the different *Idh1*$^{wt/LSL}$ *Cre*$^{-/+}$ NSC/NPCs. More consistent data were observed for α-alanine and proline metabolite levels, which were decreased in the *Idh1*$^{wt/LSL}$ *Cre*$^{-/+}$ NSC/NPCs compared to the controls with p-values of 0.1294 and 0.1796, respectively. Mean metabolite levels for methionine and phenylalanine were elevated in the *Idh1*$^{wt/LSL}$ *Cre*$^{-/+}$ NSC/NPCs compared to the controls ($p = 0.0534$, $p = 0.1865$). Unfortunately, glutamine levels were not detectable by the performed mass spectrometry. Also for most metabolites of the TCA cycle no data were available. For (iso)citrate and malate slightly decreased metabolite levels were observed ($p = 0.4282$, $p = 0.6774$) in the *Idh1*-mutant knock-in NSC/NPCs, however, marked differences were detected for the metabolite levels among the several knock-in NSC/NPC cultures **(Fig. 3.16 C)**. Metabolites branching from or into glycolysis were in general rather decreased in *Idh1*$^{wt/LSL}$ *Cre*$^{-/+}$ NSC/NPCs compared to the controls **(Fig. 3.16 C)**. Glycerol metabolite levels were unaltered ($p = 0.6965$), whereas fructose, glucose, myoinositol and sucrose mean metabolite levels were slightly decreased in *Idh1*$^{wt/LSL}$ *Cre*$^{-/+}$ NSC/NPCs compared to the controls ($p = 0.0971 - p = 0.4684$). Changes in glycolate, lactate and sorbitol metabolite levels were more consistent among the *Idh1*$^{wt/LSL}$ *Cre*$^{-/+}$ NSC/NPCs. Lactate and sorbitol mean metabolite levels were decreased with p-values of 0.1270 and 0.2090 in the knock-in NSC/NPCs compared to the controls. The mean metabolite level of glycolate was significantly decreased in *Idh1*$^{wt/LSL}$ *Cre*$^{-/+}$ NSC/NPCs compared to the controls ($p = 0.0182$).

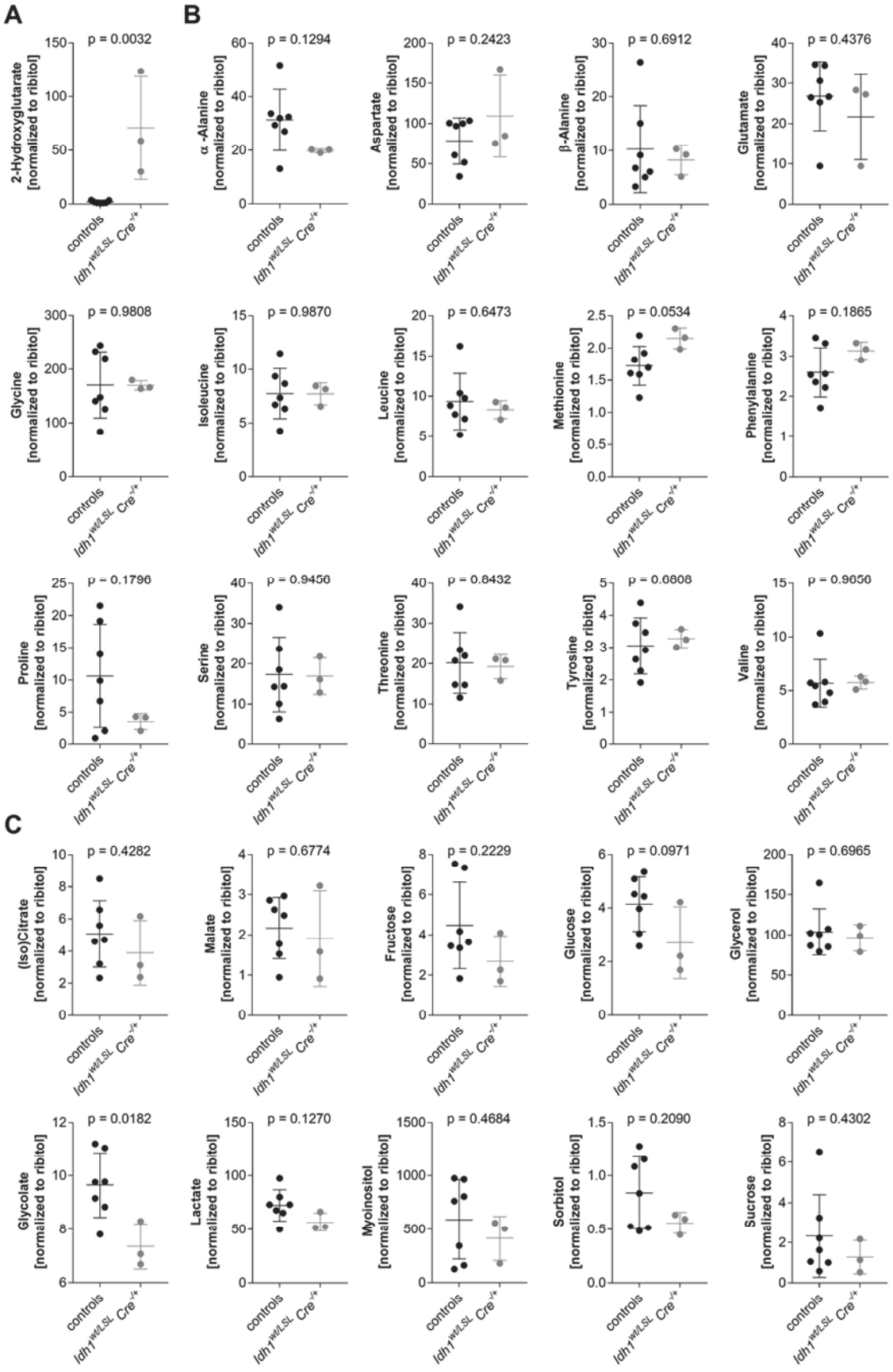

Fig. 3.16: Metabolic changes in *Idh1*-mutant NSC/NPCs compared to controls

Idh1$^{wt/wt}$ *Cre*$^{-/-}$, *Idh1*$^{wt/wt}$ *Cre*$^{-/+}$, *Idh1*$^{wt/LSL}$ *Cre*$^{-/-}$ and *Idh1*$^{wt/LSL}$ *Cre*$^{-/+}$ NSC/NPCs were cultured in 10 cm dishes with 1,500,000 cells per dish for 24 h. One NSC/NPC culture was tested for *Idh1*$^{wt/wt}$ *Cre*$^{-/-}$

(275), three NSC/NPC cultures each were tested for *Idh1*$^{wt/wt}$ *Cre*$^{-/+}$ (77, 129, 192), *Idh1*$^{wt/LSL}$ *Cre*$^{-/-}$ (42, 47, 128) and *Idh1*$^{wt/LSL}$ *Cre*$^{-/+}$ (44, 45, 75). All cells were treated with 0.5 µM 4-OHT for additional 48 h, before cells were counted and prepared for GC-coupled mass spectrometry. The graphs show metabolite levels in Idh1-mutant NSC/NPCs compared to control NSC/NPCs as determined by mass spectrometry. Individual data points for each NSC/NPC culture as well as mean values ± SEM for controls and Idh1-mutant NSC/NPCs are shown. Signal intensities of the metabolites were normalized to signal intensities of the internal control ribitol. Significances between controls and *Idh1*$^{wt/LSL}$ *Cre*$^{-/+}$ NSC/NPCs were examined by unpaired two-tailed t-tests. **(A)** 2-HG. **(B)** Amino acids. **(C)** Other metabolites.

3.4 Validation of Idh1 mutation-mediated effects in 2-HG-treated *Idh1*$^{wt/wt}$ *Cre*$^{-/-}$ NSC/NPCs

The conditional *Idh1*-mutant knock-in mouse model showed numerous limitations, wherefore an additional experimental approach was used to validate obtained results and to further characterize effects of *Idh1* mutation in NSC/NPCs. Instead of using *Idh1*-mutant knock-in cells, *Idh1*$^{wt/wt}$ *Cre*$^{-/-}$ NSC/NPCs were treated with (2R)-Octyl-α-hydroxyglutarate, a cell-permeable variant of the oncometabolite 2-HG[49], further on referred to as 2-HG for the experiments.

3.4.1 NSC/NPCs are highly sensitive to 2-HG treatment

A feasible concentration for 2-HG treatment of *Idh1*$^{wt/wt}$ *Cre*$^{-/-}$ NSC/NPCs had to be found. Therefore, MTT assays **(2.2.8)** were performed **(Fig. 3.17)**. The cells were treated with different concentrations of 2-HG for 48 h.

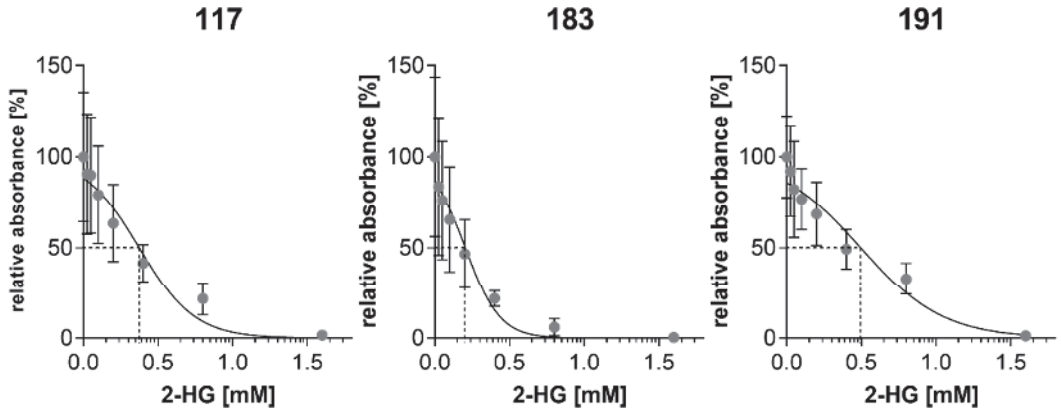

Fig. 3.17: Cytotoxicity of 2-HG in NSC/NPCs
Idh1$^{wt/wt}$ *Cre*$^{-/-}$ NSC/NPCs were cultured on 96-well plates with 10,000 cells per well for 24 h. The cells were treated with 2-HG and incubated for additional 48 h before MTT assay was performed. The $OD_{570\text{-}650\ nm}$ was measured. Results are derived from three technical replicates from three distinct NSC/NPC cultures (117, 183, 191). The graphs show a nonlinear fit of the data with mean values ± SEM being indicated for each tested concentration of 2-HG.

2-HG treatment resulted in 50 % viability in NSC/NPCs with concentrations of 0.4 mM 2-HG (117), 0.2 mM 2-HG (183) and 0.5 mM 2-HG (191). Already a concentration of 0.4 mM 2-HG decreased cell numbers in the three NSC/NPC cultures to 41.4 %, 21.8 %

and 49.3 % compared to the untreated controls. For the following experiments, the sublethal concentration of 0.4 mM 2-HG was used for treatment.

3.4.2 2-HG treatment results in stress-responsive gene expression in NSC/NPCs

The 4-OHT-mediated knock-in of mutant *Idh1* in *Idh1*$^{wt/LSL}$ *Cre*$^{-/+}$ NSC/NPCs led to elevated *Hmox1* mRNA and protein levels **(Fig. 3.15)**. To elucidate, whether this effect is 2-HG-dependent or relies on other factors like changes in NADPH levels, the mRNA expression levels and protein levels of Hmox1 in 2-HG-treated *Idh1*$^{wt/wt}$ *Cre*$^{-/-}$ NSC/NPCs were analyzed. Additional downstream targets of the main *Hmox1*-regulating transcription factors Hsp1, NF-κB, Ap-1 and Nrf2 were included[157,158] **(Fig. 3.18)**.

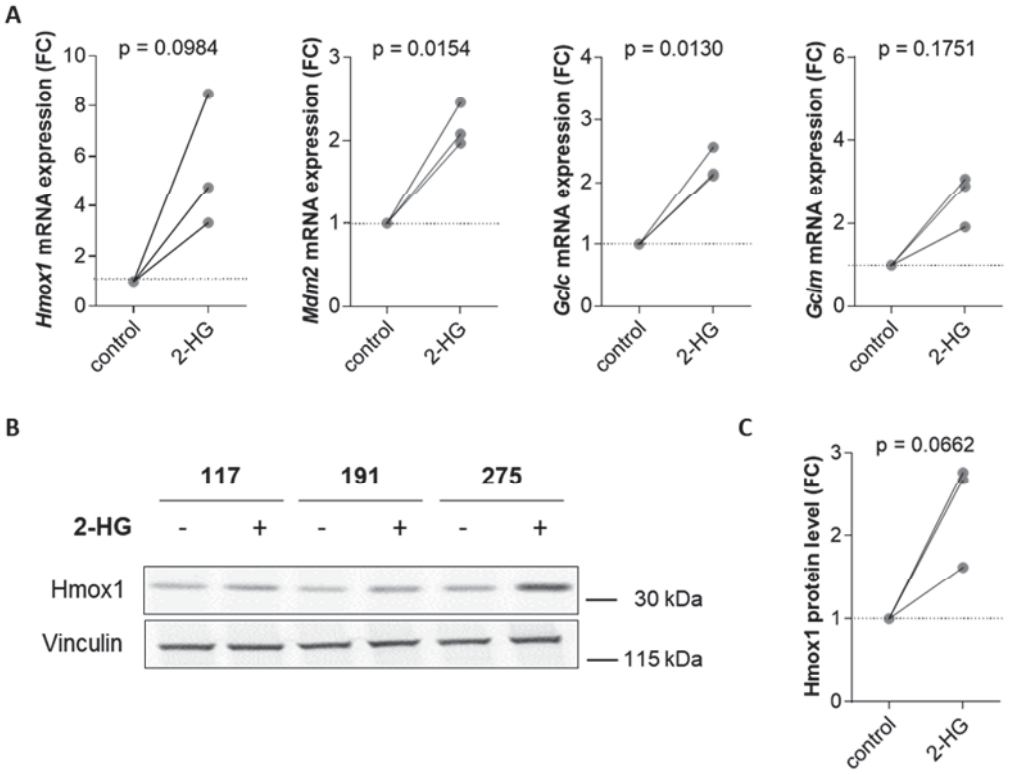

Fig. 3.18: Stress-responsive gene and protein expression in 2-HG-treated NSC/NPCs
Idh1$^{wt/wt}$ *Cre*$^{-/-}$ NSC/NPCs were cultured in 6 cm dishes with 1,000,000 cells per dish for 24 h. The cells were treated with 0.4 mM 2-HG for additional 48 h before cells were harvested and RNA or proteins were isolated. **(A)** RNA was used for cDNA synthesis and qRT-PCR analyses of *Hmox1*, *Mdm2*, *Gclc* and *Gclm* mRNA expression. **(B)** Proteins were subjected to Western blotting using vinculin expression for normalization. A representative blot is shown for one experiment with three individual NSC/NPC cultures (117, 191, 275). **(C)** Protein expression levels were analyzed densitometrically. **(A, C)** Data of the shown graphs are derived from three to five technical replicates in three distinct NSC/NPC cultures (117, 191, 275). Dots represent means for each NSC/NPC culture. Values were normalized to solvent control. Significances between untreated and treated NSC/NPCs were examined by paired two-tailed t-test analyses.

2-HG treatment resulted in elevated *Hmox1*, *Mdm2*, *Gclc* and *Gclm* mRNA expression in all tested cell lines after 48 h of exposure. *Hmox1* expression was induced 8.5-fold in NSC/NPC 117 cells, 4.8-fold in NSC/NPC 191 cells, and 3.3-fold in NSC/NPC 275 cells ($p = 0.0984$). *Mdm2* expression levels were 2.1-fold (117), 2.0-fold (191) and 2.5-fold (275) increased after 2-HG treatment, which was significant with a p-value of 0.0154. Significantly elevated mRNA expression levels were also detected for *Gclc*. In NSC/NPC 117 cells, 2-HG treatment resulted in a 2.6-fold increased *Gclc* expression, while *Gclc* expression levels were 2.1-fold increased in NSC/NPC 191 and 275 cells ($p = 0.0130$). *Gclm* levels were elevated by 2.9-fold (117), 3.1-fold (191) and 1.9-fold (275) ($p = 0.1751$). Furthermore, Hmox1 protein levels were higher in 2-HG-treated NSC/NPCs compared to the untreated NSC/NPCs. The treatment resulted in 2.7-times higher Hmox1 protein levels in NSC/NPC 117 cells. In NSC/NPC 191 and 275 cells, 1.6-fold and 2.7-fold increased Hmox1 protein levels were detected ($p = 0.0662$).

3.4.3 2-HG causes elevated ROS levels and induces an antioxidative response in NSC/NPCs

Hmox1 overexpression is an indicator of oxidative stress as its expression is regulated by ROS-responsive transcription factors like Hsp1, NF-κB, Ap-1 and Nrf2[157,158]. Besides possibly altered $NADP^+$/NADPH ratios in *Idh1*-mutant cells, also the oncometabolite 2-HG itself might lead to increased ROS levels and oxidative stress[120]. To elucidate the effect of 2-HG on the ROS homeostasis in *Idh1*$^{wt/wt}$ *Cre*$^{-/-}$ NSC/NPCs, the cells were treated with 0.4 mM 2-HG for 48 h. A DHE assay detecting superoxide levels[466] and a DCF staining indicating ROS in general[467] **(2.2.8.3)** were performed and measured by flow cytometry **(Fig. 3.19)**. Additionally, the expression of antioxidative enzymes was examined under the same conditions. Therefore, qRT-PCRs and Western blot analyses were performed **(Fig. 3.20)**.

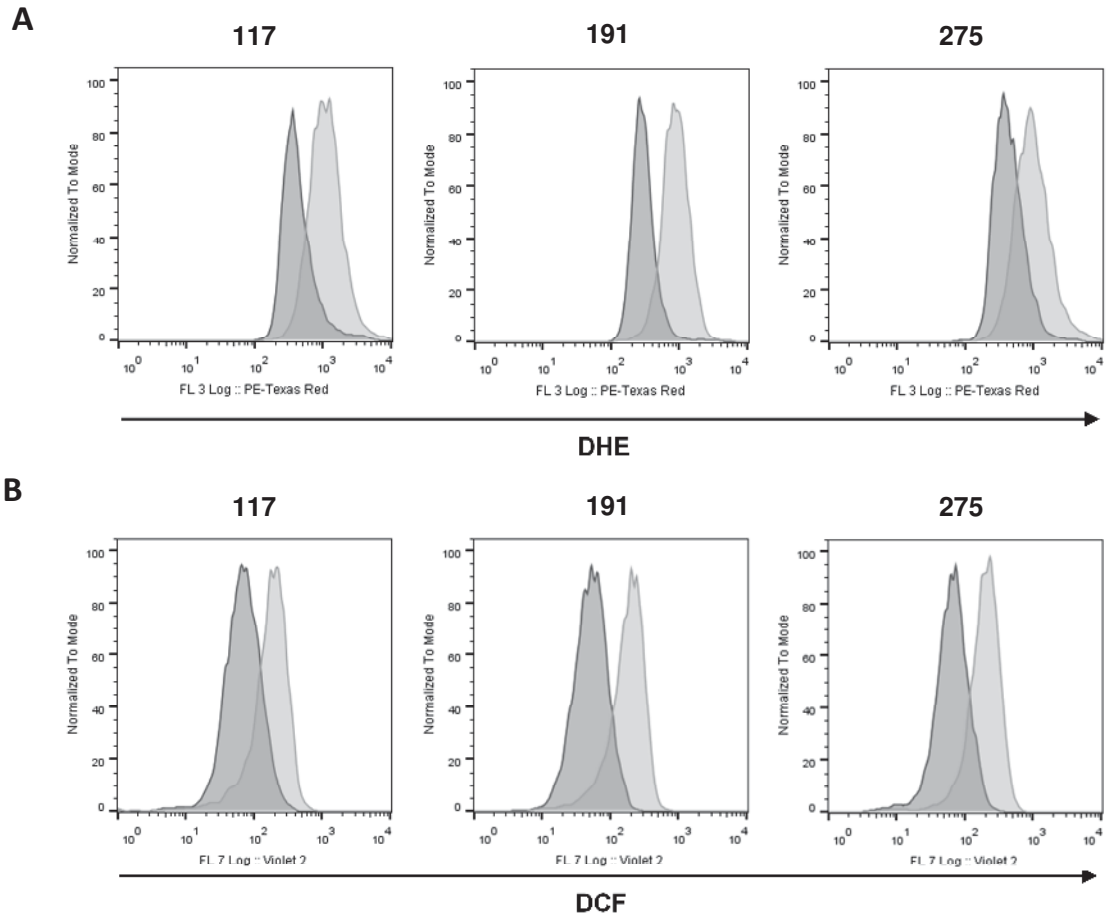

Fig. 3.19: ROS levels in 2-HG-treated NSC/NPCs
Idh1$^{wt/wt}$ *Cre*$^{-/-}$ NSC/NPCs were cultured in 6-well dishes with 500,000 cells per well for 24 h. Afterwards, the cells were treated with 0.4 mM 2-HG for additional 48 h. Then, the cells were stained with DCF or DHE, respectively, and analyzed by flow cytometry. Three technical replicates from three distinct NSC/NPC cultures were measured (117, 191, 275). Results for untreated NSC/NPCs are shown in dark gray, results for 2-HG-treated NSC/NPCs are shown in light gray. **(A)** Representative result of DHE staining in one experiment performed for each of the three distinct NSC/NPC cultures investigated. **(B)** Representative results of the DCF staining experiments in NSC/NPCs.

In all three tested NSC/NPC cultures, the 2-HG treatment resulted in increased levels of superoxide as detected by DHE staining. For 117 and 191 cells, similar results were detected for general ROS levels after 2-HG treatment. In comparison, only slightly increased ROS levels were observed for 275 cells. This was consistent in three independent replicates.

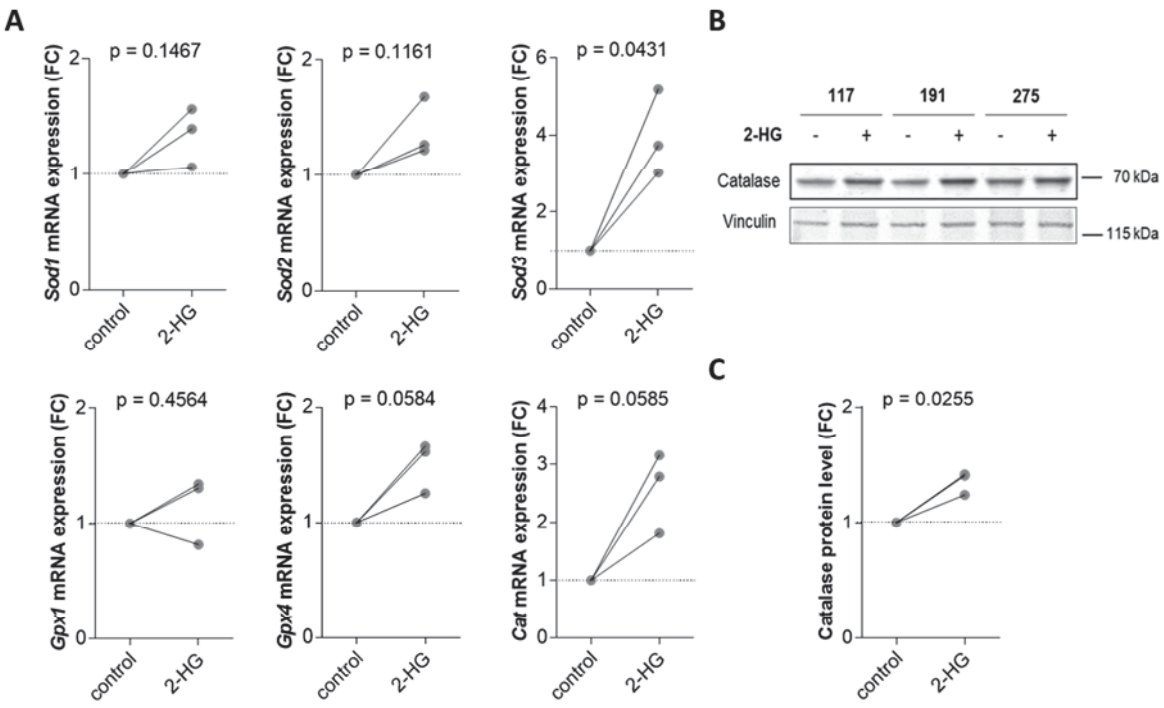

Fig. 3.20: Oxidative stress-responsive gene and protein expression in 2-HG-treated NSC/NPCs

Idh1$^{wt/wt}$ *Cre*$^{-/-}$ NSC/NPCs were cultured in 6 cm dishes with 1,000,000 cells per well for 24 h. The cells were treated with 0.4 mM 2-HG and incubated for additional 48 h, followed by RNA or proteins isolation. **(A)** cDNA synthesis and qRT-PCR were performed. **(B)** Western blotting of the protein catalase was performed using vinculin expression for normalization. A representative blot is shown for one experiment with three individual NSC/NPC cultures (117, 191, 275). **(C)** The detected bands were analyzed densitometrically. **(A, C)** Single dots represent the means for five to three technical replicates of each of the individual NSC/NPC cultures (117, 191, 275). Values were normalized to solvent controls. Significances between untreated and treated NSC/NPCs were examined by paired two-tailed t-test analyses.

Except for *Gpx1*, mRNA levels of the tested antioxidative enzymes were consistently increased in 2-HG-treated NSC/NPCs. *Sod1* mRNA expression was induced 1.6-fold (117), 1.4-fold (191) and 1.1-fold (275), compared to the untreated controls (p = 0.1467). For *Sod2,* 1.7-fold (117), 1.3-fold (191) and 1.2-fold increased mRNA expression levels were observed after 2-HG treatment (p = 0.1161). In contrary to *Sod1* and *Sod2*, *Sod3* expression levels were significantly altered (p = 0.0431). 2-HG treatment resulted in 3.7-times (117), 5.2-times (191) and 3.1-times elevated *Sod3* mRNA expression levels compared to the untreated controls. *Gpx4* expression was comparable with *Sod1* and *Sod2*. 2-HG treatment resulted in 1.7-fold (117), 1.6-fold (191) and 1.3-fold (275) higher *Gpx4* expression levels in comparison with the solvent controls (p = 0.0584). *Cat* mRNA expression was also induced by 2-HG treatment. The 2-HG-treated NSC/NPCs showed 3.2-fold (117), 2.8-fold (191) and 1.8-fold (275) increased *Cat* mRNA expression levels

compared to the solvent controls (p = 0.0585). At the protein level, catalase was significantly increased with fold changes of 1.4 (117 and 191) and 1.2 (275) after 2-HG treatment (p = 0.0255).

3.4.4 2-HG treatment of NSC/NPCs results in p38 phosphorylation

The activation of stress-responsive transcription factors like Hsf1, NF-κB, Ap-1 and Nrf2 is not solely induced by direct effects of ROS, but also by ROS-activated stress signaling pathways like Pi3k/Akt- and Mapk-signaling[157,468]. Induced p42/44 signaling has been reported for 2-HG-treated cells as well as for glioma cells[120,469]. p38 signaling is activated by ROS in glioma-initiating cells[470]. To examine a possible activation of these pathways in NSC/NPCs following 2-HG treatment, phosphorylation levels of the signaling molecules were detected by western blotting after 2-HG treatment for 48 h **(Fig. 3.21)**.

Neither total protein levels of Akt (p = 0.9270) and Jnk (p = 0.3746) nor their phosphorylation (p = 0.7395, p = 0.2371) was consistently altered in 2-HG-treated NSC/NPCs. Up- as well as downregulated protein levels were observed for these proteins. Total p42/44 protein levels were unaffected by 2-HG treatment (p = 0.3908), whereas phosphorylated p42/44 protein levels were rather decreased to 0.5 and 0.8 in NSC/NPC 117 and 191 cells or unaltered in NSC/NPC 275 cells (p = 0.1856). However, consistent changes were observed for p38 after 2-HG treatment. While total p38 protein levels decreased significantly to 0.8 (117), 0.9 (191) and 0.7 (275) (p = 0.0047), the abundance of phosphorylated p38 was on average 3.9-fold (117), 2.2-fold (191) and 3.4-fold (275) higher in 2-HG-treated cells compared to the untreated controls (p = 0.0530).

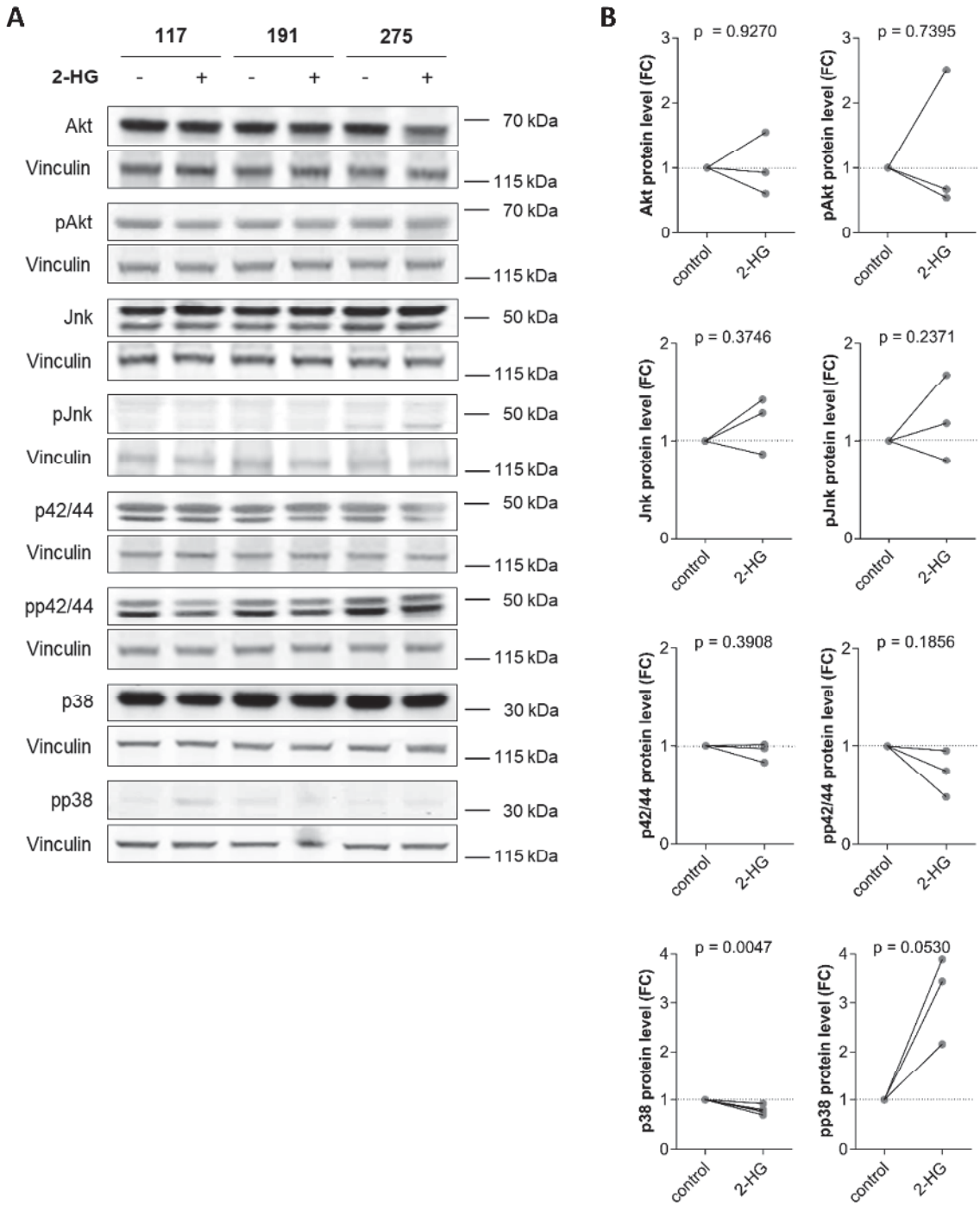

Fig. 3.21: Akt- and Mapk-signaling in 2-HG-treated NSC/NPCs

Idh1$^{wt/wt}$ *Cre*$^{-/-}$ NSC/NPCs were cultured in 6 cm dishes with 1,000,000 cells per well for 24 h. The cells were treated with 0.4 mM 2-HG and incubated for additional 48 h. Then, proteins were isolated and used for Western blotting to detect expression of total and phosphorylated Akt, Jnk, p42/44 and p38. Vinculin protein expression was used for normalization. The relative expression levels were determined densitometrically. **(A)** Representative blots are shown. **(B)** Data of the graphs are derived from one to five technical replicates and show the mean value for each tested NSC/NPC culture (117, 191, 275) normalized to the solvent controls. Significances between untreated and treated NSC/NPCs were examined by paired two-tailed t-test analyses.

3.4.5 2-HG treatment of NSC/NPCs induces the integrated stress response

Perk signaling in response to oxidative stress or unfolded proteins is an additional pathway that may activate the *Hmox1*-inducing transcription factor Nrf2[471], as well as the integrative stress response[217]. To investigate, if Perk signaling is involved in 2-HG-mediated *Hmox1* expression, the phosphorylation levels of Perk as well as downstream mediators of Perk signaling were analyzed by Western blot analysis after 2-HG treatment for 6 h or 48 h. Furthermore, qRT-PCR experiments were performed after 48 h of 2-HG treatment for detection of expression of indirectly Perk-responsive genes **(Fig. 3.22)**.

Total Perk protein levels were unaltered (117) to slightly increased after 2-HG treatment by 1.1-fold (191) and 1.3-fold (275) in comparison to the solvent controls ($p = 0.2777$). Unfortunately, it was not possible to detect phosphorylated Perk at the protein level. However, the phosphorylation of the Perk downstream target eIF2α was significantly increased in 2-HG-treated NSC/NPCs ($p = 0.0394$) to 2.9-fold (117), 3.8-fold (191) and 3.8-fold (275) after 2-HG treatment compared to the solvent controls. Total eIF2α protein levels slightly decreased to 0.9 (191) and 0.8 (275) ($p = 0.3060$). Comparable to eIF2α phosphorylation levels, elevated protein levels were also detected for Atf4. Atf4 protein levels were 3.8-times (117), 1.8-times (191) and 2.6-times (275) higher in 2-HG-treated NSC/NPCs compared to the controls ($p = 0.0975$). Grp78 protein levels were not consistently altered in the three NSC/NPC cultures after 2-HG treatment ($p = 0.3552$). Besides the effects at the protein level, the stress-responsive transcription of *Atf4* and *Chop* was also induced by 2-HG treatment. *Atf4* levels were 1.6-times (117), 1.1-times (191) and 1.4-times (275) higher in 2-HG-treated NSC/NPCs compared to the controls ($p = 0.1404$). *Chop* levels increased 12.2-fold (117), 3.4-fold (191) and 3.2-fold (275) after 2-HG treatment ($p = 0.2291$). *Gadd34* levels were not consistently altered by 2-HG in the three tested cell lines ($p = 0.2365$). Whereas 2-HG treatment resulted in 4.9-fold and 7.8-fold increased *Gadd34* levels in NSC/NPC 117 and 191 cells, mRNA levels were decreased to 0.7 compared to the untreated controls in NSC/NPC 275 cells.

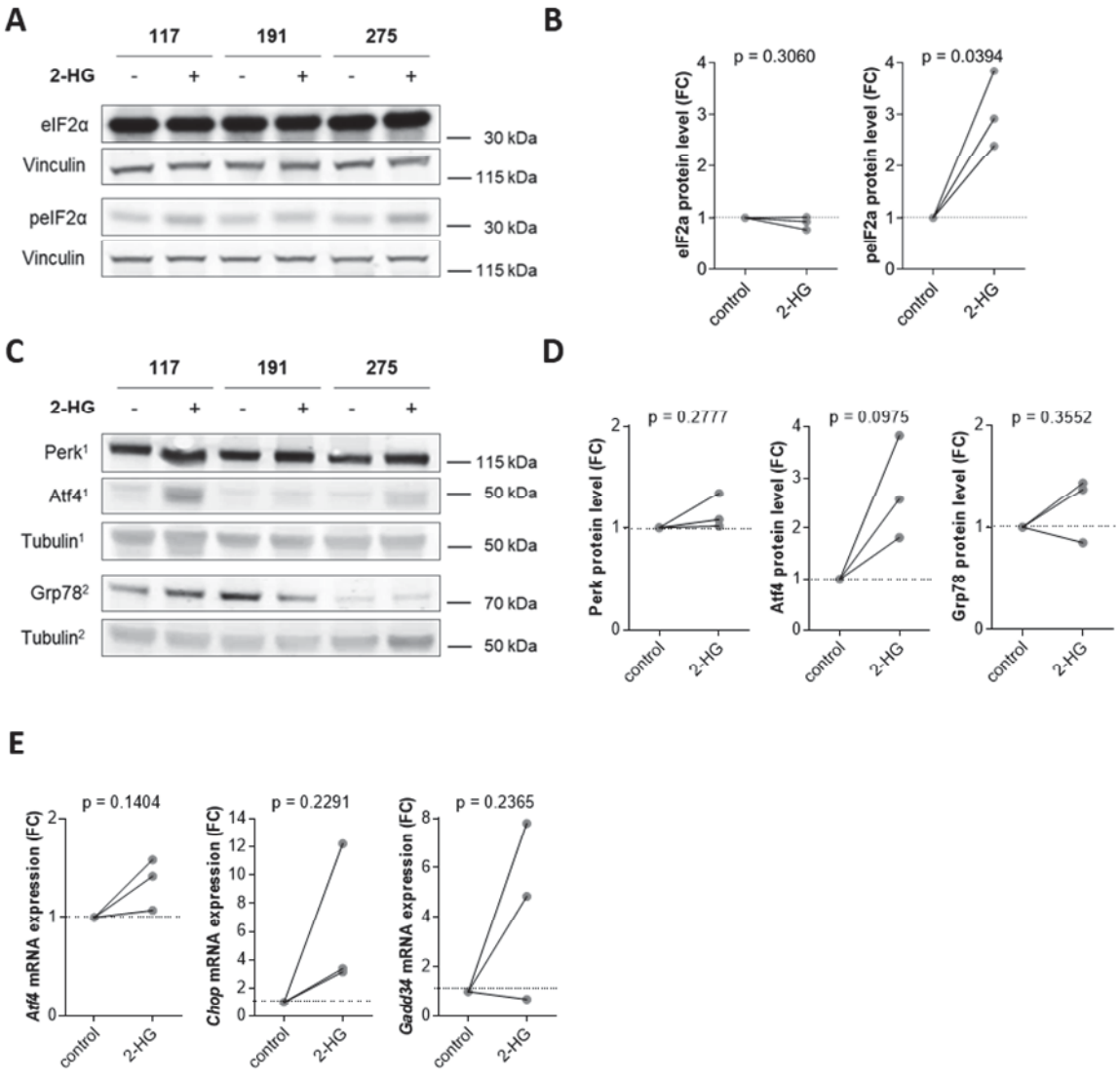

Fig. 3.22: Integrated stress response in 2-HG-treated NSC/NPCs

Idh1$^{wt/wt}$ *Cre*$^{-/-}$ NSC/NPCs were cultured in 6 cm dishes with 1,000,000 cells per well for 24 h. **(A, B, E)** The cells were treated with 0.4 mM 2-HG and incubated for additional 48 h. **(C, D)** The cells were treated with 0.4 mM 2-HG and incubated for additional 6 h. **(A-D)** Proteins were isolated and used for Western blotting of total and phosphorylated eIF2α, Perk, Atf4 and Grp78 proteins. Vinculin and tubulin expression levels were used for normalization. Relative expression levels were determined densitometrically. **(A, C)** Representative blots are shown. **(E)** RNA was isolated from treated and control cells, followed by cDNA synthesis and qRT-PCR analyses. **(B, C, E)** Data of the graphs were normalized to the solvent controls. Single dots represent the mean value, combining values for three to five technical replicates for each independent NSC/NPC culture (117, 191, 275). Significances between untreated and treated NSC/NPCs were examined by paired two-tailed t-test analyses.

3.4.6 2-HG treatment of NSC/NPCs mediates apoptotic cell death

Chop is an anti-autophagic and pro-apoptotic transcription factor, regulating for example the expression of the anti-apoptotic protein Bcl-2[220,472], as well as the apoptosis and cell cycle regulator *Gadd34* under prolonged stress conditions[222]. Since 2-HG treatment resulted in increased *Chop* levels in all tested NSC/NPCs, the effect of 2-HG on apoptotic and autophagic cell death was examined. Therefore, an Annexin V / 7-AAD staining **(2.2.7.1)** was performed with untreated and 2-HG-treated NSC/NPCs after 48 h **(Fig. 3.23)**. Furthermore, protein levels of the autophagy marker LC3II were detected by Western blotting. Moreover, the phosphorylation status of the mTorc1 downstream targets p70S6 and 4E-BP1 was analyzed **(Fig. 3.24)**.

In untreated NSC/NPCs most of the cells were unstained. For NSC/NPC 117 cells, 91 % of all gated cells were unstained. With 91 % and 90 %, comparable fractions of cells were unstained for NSC/NPC 183 and 191 cells. After 2-HG treatment, the percentage of unstained cells decreased to 87 % in the cell line 117 ($p = 0.5033$), to 57 % in the cell line 183 ($p = 0.2831$) and to 92 % in the cell line 191 ($p = 0.0019$). The fraction of Annexin V-stained NSC/NPCs generally increased after 2-HG treatment. The percentage of Annexin V-stained cells increased after treatment from 5 % to 11 % (117) ($p = 0.2611$), 6 % to 28 % (183) ($p = 0.6999$), and 7 % to 22 % (191) ($p = 0.0045$). 2-HG treatment did not consistently affect the fraction of 7-AAD-stained NSC/NPCs, i.e. changed from 1 % to 0.5 % (117) ($p > 0.9999$) and 0.5 % to 2 % (183) ($p > 0.9999$), or remained at 0.6 % (191) ($p > 0.9999$). Slightly increased fractions of double-stained NSC/NPCs were found for 183 and 191 NSC/NPCs, with an increase from 3 % to 14 % (183) ($p > 0.9999$) and from 3 % to 5 % (191) ($p > 0.9999$). In contrast, a decrease from 3 % to 2 % of double-stained cells was detected in NSC/NPC 117 cells ($p > 0.9999$).

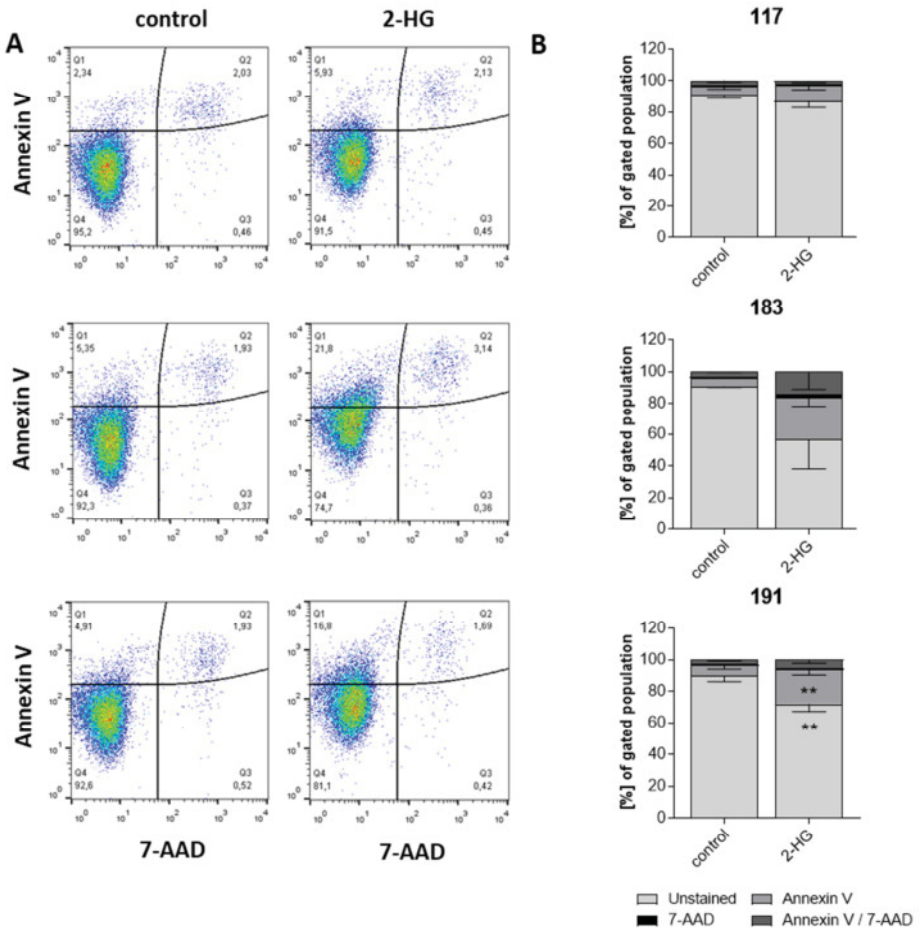

Fig. 3.23: Apoptosis in 2-HG-treated NSC/NPCs
Idh1$^{wt/wt}$ *Cre*$^{-/-}$ NSC/NPCs were cultured in 6-well plates with 500,000 cells per well for 24 h. The cells were treated with 0.4 mM 2-HG for additional 48 h before Annexin V / 7-AAD staining was performed. **(A)** After gating for the cellular population in the SSC-FSC gate, the included cells were gated corresponding to their staining. A representative gating is shown for one experiment with three NSC/NPC cultures (top to bottom: 117, 183 and 191). **(B)** The results are composed of two (183) to three (117, 191) technical replicates from each NSC/NPC culture (117, 183, 191). Data are indicated as mean values & SEM. Significances between the fractions of untreated and treated NSC/NPCs were examined by Two-way ANOVA with Bonferroni Multiple Comparison Test.

Total protein levels of the mTorc1 downstream target p70S6 were significantly decreased to 50 % (191) and 60 % (117 and 275) after 2-HG treatment compared to untreated controls ($p = 0.0031$). However, 2-HG treatment did not result in consistent alterations of p70S6 phosphorylation ($p = 0.5165$). While expression of phosphorylated p70S6 was nearly unaffected with in NSC/NPC 117 and 191 cells, an increase of 2.4-times was detected in NSC/NPC 275 cells. Total 4E-BP1 levels were significantly affected by 2-HG treatment, as increases of 1.4-fold (117, 275) and 1.2-fold (191) were detected ($p = 0.0415$). Comparable to p70S6, 4E-BP1 phosphorylation levels were not altered consistently by 2-HG treatment. In NSC/NPC 117 cells, the phosphorylation level of 4E-BP1 was unaffected, while it was slightly elevated 1.1-fold in NSC/NPC 191 cells and 1.3-

fold in NSC/NPC275 cells after 2-HG treatment (p = 0.3373). Also LC3II protein levels were not affected uniformly in the distinct NSC/NPC cultures. Whereas the protein levels of LC3II were unaffected by 2-HG treatment in 117 and 275 cells, a 1.4-fold increase was observed for 191 cells (p = 0.4149). LC3I protein levels were elevated in all three tested NSC/NPC cultures with fold changes of 1.6 (117, 275) and 2.1 (191) in response to 2-HG treatment (p = 0.0509).

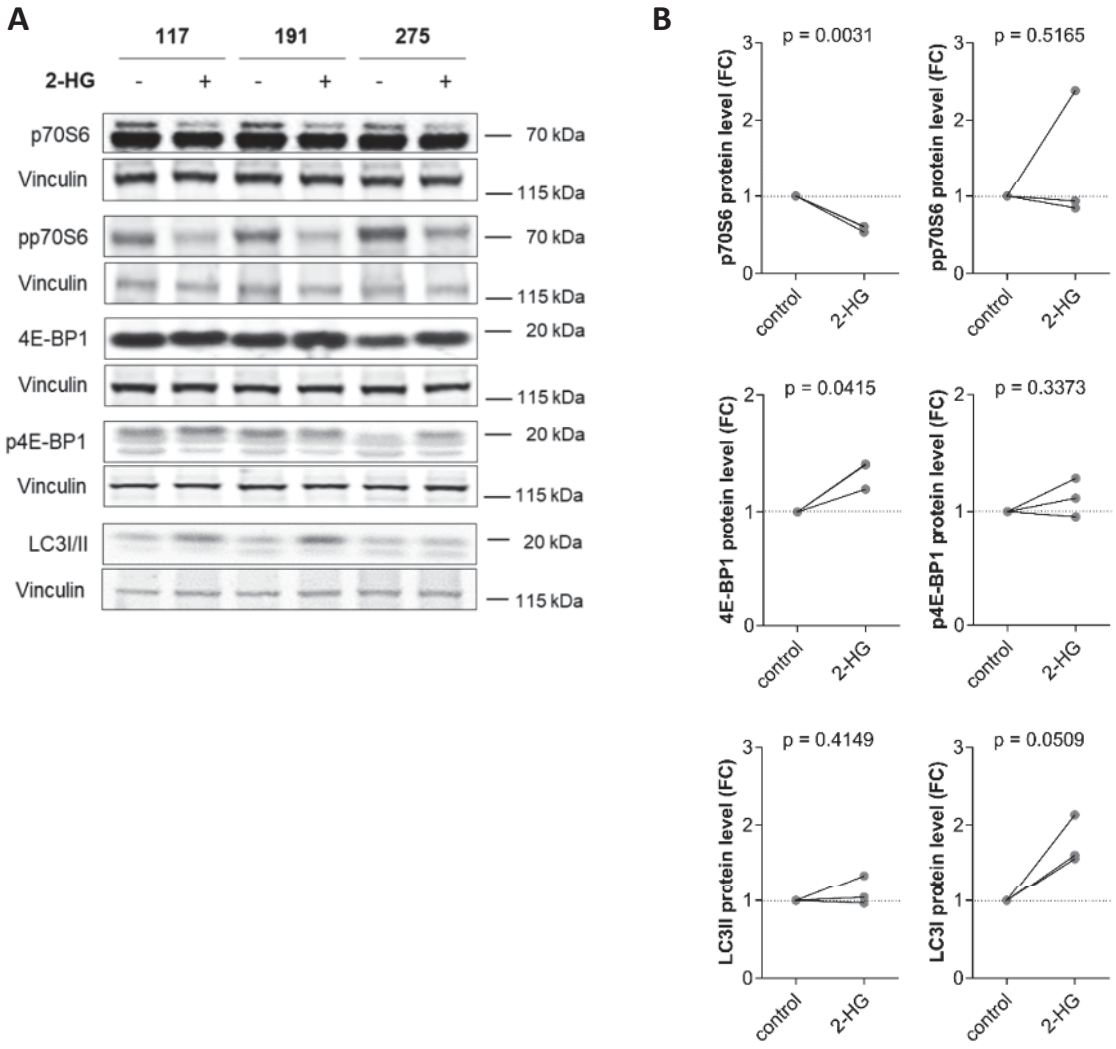

Fig. 3.24: Autophagic cell signaling in 2-HG-treated NSC/NPCs
Idh1$^{wt/wt}$ *Cre*$^{-/-}$ NSC/NPCs were cultured in 10 cm dishes with 1,000,000 cells per well for 24 h. The cells were treated with 0.4 mM 2-HG for additional 48 h. **(A, B)** Proteins were isolated and used for Western blotting of total and phosphorylated p70S6 and 4E-BP1, as well as LC3I/II. Vinculin expression was used for normalization. Relative expression levels were determined densitometrically. **(A)** Representative blots are shown for each investigated NSC/NPC culture (117, 191, 275). **(B)** Densitometic data are derived from three to five technical replicates performed for each NSC/NPC culture (117, 191, 275). Values were normalized to the solvent controls. Single dots represent mean values calculated for the technical replicates of each NSC/NPC culture. Significances between untreated and treated NSC/NPCs were examined by paired two-tailed t-test analyses.

3.4.7 2-HG treatment of NSC/NPCs induces cell cycle arrest and *Cdkn1a* expression

In 2017, Pirozzi and colleagues detected reduced proliferation as well as p53- and p21-induced cell cycle arrest in *Idh1*-mutant NSCs[473]. To elucidate, whether 2-HG mediates the same effect in NSC/NPCs, a BrdU assay was performed after 2-HG treatment for 48 h **(Fig. 3.25)**. Furthermore, p53 total protein and phosphorylation levels were detected by Western blotting and qRT-PCRs were performed for detection of expression of selected cell cycle regulators **(Fig. 26)**.

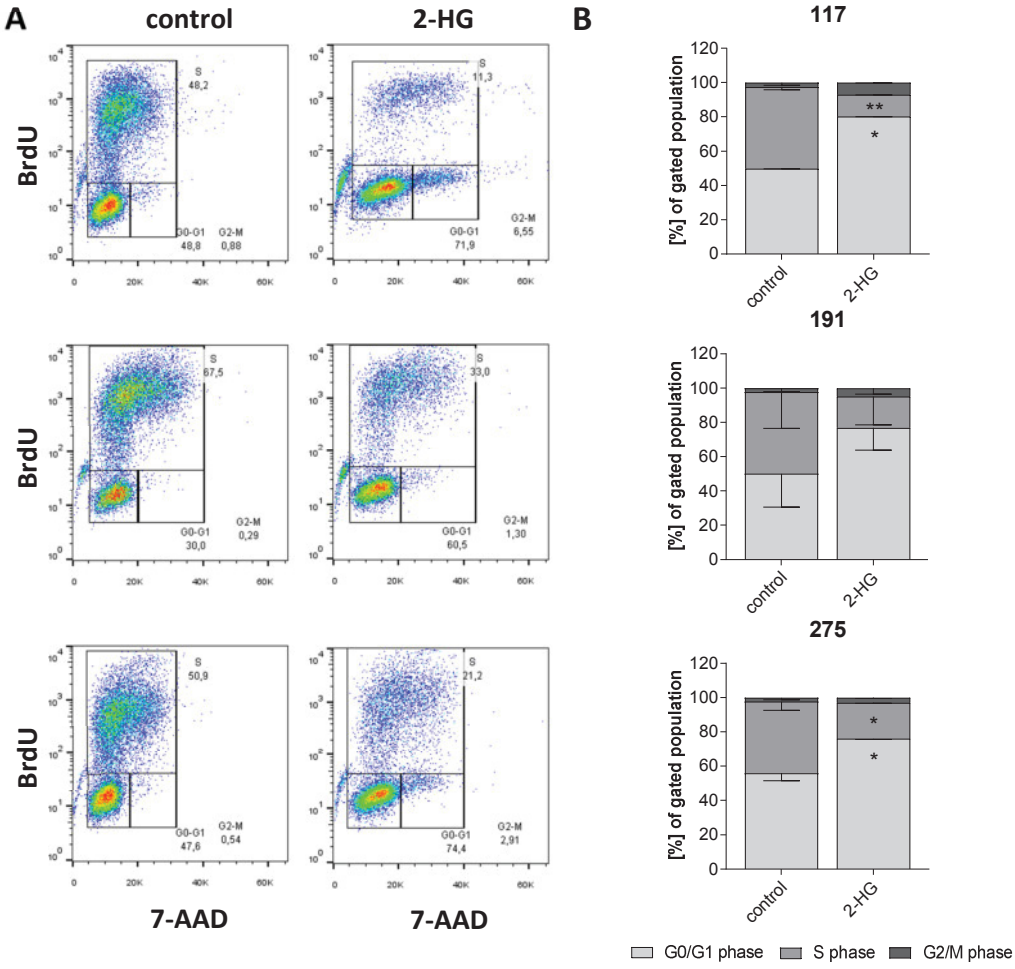

Fig. 3.25 Cell cycle analysis of 2-HG-treated NSC/NPCs
Idh1$^{wt/wt}$ *Cre*$^{-/-}$ NSC/NPCs were cultured in 6-well plates with 500,000 cells per well for 24 h. The cells were treated with 0.4 mM 2-HG for additional 48 h and incubated with BrdU for 4 h. The BrdU Flow Kit from BD Pharmingen™ was used. Cells with positivity for BrdU or the total DNA-binding 7-AAD were detected by flow cytometry. **(A)** A representative figure of gated cells in G0/G1-, S- or G2/M-phase of the cell cycle is shown. (Top to bottom: 117, 191, 275) **(B)** Summary of the results based of two (117, 191) to three (275) technical replicates from NSC/NPC cultures and show the mean values ± SEM (117, 191, 275). Significances in cell cycle distribution between untreated and treated NSC/NPCs were examined by Two-way ANOVA analyses of variance with Bonferroni Multiple Comparison Test. (* $p \leq 0.05$, ** $p \leq 0.01$).

BrdU-based cell cycle analyses showed that 2-HG treatment resulted in significantly reduced cell fractions in the S-phase of the cell cycle in all tested NSC/NPCs. BrdU-stained NSC/NPCs decreased significantly After 2-HG treatment from 48 % to 13 % (117) ($p = 0.0078$), from 48 % to 18 % (191) ($p = 0.1076$), and from 42 % to 21 % (275) ($p = 0.0297$). Subsequently, higher fractions of cells were found in the G0/G1-phase and in the G2/M-phase after 2-HG treatment, with increases from 50 % to 80 % (117) ($p = 0.0102$), from 50 % to 77 % (191) ($p = 0.1284$), and from 56 % to 76 % (275) ($p = 0.0331$). The percentage of cells in the G2/M-phase rose from 3 % to 7 % (117) ($p = 0.3790$), from 2 % to 5 % (191) ($p > 0.9999$), and from 2 % to 3 % (275) ($p > 0.9999$).

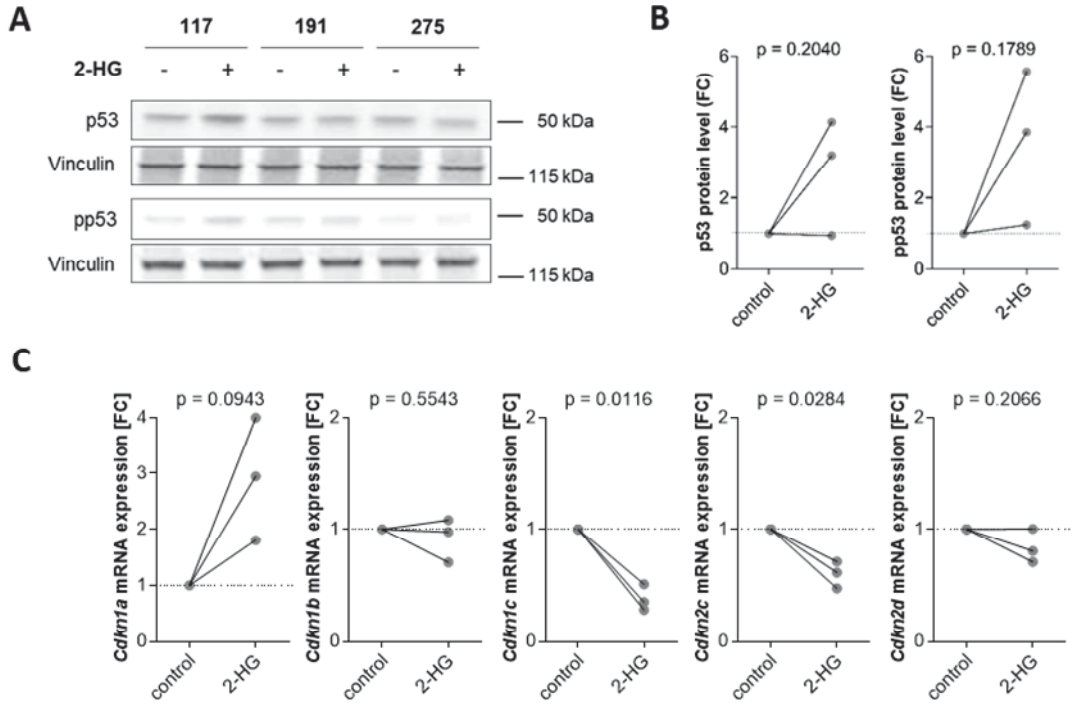

Fig. 3.26: Cell cycle regulator expression in 2-HG-treated NSC/NPCs
Idh1$^{wt/wt}$ *Cre*$^{-/-}$ NSC/NPCs were cultured in 10 cm dishes with 1,000,000 cells per well for 24 h. Afterwards, the cells were treated with 0.4 mM 2-HG for additional 48 h. **(A, B)** Proteins were isolated, subjected to gel electrophoresis and used for Western blotting to assess total and phosphorylated p53. Expression of vinculin was used for normalization and expression levels were determined by densitometry of the protein bands. **(A)** Representative blots are shown for one experiment with each of three NSC/NPC cultures (117, 191, 275), respectively. **(B)** Summary of the results based on data obtained by measuring three to five technical replicates from each culture (117, 191, 275). **(C)** RNA was isolated, followed by cDNA synthesis and qRT-PCR analyses. **(B; C)** Data were normalized to the solvent controls. Single dots represent the means calculated for each NSC/NPC culture. Significances between untreated and treated NSC/NPCs were examined by paired two-tailed t-test analyses.

Total p53 expression was not consistently altered in a single direction by 2-HG treatment. Whereas 2-HG treatment resulted in 4.1-fold and 3.2-fold higher p53 protein levels in

NSC/NPC 117 and 191 cells, p53 protein levels were unaltered in NSC/NPC 275 cells ($p = 0.2040$). Phosphorylated p53 expression was on average 3.9-fold (117), 5.6-fold (191) and 1.3-fold (275) higher after 2-HG treatment, albeit these differences remained not significant ($p = 0.1789$). 2-HG treatment also affected the mRNA expression of selected CKIs. *Cdkn1a* expression was increased 4.0-fold (117), 3.0-fold (191) and 1.8-fold (275) in 2-HG-treated NSC/NPCs ($p = 0.0943$). *Cdkn1b* expression was almost unaltered after 2-HG treatment ($p = 0.5543$). In contrast to *Cdkn1a* levels, the mRNA expression levels of *Cdkn1c* significantly decreased to 0.4 (117), 0.3 (191) and 0.5 (275) after 2-HG treatment compared to the controls ($p = 0.0116$). Similar results were obtained for *Cdkn2c* with decreases in mRNA expression levels to 0.6 (117), 0.5 (191) and 0.7 (275) compared to the controls ($p = 0.0284$). *Cdkn2d* mRNA levels were reduced to 0.8 (191) and 0.7 (275) in two NSC/NPC cultures and unaltered in NSC/NPC 117 cells ($p = 0.2066$).

3.4.8 2-HG-mediated apoptotic cell death in NSC/NPCs is attenuated by antioxidant treatment

Increased ROS levels as well as enhanced p38 expression might lead to the induction of the integrated stress response and consequently to cell death under prolonged stress conditions[197,474]. To elucidate the involvement of increased ROS levels and p38 signaling in induction of apoptosis by 2-HG treatment of NSC/NPCs, a caspase activity assay was performed **(2.2.10) (Fig. 3.27)**. Specifically, NSC/NPCs were treated with 0.4 mM 2-HG in co-incubation with either the antioxidant N-acetyl-cysteine (NAC, 2 mM) or the p38 inhibitor SB203580 (SB, 3 µM) for 48 h.

2-HG-treated NSC/NPCs showed 2.1-fold (117), 2.4-fold (183) and 3.0-fold (191) increased caspase 3 and 7 activity compared to untreated NSC/NPCs ($p = 0.0012$). Although caspase 3 and 7 activity was 1.6-fold (117), 2.0-fold (183) and 2.1-fold (191) increased in 2-HG- and NAC-treated NSC/NPCs compared to the control ($p = 0.0511$), the effect of 2-HG treatment alone was overall attenuated in the three NSC/NPC cultures ($p = 0.2759$). The co-incubation of 2-HG and SB resulted in 3.3-fold (117), 2.6-fold (183) and 2.1-fold (191) increased caspase 3 and 7 activity in NSC/NPCs compared to the control ($p = 0.0006$). Compared to NSC/NPCs treated with 2-HG alone, the co-incubation resulted in an even higher caspase 3 and 7 activity in 117 and 183 cells, whereas the co-incubation with SB led to reduced caspase 3 and 7 activity in 191 cells ($p = 0.9940$).

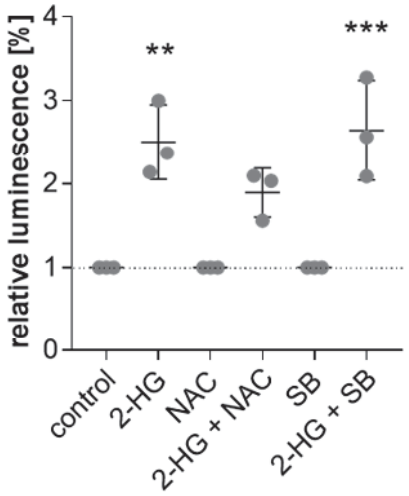

Fig. 3.27: Impact of NAC and SB203580 on 2-HG-induced apoptosis
Idh1$^{wt/wt}$ *Cre*$^{-/-}$ NSC/NPCs were cultured on white clear-bottom 96-well plates with 10,000 cells per well for 24 h. The cells were treated for additional 48 h with 0.4 mM 2-HG, 2 mM N-acetyl-cysteine (NAC) or 3 µM SB203580 (SB) either alone or in combinations as indicated in the figure. The Caspase-Glo® 3/7 Assay from Promega as well as an MTT assay were performed as described in **2.2.10**. Results are derived from two (183, 191) or three (117) technical replicates and depicted as means ± SEM. Data were normalized to the controls respectively. Significances between the respective controls and treated NSC/NPCs were examined by One-way ANOVA analyses of variance with Tukey's Post-Test. (** p = 0.0012, *** p = 0.0006).

3.5 Comparison of 2-HG-mediated effects on NSC/NPCs to RNA sequencing and proteomic data of NSC/NPCs from conditional *Idh1*-mutant knock-in mice

Results obtained by 2-HG treatment of *Idh1*$^{wt/wt}$ *Cre*$^{-/-}$ NSC/NPCs were compared to the RNA sequencing data as well as to the proteomic data performed with 4-OHT-treated *Idh1*$^{wt/LSL}$ *Cre*$^{-/+}$ NSC/NPCs. The RNA sequencing data of the knock-in NSC/NPCs were compared to controls consisting of 4-OHT-treated *Idh1*$^{wt/wt}$ *Cre*$^{-/-}$, *Idh1*$^{wt/wt}$ *Cre*$^{-/+}$ and *Idh1*$^{wt/LSL}$ *Cre*$^{-/-}$ NSC/NPCs. The proteomic data of the knock-in NSC/NPCs were compared to *Idh1*$^{wt/LSL}$ *Cre*$^{-/-}$ as controls **(Fig. 3.28, Fig. 3.29, Fig. 3.30)**.

As already described, Hmox1 mRNA and protein levels were significantly induced in the knock-in NSC/NPCs compared to the controls ($p = 0.0285$, $p = 0.0295$ respectively) **(Fig. 3.28 A)**. As in 2-HG-treated NSC/NPCs **(Fig. 3.18)**, *Mdm2* mRNA expression levels were moreover significantly increased in *Idh1*$^{wt/LSL}$ *Cre*$^{-/+}$ NSC/NPCs compared to the controls ($p = 0.0336$) **(Fig. 3.28 A)**. As in 2-HG-treated NSC/NPCs **(Fig. 3.20)**, also a significantly increased expression was detected for the antioxidative enzyme-coding gene *Sod3* in *Idh1*$^{wt/LSL}$ *Cre*$^{-/+}$ NSC/NPCs ($p = 0.0018$) **(Fig. 3.28 B)**. Unlike the *Gpx1* mRNA levels in 2-HG-treated NSC/NPCs, expression levels of *Gpx1* were significantly decreased in *Idh1*$^{wt/LSL}$ *Cre*$^{-/+}$ NSC/NPCs in the RNA sequencing data ($p = 0.0109$) **(Fig. 3.28 B)**.

Unlike the unaltered total Akt protein levels in 2-HG-treated NSC/NPCs **(Fig. 3.21)**, the proteomic data revealed significantly increased Akt protein levels in *Idh1*$^{wt/LSL}$ *Cre*$^{-/+}$ NSC/NPCs compared to the controls ($p = 0.0232$). Total p38 protein levels were significantly reduced in 2-HG-treated NSC/NPCs **(Fig. 3.22)**. mRNA expression levels of *Mapk14,* coding for p38α, were increased significantly in *Idh1*$^{wt/LSL}$ *Cre*$^{-/+}$ NSC/NPCs ($p = 0.0145$). However, mRNA expression levels of *Mapk11* and *Mapk12,* coding for p38β and p38γ, were significantly decreased in *Idh1*$^{wt/LSL}$ *Cre*$^{-/+}$ NSC/NPCs in comparison to the controls ($p = 0.0396$, $p = 0.0010$ respectively) **(Fig. 3.29 A)**. While 2-HG treatment did not significantly alter mRNA or protein levels of tested components of the integrated stress response in NSC/NPCs **(Fig. 3.22)**, significantly elevated *Chop* mRNA expression levels were detected in *Idh1*$^{wt/LSL}$ *Cre*$^{-/+}$ NSC/NPCs compared to the controls ($p = 0.0404$) **(Fig. 3.29 B)**.

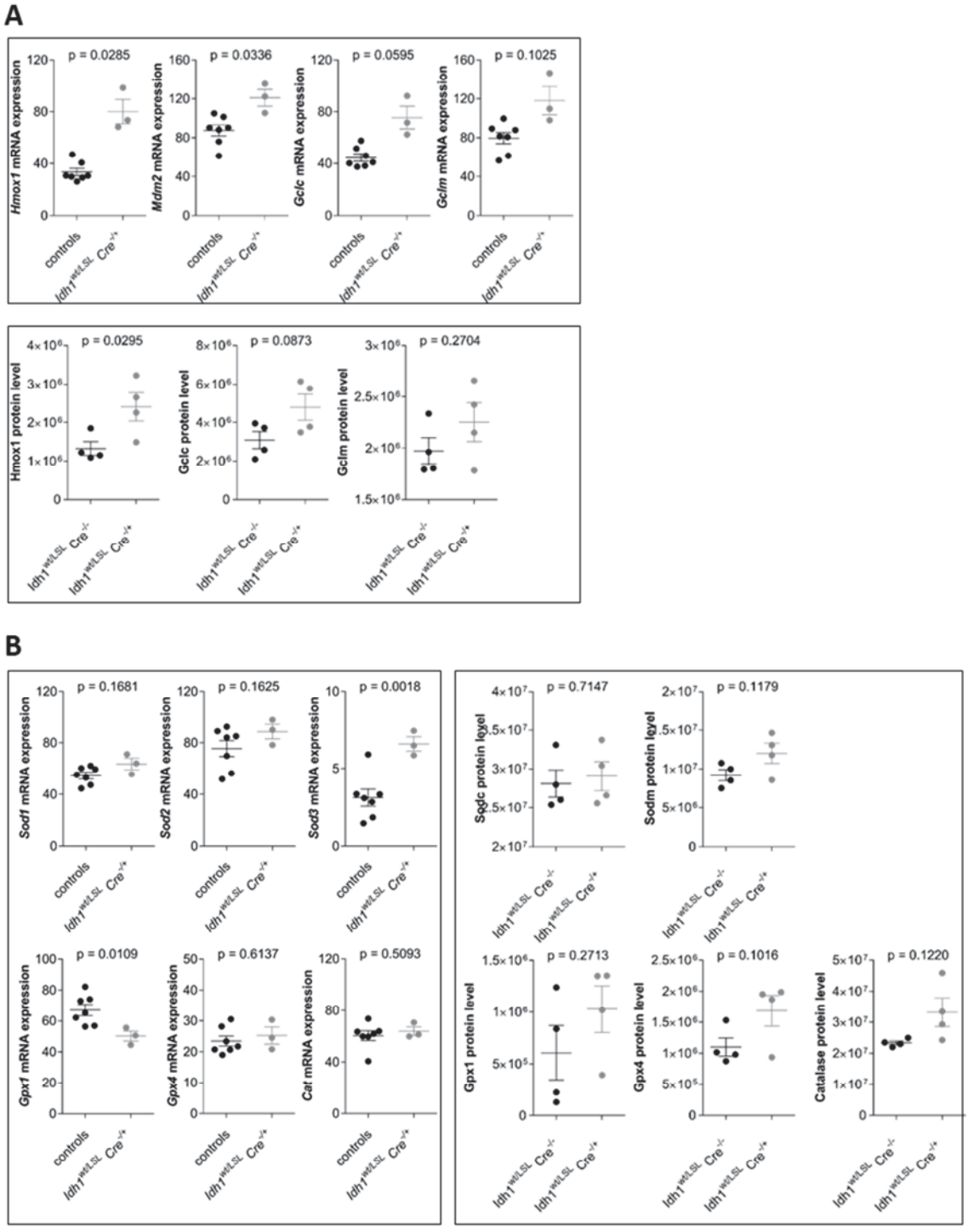

Fig. 3.28: Stress-responsive signaling in *Idh1*-mutant knock-in NSC/NPCs (1)
Results of RNA sequencing of *Idh1*$^{wt/LSL}$ *Cre*$^{-/+}$ NSC/NPCs compared to *Idh1*$^{wt/wt}$ *Cre*$^{-/-}$, *Idh1*$^{wt/wt}$ *Cre*$^{-/+}$ and *Idh1*$^{wt/LSL}$ *Cre*$^{-/-}$ NSC/NPCs (controls) (method described in **Fig. 3.14**) and corresponding proteomic analyses (method described in **Fig. 3.15 B**) Significances were examined by unpaired two-tailed t-tests for the RNA sequencing and by the proteomic data analysis software Progenesis® QI, which uses ANOVA for statistical testing for the proteomic data. Data are represented as means ± SEM. **(A)** Expression of selected ROS-responsive candidates (upper box: RNA sequencing, lower box: proteomics). Corresponding results of 2-HG-treated cells are shown in **Fig. 3.18**. **(B)** Expression of selected antioxidative enzymes (left box: RNA sequencing, right box: proteomics). Corresponding results of 2-HG-treated cells are shown in **Fig. 3.20**.

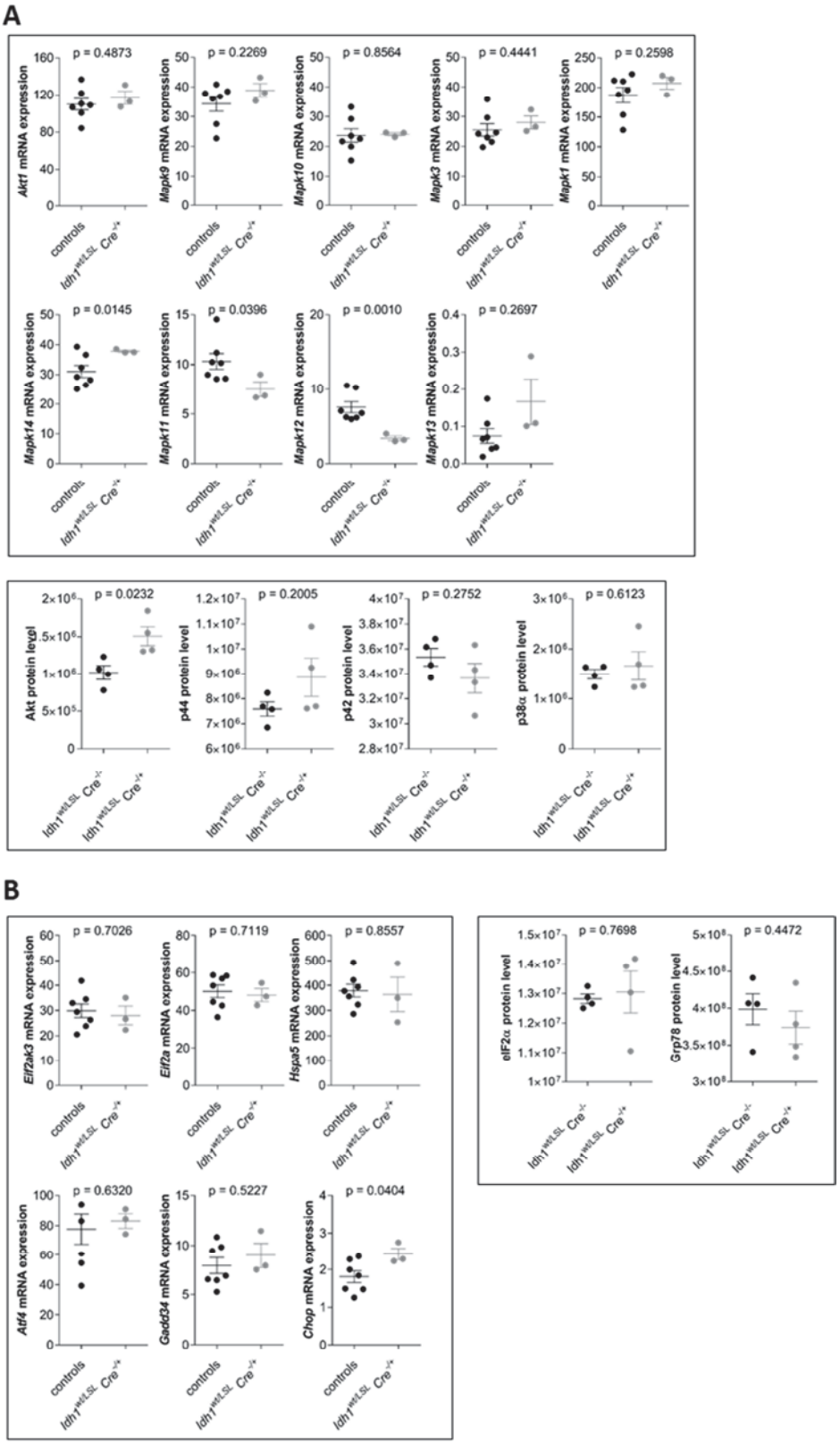

Fig. 3.29: Stress-responsive signaling in *Idh1*-mutant knock-in NSC/NPCs (2)

Experiments and analyses were performed as described in **Fig. 3.28**. **(A)** Expression of selected Akt and Mapk signaling molecules (upper box: RNA sequencing, lower box: proteomics). Corresponding results of 2-HG-treated cells are shown in **Fig. 3.21**. **(B)** Expression of selected candidates involved in the integrated stress response (left box: RNA sequencing, right box: proteomics). Corresponding results of 2-HG-treated cells are shown in **Fig. 3.22**.

2-HG-treated NSC/NPCs showed significantly diminished p70S6 protein levels, whereas total 4E-BP1 showed significantly higher abundance compared to the controls **(Fig. 3.24)**. No significant alterations for these genes were detected in the RNA sequencing and proteomic data from *Idh1*-mutant knock-in NSC/NPCs **(Fig. 3.30 A).** For 2-HG-treated NSC/NPCs, significantly reduced mRNA expression levels of the cell cycle regulator-coding genes *Cdkn1c* and *Cdkn2c* were observed **(Fig. 3.26)**. Compared to the controls, a significantly increased mRNA expression of *Cdkn1a,* coding for p21, as well as a significantly decreased mRNA expression of *Cdkn1c*, coding for p57*,* were observed in *Idh1*$^{wt/LSL}$ *Cre*$^{-/+}$ NSC/NPCs (p = 0.0234, p = 0.0290, p = 0.2242 respectively) **(Fig. 3.30 B)**.

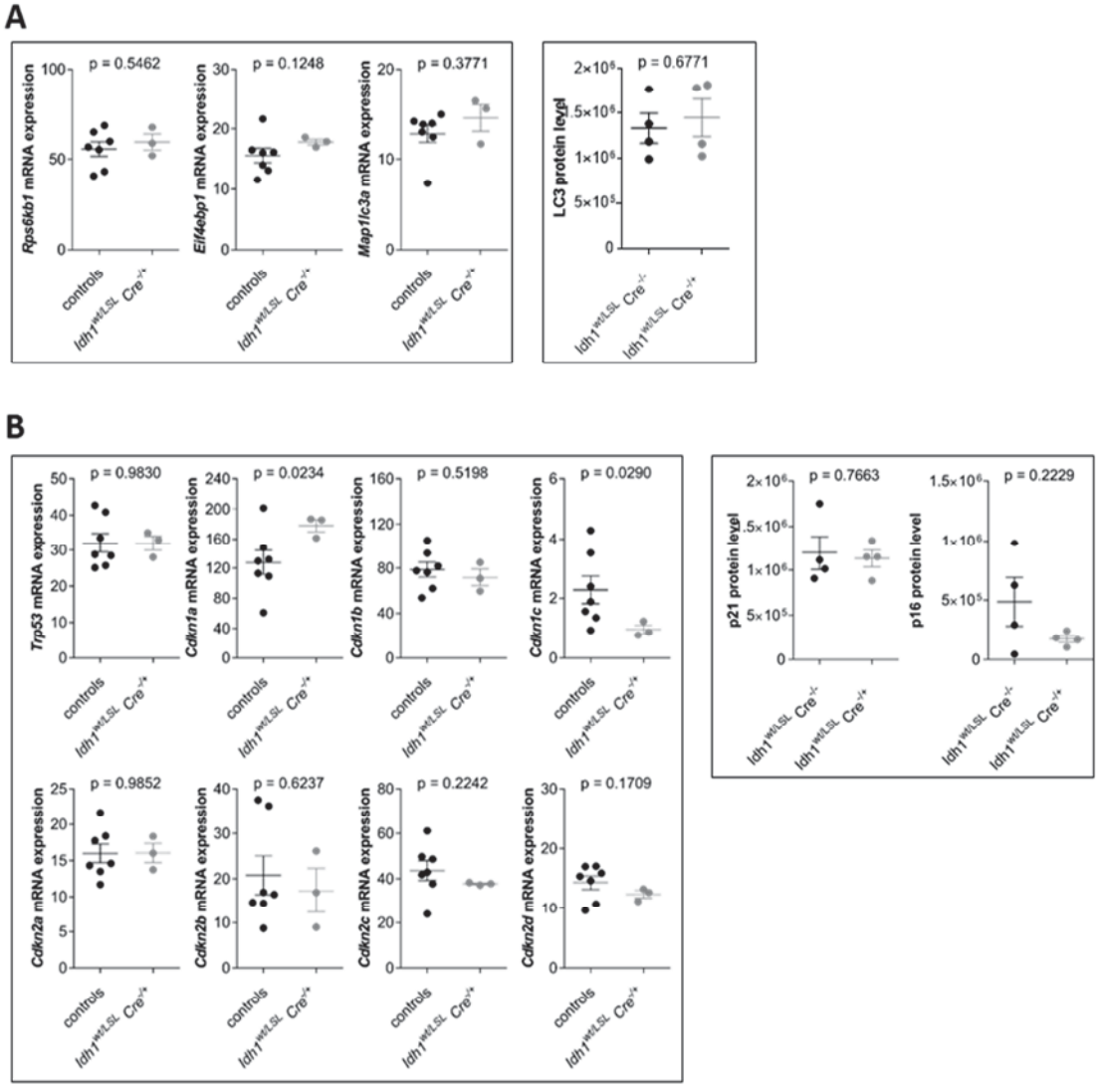

Fig. 3.30: Expression of genes involved in mTorc1 signaling and cell cycle regulation in *Idh1*-mutant knock-in NSC/NPCs

Experiments and analyses were performed as described in **Fig. 3.28**. **(A)** Expression of selected mTorc1 signaling mRNAs/proteins (left box: RNA sequencing, right box: proteomics). Corresponding results of 2-HG-treated cells are shown in **Fig. 3.24**. **(B)** Expression of selected cell cycle regulators (left box: RNA sequencing, right box: proteomics). Corresponding results of 2-HG-treated cells are shown in **Fig. 3.26**.

4.0 DISCUSSION

Heterozygous mutation of *IDH1*, coding for a metabolic enzyme located in the cytosol and in the peroxisomes, is the most frequent mutation in diffuse astrocytic and oligodendroglial gliomas of WHO grade II or III, and a subset of glioblastomas[13,16,17,45]. Wildtype IDH1 converts isocitrate to α-KG, thereby reducing $NADP^+$ to NADPH, which is important for the redox homeostasis of the cell[35,36]. The vast majority of *IDH1* mutations affect the arginine residue R132 in the active site of the enzyme, resulting in a gain-of-function mutation with increased affinity for α-KG and NADPH, wherefore the NADPH-consuming conversion of α-KG to 2-HG is favored[17,45,48-50,52]. Although several studies reported on possible oncogenic potential of 2-HG in glioblastoma cell lines and other models[101,475,476], an appropriate model reflecting relevant circumstances in human gliomas *in situ*, like a heterogeneous expression of a mutant *IDH1* allele under the endogenous promoter as well as no glioblastoma-associated background mutations, is missing. To characterize the molecular and cellular roles of mutant IDH1 proteins in an appropriate model, NSC/NPC cultures derived from a conditional *Idh1*-mutant knock-in mouse model were used.

4.1 Limitations of the use of NSC/NPCs from conditional *Idh1*-mutant knock-in mice

Conditional knock-in models using the $CreER^{tam}$/*loxP* recombinase system allow for a tight temporal regulation of recombination events and hence are a commonly used genome-tailoring tool[349]. Recombination between two *loxP* sites is induced by a 4-OHT-mediated activation of the Cre recombinase[349,356,357,362]. For validation of the system used in this thesis, a PCR assay detecting the *Idh1*-wildtype allele, the *Idh1*-mutant allele with the *LSL* sequence and the recombinant *Idh1*-mutant allele was performed after treatment with 4-OHT **(Fig. 3.2)**. Additionally, metabolite levels of the oncometabolite 2-HG after 4-OHT treatment were measured by mass spectrometry **(Fig. 3.3)**.

Although the activation of Cre recombinase with 4-OHT resulted in recombinant alleles in $Idh1^{wt/LSL}$ $Cre^{-/+}$ NSC/NPCs, a high number of cells with non-recombinant *LSL* alleles remained **(Fig. 3.2)**. Thereby, the efficiency of recombination differed among the used NSC/NPC cultures, showing the first limitation of the system. The heterogeneity of generated cell populations, consisting of *Idh1*-mutant cells as well as of non-recombinant cells, might result in variable experimental outcomes, as effects of the *Idh1* mutation are

potentially overlayed by the remaining background of non-recombinant *Idh1*$^{wt/LSL}$ *Cre*$^{-/+}$ NSC/NPCs. Therefore, only strong effects mediated by Idh1 mutation are likely to be detectable. The inefficient recombination might result from inaccessible promoter regions of *Idh1* in *Idh1*$^{wt/LSL}$ *Cre*$^{-/+}$ NSC/NPCs. Since the *Idh1* promoter contains a CpG island, epigenetic regulation might be possible[477]. However, Idh1 is highly abundant in *Idh1*$^{wt/LSL}$ *Cre*$^{-/+}$ NSC/NPCs (data not shown), wherefore no evidence is provided for this hypothesis. An additional reason for the incomplete recombination might be an insufficient activation of Cre recombinase in single NSC/NPCs or the lack of expressed Cre recombinase. However, even the expression of constitutively active Cre recombinase in *Idh1*$^{wt/LSL}$ NSC/NPCs was not sufficient for complete recombination of all *Idh1*-mutant alleles (unpublished data, C. B. Knobbe-Thomsen).

The second limitation of the used conditional *Idh1*-mutant knock-in system is the loss of recombinant cells over time in culture. Already 10 days after Cre recombinase activation with 4-OHT, only a small amount of recombinant cells remained within the *Idh1*$^{wt/LSL}$ *Cre*$^{-/+}$ NSC/NPC population **(Fig. 3.2)**. Besides the confirmation of functional mutant Idh1 by increased metabolite levels of 2-HG after recombination, metabolomic studies also revealed a decrease of 2-HG over time, validating the observed effects of vanishing recombinant NSC/NPCs from the cell population **(Fig. 3.3)**. The loss of the recombinant allele and consequently decreased 2-HG levels indicate a disadvantage in survival for *Idh1*-mutant NSC/NPCs. This effect was not 4-OHT-mediated, since *Idh1*$^{wt/LSL}$ NSC/NPCs transfected with constitutively active Cre recombinase did not show stably recombinant cells either (unpublished data, C. B. Knobbe-Thomsen). The results are consistent with the observation, that the *IDH1* mutation never appears to be the only mutation in diffuse gliomas, but is accompanied by specific additional mutations, like mutations in *P53* and *ATRX* or TERT promoter mutation and losses of 1p19q[1,11,12]. Furthermore, *Idh1* mutation alone was not sufficient for the induction of gliomagenesis during *in vivo* experiments[28,32,33]. Moreover, *IDH1*-mutant glioma cells were difficult to propagate in *in vitro* cultures, since mutant cells were eliminated from the population after passaging[478,479]. In 2017, five of eighty *IDH1*-mutant gliomas of WHO grades III-IV were successfully cultured for more than ten passages under serum-free conditions by Verheul and colleagues[480]. However, the underlying reason for the difficulties in culturing *IDH1*-mutant gliomas is not known so far[480].

As it was not possible to generate stable *Idh1*-mutant NSC/NPCs with the used model and the initially used workflow, the latter was changed to Cre recombinase activation prior to each experiment, in order to perform experiments with an at least in parts *Idh1*-mutant population of NSC/NPCs. As most of the 4-OHT-treated NSC/NPCs died shortly after

treatment, the third limitation of the used system is the cytotoxic effect of 4-OHT on NSC/NPCs, which might also affect and modulate *Idh1* mutation-mediated effects and further impede the molecular and functional characterization of the mutation in these cells.

4.2 Cytotoxic effect of 4-OHT on NSC/NPCs

The activation of Cre recombinase by 4-OHT was accompanied by cell death and reduced cell numbers of cultured NSC/NPCs. Cre recombinase-mediated growth-inhibiting genotoxic and cytotoxic effects have already been reported[481-483]. To exclude possible effects mediated by the *Idh1* mutation or active Cre recombinase, $Idh1^{wt/wt}$ $Cre^{-/-}$ NSC/NPCs were used for the evaluation of the toxic effects of 4-OHT on NSC/NPCs.

4.2.1 4-OHT-mediated cytotoxicity on NSC/NPCs is ER-independent

4-OHT treatment resulted in reduced cell numbers at commonly used concentrations for Cre recombinase activation **(Fig. 3.5)**. This might be due to either anti-proliferative or cell death-inducing effects. As the sensitivity to 4-OHT treatment markedly varied among the tested cell cultures, strong interindividual differences between the different NSC/NPC cell batches are assumed. Since the least sensitive NSC/NPC 275 cells were derived from a female mouse, whereas the NSC/NPC 117 and 191 cells were derived from male mice, and as 4-OHT is a known SERM[398,484], the ER-dependency of the cytotoxic effect was examined. The endogenous estrogen β-ES and 4-OHT bind ERs with equal affinities[372], wherefore a co-incubation should result in an increased cytotoxicity in case of an agonistic effect of 4-OHT or in a decreased cytotoxicity in case of an antagonistic effect of 4-OHT. In 2013, Chen and colleagues already reported an ER-dependent cytotoxic effect of tamoxifen on human glial progenitor cells, which was partly reduced by adding equal concentrations of β-ES to the cells[454]. However, the co-incubation of 4-OHT with β-ES in mouse NSC/NPCs did not modulate the cytotoxic effect of 4-OHT, assuming an ER-independent effect on cell viability or cell proliferation **(Fig. 3.6)**.

4.2.2 4-OHT treatment induces autophagic and apoptotic cell death in NSC/NPCs

ER-independent cytotoxic effects on brain cells have been repeatedly reported for 4-OHT and have been attributed to different kinds of cell deaths. In numerous tissues, 4-OHT treatment resulted in ER-independent autophagic cell death[409,485,486]. In own experiments, 4-OHT treatment of NSC/NPCs indeed resulted in significantly elevated protein levels of the autophagy marker LC3II **(Fig. 3.7 A, B)** indicating an activation of the autophagic cascade. However, autophagy does not only refer to ongoing cell death but even more likely to pro-survival signaling, regulating the catabolism of damaged or misfolded proteins and macromolecules and serving as a refueling pathway in case of insufficient nutrient, energy and building block demand[255,487]. Whether increased LC3II levels in 4-OHT-treated NSC/NPCs indicated autophagic cell death or rather pro-survival signaling remained therefore unsolved. However, since the inhibition of autophagy partly attenuated the cytotoxic effect of 4-OHT in three independent NSC/NPC cultures **(Fig. 3.7 C)**, autophagy might at least be involved in 4-OHT-induced cell death in NSC/NPCs.

Besides the mediation of an ER-independent autophagic cell death, 4-OHT treatment has been associated with ER-independent activation of apoptotic cell death, for instance via the activation of NF-κB[400,418,457]. Some studies also reported on ER-independent 4-OHT-mediated activation of caspases, while this feature did not result in an essentially apoptotic cell death[409,486]. By investigating the effect of 4-OHT treatment on apoptotic cell death in NSC/NPCs, diverse outcomes for the distinct cell batches were detected **(Fig. 3.8 A, B)**. Whereas one NSC/NPC culture showed a concentration-dependent increase in apoptotic cell death, increased levels of Annexin V-stained NSC/NPCs resulted from 4-OHT treatment with 0.5 µM, and unaltered fractions of apoptotic cells were found after 2 µM 4-OHT treatment in one other NSC/NPC culture. The third NSC/NPC culture showed even a slight decrease for Annexin V-stained cells after 4-OHT treatment with 0.5 µM and 2 µM. However, the percentage of double-stained NSC/NPCs, labeling cells in late apoptosis, increased for all 4-OHT-treated cell cultures. In combination with generally reduced 4-OHT-mediated cytotoxicity in NSC/NPCs treated with the apoptosis inhibitors DEVD and VAD, a contribution of apoptosis to 4-OHT-mediated cell death of NSC/NPCs is probable, although also this is highly dependent on the individual cell cultures **(Fig. 3.8 C)**. 4-OHT-induced necrotic cell death seems to be rather unlikely, since the number of cells solely stained with 7-AAD did not change after 4-OHT treatment. Since neither autophagy nor apoptosis alone was responsible for 4-OHT-mediated cell death in NSC/NPCs, the induction of both kinds of cell death by 4-OHT is likely, making it difficult

to define a potential trigger for the 4-OHT-mediated cytotoxicity and to overcome this cytotoxic effect.

4.2.3 4-OHT treatment affects Jak/Stat signaling and NF-κB signaling in NSC/NPCs

In order to further characterize the cytotoxic effect and the type of cell death mediated by 4-OHT on NSC/NPCs, microarray-based expression profiling was performed for comparison of 4-OHT-treated and –untreated *Idh1*$^{wt/wt}$ *Cre*$^{-/-}$ NSC/NPCs. Due to the interindividual differences of the individual NSC/NPC cultures, paired t-test analyses had to be performed **(Fig. 3.9 A)**. Although the expression of several genes was significantly altered, enrichment analyses did not reveal striking indications for one or the other kind of cell death or for one or another signaling pathway responsible for the cellular outcome. Solely lysosome KEGG signaling was significantly enriched, underlining the partially mediated autophagic cell death by 4-OHT treatment. Screening for single significantly regulated candidate genes, *Socs2* mRNA expression levels were found to be upregulated in all tested NSC/NPC cultures after 4-OHT treatment **(Fig. 3.9 B, C)**. Socs2 is known as the main negative regulator of cytokine and growth factor signaling, and is expressed in a feedback loop upon Jak/Stat signaling[488-495]. Thus, its expression induction points to the activation of Jak/Stat signaling by 4-OHT. Socs2 binds to phosphorylated tyrosine residues of activated Jak, associated with cytokine and growth hormone (GH) receptors[494,496-498]. This binding results in a block of the Stat activation site within Jak as well as in the targeting of Jak for proteosomal degradation by Socs2, functioning as ubiquitin ligase[494,496-498]. *SOCS2* mRNA expression was already shown to be upregulated by estrogen signaling, resulting in the inhibition of GH signaling via the JAK/STAT signaling pathway[499]. Whether this effect was ER-dependent or –independent was not elucidated[500]. However, for 4-OHT treatment, the opposite effect is described on GH signaling in HEK293 cells[499]. GH signaling was SOCS2-independently enhanced 1-2 h after 4-OHT treatment[499]. Although *Socs2* mRNA expression obviously increased in 4-OHT-treated NSC/NPCs, protein levels of phosphorylated Stat3 increased instead of decreased after 4-OHT treatment **(Fig. 3.10)**. The findings of the kinase inhibitor screen pointed into the same direction, since 4-OHT attenuated the cytotoxic effect of the Jak2 inhibitor AG 490, assuming a 4-OHT-mediated AG 490-opposing effect of Jak2/Stat3 activation **(Fig. 3.11 A)**. The co-incubation of 4-OHT with AG 490 attenuated *vice versa* the cytotoxicity of 4-OHT, moreover assuming the involvement of Jak2/Stat3 signaling in 4-OHT-mediated cell death **(Fig. 3.11 C)**. However, all these results point towards Jak2/Stat3-activating effects of 4-OHT instead of inhibiting functions of Socs2 in 4-OHT-

treated NSC/NPCs. Although increased levels of Socs2 were mostly associated with an inhibitory effect on Jak2/Stat3 signaling[489-495], in the last years several studies have been published that reported on an activating effect of heavily increased Socs2 on growth hormone signaling[490,495,501,502]. This dualistic effect may be due to differing affinities for possible binding partner. Besides binding the phosphotyrosine residues of the GH receptor and Jak, Socs2 binds and inhibits also other Jak/Stat signaling-inhibiting Socs proteins, thereby leading to enhanced cytokine and GH signaling[495,503-505].

Interestingly, 4-OHT moreover strengthens the cytotoxic effect of IKK 16, an indirect inhibitor of NF-κB **(Fig. 3.11 B, C)**. IKK 16 inhibits IKKs, resulting in the stabilization of IκBs and the consequent inhibition of NF-κB[462]. Similar effects were described for tamoxifen treatment in neural tissue, which also resulted in a decreased phosphorylation of IκBs and a consequent inhibitory effect on NF-κB[407]. Furthermore, persistently activated Stat3 signaling as well as Socs2 inhibit IKK/NF-κB signaling[281,506,507]. The amplified cytotoxic effect of NF-κB inhibition by 4-OHT might therefore result from a 4-OHT-mediated Stat3 signaling activation, the consequent expression of Socs2 and the consequent Stat3 signaling- and Socs2-dependent inhibition of IKK. In contrast to Socs2, Socs1 and Socs3 activate NF-κB signaling[508], wherefore a Socs2-mediated inhibition of NF-κB signaling would again point to an inhibitory effect of Socs2 on Socs1 and Socs3.

4.2.4 4-OHT-mediated apoptotic and autophagic cell death might result from NF-κB signaling inhibition

Stat3 as well as NF-κB are involved in pro-survival and anti-apoptotic signaling by regulating the transcription of autophagy- and apoptosis-related genes[266-269]. Numerous genes are thereby regulated by both transcriptions factors. Amongst the positively regulated genes is, for instance, the anti-apoptotic gene *Bcl-2*, while the expression of pro-apoptotic *p53* as well as pro-autophagic *Bcl2-interacting protein 3* (*Bnip3)* is repressed by both transcription factors[281,509]. NF-κB activity is furthermore accompanied by increased p62 expression and accumulating autophagosomes as well as by induced mTORC1 signaling, further indicating inhibited autophagy[268,280,510]. The inhibition of NF-κB signaling consequently induces the lipidation of LC3 and autophagic cell death as well as apoptotic cell death[511-513]. Since active NF-κB is moreover leading to the expression of cyclin D1 and consequent cell cycle progression, and as the inhibition of NF-κB or cyclin D1 leads to an impaired G1-phase to S-phase transition[514-517], it is not surprising that 4-OHT-treated NSC/NPCs arrested in G0/G1-phase of the cell cycle **(Fig. 3.13)**. Therefore

4-OHT-mediated autophagy, apoptosis and G0/G1 cell cycle arrest in NSC/NPCs might result from the inhibition of NF-κB signaling. If this inhibition is truly mediated by the activation of Stat3 and the induction of Socs2 in 4-OHT-treated NSC/NPCs, a co-incubation of 4-OHT and AG 490 would result in attenuated NF-κB inhibition as well as in potentially attenuated cell death of 4-OHT-treated NSC/NPCs, as it was shown in **Fig. 3.11 C**. However, although the co-incubation of 4-OHT and AG 490 resulted on average in reduced protein levels of phosphorylated Stat3 and led to reduced Socs2 protein levels compared to 4-OHT-treated NSC/NPCs, LC3II protein levels were further increased in 4-OHT- and AG 490-treated NSC/NPCs **(Fig. 3.12)**. However, elevated LC3II levels might either be indicative for increased autophagic cell death or for decreased autophagic cell death and the consequent accumulation of lipidated LC3II[518]. Thus, further experiments are needed to elucidate the impact of the co-incubation with AG 490 on 4-OHT-mediated cell death in NSC/NPCs.

4.3 Characterization of *Idh1* mutation using NSC/NPCs from a conditional knock-in mouse model

In the last years, numerous studies about the effects of mutant *Idh1* were performed. However, most experiments were done in glioblastoma cell lines transfected with overexpressed wildtype or mutant *IDH1*[63,423-425]. These models, however, do not reflect the natural situation of IDH mutations found in gliomas or AML patients, in which the mutation is always heterozygous and the mutant protein forms heterodimers with its wildtype counterpart[52]. Furthermore, glioblastoma cell lines in general emerge from IDH-wildtype glioblastomas harboring numerous other mutations and hence a wrong genetic background for IDH mutations, making it difficult to characterize IDH-mediated effects in an appropriate pathophysiological environment. As NSCs were shown to be more similar to dissected glioma cells and as IDH mutation is believed to be among the first mutations to occur in gliomagenesis[1,16,17,30,31], murine NSC/NPCs with a conditional knock-in of mutant *Idh1* were used for *in vitro* molecular and functional characterization of mutant *Idh1*.

4.3.1 *Idh1*-mutant NSC/NPCs show induced stress-responsive *Hmox1* expression

To investigate *Idh1* mutation-induced alterations in NSC/NPCs, RNA sequencing was performed with 4-OHT-treated *Idh1*$^{wt/wt}$ *Cre*$^{-/-}$, *Idh1*$^{wt/wt}$ *Cre*$^{-/+}$, *Idh1*$^{wt/LSL}$ *Cre*$^{-/-}$ and *Idh1*$^{wt/LSL}$ *Cre*$^{-/+}$ NSC/NPCs. Comparable to the effects observed in the microarray analyses of 4-OHT-treated *Idh1*$^{wt/wt}$ *Cre*$^{-/-}$ NSC/NPCs, interindividual background was detected among the cells of the different genotypes **(Fig. 3.14 A, B)**. Since the controls did not cluster according to their genotypes, all controls were combined and compared against the knock-in NSC/NPCs which clustered together **(Fig. 3.14 C)**. By performing enrichment analyses for exclusively expressed genes in either the controls or the *Idh1*$^{wt/LSL}$ *Cre*$^{-/+}$ NSC/NPCs with the PANTHER enrichment tool, significant expression differences were detected for many genes. However, most results concerned rather universal processes in cells, without hinting to specifically involved processes or processes that had been connected to already reported effects of *Idh1* mutation, like those affecting ROS homeostasis, DNA damage or endoplasmic reticulum stress signaling. By comparing the exclusively expressed genes for either the controls or the knock-in cells with the proteomic data sets from Dr. Nina Overbeck (MPL, BMFZ) obtained within her Ph.D. thesis entitled 'Charakterisierung der Isocitrat-Dehydrogenase 1 im Zusammenhang der Tumorgenese von Gliomen mithilfe der Proteomanalyse', no coincidences were detected for regulated candidates in *Idh1*-mutant NSC/NPCs at the RNA and protein levels. Further on, significantly overexpressed and repressed genes among the commonly expressed genes in the knock-in cells and the controls were detected and also compared to the proteomic data set **(Tab. 3.1, Fig. 3.15 A, B)**. Four genes and the encoded proteins were consistently altered within the RNA sequencing and the proteomic data set. Cd93 was significantly downregulated at the RNA and protein levels in *Idh1* knock-in cells. However, Cd93 was shown to be elevated in glioblastoma, regulating glioma angiogenesis and vascular function[519]. Furthermore, high Cd93 levels have been associated with worse outcome for glioma patients[520]. Since IDH-mutant glioma patients show better survival rates than IDH-wildtype glioma patients[17,34], the decreased abundance of Cd93 in *Idh1*-mutant cells might be associated to the underlying effects. For Kctd12 and Arsb no relations to gliomas were described until now, however, a role for KCTD12 was reported for several cancers[521-523]. Since KCTD12 reduces the stemness of cancer stem cells[522,523] and is associated with a better outcome in renal cancer[520], it might also play a role in the better outcome of IDH-mutant gliomas. However, *Hmox1* was the most interesting candidate. It codes for a heat shock protein induced by four main transcription factors - Nrf2, Ap-1, Hsf1 and NF-κB - in response to cellular stresses[157]. Possible activators of these transcription factors are the Mapks p42/44, Jnk and p38 in response to cellular

stresses like oxidative stress[157,204-210]. Furthermore, a direct activation by ROS was described[174,178,524]. Since glioma-associated mutations of *Idh1* result in the consumption of NADPH[49], elevated ROS levels and the consequent activation of stress-responsive signaling might be reasonable. HMOX1 was moreover found to be one of five surface markers elevated in glioblastoma cancer stem cells compared to NSCs[187]. Therefore, the enhanced expression of *Hmox1* in *Idh1*-mutant NSC/NPCs might indicate a step towards gliomagenesis, corresponding to the hypothesis that *Idh1* is the first mutation occurring in this process[1,16]. Increased levels of *HMOX1* in diffuse and anaplastic gliomas as well as glioblastomas relative to non-neoplastic brain tissue further point to a relevant effect in glioma pathogenesis **(Fig. 3.15 C)**.

Studies examining the connection between gliomas and HMOX1, showed a positive correlation between HMOX1 levels and tumor grade, invasiveness and stemness, making it to an interesting candidate to elucidate[186,187,525-527]. During the last years, several studies were published, hypothesizing that the inhibition of the *HMOX1*-inducing NRF2 could be a possible treatment option for glioblastomas, since this in turn leads to the sensitization of the tumor cells to temozolomide treatment by favoring apoptotic cell death[188,189,528]. Although numerous studies followed up on the connection between HMOX1 and gliomas, most data did not consider a potential role of the IDH status in HMOX1 induction, focusing on the differences between IDH-wildtype and IDH-mutant tumors instead of comparing IDH-mutant cells to normal brain tissue. *NRF2* expression as well as the expression of *NRF2*-target genes correlate negatively with *IDH1* mutation in anaplastic glioma and in IDH1-R132H-transfected glioblastoma cell lines[529,530]. This effect is reflected by the *HMOX1* mRNA expression levels in the patient tissue samples investigated by Toedt and colleagues[465], where IDH-mutant gliomas showed increased *Hmox1* expression levels compared to normal brain but lower *Hmox1* expression levels compared to IDH-wildtype glioblastomas **(Fig. 3.15 C)**. Since high NRF2 levels as well as elevated NRF2-target gene expression are associated with worse progression-free survival and overall survival rates in astrocytoma patients, and an inhibition of NRF2 signaling sensitizes glioma cells to temozolomide treatment[189,530,531], lower NRF2 levels in IDH-mutant cells might contribute to the better overall outcome of patients with IDH-mutant gliomas[530]. High NRF2 signaling and HMOX1 expression levels in IDH-wildtype glioblastomas might result from specific genetic alterations within these tumors, like *EGFR* amplification. It has already been shown, that EGFR signaling enhances NRF2 signaling in cancer cells[532,533]. Furthermore, loss of PTEN *function* by *PTEN* mutation and/or deletion results in induced NRF2 signaling[534,535]. Also, P53 has been linked to NRF2 signaling[536-538]. Under conditions of mild stress, wildtype P53 induces p21 expression, disrupting NRF2-inhibition by KEAP1 and consequently activating NRF2 signaling. However, under severe stress conditions,

wildtype P53 represses pro-survival NRF2 signaling and induces apoptosis[536-538]. Since gliomas and glioblastomas show frequent gain-of-function mutations of P53, leading to the differential expression of NRF2 target genes[344,536], a possibly altered regulation of NRF2 signaling by mutant P53 is likely in these tumors.

4.3.2 *Idh1*-mutant NSC/NPCs show increased 2-HG and decreased glycolate metabolite levels

Numerous studies with Idh-mutant cells showed alterations on metabolite levels compared to wildtype cells[28,64,539]. As expected, metabolomic studies with 4-OHT-treated *Idh1*$^{wt/wt}$ *Cre*$^{-/-}$, *Idh1*$^{wt/wt}$ *Cre*$^{-/+}$, *Idh1*$^{wt/LSL}$ *Cre*$^{-/-}$ and *Idh1*$^{wt/LSL}$ *Cre*$^{-/+}$ NSC/NPCs revealed significantly increased 2-HG metabolite levels in *Idh1*$^{wt/LSL}$ *Cre*$^{-/+}$ NSC/NPCs **(Fig. 3.16 A)**. As already noticed by PCR **(Fig. 3.2)**, recombination efficiency and manifestation of the mutant phenotype differed between different NSC/NPC cultures. Although 2-HG metabolite levels were obviously increased in the *Idh1*$^{wt/LSL}$ *Cre*$^{-/+}$ NSC/NPCs, the extent of this effect differed strongly between different cultures, pointing again to the difficulty of detecting comparable *Idh1* mutation- and 2-HG-mediated results for multiple cell cultures within the used system. Detectable results have to be really strong to overcome interindividual differences and the manifested phenotype. Also, for several metabolites high variances were detected that could not be attributed to the different genotypes.

Among the amino acids **(Fig. 3.16 B)**, no significant differences were observed between the *Idh1*$^{wt/LSL}$ *Cre*$^{-/+}$ NSC/NPCs and the controls. Slightly decreased proline metabolite levels might point toward amino acid catabolism in order to replenish Idh1 mutation-dependent α-KG consumption[70]. However, since α-KG and also glutamine were not detected by mass spectrometry, further hints supporting this hypothesis are missing. Contradictory, the increased synthesis of glutamine-derived proline was shown for transfected IDH-mutant human anaplastic oligodendroglioma compared to IDH-wildtype cells[539]. This was attributable to an increased expression of pyrroline 5-carboxylate reductase 1, which was moreover also found increased in IDH-mutant gliomas compared to IDH-wildtype gliomas[539]. However, other factors like additional mutations might have influenced this effect. Increased methionine and phenylalanine metabolite levels, as shown for knock-in NSC/NPCs compared to the controls, have already been reported for IDH1-mutant or 2-HG-treated cells, however, these effects were affiliated to gene methylations[479]. Since the establishment of a hypermethylation phenotype was observed to occur first after fifteen passages[110], epigenetic changes might not be reasonable for the

observed effects in the NSC/NPCs. Decreased α-alanine metabolite levels were not linked to IDH mutation so far.

Among other metabolites **(Fig. 3.16 C)**, glycolate levels were significantly decreased in *Idh1*$^{wt/LSL}$ *Cre*$^{-/+}$ NSC/NPCs. This effect was not linked to IDH mutation so far. However, the hypermethylation and consequent suppression of the enzyme glyoxylate reductase / hydroxypyruvate reductase, catalyzing the reaction from glyoxylate to glycolate in an NADPH-wasting step, was found to induce glioma cell death[540,541]. This potentially indicates that a decreased glycolate metabolite level in Idh1-mutant tumors might also induce cell death. Reduced glycolate levels might thereby be attributable to decreased NADPH levels that were already described for Idh1-mutant cells[58]. Additional non-significant changes were observed for metabolites branching from or into glycolysis being in general rather decreased in *Idh1*$^{wt/LSL}$ *Cre*$^{-/+}$ NSC/NPCs compared to the controls. When compared to IDH-wildtype gliomas and normal brain, IDH-mutant gliomas show a reduced glucose turnover[542]. Decreased lactate levels were moreover detected in IDH1-mutant overexpressing glioblastoma cell lines compared to IDH1-wildtype overexpressing glioblastoma cell lines[425]. It was already described that IDH-mutant glioma cell lines show a metabolic phenotype that relies less on glycolysis than IDH-wildtype gliomas[543]. However, the metabolic phenotype is influenced by many factors and further mutations of the tested cells have to be taken into account. For the experiments with *Idh1*$^{wt/LSL}$ *Cre*$^{-/+}$ NSC/NPCs, many metabolites were not detected by mass spectrometry, making it difficult to draw conclusions about the metabolic phenotype of Idh1-mutant NSC/NPCs.

4.4 Validation of *Idh1* mutation-dependent effects by 2-HG treatment of NSC/NPCs

Since the conditional *Idh1*-mutant knock-in mouse model showed limitations, like the incomplete recombination or the sensitivity of the NSC/NPCs against 4-OHT **(Fig. 3.2, Fig. 3.3, Fig. 3.5)**, an alternative model was used to validate the *Idh1* mutation-induced *Hmox1* expression and to further elucidate possible underlying mechanisms. Therefore, *Idh1*$^{wt/wt}$ *Cre*$^{-/-}$ NSC/NPCs were treated with a membrane-permeable derivative of 2-HG.

4.4.1 *Hmox1* overexpression was validated in 2-HG-treated NSC/NPCs

A sublethal concentration of 2-HG was determined by MTT assays and further on used for NSC/NPCs treatment. Surprisingly, the NSC/NPCs were very sensitive to 2-HG treatment **(Fig. 3.17)**. Although concentrations of 2-HG found in tumor tissue range from around 5 to 35 mM[49,97], the IC_{50} for NSC/NPCs was within the micromolar range, which might be due to the cell culture microenvironment, the lack of additional mutations or a deviant differentiation state of the tumor cells, all of which are factors that might desensitize tumor cells to 2-HG. The carrier octyl-group of the used 2-HG might moreover mediate a toxic effect on NSC/NPCs. In lack of an appropriate control, a possible involvement of the carrier octyl-group on the cytotoxicity of 2-HG on NSC/NPCs cannot be excluded. The sensitivity to 2-HG treatment furthermore highly varied among the respective NSC/NPC cultures. At the end, a concentration of 0.4 µM 2-HG was chosen for NSC/NPC treatment. In accordance to RNA sequencing data as well as proteomic data of the knock-in NSC/NPCs, 2-HG treatment of *Idh1*$^{wt/wt}$ *Cre*$^{-/-}$ NSC/NPCs caused elevated Hmox1 mRNA and protein levels **(Fig. 3.18 A-C)**. Furthermore, additional downstream targets of *Hmox1*-inducing transcription factors, like *Gclc*, *Gclm* and *Mdm2* were elevated at the mRNA level in 2-HG-treated *Idh1*$^{wt/wt}$ *Cre*$^{-/-}$ NSC/NPCs as well as in knock-in NSC/NPCs **(Fig. 3.18 A, Fig. 3.28 A)**, pointing to an effect of 2-HG on the activation of stress-responsive transcription factors like Nrf2, Ap-1, Hsf1 or NF-κB[157]. Numerous triggers are known to result in the activation of these transcription factors and in *Hmox1* expression.

4.4.2 2-HG treatment of NSC/NPCs results in elevated ROS levels

The transcription factors NF-κB, Nrf2, Ap-1 and Hsf1 that are potential activators of *Hmox1* transcription were shown to be activated for instance by a disturbed redox homeostasis and elevated ROS levels[161,171,178,184,544]. Subsequently expressed genes decrease the susceptibility of the cell to oxidative stress[545,546]. *Idh1*-mutant cells are predisposed to develop elevated ROS levels, since the conversion of α-KG to 2-HG utilizes NADPH, an important reduction equivalent for the antioxidative response of, for instance, glutathione peroxidase[41]. A decreased ratio for NADPH/$NADP^+$ and increased ROS levels, as already described in several studies[58,63,64], might therefore activate stress-responsive signaling pathways in *Idh1*-mutant knock-in NSC/NPCs. Since 2-HG itself was also described to induce oxidative stress[120,121], a ROS-induced *Hmox1* overexpression is also conceivable in 2-HG-treated *Idh1*$^{wt/wt}$ *Cre*$^{-/-}$ NSC/NPCs. As shown by DHE and DCF

assays, 2-HG treatment indeed resulted in increased ROS levels in *Idh1*$^{wt/wt}$ *Cre*$^{-/-}$ NSC/NPCs **(Fig. 3.19)**. The severity of this effect was again highly dependent on the distinct cell cultures. This might be due to a different stress-response, for instance for the NSC/NPC 275 cells. The lowest increase in ROS levels correlated with the highest increase in the stress-response gene expression of *Gclc* as well as with the highest protein levels of Hmox1, indicating a possible option of coping with high ROS levels. Elevated ROS levels were accompanied by the induced expression of genes encoding for antioxidative enzymes like Gpx4, catalase, Sod1, Sod2 and Sod3 **(Fig. 3.20 A)**. *Sod1*, *Sod2* and *Sod3* expression levels of 2-HG-treated *Idh1*$^{wt/wt}$ *Cre*$^{-/-}$ NSC/NPCs mirrored thereby the RNA sequencing results from *Idh1*-mutant knock-in NSC/NPCs **(Fig. 3.28 B)**. Correlating with its transcript expression, catalase protein levels were increased in 2-HG-treated NSC/NPCs **(Fig. 3.20 B, C)**. Elevated protein levels of catalase were moreover also detected in *Idh1*$^{wt/LSL}$ *Cre*$^{-/+}$ NSC/NPCs in the proteomic data sets from Nina Overbeck **(Fig. 3.28 B,** 'Charakterisierung der Isocitrat-Dehydrogenase 1 im Zusammenhang der Tumorgenese von Gliomen mithilfe der Proteomanalyse'**)**. Although catalase protein levels were unaltered in *Idh1*-mutant cells using Nestin expression as control, catalase activity was shown to be enhanced in these *Idh1*-mutant cells[64]. Similar effects were observed for *Idh2*-mutant leukemic cells in combination with elevated H_2O_2 levels[121]. Furthermore, induced *SOD2* levels were already reported for *Idh1*-mutant cells as mediated by the oncometabolite 2-HG[547], whereas *SOD1* and *SOD3* upregulation was not reported in connection to gliomas or IDH mutation so far. However, significantly induced *Sod3* expression levels in 2-HG-treated NSC/NPCs as well as in *Idh1*-mutant knock-in cells might be an additional hint for 2-HG-mediated transcriptional activity of Nrf2, as Sod3 is a Nrf2-target gene[548]. The results obtained for 2-HG-treated *Idh1*$^{wt/wt}$ *Cre*$^{-/-}$ NSC/NPCs point to a 2-HG-mediated induction of ROS that is not solely dependent on NADPH depletion. Elevated ROS levels might in turn induce the expression of *Hmox1* in NSC/NPCs.

4.4.3 p38 signaling is induced in 2-HG-treated NSC/NPCs

Besides the possible direct activation by ROS, the transcription factors NF-κB, Nrf2, Ap-1 and Hsf1 were also shown to be activated by several signaling pathways. Most frequently, Pi3k/Akt signaling, Mapk signaling via Jnk, p42/44 or p38, as well as Perk signaling in response to endoplasmic reticulum stress are involved, depending on the mediating factors and the tissue[468,549-552]. Overall, p38 signaling appears to be the most commonly mediating pathway for *Hmox1* expression[157,550]. Whereas Akt and Jnk signaling were not

consistently altered and pp42/44 protein levels even decreased in 2-HG-treated NSC/NPCs, protein levels of phosphorylated p38 increased in all three tested NSC/NPC cultures **(Fig. 3.21)**. Activation of p38 has not been linked so far to *Idh1* mutation, however, increased p38 signaling has been reported for gliomas and associated with a poor prognosis in glioblastoma patients[553]. Since the inhibition of p38 and the consequent inhibition of NRF2 signaling increased sensitivity of glioma cells to chemotherapeutics[188,553,554], it is likely that NRF2 signaling in gliomas may be regulated by p38 and that induction of *Hmox1* expression in 2-HG-treated NSC/NPCs might result from activation of p38. As p38 is also activated upon cellular stresses like increased ROS[470,555], the activation of p38 in NSC/NPCs might result from 2-HG-induced ROS levels **(Fig. 3.19)**.

2-HG treatment resulted not only in higher phosphorylation levels of p38 but also in decreased total p38 protein levels **(Fig.21)**. Similar results were obtained for the expression levels of *Mapk11* and *Mapk12,* coding for p38β and p38γ, in the *Idh1*-mutant knock-in NSC/NPCs **(Fig. 3.29 A)**. Expression of p38γ was shown to increase with tumor grade in gliomas and to be involved in pro-proliferative and anti-apoptotic mechanisms in several cancers[556]. Therefore, decreased *Mapk12* expression in *Idh1*-mutant NSC/NPCs as well as decreased total p38 protein levels in 2-HG-treated NSC/NPCs might point to an inhibitory effect on tumor progression by favoring apoptosis, possibly supporting the requirement of additional mutations for tumor initiation in *Idh1*-mutant cells.

4.4.4 2-HG treatment activates the integrated stress response in NSC/NPCs

An additional kinase involved in *Hmox1* expression is Perk[471]. Active Perk is able to phosphorylate Nrf2 in response to endoplasmic reticulum stress caused by oxidative stress and unfolded proteins. Nrf2 phosphorylation results in the dissociation of Nrf2 from its repressor Keap1 and induces nuclear translocation of Nrf2[471,557]. Since 2-HG-treated NSC/NPCs showed elevated ROS levels **(Fig. 3.19)**, an activation of Perk is likely. In addition, 2-HG possibly mediates Perk activation via the inhibition of α-KG dependent prolyl hydroxylases, resulting in the accumulation of unfolded proteins within the endoplasmic reticulum[64]. Zhang and colleagues already linked *Idh1*-mutant glioma-initiating cells to Perk signaling, since *Idh1* mutation-induced endoplasmic reticulum stress resulted in Perk signaling-mediated apoptotic cell death[447]. Unfortunately, the detection of phosphorylated Perk after 2-HG treatment in NSC/NPCs was not possible. However, downstream effects of Perk activation, like phosphorylation of the translation-initiation

factor eIF2α and the induced expression of Atf4, were observed **(Fig. 3.22 A-D)**, thus pointing to a potential involvement of Perk in Nrf2 activation and *Hmox1* gene expression after 2-HG treatment of NSC/NPCs. Since Grp78, one of the commonly used targets to monitor for endoplasmic reticulum stress in response to unfolded proteins[558], was not consistently overexpressed within the three tested NSC/NPC cultures after 2-HG exposure **(Fig. 3.22 C, D)**, the involvement of other eIF2α kinases like Gcn2, Prk or Hri[213] should also be considered for the 2-HG-mediated phosphorylation of eIF2α. Although Perk represents the major eIF2α kinase induced upon oxidative stress as well as the only eIF2α kinase induced by unfolded proteins, all eIF2α kinases were reported to phosphorylate eIF2α in response to elevated ROS[212,474,559].

Independently of the involved eIF2α kinase, the phosphorylation of eIF2α itself also might result in induced expression levels of *Hmox1* after 2-HG treatment. Active eIF2α is known to attenuate protein translation and proliferation since it prevents the formation of the ternary complex that transports the initiator methionyl-tRNAi^{Met} to the translation initiation side[560]. However, cap-independent translation via open-reading-frames is still ongoing under these conditions, leading to the selective increase of specific mRNAs[561]. This often involves non-AUG start codons[562,563]. One of the selectively expressed candidates and therefore a marker for cap-independent translation is Atf4, which is frequently overexpressed in tumor tissues[564,565]. As a transcriptional activator of the integrated stress response, Atf4 is known to induce the expression of cytoprotective genes like *Hmox1*[217]. Furthermore, an Atf4 / Nrf2 dimer was reported to regulate stress-induced *Hmox1* expression in several mammalian cell types[217,566]. Elevated eIF2α phosphorylation levels and an induced integrated stress response in *Idh1*-mutant cells have been reported[64,447]. Moreover, *Idh1* mutation in human astrocytes has been linked to a shut-down of global protein expression[567]. Since eIF2α phosphorylation as well as Atf4 mRNA and protein levels were induced by 2-HG treatment in NSC/NPCs **(Fig. 3.22)**, the integrated stress response leading to cap-independent translation may also play a role for elevated *Hmox1* expression. Also increased methionine metabolite levels in the Idh1-mutant knock-in NSC/NPCs might be a hint for cap-independent translation **(Fig. 3.16)**. The phosphorylation of eIF2α might occur upon oxidative stress and elevated ROS levels[212], wherefore the 2-HG-mediated increase in ROS is possibly involved in the activation of the integrated stress response. Furthermore, eIF2α phosphorylation might be mediated by activated p38 signaling via a p53-activating mechanism[197].

4.4.5 2-HG treatment results in cell cycle arrest and apoptotic cell death in NSC/NPCs

The integrated stress response induced by Atf4 is in first line a cytoprotective mechanism linked to autophagy since the expression of autophagy-related genes like LC3I and 4E-BP1 are favored[568-571]. LC3I as well as total 4E-BP1 protein levels were indeed elevated after 2-HG treatment **(Fig. 3.24)**. Slightly increased mRNA and protein levels were furthermore observed in the RNA sequencing data and proteomic data **(Fig. 3.30 A)**, further supporting a role of Idh1 mutation- or 2-HG-induced integrated stress response in NSC/NPCs. Increased total 4E-BP1 protein levels might also foster ongoing cap-independent translation. Unphosphorylated 4E-BP1 binds to and inhibits eIF4E, a part of the eIF4F complex, normally recruiting the ternary complex as well as the 40S ribosomal subunit to the cap-structure at the 5'-end of the mRNA[572]. Although 4E-BP1 and LC3I protein levels were increased, indicating induced integrative stress response, autophagy was not induced, since protein levels of the autophagy marker LC3II remained unaltered after 2-HG treatment of NSC/NPCs **(Fig. 3.24)**. Also the phosphorylation levels of 4E-BP1 and p70S6, as major indicators of mTorc1 activity[573], were unaffected by 2-HG treatment **(Fig. 3.24)**, thus 2-HG-induced autophagy in NSC/NPCs is unlikely.

However, the integrated stress response does not solely trigger cytoprotective autophagy. Under prolonged stress conditions, translation of apoptosis-inducing genes is favored[574,575], whereby the major Atf4-responsive gene connected to the induction of apoptotic cell death is *Chop*[576]. Induced *Chop* mRNA levels were observed in 2-HG-treated NSC/NPCs **(Fig. 3.22 E)** as well as in *Idh1*-mutant knock-in NSC/NPCs **(Fig. 3.29 B)**. Furthermore, 2-HG treatment resulted in apoptosis in all tested NSC/NPC cultures, whereas the severity of the effect differed **(Fig. 3.23)**. Both effects do not only support a role of an induced integrated stress response by *Idh1* mutation and 2-HG, but also indicate prolonged stress conditions which ultimately may result in apoptotic cell death. The pro-apoptotic effect of Chop is mainly attributable to induced expression of the pro-apoptotic gene *Gadd34* and to the inhibition of autophagy[220,577-579]. Interestingly, an involvement of activated p38 in induced *Chop* transcription is conceivable, as phosphorylated p38 favors the switch from autophagy to apoptosis under severe stress conditions. Therefore, active p38 directs Atf4 towards binding to the *Chop* promoter instead of favoring the transcription of *Map1LC3A*[197]. However, although *Chop* mRNA levels increased in all tested NSC/NPC cultures, its pro-apoptotic downstream target *Gadd34* was solely upregulated in two tested cultures after 2-HG treatment **(Fig. 3.22 E)**. In contrast, decreased *Gadd34* expression was detected for NSC/NPC 275 cells. As

decreased *Gadd34* was paralleled by the slightest increase in *Chop* mRNA levels **(Fig. 3.22 E),** as well as by the lowest p38 phosphorylation levels after 2-HG treatment **(Fig. 3.21)**, a possible involvement of p38 signaling in regulating *Chop* transcription and the consequent induction of *Gadd34* is conceivable. Besides increased *Atf4* and *Chop* transcript levels, also increased levels of *Gadd34* were already described for *Idh1*-mutant cells[64].

Gadd34 is able to induce total p53 protein levels and increase p53 phosphorylation levels as well as *Cdkn1a* transcription, thereby mediating cell cycle arrest and apoptosis[222,577,579]. These effects were indeed detected in 2-HG-treated NSC/NPCs, where high *Gadd34* transcript levels correlated with higher protein levels of total p53 and phosphorylated p53 **(Fig. 3.26 A, B)**, as well as with higher transcript levels of *Cdkn1a* **(Fig. 3.26 C)**. Overexpression of *Cdkn1a* transcripts was also found in the RNA sequencing data of *Idh1*-mutant knock-in NSC/NPCs **(Fig.3.30 B).** Furthermore, 2-HG treatment resulted in a G0/G1-arrest of NSC/NPCs **(Fig. 3.25)**. Lower p38 phosphorylation levels, *Chop*, *Gadd34* and *Cdkn1a* transcript levels as well as total p53 and phosphorylated p53 protein levels were associated with the least-sensitive response to 2-HG treatment **(Fig. 3.17)**. A P53-independent increase of *CDKN1A* mRNA levels was already shown in *IDH1*-mutant glioblastoma cell lines[580]. An *IDH1* mutation-associated cell cycle arrest in the G0/G1-phase was furthermore reported by Wang and colleagues[581]. However, the mutation did not result in apoptotic cell death[581], probably attributable to numerous background mutations of the transfected glioblastoma cell line, preventing the possible *IDH1* mutation-mediated apoptotic effect. In NSCs with conditional knock-in of *Idh1* mutation, Zhang and colleagues also detected increased apoptotic cell death as compared to normal NSCs[447], supporting the effects observed in the own studies **(Fig. 3.23)**. The aggregate of results for 2-HG-treated NSC/NPCs points to a possible role of Chop and Gadd34 as players of the integrated stress response for 2-HG-induced apoptosis, with a conceivable involvement of active p38. A consequent overexpression of Cdkn1a might furthermore strengthen Nrf2 activation and *Hmox1* transcription by impairing the binding of Nrf2 to its negative regulator Keap1[537].

Additional 2-HG-mediated alterations were a significant downregulation of *Cdkn1c* and *Cdkn2c* mRNA levels **(Fig. 3.26 C)**. A similar effect was observed in the RNA sequencing data of *Idh1*-mutant NSC/NPCs **(Fig. 3.30 B)**. Decreased *Cdkn1c* transcript levels have been observed in diverse cancer cells, e.g. due to epigenetic changes repressing transcription, such as aberrant DNA-methylation or histone-methylation as well as miRNA-mediated mechanisms[582-584]. However, no link to *Idh1* mutation exists so far. A decreased expression resulting from 2-HG-mediated epigenetic changes might be conceivable,

however, *IDH1* mutation-derived epigenetic changes need around 15 passages to be established[110]. Comparable to *CDKN2A*, *CDKN2C* is a tumor suppressor gene in gliomas that is homozygously deleted in a subset of glioblastomas[585,586]. As for *Cdkn1c*, decreased *Cdkn2c* expression has not been connected to *Idh1* mutation until now. Since both cell cycle regulators are tumor suppressive, their reduced expression in *Idh1*-mutant or 2-HG-treated cells might have tumor promoting effects. However, the 2-HG-mediated expression of p53 and p21 **(Fig. 3.26)** as well as the cell cycle arrest and apoptosis **(Fig. 3.25, Fig. 3.23)** emphasize the requirement of the acquisition of an anti-apoptotic mutation for tumor initiation.

4.4.6 2-HG-induced apoptotic cell death in NSC/NPCs is mediated by ROS

2-HG treatment resulted in elevated ROS levels as well as in the activation of p38 signaling in NSC/NPCs **(Fig. 3.19, Fig. 3.21)**. By performing a caspase activity assay with 2-HG-treated NSC/NPCs in combination with the antioxidant NAC or the p38 inhibitor SB, the apoptosis-mediating effects of 2-HG were elucidated **(Fig. 3.27)**. The significant increase of caspase activity after 2-HG treatment supports the induction of apoptotic cell death. Interestingly, co-incubation with NAC attenuated the 2-HG-mediated increase of caspase activity, indicating elevated ROS levels **(Fig. 19)** as a trigger for the apoptotic cell death **(Fig. 3.23)**. Inhibition of p38, however, further induced caspase activity in 2-HG-treated NSC/NPCs instead of attenuating the 2-HG-mediated effect. Since the p38-mediated induction of the PERK/eIF2α/ATF4 axis, as well as the switch from autophagy to apoptosis were shown to be attenuated by the inhibition of p38 by SB[197,587], the results of the caspase assay are indicative for a p38 signaling-independent induction of apoptosis in 2-HG-treated NSC/NPCs. However, a possible impact of p38 on Idh1-mutant cells has to be investigated in future experiments.

5.0 SUMMARY AND OUTLOOK

For the functional investigation of Idh1 mutation, a conditional knock-in mouse model relying on the 4-OHT-inducible CreER^{tam}/*loxP* system was used **(2.2.1)**. As the cell type of choice, NSC/NPCs from P0-P2 mice were used, as it was suggested that glioma stem cells most likely originate from NSC/NPCs. The heterozygous expression under the endogenous promoter, as well as the non-neoplastic background allowed for molecular and functional analyses of mutant Idh1 as an initial event in gliomagenesis, independent from other genetic alterations **(Tab. 5.1)**.

Tab. 5.1: Advantages and disadvantages of Idh1-mutant NSC/NPCs derived from a 4-OHT-inducible conditional knock-in mouse model

Advantages	Disadvantages
Heterozygous expression of mutant *Idh1*	Cytotoxic effect of 4-OHT on NSC/NPCs
Expression of mutant *Idh1* under the endogenous promoter	Inefficient recombination rate
Free of common glioblastoma-associated background mutations	Loss of recombinant NSC/NPCs over time
Similarity of NSC/NPCs to glioma stem cells	Interindividual differences between NSC/NPCs cultures
	Intensive cell culture maintenance

Besides numerous advantages, usage of this model system was also accompanied by several limitations **(Tab. 5.1)**. Recombination occurred but was rather inefficient, resulting in heterogeneous cell populations consisting of Idh1-wildtype and Idh1-mutant NSC/NPCs **(Fig. 3.2)** and subsequently variable experimental outcomes. Therefore, only strong Idh1 mutation-derived alterations are likely to be detectable. Marked interindividual differences among several NSC/NPC cultures, as it became obvious in transcriptomic approaches **(Fig. 3.9, Fig. 3.14)**, moreover impede the detection of Idh1 mutation-mediated effects in NSC/NPCs. Furthermore, only acute effects on the cells can be studied since recombinant NSC/NPCs vanished from the cell populations over time **(Fig. 3.2, Fig. 3.3)**. Long-term effects, e.g. resulting from 2-HG-mediated epigenetic changes, cannot be detected with the used model system. Another limitation is the strong cytotoxic effect of 4-OHT on NSC/NPCs **(Fig. 3.5)**. The ER-independent induction of autophagic and apoptotic cell

death could not be entirely enlightened in this study. However, several indications for a possible mode of action were given **(Tab. 5.1)**. Microarray analysis revealed a possible involvement of Jak/Stat signaling, as *Socs2* transcript levels were upregulated in 4-OHT-treated NSC/NPCs **(Fig. 3.9)**. Results from a kinase inhibitor screen and following experiments also pointed towards a role of Jak signaling in 4-OHT-mediated induction of cell death in NSC/NPCs, as a co-incubation of 4-OHT with the Jak2 inhibitor AG 490 attenuated the cytotoxic effect of the former **(Fig. 3.11)**. The inhibition of NF-κB signaling by 4-OHT itself, Stat3 and Socs2 might be reasonable according to literature. However, this was not proven in this thesis and has to be experimentally verified in further experiments.

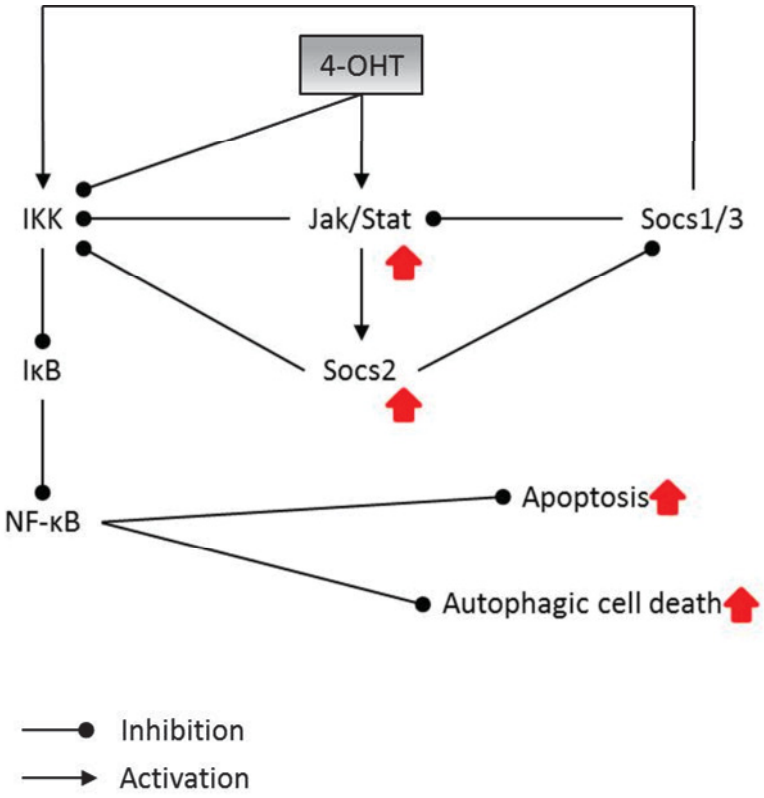

Fig. 5.1: Possible mechanisms underlying the cytotoxic effect of 4-OHT in NSC/NPCs
Red arrows indicate observed results in this thesis. Links were drawn according to literature review and have to be proven experimentally.

As the cytotoxic effect of 4-OHT on NSC/NPCs could not be elucidated and adequately attenuated, 4-OHT-treated controls were indispensable to distinguish between 4-OHT-mediated effects and Idh1 mutation-derived implications during the experiments. An additional confounder might be active Cre, leading to unspecific side effects. Therefore, 4-OHT-treated *Idh1*$^{wt/wt}$ *Cre*$^{-/-}$, *Idh1*$^{wt/wt}$ *Cre*$^{-/+}$ and *Idh1*$^{wt/LSL}$ *Cre*$^{-/-}$ NSC/NPC cultures were used as controls in experiments with the *Idh1*$^{wt/LSL}$ *Cre*$^{-/+}$ knock-in NSC/NPCs. Using NSC/NPCs of four genotypes, plus biological replicates should achieve the detection of

Idh1 mutation-mediated effects instead of individual characteristics of the respective NSC/NPC cultures. However, this resulted in a complex cell culture maintenance and experimental set up **(Tab. 5.1)**. Therefore, the usage of NSC/NPCs derived from conditional Idh1-mutant knock-in mice was rather restricted to large-scale experiments than to standard cell culture experiments. Although a strong interindividual background was detected for the several NSC/NPC cultures, RNA sequencing revealed numerous significantly altered transcript levels in *Idh1*-mutant knock-in NSC/NPCs **(Fig. 3.14)**. One significantly regulated candidate, already detected as altered on protein level in *Idh1*-mutant knock-in NSC/NPCs, was *Hmox1* **(Fig. 3.15)**. As the detected effect could still have been mediated or influenced by 4-OHT treatment or active Cre, an additional model was used to validate the effects as Idh1 mutation-derived. The treatment of *Idh1*$^{wt/wt}$ *Cre*$^{-/-}$ NSC/NPCs with membrane-permeable 2-HG proved that the induced expression of Hmox1 was 2-HG- and thereby Idh1 mutation-dependent **(Fig. 3.18)**, and that the conditional Idh1-mutant knock-in mouse model is, despite all limitations, suitable to detect Idh1 mutation-derived effects. Follow-up experiments were performed with 2-HG-treated wildtype NSC/NPCs for the further characterization of the observed effects. Several reasonable triggers leading to 2-HG-induced Hmox1 expression were found **(Fig. 5.2)**, e.g. increased ROS levels **(Fig. 3.19)** or an enhanced integrated stress response shown by induced phosphorylation of eIF2α and upregulated Atf4 expression **(Fig. 3.22)**. Whether the phosphorylation of eIF2α results from the activation of Perk as a response to impaired protein folding or via other eIF2α kinases has to be further elucidated and was not examined in this thesis. Furthermore, a peIF2α- and 4E-BP1-mediated shutdown of global translation in favor of cap-independent translation has to be proven in additional experiments. Another reason for induced Hmox1 expression after 2-HG treatment might be an elevated level of active p38 **(Fig. 3.21)**. This was not linked to Idh1 mutation so far. Elevated ROS levels as well as pp38 and pPerk might exert a possible Hmox1-inducing action by the activation of the transcription factors Nrf2, NF-κB, Ap-1 or Hsf. Whether those transcription factors are involved in the 2-HG-mediated Hmox1 expression in NSC/NPCs was, however, not evaluated. Thus, additional experiments have to be performed to clarify these open issues.

The induction of G0/G1-phase arrest **(Fig. 3.25)** and apoptosis **(Fig. 3.23)** in 2-HG-treated NSC/NPCs might result from a pp38- and Atf4-mediated switch from LC3 to Chop expression and the consequent induction of Gadd34, p53 and p21 expression upon severe stress conditions in the cells **(Fig. 5.2)**. Further experiments have to be performed to clarify this potential mode of action. However, the coincubation of NSC/NPCs with 2-HG and an inhibitor of p38 was, in contrast to a coincubation with the antioxidant NAC, not sufficient to attenuate 2-HG-mediated apoptosis in NSC/NPCs **(Fig. 3.27)**. The

downregulation of *Cdkn1a* and *Cdkn1c* expression and its implications are worth to perform further experiments with 2-HG-treated NSC/NPCs.

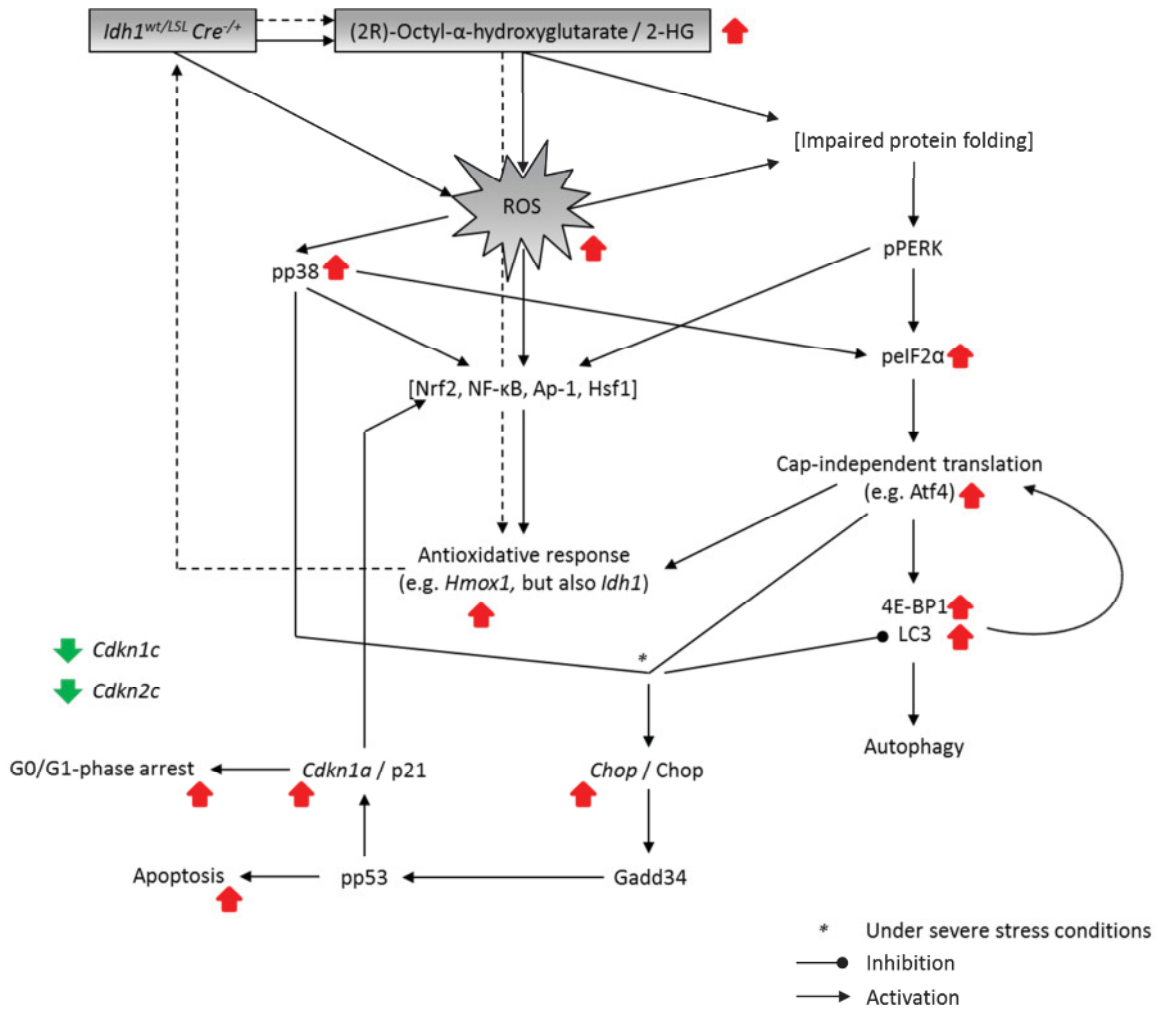

Fig. 5.2: Potential effects of mutant Idh1 in NSC/NPCs
Red and green arrows indicate observed results in this thesis. Not-continuous lines depict results from experiments with the Idh1-mutant knock-in NSC/NPCs. Links were drawn according to literature review and have to be validated experimentally.

Idh1 mutation and 2-HG obviously led to induced expression of ARE-responsive genes (e.g. Hmox1). As *Idh1* is also an ARE-responsive gene, even more mutant Idh1 is expressed under the endogenous promoter, subsequently inducing again ARE-responsive gene expression. Since this constitutes maintained stress conditions, Idh1-mutant NSC/NPCs undergo apoptosis, what might explain difficulties in culturing Idh1-mutant cells. Hence, the necessity for additional apoptosis-preventing mutations, like mutations in *p53*, for gliomagenesis of Idh1-mutant cells is plausible. In summary, the conditional Idh1-mutant knock-in mouse model expressing mutant Idh1 under the endogenous promoter is not only a possible but also a valid model for mechanistic characterization of Idh1 mutation-dependent effects.

6.0 LITERATURE

1 Louis, D. N., Perry, A., Reifenberger, G., von Deimling, A., Figarella-Branger, D., Cavenee, W. K. *et al.* The 2016 World Health Organization Classification of Tumors of the Central Nervous System: a summary. *Acta Neuropathol* **131**, 803-820, doi:10.1007/s00401-016-1545-1 (2016).

2 Crocetti, E., Trama, A., Stiller, C., Caldarella, A., Soffietti, R., Jaal, J. *et al.* Epidemiology of glial and non-glial brain tumours in Europe. *Eur J Cancer* **48**, 1532-1542, doi:10.1016/j.ejca.2011.12.013 (2012).

3 Zong, H., Verhaak, R. G. & Canoll, P. The cellular origin for malignant glioma and prospects for clinical advancements. *Expert Rev Mol Diagn* **12**, 383-394, doi:10.1586/erm.12.30 (2012).

4 Goffart, N., Kroonen, J. & Rogister, B. Glioblastoma-initiating cells: relationship with neural stem cells and the micro-environment. *Cancers (Basel)* **5**, 1049-1071, doi:10.3390/cancers5031049 (2013).

5 Lim, D. A., Cha, S., Mayo, M. C., Chen, M. H., Keles, E., VandenBerg, S. *et al.* Relationship of glioblastoma multiforme to neural stem cell regions predicts invasive and multifocal tumor phenotype. *Neuro Oncol* **9**, 424-429, doi:10.1215/15228517-2007-023 (2007).

6 Grier, J. T. & Batchelor, T. Low-grade gliomas in adults. *Oncologist* **11**, 681-693, doi:10.1634/theoncologist.11-6-681 (2006).

7 Louis, D. N., Ohgaki, H., Wiestler, O. D., Cavenee, W. K., Burger, P. C., Jouvet, A. *et al.* The 2007 WHO classification of tumours of the central nervous system. *Acta Neuropathol* **114**, 97-109, doi:10.1007/s00401-007-0243-4 (2007).

8 Weller, M., van den Bent, M., Tonn, J. C., Stupp, R., Preusser, M., Cohen-Jonathan-Moyal, E. *et al.* European Association for Neuro-Oncology (EANO) guideline on the diagnosis and treatment of adult astrocytic and oligodendroglial gliomas. *Lancet Oncol* **18**, e315-e329, doi:10.1016/S1470-2045(17)30194-8 (2017).

9 Stupp, R., Brada, M., van den Bent, M. J., Tonn, J. C., Pentheroudakis, G. & Grp, E. G. W. High-grade glioma: ESMO Clinical Practice Guidelines for diagnosis, treatment and follow-up. *Ann Oncol* **25**, 93-101, doi:10.1093/annonc/mdu050 (2014).

10 Gramatzki, D., Dehler, S., Rushing, E. J., Zaugg, K., Hofer, S., Yonekawa, Y. *et al.* Glioblastoma in the Canton of Zurich, Switzerland revisited: 2005 to 2009. *Cancer* **122**, 2206-2215, doi:10.1002/cncr.30023 (2016).

11 Reifenberger, G., Wirsching, H. G., Knobbe-Thomsen, C. B. & Weller, M. Advances in the molecular genetics of gliomas - implications for classification and therapy. *Nat Rev Clin Oncol* **14**, 434-452, doi:10.1038/nrclinonc.2016.204 (2017).

12 Wirsching, H. G., Weiss, T., Roth, P. & Weller, M. [Basic principles of diagnosis and treatment of gliomas]. *Nervenarzt* **89**, 692-698, doi:10.1007/s00115-018-0519-z (2018).

13 Parsons, D. W., Jones, S., Zhang, X., Lin, J. C., Leary, R. J., Angenendt, P. *et al.* An integrated genomic analysis of human glioblastoma multiforme. *Science* **321**, 1807-1812, doi:10.1126/science.1164382 (2008).

14 Balss, J., Meyer, J., Mueller, W., Korshunov, A., Hartmann, C. & von Deimling, A. Analysis of the IDH1 codon 132 mutation in brain tumors. *Acta Neuropathol* **116**, 597-602, doi:10.1007/s00401-008-0455-2 (2008).

15 Hartmann, C., Meyer, J., Balss, J., Capper, D., Mueller, W., Christians, A. *et al.* Type and frequency of IDH1 and IDH2 mutations are related to astrocytic and oligodendroglial differentiation and age: a study of 1,010 diffuse gliomas. *Acta Neuropathol* **118**, 469-474, doi:10.1007/s00401-009-0561-9 (2009).

16 Watanabe, T., Nobusawa, S., Kleihues, P. & Ohgaki, H. IDH1 mutations are early events in the development of astrocytomas and oligodendrogliomas. *Am J Pathol* **174**, 1149-1153, doi:10.2353/ajpath.2009.080958 (2009).
17 Yan, H., Parsons, D. W., Jin, G., McLendon, R., Rasheed, B. A., Yuan, W. *et al.* IDH1 and IDH2 mutations in gliomas. *N Engl J Med* **360**, 765-773, doi:10.1056/NEJMoa0808710 (2009).
18 Wang, P., Dong, Q., Zhang, C., Kuan, P. F., Liu, Y., Jeck, W. R. *et al.* Mutations in isocitrate dehydrogenase 1 and 2 occur frequently in intrahepatic cholangiocarcinomas and share hypermethylation targets with glioblastomas. *Oncogene* **32**, 3091-3100, doi:10.1038/onc.2012.315 (2013).
19 Schnittger, S., Haferlach, C., Ulke, M., Alpermann, T., Kern, W. & Haferlach, T. IDH1 mutations are detected in 6.6% of 1414 AML patients and are associated with intermediate risk karyotype and unfavorable prognosis in adults younger than 60 years and unmutated NPM1 status. *Blood* **116**, 5486-5496, doi:10.1182/blood-2010-02-267955 (2010).
20 Mardis, E. R., Ding, L., Dooling, D. J., Larson, D. E., McLellan, M. D., Chen, K. *et al.* Recurring mutations found by sequencing an acute myeloid leukemia genome. *N Engl J Med* **361**, 1058-1066, doi:10.1056/NEJMoa0903840 (2009).
21 Medeiros, B. C., Fathi, A. T., DiNardo, C. D., Pollyea, D. A., Chan, S. M. & Swords, R. Isocitrate dehydrogenase mutations in myeloid malignancies. *Leukemia* **31**, 272-281, doi:10.1038/leu.2016.275 (2017).
22 Amary, M. F., Bacsi, K., Maggiani, F., Damato, S., Halai, D., Berisha, F. *et al.* IDH1 and IDH2 mutations are frequent events in central chondrosarcoma and central and periosteal chondromas but not in other mesenchymal tumours. *J Pathol* **224**, 334-343, doi:10.1002/path.2913 (2011).
23 Ward, P. S., Patel, J., Wise, D. R., Abdel-Wahab, O., Bennett, B. D., Coller, H. A. *et al.* The common feature of leukemia-associated IDH1 and IDH2 mutations is a neomorphic enzyme activity converting alpha-ketoglutarate to 2-hydroxyglutarate. *Cancer Cell* **17**, 225-234, doi:10.1016/j.ccr.2010.01.020 (2010).
24 Chen, C., Liu, Y., Lu, C., Cross, J. R., Morris, J. P. t., Shroff, A. S. *et al.* Cancer-associated IDH2 mutants drive an acute myeloid leukemia that is susceptible to Brd4 inhibition. *Genes Dev* **27**, 1974-1985, doi:10.1101/gad.226613.113 (2013).
25 Lu, C., Venneti, S., Akalin, A., Fang, F., Ward, P. S., Dematteo, R. G. *et al.* Induction of sarcomas by mutant IDH2. *Genes Dev* **27**, 1986-1998, doi:10.1101/gad.226753.113 (2013).
26 Lu, C., Ward, P. S., Kapoor, G. S., Rohle, D., Turcan, S., Abdel-Wahab, O. *et al.* IDH mutation impairs histone demethylation and results in a block to cell differentiation. *Nature* **483**, 474-478, doi:10.1038/nature10860 (2012).
27 Sasaki, M., Knobbe, C. B., Munger, J. C., Lind, E. F., Brenner, D., Brustle, A. *et al.* IDH1(R132H) mutation increases murine haematopoietic progenitors and alters epigenetics. *Nature* **488**, 656-659, doi:10.1038/nature11323 (2012).
28 Bardella, C., Al-Dalahmah, O., Krell, D., Brazauskas, P., Al-Qahtani, K., Tomkova, M. *et al.* Expression of Idh1(R132H) in the Murine Subventricular Zone Stem Cell Niche Recapitulates Features of Early Gliomagenesis. *Cancer Cell* **30**, 578-594, doi:10.1016/j.ccell.2016.08.017 (2016).
29 Rosiak, K., Smolarz, M., Stec, W. J., Peciak, J., Grzela, D., Winiecka-Klimek, M. *et al.* IDH1R132H in Neural Stem Cells: Differentiation Impaired by Increased Apoptosis. *PLoS One* **11**, e0154726, doi:10.1371/journal.pone.0154726 (2016).
30 Lai, A., Kharbanda, S., Pope, W. B., Tran, A., Solis, O. E., Peale, F. *et al.* Evidence for sequenced molecular evolution of IDH1 mutant glioblastoma from a distinct cell of origin. *J Clin Oncol* **29**, 4482-4490, doi:10.1200/JCO.2010.33.8715 (2011).
31 Dang, L. & Su, S. M. Isocitrate Dehydrogenase Mutation and (R)-2-Hydroxyglutarate: From Basic Discovery to Therapeutics Development. *Annu Rev Biochem* **86**, 305-331, doi:10.1146/annurev-biochem-061516-044732 (2017).

32 Amankulor, N. M., Kim, Y., Arora, S., Kargl, J., Szulzewsky, F., Hanke, M. *et al.* Mutant IDH1 regulates the tumor-associated immune system in gliomas. *Genes Dev* **31**, 774-786, doi:10.1101/gad.294991.116 (2017).

33 Philip, B., Yu, D. X., Silvis, M. R., Shin, C. H., Robinson, J. P., Robinson, G. L. *et al.* Mutant IDH1 Promotes Glioma Formation In Vivo. *Cell Rep* **23**, 1553-1564, doi:10.1016/j.celrep.2018.03.133 (2018).

34 Bleeker, F. E., Atai, N. A., Lamba, S., Jonker, A., Rijkeboer, D., Bosch, K. S. *et al.* The prognostic IDH1(R132) mutation is associated with reduced NADP+-dependent IDH activity in glioblastoma. *Acta Neuropathol* **119**, 487-494, doi:10.1007/s00401-010-0645-6 (2010).

35 Geisbrecht, B. V. & Gould, S. J. The human PICD gene encodes a cytoplasmic and peroxisomal NADP(+)-dependent isocitrate dehydrogenase. *J Biol Chem* **274**, 30527-30533 (1999).

36 Haselbeck, R. J. & McAlister-Henn, L. Function and expression of yeast mitochondrial NAD- and NADP-specific isocitrate dehydrogenases. *J Biol Chem* **268**, 12116-12122 (1993).

37 Lee, S. M., Koh, H. J., Park, D. C., Song, B. J., Huh, T. L. & Park, J. W. Cytosolic NADP(+)-dependent isocitrate dehydrogenase status modulates oxidative damage to cells. *Free Radic Biol Med* **32**, 1185-1196 (2002).

38 Kim, S. Y. & Park, J. W. Cellular defense against singlet oxygen-induced oxidative damage by cytosolic NADP+-dependent isocitrate dehydrogenase. *Free Radic Res* **37**, 309-316 (2003).

39 Jo, S. H., Son, M. K., Koh, H. J., Lee, S. M., Song, I. H., Kim, Y. O. *et al.* Control of mitochondrial redox balance and cellular defense against oxidative damage by mitochondrial NADP+-dependent isocitrate dehydrogenase. *J Biol Chem* **276**, 16168-16176, doi:10.1074/jbc.M010120200 (2001).

40 Fernandez-Fernandez, S., Almeida, A. & Bolanos, J. P. Antioxidant and bioenergetic coupling between neurons and astrocytes. *Biochem J* **443**, 3-11, doi:10.1042/BJ20111943 (2012).

41 Wu, G., Fang, Y. Z., Yang, S., Lupton, J. R. & Turner, N. D. Glutathione metabolism and its implications for health. *J Nutr* **134**, 489-492, doi:10.1093/jn/134.3.489 (2004).

42 Hartong, D. T., Dange, M., McGee, T. L., Berson, E. L., Dryja, T. P. & Colman, R. F. Insights from retinitis pigmentosa into the roles of isocitrate dehydrogenases in the Krebs cycle. *Nat Genet* **40**, 1230-1234, doi:10.1038/ng.223 (2008).

43 Weiss, C., Zeng, Y., Huang, J., Sobocka, M. B. & Rushbrook, J. I. Bovine NAD+-dependent isocitrate dehydrogenase: alternative splicing and tissue-dependent expression of subunit 1. *Biochemistry* **39**, 1807-1816 (2000).

44 Krell, D., Assoku, M., Galloway, M., Mulholland, P., Tomlinson, I. & Bardella, C. Screen for IDH1, IDH2, IDH3, D2HGDH and L2HGDH mutations in glioblastoma. *PLoS One* **6**, e19868, doi:10.1371/journal.pone.0019868 (2011).

45 Yan, H., Bigner, D. D., Velculescu, V. & Parsons, D. W. Mutant metabolic enzymes are at the origin of gliomas. *Cancer Res* **69**, 9157-9159, doi:10.1158/0008-5472.CAN-09-2650 (2009).

46 Al-Khallaf, H. Isocitrate dehydrogenases in physiology and cancer: biochemical and molecular insight. *Cell Biosci* **7**, 37, doi:10.1186/s13578-017-0165-3 (2017).

47 Molenaar, R., Sanikommu, S. R., Patel, B. J., Przychodzen, B., van Noorden, C. J., Radivoyevitch, T. *et al.* Whole-Exome Sequencing Identifies Germline IDH2 and IDH3 mutations That Predispose to Myeloid Neoplasms. *Blood* **126** (2015).

48 Ward, P. S., Cross, J. R., Lu, C., Weigert, O., Abel-Wahab, O., Levine, R. L. *et al.* Identification of additional IDH mutations associated with oncometabolite R(-)-2-hydroxyglutarate production. *Oncogene* **31**, 2491-2498, doi:10.1038/onc.2011.416 (2012).

49 Dang, L., White, D. W., Gross, S., Bennett, B. D., Bittinger, M. A., Driggers, E. M. *et al.* Cancer-associated IDH1 mutations produce 2-hydroxyglutarate. *Nature* **462**, 739-744, doi:10.1038/nature08617 (2009).

50 Yang, H., Ye, D., Guan, K. L. & Xiong, Y. IDH1 and IDH2 mutations in tumorigenesis: mechanistic insights and clinical perspectives. *Clin Cancer Res* **18**, 5562-5571, doi:10.1158/1078-0432.CCR-12-1773 (2012).

51 Gross, S., Cairns, R. A., Minden, M. D., Driggers, E. M., Bittinger, M. A., Jang, H. G. *et al.* Cancer-associated metabolite 2-hydroxyglutarate accumulates in acute myelogenous leukemia with isocitrate dehydrogenase 1 and 2 mutations. *J Exp Med* **207**, 339-344, doi:10.1084/jem.20092506 (2010).

52 Ward, P. S., Lu, C., Cross, J. R., Abdel-Wahab, O., Levine, R. L., Schwartz, G. K. *et al.* The potential for isocitrate dehydrogenase mutations to produce 2-hydroxyglutarate depends on allele specificity and subcellular compartmentalization. *J Biol Chem* **288**, 3804-3815, doi:10.1074/jbc.M112.435495 (2013).

53 Gupta, R., Webb-Myers, R., Flanagan, S. & Buckland, M. E. Isocitrate dehydrogenase mutations in diffuse gliomas: clinical and aetiological implications. *J Clin Pathol* **64**, 835-844, doi:10.1136/jclinpath-2011-200227 (2011).

54 Levine, A. J. & Puzio-Kuter, A. M. The control of the metabolic switch in cancers by oncogenes and tumor suppressor genes. *Science* **330**, 1340-1344, doi:10.1126/science.1193494 (2010).

55 Waitkus, M. S., Diplas, B. H. & Yan, H. Isocitrate dehydrogenase mutations in gliomas. *Neuro Oncol* **18**, 16-26, doi:10.1093/neuonc/nov136 (2016).

56 Tiwari, M. Glucose 6 phosphatase dehydrogenase (G6PD) and neurodegenerative disorders: Mapping diagnostic and therapeutic opportunities. *Genes Dis* **4**, 196-203, doi:10.1016/j.gendis.2017.09.001 (2017).

57 Sarfraz, I., Rasul, A., Hussain, G., Hussain, S. M., Ahmad, M., Nageen, B. *et al.* Malic enzyme 2 as a potential therapeutic drug target for cancer. *IUBMB Life* **70**, 1076-1083, doi:10.1002/iub.1930 (2018).

58 Gelman, S. J., Naser, F., Mahieu, N. G., McKenzie, L. D., Dunn, G. P., Chheda, M. G. *et al.* Consumption of NADPH for 2-HG Synthesis Increases Pentose Phosphate Pathway Flux and Sensitizes Cells to Oxidative Stress. *Cell Rep* **22**, 512-522, doi:10.1016/j.celrep.2017.12.050 (2018).

59 Li, S., Chou, A. P., Chen, W., Chen, R., Deng, Y., Phillips, H. S. *et al.* Overexpression of isocitrate dehydrogenase mutant proteins renders glioma cells more sensitive to radiation. *Neuro Oncol* **15**, 57-68, doi:10.1093/neuonc/nos261 (2013).

60 Shi, X., He, B. L., Ma, A. C., Guo, Y., Chi, Y., Man, C. H. *et al.* Functions of idh1 and its mutation in the regulation of developmental hematopoiesis in zebrafish. *Blood* **125**, 2974-2984, doi:10.1182/blood-2014-09-601187 (2015).

61 Zhu, H., Zhang, Y., Chen, J., Qiu, J., Huang, K., Wu, M. *et al.* IDH1 R132H Mutation Enhances Cell Migration by Activating AKT-mTOR Signaling Pathway, but Sensitizes Cells to 5-FU Treatment as NADPH and GSH Are Reduced. *PLoS One* **12**, e0169038, doi:10.1371/journal.pone.0169038 (2017).

62 Shi, J., Sun, B., Shi, W., Zuo, H., Cui, D., Ni, L. *et al.* Decreasing GSH and increasing ROS in chemosensitivity gliomas with IDH1 mutation. *Tumour Biol* **36**, 655-662, doi:10.1007/s13277-014-2644-z (2015).

63 Shi, J., Zuo, H., Ni, L., Xia, L., Zhao, L., Gong, M. *et al.* An IDH1 mutation inhibits growth of glioma cells via GSH depletion and ROS generation. *Neurol Sci* **35**, 839-845, doi:10.1007/s10072-013-1607-2 (2014).

64 Sasaki, M., Knobbe, C. B., Itsumi, M., Elia, A. J., Harris, I. S., Chio, II *et al.* D-2-hydroxyglutarate produced by mutant IDH1 perturbs collagen maturation and basement membrane function. *Genes Dev* **26**, 2038-2049, doi:10.1101/gad.198200.112 (2012).

65 Seltzer, M. J., Bennett, B. D., Joshi, A. D., Gao, P., Thomas, A. G., Ferraris, D. V. *et al.* Inhibition of glutaminase preferentially slows growth of glioma cells with mutant IDH1. *Cancer Res* **70**, 8981-8987, doi:10.1158/0008-5472.CAN-10-1666 (2010).

66 Gaglio, D., Metallo, C. M., Gameiro, P. A., Hiller, K., Danna, L. S., Balestrieri, C. *et al.* Oncogenic K-Ras decouples glucose and glutamine metabolism to support cancer cell growth. *Mol Syst Biol* **7**, 523, doi:10.1038/msb.2011.56 (2011).

67 Son, J., Lyssiotis, C. A., Ying, H., Wang, X., Hua, S., Ligorio, M. *et al.* Glutamine supports pancreatic cancer growth through a KRAS-regulated metabolic pathway. *Nature* **496**, 101-105, doi:10.1038/nature12040 (2013).

68 Grassian, A. R., Parker, S. J., Davidson, S. M., Divakaruni, A. S., Green, C. R., Zhang, X. *et al.* IDH1 mutations alter citric acid cycle metabolism and increase dependence on oxidative mitochondrial metabolism. *Cancer Res* **74**, 3317-3331, doi:10.1158/0008-5472.CAN-14-0772-T (2014).

69 Chen, R., Nishimura, M. C., Kharbanda, S., Peale, F., Deng, Y., Daemen, A. *et al.* Hominoid-specific enzyme GLUD2 promotes growth of IDH1R132H glioma. *Proc Natl Acad Sci U S A* **111**, 14217-14222, doi:10.1073/pnas.1409653111 (2014).

70 Wu, G. Y., Bazer, F. W., Burghardt, R. C., Johnson, G. A., Kim, S. W., Knabe, D. A. *et al.* Proline and hydroxyproline metabolism: implications for animal and human nutrition. *Amino Acids* **40**, 1053-1063, doi:10.1007/s00726-010-0715-z (2011).

71 Son, E. D., Choi, G. H., Kim, H., Lee, B., Chang, I. S. & Hwang, J. S. Alpha-ketoglutarate stimulates procollagen production in cultured human dermal fibroblasts, and decreases UVB-induced wrinkle formation following topical application on the dorsal skin of hairless mice. *Biol Pharm Bull* **30**, 1395-1399 (2007).

72 Dakshayani, K. B. & Subramanian, P. Alpha-ketoglutarate modulates the circadian patterns of lipid peroxidation and antioxidant status during N-nitrosodiethylamine-induced hepatocarcinogenesis in rats. *J Med Food* **9**, 90-97, doi:10.1089/jmf.2006.9.90 (2006).

73 Lambert, B. D., Filip, R., Stoll, B., Junghans, P., Derno, M., Hennig, U. *et al.* First-pass metabolism limits the intestinal absorption of enteral alpha-ketoglutarate in young pigs. *J Nutr* **136**, 2779-2784, doi:10.1093/jn/136.11.2779 (2006).

74 Gregersen, N., Ingerslev, J. & Rasmussen, K. Low molecular weight organic acids in the urine of the newborn. *Acta Paediatr Scand* **66**, 85-89 (1977).

75 Kranendijk, M., Struys, E. A., Salomons, G. S., Van der Knaap, M. S. & Jakobs, C. Progress in understanding 2-hydroxyglutaric acidurias. *J Inherit Metab Dis* **35**, 571-587, doi:10.1007/s10545-012-9462-5 (2012).

76 Rzem, R., Vincent, M. F., Van Schaftingen, E. & Veiga-da-Cunha, M. L-2-hydroxyglutaric aciduria, a defect of metabolite repair. *J Inherit Metab Dis* **30**, 681-689, doi:10.1007/s10545-007-0487-0 (2007).

77 Fan, J., Teng, X., Liu, L., Mattaini, K. R., Looper, R. E., Vander Heiden, M. G. *et al.* Human phosphoglycerate dehydrogenase produces the oncometabolite D-2-hydroxyglutarate. *ACS Chem Biol* **10**, 510-516, doi:10.1021/cb500683c (2015).

78 Struys, E. A., Gibson, K. M. & Jakobs, C. Novel insights into L-2-hydroxyglutaric aciduria: mass isotopomer studies reveal 2-oxoglutaric acid as the metabolic precursor of L-2-hydroxyglutaric acid. *J Inherit Metab Dis* **30**, 690-693, doi:10.1007/s10545-007-0697-5 (2007).

79 Steenweg, M. E., Jakobs, C., Errami, A., van Dooren, S. J., Adeva Bartolome, M. T., Aerssens, P. *et al.* An overview of L-2-hydroxyglutarate dehydrogenase gene (L2HGDH) variants: a genotype-phenotype study. *Hum Mutat* **31**, 380-390, doi:10.1002/humu.21197 (2010).

80 Achouri, Y., Noel, G., Vertommen, D., Rider, M. H., Veiga-Da-Cunha, M. & Van Schaftingen, E. Identification of a dehydrogenase acting on D-2-hydroxyglutarate. *Biochem J* **381**, 35-42, doi:10.1042/BJ20031933 (2004).

81 Rzem, R., Veiga-da-Cunha, M., Noel, G., Goffette, S., Nassogne, M. C., Tabarki, B. *et al.* A gene encoding a putative FAD-dependent L-2-hydroxyglutarate dehydrogenase is mutated in L-2-hydroxyglutaric aciduria. *Proc Natl Acad Sci U S A* **101**, 16849-16854, doi:10.1073/pnas.0404840101 (2004).

82 Topcu, M., Jobard, F., Halliez, S., Coskun, T., Yalcinkayal, C., Gerceker, F. O. *et al.* L-2-Hydroxyglutaric aciduria: identification of a mutant gene C14orf160,

localized on chromosome 14q22.1. *Hum Mol Genet* **13**, 2803-2811, doi:10.1093/hmg/ddh300 (2004).

83 Struys, E. A., Verhoeven, N. M., Jansen, E. E., Ten Brink, H. J., Gupta, M., Burlingame, T. G. *et al.* Metabolism of gamma-hydroxybutyrate to d-2-hydroxyglutarate in mammals: further evidence for d-2-hydroxyglutarate transhydrogenase. *Metabolism* **55**, 353-358, doi:10.1016/j.metabol.2005.09.009 (2006).

84 Struys, E. A., Salomons, G. S., Achouri, Y., Van Schaftingen, E., Grosso, S., Craigen, W. J. *et al.* Mutations in the D-2-hydroxyglutarate dehydrogenase gene cause D-2-hydroxyglutaric aciduria. *Am J Hum Genet* **76**, 358-360, doi:10.1086/427890 (2005).

85 Kranendijk, M., Struys, E. A., Gibson, K. M., Wickenhagen, W. V., Abdenur, J. E., Buechner, J. *et al.* Evidence for genetic heterogeneity in D-2-hydroxyglutaric aciduria. *Hum Mutat* **31**, 279-283, doi:10.1002/humu.21186 (2010).

86 Kranendijk, M., Struys, E. A., van Schaftingen, E., Gibson, K. M., Kanhai, W. A., van der Knaap, M. S. *et al.* IDH2 mutations in patients with D-2-hydroxyglutaric aciduria. *Science* **330**, 336, doi:10.1126/science.1192632 (2010).

87 Wang, Q. & Yang, Y. L. [Complex heterogeneity phenotypes and genotypes of glutaric aciduria type 1]. *Zhongguo Dang Dai Er Ke Za Zhi* **18**, 460-465 (2016).

88 van der Knaap, M. S., Jakobs, C., Hoffmann, G. F., Duran, M., Muntau, A. C., Schweitzer, S. *et al.* D-2-hydroxyglutaric aciduria: further clinical delineation. *J Inherit Metab Dis* **22**, 404-413 (1999).

89 van der Knaap, M. S., Jakobs, C., Hoffmann, G. F., Nyhan, W. L., Renier, W. O., Smeitink, J. A. *et al.* D-2-Hydroxyglutaric aciduria: biochemical marker or clinical disease entity? *Ann Neurol* **45**, 111-119 (1999).

90 Rzem, R., Van Schaftingen, E. & Veiga-da-Cunha, M. The gene mutated in l-2-hydroxyglutaric aciduria encodes l-2-hydroxyglutarate dehydrogenase. *Biochimie* **88**, 113-116, doi:10.1016/j.biochi.2005.06.005 (2006).

91 Aghili, M., Zahedi, F. & Rafiee, E. Hydroxyglutaric aciduria and malignant brain tumor: a case report and literature review. *J Neurooncol* **91**, 233-236, doi:10.1007/s11060-008-9706-2 (2009).

92 Moroni, I., Bugiani, M., D'Incerti, L., Maccagnano, C., Rimoldi, M., Bissola, L. *et al.* L-2-hydroxyglutaric aciduria and brain malignant tumors: a predisposing condition? *Neurology* **62**, 1882-1884 (2004).

93 Barbot, C., Fineza, I., Diogo, L., Maia, M., Melo, J., Guimaraes, A. *et al.* L-2-Hydroxyglutaric aciduria: clinical, biochemical and magnetic resonance imaging in six Portuguese pediatric patients. *Brain Dev* **19**, 268-273 (1997).

94 Patay, Z., Orr, B. A., Shulkin, B. L., Hwang, S. N., Ying, Y., Broniscer, A. *et al.* Successive distinct high-grade gliomas in L-2-hydroxyglutaric aciduria. *J Inherit Metab Dis* **38**, 273-277, doi:10.1007/s10545-014-9782-8 (2015).

95 Ozisik, P. A., Akalan, N., Palaoglu, S. & Topcu, M. Medulloblastoma in a child with the metabolic disease L-2-hydroxyglutaric aciduria. *Pediatr Neurosurg* **37**, 22-26, doi:10.1159/000065097 (2002).

96 Wilcken, B., Pitt, J., Heath, D., Walsh, P., Wilson, G. & Buchanan, N. L-2-hydroxyglutaric aciduria: three Australian cases. *J Inherit Metab Dis* **16**, 501-504 (1993).

97 Andronesi, O. C., Kim, G. S., Gerstner, E., Batchelor, T., Tzika, A. A., Fantin, V. R. *et al.* Detection of 2-hydroxyglutarate in IDH-mutated glioma patients by in vivo spectral-editing and 2D correlation magnetic resonance spectroscopy. *Sci Transl Med* **4**, 116ra114, doi:10.1126/scitranslmed.3002693 (2012).

98 Capper, D., Simon, M., Langhans, C. D., Okun, J. G., Tonn, J. C., Weller, M. *et al.* 2-Hydroxyglutarate concentration in serum from patients with gliomas does not correlate with IDH1/2 mutation status or tumor size. *Int J Cancer* **131**, 766-768, doi:10.1002/ijc.26425 (2012).

99 Lombardi, G., Corona, G., Bellu, L., Della Puppa, A., Pambuku, A., Fiduccia, P. *et al.* Diagnostic value of plasma and urinary 2-hydroxyglutarate to identify patients

with isocitrate dehydrogenase-mutated glioma. *Oncologist* **20**, 562-567, doi:10.1634/theoncologist.2014-0266 (2015).

100 Chowdhury, R., Yeoh, K. K., Tian, Y. M., Hillringhaus, L., Bagg, E. A., Rose, N. R. *et al.* The oncometabolite 2-hydroxyglutarate inhibits histone lysine demethylases. *EMBO Rep* **12**, 463-469, doi:10.1038/embor.2011.43 (2011).

101 Xu, W., Yang, H., Liu, Y., Yang, Y., Wang, P., Kim, S. H. *et al.* Oncometabolite 2-hydroxyglutarate is a competitive inhibitor of alpha-ketoglutarate-dependent dioxygenases. *Cancer Cell* **19**, 17-30, doi:10.1016/j.ccr.2010.12.014 (2011).

102 Joberty, G., Boesche, M., Brown, J. A., Eberhard, D., Garton, N. S., Humphreys, P. G. *et al.* Interrogating the Druggability of the 2-Oxoglutarate-Dependent Dioxygenase Target Class by Chemical Proteomics. *ACS Chem Biol* **11**, 2002-2010, doi:10.1021/acschembio.6b00080 (2016).

103 Tahiliani, M., Koh, K. P., Shen, Y., Pastor, W. A., Bandukwala, H., Brudno, Y. *et al.* Conversion of 5-methylcytosine to 5-hydroxymethylcytosine in mammalian DNA by MLL partner TET1. *Science* **324**, 930-935, doi:10.1126/science.1170116 (2009).

104 Ito, S., D'Alessio, A. C., Taranova, O. V., Hong, K., Sowers, L. C. & Zhang, Y. Role of Tet proteins in 5mC to 5hmC conversion, ES-cell self-renewal and inner cell mass specification. *Nature* **466**, 1129-1133, doi:10.1038/nature09303 (2010).

105 Ito, S., Shen, L., Dai, Q., Wu, S. C., Collins, L. B., Swenberg, J. A. *et al.* Tet proteins can convert 5-methylcytosine to 5-formylcytosine and 5-carboxylcytosine. *Science* **333**, 1300-1303, doi:10.1126/science.1210597 (2011).

106 He, Y. F., Li, B. Z., Li, Z., Liu, P., Wang, Y., Tang, Q. *et al.* Tet-mediated formation of 5-carboxylcytosine and its excision by TDG in mammalian DNA. *Science* **333**, 1303-1307, doi:10.1126/science.1210944 (2011).

107 Raiber, E. A., Beraldi, D., Ficz, G., Burgess, H. E., Branco, M. R., Murat, P. *et al.* Genome-wide distribution of 5-formylcytosine in embryonic stem cells is associated with transcription and depends on thymine DNA glycosylase. *Genome Biol* **13**, R69, doi:10.1186/gb-2012-13-8-r69 (2012).

108 Koivunen, P., Lee, S., Duncan, C. G., Lopez, G., Lu, G., Ramkissoon, S. *et al.* Transformation by the (R)-enantiomer of 2-hydroxyglutarate linked to EGLN activation. *Nature* **483**, 484-488, doi:10.1038/nature10898 (2012).

109 Noushmehr, H., Weisenberger, D. J., Diefes, K., Phillips, H. S., Pujara, K., Berman, B. P. *et al.* Identification of a CpG island methylator phenotype that defines a distinct subgroup of glioma. *Cancer Cell* **17**, 510-522, doi:10.1016/j.ccr.2010.03.017 (2010).

110 Turcan, S., Rohle, D., Goenka, A., Walsh, L. A., Fang, F., Yilmaz, E. *et al.* IDH1 mutation is sufficient to establish the glioma hypermethylator phenotype. *Nature* **483**, 479-483, doi:10.1038/nature10866 (2012).

111 Duncan, C. G., Barwick, B. G., Jin, G., Rago, C., Kapoor-Vazirani, P., Powell, D. R. *et al.* A heterozygous IDH1R132H/WT mutation induces genome-wide alterations in DNA methylation. *Genome Res* **22**, 2339-2355, doi:10.1101/gr.132738.111 (2012).

112 Klose, R. J., Kallin, E. M. & Zhang, Y. JmjC-domain-containing proteins and histone demethylation. *Nat Rev Genet* **7**, 715-727, doi:10.1038/nrg1945 (2006).

113 Shilatifard, A. Chromatin modifications by methylation and ubiquitination: implications in the regulation of gene expression. *Annu Rev Biochem* **75**, 243-269, doi:10.1146/annurev.biochem.75.103004.142422 (2006).

114 Kaelin, W. G., Jr. & Ratcliffe, P. J. Oxygen sensing by metazoans: the central role of the HIF hydroxylase pathway. *Mol Cell* **30**, 393-402, doi:10.1016/j.molcel.2008.04.009 (2008).

115 Semenza, G. L. Targeting HIF-1 for cancer therapy. *Nat Rev Cancer* **3**, 721-732, doi:10.1038/nrc1187 (2003).

116 Semenza, G. L. Oxygen sensing, hypoxia-inducible factors, and disease pathophysiology. *Annu Rev Pathol* **9**, 47-71, doi:10.1146/annurev-pathol-012513-104720 (2014).

117 Zhao, S., Lin, Y., Xu, W., Jiang, W., Zha, Z., Wang, P. *et al.* Glioma-derived mutations in IDH1 dominantly inhibit IDH1 catalytic activity and induce HIF-1alpha. *Science* **324**, 261-265, doi:10.1126/science.1170944 (2009).

118 Qi, Y. & Xu, R. Roles of PLODs in Collagen Synthesis and Cancer Progression. *Front Cell Dev Biol* **6**, 66, doi:10.3389/fcell.2018.00066 (2018).

119 Latini, A., Scussiato, K., Rosa, R. B., Llesuy, S., Bello-Klein, A., Dutra-Filho, C. S. *et al.* D-2-hydroxyglutaric acid induces oxidative stress in cerebral cortex of young rats. *Eur J Neurosci* **17**, 2017-2022 (2003).

120 Chen, J. Y., Lai, Y. S., Tsai, H. J., Kuo, C. C., Yen, B. L., Yeh, S. P. *et al.* The oncometabolite R-2-hydroxyglutarate activates NF-kappaB-dependent tumor-promoting stromal niche for acute myeloid leukemia cells. *Sci Rep* **6**, 32428, doi:10.1038/srep32428 (2016).

121 Karlstaedt, A., Zhang, X., Vitrac, H., Harmancey, R., Vasquez, H., Wang, J. H. *et al.* Oncometabolite d-2-hydroxyglutarate impairs alpha-ketoglutarate dehydrogenase and contractile function in rodent heart. *Proc Natl Acad Sci U S A* **113**, 10436-10441, doi:10.1073/pnas.1601650113 (2016).

122 Mates, J. M. Effects of antioxidant enzymes in the molecular control of reactive oxygen species toxicology. *Toxicology* **153**, 83-104 (2000).

123 Riley, P. A. Free radicals in biology: oxidative stress and the effects of ionizing radiation. *Int J Radiat Biol* **65**, 27-33 (1994).

124 Turrens, J. F. Mitochondrial formation of reactive oxygen species. *J Physiol* **552**, 335-344, doi:10.1113/jphysiol.2003.049478 (2003).

125 Gough, D. R. & Cotter, T. G. Hydrogen peroxide: a Jekyll and Hyde signalling molecule. *Cell Death Dis* **2**, e213, doi:10.1038/cddis.2011.96 (2011).

126 Sies, H. Strategies of antioxidant defense. *Eur J Biochem* **215**, 213-219 (1993).

127 Steinbrenner, H. & Sies, H. Protection against reactive oxygen species by selenoproteins. *Biochim Biophys Acta* **1790**, 1478-1485, doi:10.1016/j.bbagen.2009.02.014 (2009).

128 Commoner, B., Townsend, J. & Pake, G. E. Free radicals in biological materials. *Nature* **174**, 689-691 (1954).

129 Jones, O. T. The regulation of superoxide production by the NADPH oxidase of neutrophils and other mammalian cells. *Bioessays* **16**, 919-923, doi:10.1002/bies.950161211 (1994).

130 Lambeth, J. D. NOX enzymes and the biology of reactive oxygen. *Nat Rev Immunol* **4**, 181-189, doi:10.1038/nri1312 (2004).

131 Brand, M. D. The sites and topology of mitochondrial superoxide production. *Exp Gerontol* **45**, 466-472, doi:10.1016/j.exger.2010.01.003 (2010).

132 Dupuy, C., Virion, A., Ohayon, R., Kaniewski, J., Deme, D. & Pommier, J. Mechanism of hydrogen peroxide formation catalyzed by NADPH oxidase in thyroid plasma membrane. *J Biol Chem* **266**, 3739-3743 (1991).

133 Sies, H. & Cadenas, E. Oxidative stress: damage to intact cells and organs. *Philos Trans R Soc Lond B Biol Sci* **311**, 617-631, doi:10.1098/rstb.1985.0168 (1985).

134 Halliwell, B. Free radicals, reactive oxygen species and human disease: a critical evaluation with special reference to atherosclerosis. *Br J Exp Pathol* **70**, 737-757 (1989).

135 Birben, E., Sahiner, U. M., Sackesen, C., Erzurum, S. & Kalayci, O. Oxidative stress and antioxidant defense. *World Allergy Organ J* **5**, 9-19, doi:10.1097/WOX.0b013e3182439613 (2012).

136 Miller, A. F. Superoxide dismutases: ancient enzymes and new insights. *FEBS Lett* **586**, 585-595, doi:10.1016/j.febslet.2011.10.048 (2012).

137 Wang, Y., Branicky, R., Noe, A. & Hekimi, S. Superoxide dismutases: Dual roles in controlling ROS damage and regulating ROS signaling. *J Cell Biol* **217**, 1915-1928, doi:10.1083/jcb.201708007 (2018).

138 Flynn, J. M. & Melov, S. SOD2 in mitochondrial dysfunction and neurodegeneration. *Free Radic Biol Med* **62**, 4-12, doi:10.1016/j.freeradbiomed.2013.05.027 (2013).

139 Karlsson, K. & Marklund, S. L. Extracellular superoxide dismutase in the vascular system of mammals. *Biochem J* **255**, 223-228 (1988).
140 Karlsson, K. & Marklund, S. L. Extracellular-superoxide dismutase association with cell surface-bound sulfated glucosaminoglycans. *Basic Life Sci* **49**, 647-650 (1988).
141 Schieber, M. & Chandel, N. S. ROS function in redox signaling and oxidative stress. *Curr Biol* **24**, R453-462, doi:10.1016/j.cub.2014.03.034 (2014).
142 Rotruck, J. T., Pope, A. L., Ganther, H. E., Swanson, A. B., Hafeman, D. G. & Hoekstra, W. G. Selenium: biochemical role as a component of glutathione peroxidase. *Science* **179**, 588-590 (1973).
143 Percy, M. E. Catalase: an old enzyme with a new role? *Can J Biochem Cell Biol* **62**, 1006-1014 (1984).
144 Mills, G. C. Hemoglobin catabolism. I. Glutathione peroxidase, an erythrocyte enzyme which protects hemoglobin from oxidative breakdown. *J Biol Chem* **229**, 189-197 (1957).
145 Schrader, M. & Fahimi, H. D. Peroxisomes and oxidative stress. *Biochim Biophys Acta* **1763**, 1755-1766, doi:10.1016/j.bbamcr.2006.09.006 (2006).
146 Lubos, E., Loscalzo, J. & Handy, D. E. Glutathione peroxidase-1 in health and disease: from molecular mechanisms to therapeutic opportunities. *Antioxid Redox Signal* **15**, 1957-1997, doi:10.1089/ars.2010.3586 (2011).
147 Dringen, R. Metabolism and functions of glutathione in brain. *Prog Neurobiol* **62**, 649-671 (2000).
148 Muse, K. E., Oberley, T. D., Sempf, J. M. & Oberley, L. W. Immunolocalization of antioxidant enzymes in adult hamster kidney. *Histochem J* **26**, 734-753 (1994).
149 Margis, R., Dunand, C., Teixeira, F. K. & Margis-Pinheiro, M. Glutathione peroxidase family - an evolutionary overview. *FEBS J* **275**, 3959-3970, doi:10.1111/j.1742-4658.2008.06542.x (2008).
150 Finkel, T. Reactive oxygen species and signal transduction. *IUBMB Life* **52**, 3-6, doi:10.1080/15216540252774694 (2001).
151 Rhee, S. G. Cell signaling. H2O2, a necessary evil for cell signaling. *Science* **312**, 1882-1883, doi:10.1126/science.1130481 (2006).
152 Brieger, K., Schiavone, S., Miller, F. J., Jr. & Krause, K. H. Reactive oxygen species: from health to disease. *Swiss Med Wkly* **142**, w13659, doi:10.4414/smw.2012.13659 (2012).
153 Gutowski, M. & Kowalczyk, S. A study of free radical chemistry: their role and pathophysiological significance. *Acta Biochim Pol* **60**, 1-16 (2013).
154 den Hertog, J., Groen, A. & van der Wijk, T. Redox regulation of protein-tyrosine phosphatases. *Arch Biochem Biophys* **434**, 11-15, doi:10.1016/j.abb.2004.05.024 (2005).
155 Liou, G. Y. & Storz, P. Reactive oxygen species in cancer. *Free Radic Res* **44**, 479-496, doi:10.3109/10715761003667554 (2010).
156 Kawanishi, S. & Murata, M. Mechanism of DNA damage induced by bromate differs from general types of oxidative stress. *Toxicology* **221**, 172-178, doi:10.1016/j.tox.2006.01.002 (2006).
157 Alam, J. & Cook, J. L. How many transcription factors does it take to turn on the heme oxygenase-1 gene? *Am J Respir Cell Mol Biol* **36**, 166-174, doi:10.1165/rcmb.2006-0340TR (2007).
158 Pronk, T. E., van der Veen, J. W., Vandebriel, R. J., van Loveren, H., de Vink, E. P. & Pennings, J. L. Comparison of the molecular topologies of stress-activated transcription factors HSF1, AP-1, NRF2, and NF-kappaB in their induction kinetics of HMOX1. *Biosystems* **124**, 75-85, doi:10.1016/j.biosystems.2014.09.005 (2014).
159 Martindale, J. L. & Holbrook, N. J. Cellular response to oxidative stress: signaling for suicide and survival. *J Cell Physiol* **192**, 1-15, doi:10.1002/jcp.10119 (2002).
160 Schreck, R., Rieber, P. & Baeuerle, P. A. Reactive oxygen intermediates as apparently widely used messengers in the activation of the NF-kappa B transcription factor and HIV-1. *EMBO J* **10**, 2247-2258 (1991).

161 Takada, Y., Mukhopadhyay, A., Kundu, G. C., Mahabeleshwar, G. H., Singh, S. & Aggarwal, B. B. Hydrogen peroxide activates NF-kappa B through tyrosine phosphorylation of I kappa B alpha and serine phosphorylation of p65: evidence for the involvement of I kappa B alpha kinase and Syk protein-tyrosine kinase. *J Biol Chem* **278**, 24233-24241, doi:10.1074/jbc.M212389200 (2003).

162 Schreiber, J., Jenner, R. G., Murray, H. L., Gerber, G. K., Gifford, D. K. & Young, R. A. Coordinated binding of NF-kappaB family members in the response of human cells to lipopolysaccharide. *Proc Natl Acad Sci U S A* **103**, 5899-5904, doi:10.1073/pnas.0510996103 (2006).

163 Zhou, L. Z., Johnson, A. P. & Rando, T. A. NF kappa B and AP-1 mediate transcriptional responses to oxidative stress in skeletal muscle cells. *Free Radic Biol Med* **31**, 1405-1416 (2001).

164 Rojo, A. I., Salinas, M., Martin, D., Perona, R. & Cuadrado, A. Regulation of Cu/Zn-superoxide dismutase expression via the phosphatidylinositol 3 kinase/Akt pathway and nuclear factor-kappaB. *J Neurosci* **24**, 7324-7334, doi:10.1523/JNEUROSCI.2111-04.2004 (2004).

165 Das, K. C., Lewis-Molock, Y. & White, C. W. Activation of NF-kappa B and elevation of MnSOD gene expression by thiol reducing agents in lung adenocarcinoma (A549) cells. *Am J Physiol* **269**, L588-602, doi:10.1152/ajplung.1995.269.5.L588 (1995).

166 Kimura, T., Kawasaki, Y., Okumura, F., Sone, T., Natsuki, R. & Isobe, M. Ethanol-induced expression of glutamate-cysteine ligase catalytic subunit gene is mediated by NF-kappaB. *Toxicol Lett* **185**, 110-115, doi:10.1016/j.toxlet.2008.12.006 (2009).

167 Webster, G. A. & Perkins, N. D. Transcriptional cross talk between NF-kappaB and p53. *Mol Cell Biol* **19**, 3485-3495 (1999).

168 Osburn, W. O., Wakabayashi, N., Misra, V., Nilles, T., Biswal, S., Trush, M. A. *et al.* Nrf2 regulates an adaptive response protecting against oxidative damage following diquat-mediated formation of superoxide anion. *Arch Biochem Biophys* **454**, 7-15, doi:10.1016/j.abb.2006.08.005 (2006).

169 Kobayashi, A., Kang, M. I., Watai, Y., Tong, K. I., Shibata, T., Uchida, K. *et al.* Oxidative and electrophilic stresses activate Nrf2 through inhibition of ubiquitination activity of Keap1. *Mol Cell Biol* **26**, 221-229, doi:10.1128/MCB.26.1.221-229.2006 (2006).

170 Kobayashi, M. & Yamamoto, M. Nrf2-Keap1 regulation of cellular defense mechanisms against electrophiles and reactive oxygen species. *Adv Enzyme Regul* **46**, 113-140, doi:10.1016/j.advenzreg.2006.01.007 (2006).

171 Yamamoto, T., Suzuki, T., Kobayashi, A., Wakabayashi, J., Maher, J., Motohashi, H. *et al.* Physiological significance of reactive cysteine residues of Keap1 in determining Nrf2 activity. *Mol Cell Biol* **28**, 2758-2770, doi:10.1128/MCB.01704-07 (2008).

172 Thimmulappa, R. K., Mai, K. H., Srisuma, S., Kensler, T. W., Yamamoto, M. & Biswal, S. Identification of Nrf2-regulated genes induced by the chemopreventive agent sulforaphane by oligonucleotide microarray. *Cancer Res* **62**, 5196-5203 (2002).

173 Jain, A., Lamark, T., Sjottem, E., Larsen, K. B., Awuh, J. A., Overvatn, A. *et al.* p62/SQSTM1 is a target gene for transcription factor NRF2 and creates a positive feedback loop by inducing antioxidant response element-driven gene transcription. *J Biol Chem* **285**, 22576-22591, doi:10.1074/jbc.M110.118976 (2010).

174 Cullinan, S. B., Gordan, J. D., Jin, J., Harper, J. W. & Diehl, J. A. The Keap1-BTB protein is an adaptor that bridges Nrf2 to a Cul3-based E3 ligase: oxidative stress sensing by a Cul3-Keap1 ligase. *Mol Cell Biol* **24**, 8477-8486, doi:10.1128/MCB.24.19.8477-8486.2004 (2004).

175 Wu, K. C., Cui, J. Y. & Klaassen, C. D. Beneficial role of Nrf2 in regulating NADPH generation and consumption. *Toxicol Sci* **123**, 590-600, doi:10.1093/toxsci/kfr183 (2011).

176 Mitsuishi, Y., Taguchi, K., Kawatani, Y., Shibata, T., Nukiwa, T., Aburatani, H. *et al.* Nrf2 redirects glucose and glutamine into anabolic pathways in metabolic reprogramming. *Cancer Cell* **22**, 66-79, doi:10.1016/j.ccr.2012.05.016 (2012).
177 Dinkova-Kostova, A. T. & Abramov, A. Y. The emerging role of Nrf2 in mitochondrial function. *Free Radic Biol Med* **88**, 179-188, doi:10.1016/j.freeradbiomed.2015.04.036 (2015).
178 Ahn, S. G. & Thiele, D. J. Redox regulation of mammalian heat shock factor 1 is essential for Hsp gene activation and protection from stress. *Genes Dev* **17**, 516-528, doi:10.1101/gad.1044503 (2003).
179 Lu, M., Kim, H. E., Li, C. R., Kim, S., Kwak, I. J., Lee, Y. J. *et al.* Two distinct disulfide bonds formed in human heat shock transcription factor 1 act in opposition to regulate its DNA binding activity. *Biochemistry* **47**, 6007-6015, doi:10.1021/bi702185u (2008).
180 Samarasinghe, B., Wales, C. T., Taylor, F. R. & Jacobs, A. T. Heat shock factor 1 confers resistance to Hsp90 inhibitors through p62/SQSTM1 expression and promotion of autophagic flux. *Biochem Pharmacol* **87**, 445-455, doi:10.1016/j.bcp.2013.11.014 (2014).
181 Maines, M. D. & Ewing, J. F. Stress response of the rat testis: in situ hydridization and immunohistochemical analysis of heme oxygenase-1 (HSP32) induction by hyperthermia. *Biol Reprod* **54**, 1070-1079 (1996).
182 Preville, X., Salvemini, F., Giraud, S., Chaufour, S., Paul, C., Stepien, G. *et al.* Mammalian small stress proteins protect against oxidative stress through their ability to increase glucose-6-phosphate dehydrogenase activity and by maintaining optimal cellular detoxifying machinery. *Exp Cell Res* **247**, 61-78, doi:10.1006/excr.1998.4347 (1999).
183 Wu, S., Gao, J., Ohlemeyer, C., Roos, D., Niessen, H., Kottgen, E. *et al.* Activation of AP-1 through reactive oxygen species by angiotensin II in rat cardiomyocytes. *Free Radic Biol Med* **39**, 1601-1610, doi:10.1016/j.freeradbiomed.2005.08.006 (2005).
184 Aharoni-Simon, M., Reifen, R. & Tirosh, O. ROS-production-mediated activation of AP-1 but not NFkappaB inhibits glutamate-induced HT4 neuronal cell death. *Antioxid Redox Signal* **8**, 1339-1349, doi:10.1089/ars.2006.8.1339 (2006).
185 Was, H., Dulak, J. & Jozkowicz, A. Heme oxygenase-1 in tumor biology and therapy. *Curr Drug Targets* **11**, 1551-1570 (2010).
186 Gandini, N. A., Fermento, M. E., Salomon, D. G., Obiol, D. J., Andres, N. C., Zenklusen, J. C. *et al.* Heme oxygenase-1 expression in human gliomas and its correlation with poor prognosis in patients with astrocytoma. *Tumour Biol* **35**, 2803-2815, doi:10.1007/s13277-013-1373-z (2014).
187 Ghosh, D., Ulasov, I. V., Chen, L., Harkins, L. E., Wallenborg, K., Hothi, P. *et al.* TGFbeta-Responsive HMOX1 Expression Is Associated with Stemness and Invasion in Glioblastoma Multiforme. *Stem Cells* **34**, 2276-2289, doi:10.1002/stem.2411 (2016).
188 Ma, L., Liu, J., Zhang, X., Qi, J., Yu, W. & Gu, Y. p38 MAPK-dependent Nrf2 induction enhances the resistance of glioma cells against TMZ. *Med Oncol* **32**, 69, doi:10.1007/s12032-015-0517-y (2015).
189 Zhang, L. & Wang, H. FTY720 inhibits the Nrf2/ARE pathway in human glioblastoma cell lines and sensitizes glioblastoma cells to temozolomide. *Pharmacol Rep* **69**, 1186-1193, doi:10.1016/j.pharep.2017.07.003 (2017).
190 Meyer, N., Zielke, S., Michaelis, J. B., Linder, B., Warnsmann, V., Rakel, S. *et al.* AT 101 induces early mitochondrial dysfunction and HMOX1 (heme oxygenase 1) to trigger mitophagic cell death in glioma cells. *Autophagy* **14**, 1693-1709, doi:10.1080/15548627.2018.1476812 (2018).
191 Son, Y., Cheong, Y. K., Kim, N. H., Chung, H. T., Kang, D. G. & Pae, H. O. Mitogen-Activated Protein Kinases and Reactive Oxygen Species: How Can ROS Activate MAPK Pathways? *J Signal Transduct* **2011**, 792639, doi:10.1155/2011/792639 (2011).

192 Runchel, C., Matsuzawa, A. & Ichijo, H. Mitogen-activated protein kinases in mammalian oxidative stress responses. *Antioxid Redox Signal* **15**, 205-218, doi:10.1089/ars.2010.3733 (2011).
193 Plotnikov, A., Zehorai, E., Procaccia, S. & Seger, R. The MAPK cascades: signaling components, nuclear roles and mechanisms of nuclear translocation. *Biochim Biophys Acta* **1813**, 1619-1633, doi:10.1016/j.bbamcr.2010.12.012 (2011).
194 Yoon, S. & Seger, R. The extracellular signal-regulated kinase: multiple substrates regulate diverse cellular functions. *Growth Factors* **24**, 21-44, doi:10.1080/02699050500284218 (2006).
195 Cuadrado, A. & Nebreda, A. R. Mechanisms and functions of p38 MAPK signalling. *Biochem J* **429**, 403-417, doi:10.1042/BJ20100323 (2010).
196 Bogoyevitch, M. A., Ngoei, K. R., Zhao, T. T., Yeap, Y. Y. & Ng, D. C. c-Jun N-terminal kinase (JNK) signaling: recent advances and challenges. *Biochim Biophys Acta* **1804**, 463-475, doi:10.1016/j.bbapap.2009.11.002 (2010).
197 Jiang, Q., Li, F., Shi, K., Wu, P., An, J., Yang, Y. *et al.* Involvement of p38 in signal switching from autophagy to apoptosis via the PERK/eIF2alpha/ATF4 axis in selenite-treated NB4 cells. *Cell Death Dis* **5**, e1270, doi:10.1038/cddis.2014.200 (2014).
198 Karin, M. The regulation of AP-1 activity by mitogen-activated protein kinases. *J Biol Chem* **270**, 16483-16486 (1995).
199 Catarzi, S., Romagnoli, C., Marcucci, G., Favilli, F., Iantomasi, T. & Vincenzini, M. T. Redox regulation of ERK1/2 activation induced by sphingosine 1-phosphate in fibroblasts: involvement of NADPH oxidase and platelet-derived growth factor receptor. *Biochim Biophys Acta* **1810**, 446-456, doi:10.1016/j.bbagen.2011.01.005 (2011).
200 Meves, A., Stock, S. N., Beyerle, A., Pittelkow, M. R. & Peus, D. H(2)O(2) mediates oxidative stress-induced epidermal growth factor receptor phosphorylation. *Toxicol Lett* **122**, 205-214 (2001).
201 Nagai, H., Noguchi, T., Takeda, K. & Ichijo, H. Pathophysiological roles of ASK1-MAP kinase signaling pathways. *J Biochem Mol Biol* **40**, 1-6 (2007).
202 Kamata, H., Honda, S., Maeda, S., Chang, L., Hirata, H. & Karin, M. Reactive oxygen species promote TNFalpha-induced death and sustained JNK activation by inhibiting MAP kinase phosphatases. *Cell* **120**, 649-661, doi:10.1016/j.cell.2004.12.041 (2005).
203 Soga, M., Matsuzawa, A. & Ichijo, H. Oxidative Stress-Induced Diseases via the ASK1 Signaling Pathway. *Int J Cell Biol* **2012**, 439587, doi:10.1155/2012/439587 (2012).
204 Kyriakis, J. M. & Avruch, J. Mammalian mitogen-activated protein kinase signal transduction pathways activated by stress and inflammation. *Physiol Rev* **81**, 807-869, doi:10.1152/physrev.2001.81.2.807 (2001).
205 Dai, R., Frejtag, W., He, B., Zhang, Y. & Mivechi, N. F. c-Jun NH2-terminal kinase targeting and phosphorylation of heat shock factor-1 suppress its transcriptional activity. *J Biol Chem* **275**, 18210-18218, doi:10.1074/jbc.M000958200 (2000).
206 Chu, B., Soncin, F., Price, B. D., Stevenson, M. A. & Calderwood, S. K. Sequential phosphorylation by mitogen-activated protein kinase and glycogen synthase kinase 3 represses transcriptional activation by heat shock factor-1. *J Biol Chem* **271**, 30847-30857 (1996).
207 Zipper, L. M. & Mulcahy, R. T. Erk activation is required for Nrf2 nuclear localization during pyrrolidine dithiocarbamate induction of glutamate cysteine ligase modulatory gene expression in HepG2 cells. *Toxicol Sci* **73**, 124-134, doi:10.1093/toxsci/kfg083 (2003).
208 Oguro, T., Hayashi, M., Nakajo, S., Numazawa, S. & Yoshida, T. The expression of heme oxygenase-1 gene responded to oxidative stress produced by phorone, a glutathione depletor, in the rat liver; the relevance to activation of c-jun n-terminal kinase. *J Pharmacol Exp Ther* **287**, 773-778 (1998).

209 Brenner, D. A., O'Hara, M., Angel, P., Chojkier, M. & Karin, M. Prolonged activation of jun and collagenase genes by tumour necrosis factor-alpha. *Nature* **337**, 661-663, doi:10.1038/337661a0 (1989).
210 McCubrey, J. A., Lahair, M. M. & Franklin, R. A. Reactive oxygen species-induced activation of the MAP kinase signaling pathways. *Antioxid Redox Signal* **8**, 1775-1789, doi:10.1089/ars.2006.8.1775 (2006).
211 Pakos-Zebrucka, K., Koryga, I., Mnich, K., Ljujic, M., Samali, A. & Gorman, A. M. The integrated stress response. *EMBO Rep* **17**, 1374-1395, doi:10.15252/embr.201642195 (2016).
212 Rajesh, K., Krishnamoorthy, J., Kazimierczak, U., Tenkerian, C., Papadakis, A. I., Wang, S. *et al.* Phosphorylation of the translation initiation factor eIF2alpha at serine 51 determines the cell fate decisions of Akt in response to oxidative stress. *Cell Death Dis* **6**, e1591, doi:10.1038/cddis.2014.554 (2015).
213 Donnelly, N., Gorman, A. M., Gupta, S. & Samali, A. The eIF2alpha kinases: their structures and functions. *Cell Mol Life Sci* **70**, 3493-3511, doi:10.1007/s00018-012-1252-6 (2013).
214 Taniuchi, S., Miyake, M., Tsugawa, K., Oyadomari, M. & Oyadomari, S. Integrated stress response of vertebrates is regulated by four eIF2alpha kinases. *Sci Rep* **6**, 32886, doi:10.1038/srep32886 (2016).
215 Jackson, R. J., Hellen, C. U. & Pestova, T. V. The mechanism of eukaryotic translation initiation and principles of its regulation. *Nat Rev Mol Cell Biol* **11**, 113-127, doi:10.1038/nrm2838 (2010).
216 Spriggs, K. A., Bushell, M. & Willis, A. E. Translational regulation of gene expression during conditions of cell stress. *Mol Cell* **40**, 228-237, doi:10.1016/j.molcel.2010.09.028 (2010).
217 Dey, S., Sayers, C. M., Verginadis, II, Lehman, S. L., Cheng, Y., Cerniglia, G. J. *et al.* ATF4-dependent induction of heme oxygenase 1 prevents anoikis and promotes metastasis. *J Clin Invest* **125**, 2592-2608, doi:10.1172/JCI78031 (2015).
218 Kroemer, G., Marino, G. & Levine, B. Autophagy and the integrated stress response. *Mol Cell* **40**, 280-293, doi:10.1016/j.molcel.2010.09.023 (2010).
219 Matsumoto, H., Miyazaki, S., Matsuyama, S., Takeda, M., Kawano, M., Nakagawa, H. *et al.* Selection of autophagy or apoptosis in cells exposed to ER-stress depends on ATF4 expression pattern with or without CHOP expression. *Biol Open* **2**, 1084-1090, doi:10.1242/bio.20135033 (2013).
220 Lei, Y., Wang, S., Ren, B., Wang, J., Chen, J., Lu, J. *et al.* CHOP favors endoplasmic reticulum stress-induced apoptosis in hepatocellular carcinoma cells via inhibition of autophagy. *PLoS One* **12**, e0183680, doi:10.1371/journal.pone.0183680 (2017).
221 Urra, H., Dufey, E., Lisbona, F., Rojas-Rivera, D. & Hetz, C. When ER stress reaches a dead end. *Biochim Biophys Acta* **1833**, 3507-3517, doi:10.1016/j.bbamcr.2013.07.024 (2013).
222 Yagi, A., Hasegawa, Y., Xiao, H. Y., Haneda, M., Kojima, E., Nishikimi, A. *et al.* GADD34 induces p53 phosphorylation and p21/WAF1 transcription. *Journal of Cellular Biochemistry* **90**, 1242-1249, doi:10.1002/jcb.10711 (2003).
223 Fulda, S., Gorman, A. M., Hori, O. & Samali, A. Cellular stress responses: cell survival and cell death. *Int J Cell Biol* **2010**, 214074, doi:10.1155/2010/214074 (2010).
224 Green, D. R. & Llambi, F. Cell Death Signaling. *Cold Spring Harb Perspect Biol* **7**, doi:10.1101/cshperspect.a006080 (2015).
225 Tsujimoto, Y. & Shimizu, S. Another way to die: autophagic programmed cell death. *Cell Death Differ* **12 Suppl 2**, 1528-1534, doi:10.1038/sj.cdd.4401777 (2005).
226 Grooten, J., Goossens, V., Vanhaesebroeck, B. & Fiers, W. Cell membrane permeabilization and cellular collapse, followed by loss of dehydrogenase activity: early events in tumour necrosis factor-induced cytotoxicity. *Cytokine* **5**, 546-555 (1993).

227 Ellis, H. M. & Horvitz, H. R. Genetic control of programmed cell death in the nematode C. elegans. *Cell* **44**, 817-829 (1986).
228 Ashkenazi, A. & Salvesen, G. Regulated cell death: signaling and mechanisms. *Annu Rev Cell Dev Biol* **30**, 337-356, doi:10.1146/annurev-cellbio-100913-013226 (2014).
229 Kerr, J. F., Wyllie, A. H. & Currie, A. R. Apoptosis: a basic biological phenomenon with wide-ranging implications in tissue kinetics. *Br J Cancer* **26**, 239-257 (1972).
230 Majno, G. & Joris, I. Apoptosis, oncosis, and necrosis. An overview of cell death. *Am J Pathol* **146**, 3-15 (1995).
231 Arends, M. J., Morris, R. G. & Wyllie, A. H. Apoptosis. The role of the endonuclease. *Am J Pathol* **136**, 593-608 (1990).
232 Coleman, M. L., Sahai, E. A., Yeo, M., Bosch, M., Dewar, A. & Olson, M. F. Membrane blebbing during apoptosis results from caspase-mediated activation of ROCK I. *Nat Cell Biol* **3**, 339-345, doi:10.1038/35070009 (2001).
233 Fadok, V. A., Voelker, D. R., Campbell, P. A., Cohen, J. J., Bratton, D. L. & Henson, P. M. Exposure of phosphatidylserine on the surface of apoptotic lymphocytes triggers specific recognition and removal by macrophages. *J Immunol* **148**, 2207-2216 (1992).
234 Sen, S. Programmed cell death: concept, mechanism and control. *Biol Rev Camb Philos Soc* **67**, 287-319 (1992).
235 Anilkumar, T. V., Sarraf, C. E. & Alison, M. R. The biology and pathology of programmed cell death (apoptosis). *Vet Hum Toxicol* **34**, 251-254 (1992).
236 Van Cruchten, S. & Van Den Broeck, W. Morphological and biochemical aspects of apoptosis, oncosis and necrosis. *Anat Histol Embryol* **31**, 214-223 (2002).
237 Cohen, G. M. Caspases: the executioners of apoptosis. *Biochem J* **326 (Pt 1)**, 1-16 (1997).
238 Shi, Y. Mechanisms of caspase activation and inhibition during apoptosis. *Mol Cell* **9**, 459-470 (2002).
239 Shi, Y. Caspase activation, inhibition, and reactivation: a mechanistic view. *Protein Sci* **13**, 1979-1987, doi:10.1110/ps.04789804 (2004).
240 Degterev, A., Boyce, M. & Yuan, J. A decade of caspases. *Oncogene* **22**, 8543-8567, doi:10.1038/sj.onc.1207107 (2003).
241 Shi, Y. Apoptosome: the cellular engine for the activation of caspase-9. *Structure* **10**, 285-288 (2002).
242 McIlwain, D. R., Berger, T. & Mak, T. W. Caspase functions in cell death and disease. *Cold Spring Harb Perspect Biol* **5**, a008656, doi:10.1101/cshperspect.a008656 (2013).
243 Bao, Q. & Shi, Y. Apoptosome: a platform for the activation of initiator caspases. *Cell Death Differ* **14**, 56-65, doi:10.1038/sj.cdd.4402028 (2007).
244 Gibson, E. M., Henson, E. S., Villanueva, J. & Gibson, S. B. MEK kinase 1 induces mitochondrial permeability transition leading to apoptosis independent of cytochrome c release. *J Biol Chem* **277**, 10573-10580, doi:10.1074/jbc.M108366200 (2002).
245 Fulda, S. & Debatin, K. M. Extrinsic versus intrinsic apoptosis pathways in anticancer chemotherapy. *Oncogene* **25**, 4798-4811, doi:10.1038/sj.onc.1209608 (2006).
246 Galluzzi, L., Vitale, I., Aaronson, S. A., Abrams, J. M., Adam, D., Agostinis, P. *et al.* Molecular mechanisms of cell death: recommendations of the Nomenclature Committee on Cell Death 2018. *Cell Death Differ* **25**, 486-541, doi:10.1038/s41418-017-0012-4 (2018).
247 Lavrik, I. N., Golks, A. & Krammer, P. H. Caspases: pharmacological manipulation of cell death. *J Clin Invest* **115**, 2665-2672, doi:10.1172/JCI26252 (2005).
248 Wang, S. & El-Deiry, W. S. TRAIL and apoptosis induction by TNF-family death receptors. *Oncogene* **22**, 8628-8633, doi:10.1038/sj.onc.1207232 (2003).

249 Nakagawa, T., Zhu, H., Morishima, N., Li, E., Xu, J., Yankner, B. A. *et al.* Caspase-12 mediates endoplasmic-reticulum-specific apoptosis and cytotoxicity by amyloid-beta. *Nature* **403**, 98-103, doi:10.1038/47513 (2000).

250 Kroemer, G., Galluzzi, L. & Brenner, C. Mitochondrial membrane permeabilization in cell death. *Physiol Rev* **87**, 99-163, doi:10.1152/physrev.00013.2006 (2007).

251 Denton, D., Xu, T. & Kumar, S. Autophagy as a pro-death pathway. *Immunol Cell Biol* **93**, 35-42, doi:10.1038/icb.2014.85 (2015).

252 Levine, B. & Kroemer, G. Autophagy in the pathogenesis of disease. *Cell* **132**, 27-42, doi:10.1016/j.cell.2007.12.018 (2008).

253 Rabanal-Ruiz, Y., Otten, E. G. & Korolchuk, V. I. mTORC1 as the main gateway to autophagy. *Essays Biochem* **61**, 565-584, doi:10.1042/EBC20170027 (2017).

254 Yu, L., McPhee, C. K., Zheng, L., Mardones, G. A., Rong, Y., Peng, J. *et al.* Termination of autophagy and reformation of lysosomes regulated by mTOR. *Nature* **465**, 942-946, doi:10.1038/nature09076 (2010).

255 Tsukada, M. & Ohsumi, Y. Isolation and characterization of autophagy-defective mutants of Saccharomyces cerevisiae. *FEBS Lett* **333**, 169-174 (1993).

256 Nikoletopoulou, V., Markaki, M., Palikaras, K. & Tavernarakis, N. Crosstalk between apoptosis, necrosis and autophagy. *Biochim Biophys Acta* **1833**, 3448-3459, doi:10.1016/j.bbamcr.2013.06.001 (2013).

257 Shimizu, S., Kanaseki, T., Mizushima, N., Mizuta, T., Arakawa-Kobayashi, S., Thompson, C. B. *et al.* Role of Bcl-2 family proteins in a non-apoptotic programmed cell death dependent on autophagy genes. *Nat Cell Biol* **6**, 1221-1228, doi:10.1038/ncb1192 (2004).

258 Bursch, W. The autophagosomal-lysosomal compartment in programmed cell death. *Cell Death Differ* **8**, 569-581, doi:10.1038/sj.cdd.4400852 (2001).

259 Liu, W. J., Ye, L., Huang, W. F., Guo, L. J., Xu, Z. G., Wu, H. L. *et al.* p62 links the autophagy pathway and the ubiqutin-proteasome system upon ubiquitinated protein degradation. *Cell Mol Biol Lett* **21**, 29, doi:10.1186/s11658-016-0031-z (2016).

260 Hansen, T. E. & Johansen, T. Following autophagy step by step. *BMC Biol* **9**, 39, doi:10.1186/1741-7007-9-39 (2011).

261 Fan, Y. J. & Zong, W. X. The cellular decision between apoptosis and autophagy. *Chin J Cancer* **32**, 121-129, doi:10.5732/cjc.012.10106 (2013).

262 Li, Y., Zhu, H., Zeng, X., Fan, J., Qian, X., Wang, S. *et al.* Suppression of autophagy enhanced growth inhibition and apoptosis of interferon-beta in human glioma cells. *Mol Neurobiol* **47**, 1000-1010, doi:10.1007/s12035-013-8403-0 (2013).

263 Li, H., Jin, X., Zhang, Z., Xing, Y. & Kong, X. Inhibition of autophagy enhances apoptosis induced by the PI3K/AKT/mTor inhibitor NVP-BEZ235 in renal cell carcinoma cells. *Cell Biochem Funct* **31**, 427-433, doi:10.1002/cbf.2917 (2013).

264 Liang, J., Shao, S. H., Xu, Z. X., Hennessy, B., Ding, Z., Larrea, M. *et al.* The energy sensing LKB1-AMPK pathway regulates p27(kip1) phosphorylation mediating the decision to enter autophagy or apoptosis. *Nat Cell Biol* **9**, 218-224, doi:10.1038/ncb1537 (2007).

265 Marino, G., Niso-Santano, M., Baehrecke, E. H. & Kroemer, G. Self-consumption: the interplay of autophagy and apoptosis. *Nat Rev Mol Cell Biol* **15**, 81-94, doi:10.1038/nrm3735 (2014).

266 Grivennikov, S. I. & Karin, M. Dangerous liaisons: STAT3 and NF-kappaB collaboration and crosstalk in cancer. *Cytokine Growth Factor Rev* **21**, 11-19, doi:10.1016/j.cytogfr.2009.11.005 (2010).

267 Jonchere, B., Belanger, A., Guette, C., Barre, B. & Coqueret, O. STAT3 as a new autophagy regulator. *JAKSTAT* **2**, e24353, doi:10.4161/jkst.24353 (2013).

268 Djavaheri-Mergny, M., Amelotti, M., Mathieu, J., Besancon, F., Bauvy, C., Souquere, S. *et al.* NF-kappaB activation represses tumor necrosis factor-alpha-induced autophagy. *J Biol Chem* **281**, 30373-30382, doi:10.1074/jbc.M602097200 (2006).

269 Fan, Y., Mao, R. & Yang, J. NF-kappaB and STAT3 signaling pathways collaboratively link inflammation to cancer. *Protein Cell* **4**, 176-185, doi:10.1007/s13238-013-2084-3 (2013).
270 Karin, M. How NF-kappaB is activated: the role of the IkappaB kinase (IKK) complex. *Oncogene* **18**, 6867-6874, doi:10.1038/sj.onc.1203219 (1999).
271 Karin, M. The beginning of the end: IkappaB kinase (IKK) and NF-kappaB activation. *J Biol Chem* **274**, 27339-27342 (1999).
272 Rawlings, J. S., Rosler, K. M. & Harrison, D. A. The JAK/STAT signaling pathway. *J Cell Sci* **117**, 1281-1283, doi:10.1242/jcs.00963 (2004).
273 Han, Y., Leaman, D. W., Watling, D., Rogers, N. C., Groner, B., Kerr, I. M. *et al.* Participation of JAK and STAT proteins in growth hormone-induced signaling. *J Biol Chem* **271**, 5947-5952 (1996).
274 Darnell, J. E., Jr., Kerr, I. M. & Stark, G. R. Jak-STAT pathways and transcriptional activation in response to IFNs and other extracellular signaling proteins. *Science* **264**, 1415-1421 (1994).
275 Niu, G., Wright, K. L., Ma, Y., Wright, G. M., Huang, M., Irby, R. *et al.* Role of Stat3 in regulating p53 expression and function. *Mol Cell Biol* **25**, 7432-7440, doi:10.1128/MCB.25.17.7432-7440.2005 (2005).
276 Tergaonkar, V., Pando, M., Vafa, O., Wahl, G. & Verma, I. p53 stabilization is decreased upon NFkappaB activation: a role for NFkappaB in acquisition of resistance to chemotherapy. *Cancer Cell* **1**, 493-503 (2002).
277 Hanahan, D. & Weinberg, R. A. Hallmarks of cancer: the next generation. *Cell* **144**, 646-674, doi:10.1016/j.cell.2011.02.013 (2011).
278 McFarland, B. C., Gray, G. K., Nozell, S. E., Hong, S. W. & Benveniste, E. N. Activation of the NF-kappa B Pathway by the STAT3 Inhibitor JSI-124 in Human Glioblastoma Cells. *Molecular Cancer Research* **11**, 494-505, doi:10.1158/1541-7786.Mcr-12-0528 (2013).
279 Atkinson, G. P., Nozell, S. E. & Benveniste, E. T. NF-kappaB and STAT3 signaling in glioma: targets for future therapies. *Expert Rev Neurother* **10**, 575-586, doi:10.1586/ern.10.21 (2010).
280 Trocoli, A. & Djavaheri-Mergny, M. The complex interplay between autophagy and NF-kappaB signaling pathways in cancer cells. *Am J Cancer Res* **1**, 629-649 (2011).
281 You, L., Wang, Z., Li, H., Shou, J., Jing, Z., Xie, J. *et al.* The role of STAT3 in autophagy. *Autophagy* **11**, 729-739, doi:10.1080/15548627.2015.1017192 (2015).
282 Mathew, R. & White, E. Autophagy in tumorigenesis and energy metabolism: friend by day, foe by night. *Curr Opin Genet Dev* **21**, 113-119, doi:10.1016/j.gde.2010.12.008 (2011).
283 Mukhtar, E., Adhami, V. M., Khan, N. & Mukhtar, H. Apoptosis and autophagy induction as mechanism of cancer prevention by naturally occurring dietary agents. *Curr Drug Targets* **13**, 1831-1841 (2012).
284 Barnum, K. J. & O'Connell, M. J. Cell cycle regulation by checkpoints. *Methods Mol Biol* **1170**, 29-40, doi:10.1007/978-1-4939-0888-2_2 (2014).
285 Peddibhotla, S. & Rosen, J. M. Chking and executing cell division to prevent genomic instability. *Cell Cycle* **8**, 2339-2342, doi:10.4161/cc.8.15.9169 (2009).
286 Ishikawa, K., Ishii, H. & Saito, T. DNA damage-dependent cell cycle checkpoints and genomic stability. *DNA Cell Biol* **25**, 406-411, doi:10.1089/dna.2006.25.406 (2006).
287 Beach, D., Durkacz, B. & Nurse, P. Functionally homologous cell cycle control genes in budding and fission yeast. *Nature* **300**, 706-709 (1982).
288 Nurse, P. & Thuriaux, P. Regulatory genes controlling mitosis in the fission yeast Schizosaccharomyces pombe. *Genetics* **96**, 627-637 (1980).
289 Nurse, P., Thuriaux, P. & Nasmyth, K. Genetic control of the cell division cycle in the fission yeast Schizosaccharomyces pombe. *Mol Gen Genet* **146**, 167-178 (1976).

290 Mitchison, J. M. & Creanor, J. Further measurements of DNA synthesis and enzyme potential during cell cycle of fission yeast Schizosaccharomyces pombe. *Exp Cell Res* **69**, 244-247 (1971).
291 Mitchison, J. M. & Creanor, J. Induction synchrony in the fission yeast. Schizosaccharomyces pombe. *Exp Cell Res* **67**, 368-374 (1971).
292 Glotzer, M., Murray, A. W. & Kirschner, M. W. Cyclin is degraded by the ubiquitin pathway. *Nature* **349**, 132-138, doi:10.1038/349132a0 (1991).
293 Bai, C., Sen, P., Hofmann, K., Ma, L., Goebl, M., Harper, J. W. *et al.* SKP1 connects cell cycle regulators to the ubiquitin proteolysis machinery through a novel motif, the F-box. *Cell* **86**, 263-274 (1996).
294 Malumbres, M. & Barbacid, M. Mammalian cyclin-dependent kinases. *Trends Biochem Sci* **30**, 630-641, doi:10.1016/j.tibs.2005.09.005 (2005).
295 Malumbres, M. & Barbacid, M. To cycle or not to cycle: a critical decision in cancer. *Nat Rev Cancer* **1**, 222-231, doi:10.1038/35106065 (2001).
296 Lundberg, A. S. & Weinberg, R. A. Functional inactivation of the retinoblastoma protein requires sequential modification by at least two distinct cyclin-cdk complexes. *Mol Cell Biol* **18**, 753-761 (1998).
297 Weinberg, R. A. The retinoblastoma protein and cell cycle control. *Cell* **81**, 323-330 (1995).
298 Dyson, N. The regulation of E2F by pRB-family proteins. *Genes Dev* **12**, 2245-2262 (1998).
299 Matsushime, H., Quelle, D. E., Shurtleff, S. A., Shibuya, M., Sherr, C. J. & Kato, J. Y. D-type cyclin-dependent kinase activity in mammalian cells. *Mol Cell Biol* **14**, 2066-2076 (1994).
300 Ross, J. F., Liu, X. & Dynlacht, B. D. Mechanism of transcriptional repression of E2F by the retinoblastoma tumor suppressor protein. *Mol Cell* **3**, 195-205 (1999).
301 Magnaghi-Jaulin, L., Groisman, R., Naguibneva, I., Robin, P., Lorain, S., Le Villain, J. P. *et al.* Retinoblastoma protein represses transcription by recruiting a histone deacetylase. *Nature* **391**, 601-605, doi:10.1038/35410 (1998).
302 Brehm, A., Miska, E. A., McCance, D. J., Reid, J. L., Bannister, A. J. & Kouzarides, T. Retinoblastoma protein recruits histone deacetylase to repress transcription. *Nature* **391**, 597-601, doi:10.1038/35404 (1998).
303 Luo, R. X., Postigo, A. A. & Dean, D. C. Rb interacts with histone deacetylase to repress transcription. *Cell* **92**, 463-473 (1998).
304 Johnson, D. G. & Schneider-Broussard, R. Role of E2F in cell cycle control and cancer. *Front Biosci* **3**, d447-448 (1998).
305 Feaver, W. J., Svejstrup, J. Q., Henry, N. L. & Kornberg, R. D. Relationship of CDK-activating kinase and RNA polymerase II CTD kinase TFIIH/TFIIK. *Cell* **79**, 1103-1109 (1994).
306 Cisek, L. J. & Corden, J. L. Phosphorylation of RNA polymerase by the murine homologue of the cell-cycle control protein cdc2. *Nature* **339**, 679-684, doi:10.1038/339679a0 (1989).
307 Cheng, S. W., Kuzyk, M. A., Moradian, A., Ichu, T. A., Chang, V. C., Tien, J. F. *et al.* Interaction of cyclin-dependent kinase 12/CrkRS with cyclin K1 is required for the phosphorylation of the C-terminal domain of RNA polymerase II. *Mol Cell Biol* **32**, 4691-4704, doi:10.1128/MCB.06267-11 (2012).
308 Russo, A. A., Jeffrey, P. D., Patten, A. K., Massague, J. & Pavletich, N. P. Crystal structure of the p27Kip1 cyclin-dependent-kinase inhibitor bound to the cyclin A-Cdk2 complex. *Nature* **382**, 325-331, doi:10.1038/382325a0 (1996).
309 Besson, A., Dowdy, S. F. & Roberts, J. M. CDK inhibitors: cell cycle regulators and beyond. *Dev Cell* **14**, 159-169, doi:10.1016/j.devcel.2008.01.013 (2008).
310 Guan, K. L., Jenkins, C. W., Li, Y., Nichols, M. A., Wu, X., O'Keefe, C. L. *et al.* Growth suppression by p18, a p16INK4/MTS1- and p14INK4B/MTS2-related CDK6 inhibitor, correlates with wild-type pRb function. *Genes Dev* **8**, 2939-2952 (1994).

311 Hannon, G. J. & Beach, D. p15INK4B is a potential effector of TGF-beta-induced cell cycle arrest. *Nature* **371**, 257-261, doi:10.1038/371257a0 (1994).
312 Serrano, M., Hannon, G. J. & Beach, D. A new regulatory motif in cell-cycle control causing specific inhibition of cyclin D/CDK4. *Nature* **366**, 704-707, doi:10.1038/366704a0 (1993).
313 Hirai, H., Roussel, M. F., Kato, J. Y., Ashmun, R. A. & Sherr, C. J. Novel INK4 proteins, p19 and p18, are specific inhibitors of the cyclin D-dependent kinases CDK4 and CDK6. *Mol Cell Biol* **15**, 2672-2681 (1995).
314 Chan, F. K., Zhang, J., Cheng, L., Shapiro, D. N. & Winoto, A. Identification of human and mouse p19, a novel CDK4 and CDK6 inhibitor with homology to p16ink4. *Mol Cell Biol* **15**, 2682-2688 (1995).
315 Gu, Y., Turck, C. W. & Morgan, D. O. Inhibition of CDK2 activity in vivo by an associated 20K regulatory subunit. *Nature* **366**, 707-710, doi:10.1038/366707a0 (1993).
316 Harper, J. W., Adami, G. R., Wei, N., Keyomarsi, K. & Elledge, S. J. The p21 Cdk-interacting protein Cip1 is a potent inhibitor of G1 cyclin-dependent kinases. *Cell* **75**, 805-816 (1993).
317 Lee, M. H., Reynisdottir, I. & Massague, J. Cloning of p57KIP2, a cyclin-dependent kinase inhibitor with unique domain structure and tissue distribution. *Genes Dev* **9**, 639-649 (1995).
318 Polyak, K., Kato, J. Y., Solomon, M. J., Sherr, C. J., Massague, J., Roberts, J. M. *et al.* p27Kip1, a cyclin-Cdk inhibitor, links transforming growth factor-beta and contact inhibition to cell cycle arrest. *Genes Dev* **8**, 9-22 (1994).
319 Polyak, K., Lee, M. H., Erdjument-Bromage, H., Koff, A., Roberts, J. M., Tempst, P. *et al.* Cloning of p27Kip1, a cyclin-dependent kinase inhibitor and a potential mediator of extracellular antimitogenic signals. *Cell* **78**, 59-66 (1994).
320 Sherr, C. J. & Roberts, J. M. CDK inhibitors: positive and negative regulators of G1-phase progression. *Genes Dev* **13**, 1501-1512 (1999).
321 Filmus, J., Robles, A. I., Shi, W., Wong, M. J., Colombo, L. L. & Conti, C. J. Induction of cyclin D1 overexpression by activated ras. *Oncogene* **9**, 3627-3633 (1994).
322 Lavoie, J. N., Rivard, N., L'Allemain, G. & Pouyssegur, J. A temporal and biochemical link between growth factor-activated MAP kinases, cyclin D1 induction and cell cycle entry. *Prog Cell Cycle Res* **2**, 49-58 (1996).
323 Weber, J. D., Raben, D. M., Phillips, P. J. & Baldassare, J. J. Sustained activation of extracellular-signal-regulated kinase 1 (ERK1) is required for the continued expression of cyclin D1 in G1 phase. *Biochem J* **326 (Pt 1)**, 61-68 (1997).
324 Diehl, J. A., Cheng, M., Roussel, M. F. & Sherr, C. J. Glycogen synthase kinase-3beta regulates cyclin D1 proteolysis and subcellular localization. *Genes Dev* **12**, 3499-3511 (1998).
325 Bellido, T., O'Brien, C. A., Roberson, P. K. & Manolagas, S. C. Transcriptional activation of the p21(WAF1,CIP1,SDI1) gene by interleukin-6 type cytokines. A prerequisite for their pro-differentiating and anti-apoptotic effects on human osteoblastic cells. *J Biol Chem* **273**, 21137-21144 (1998).
326 Chin, Y. E., Kitagawa, M., Su, W. C., You, Z. H., Iwamoto, Y. & Fu, X. Y. Cell growth arrest and induction of cyclin-dependent kinase inhibitor p21 WAF1/CIP1 mediated by STAT1. *Science* **272**, 719-722 (1996).
327 Florenes, V. A., Lu, C., Bhattacharya, N., Rak, J., Sheehan, C., Slingerland, J. M. *et al.* Interleukin-6 dependent induction of the cyclin dependent kinase inhibitor p21WAF1/CIP1 is lost during progression of human malignant melanoma. *Oncogene* **18**, 1023-1032, doi:10.1038/sj.onc.1202382 (1999).
328 Sinibaldi, D., Wharton, W., Turkson, J., Bowman, T., Pledger, W. J. & Jove, R. Induction of p21WAF1/CIP1 and cyclin D1 expression by the Src oncoprotein in mouse fibroblasts: role of activated STAT3 signaling. *Oncogene* **19**, 5419-5427, doi:10.1038/sj.onc.1203947 (2000).

329 Brunet, A., Roux, D., Lenormand, P., Dowd, S., Keyse, S. & Pouyssegur, J. Nuclear translocation of p42/p44 mitogen-activated protein kinase is required for growth factor-induced gene expression and cell cycle entry. *EMBO J* **18**, 664-674, doi:10.1093/emboj/18.3.664 (1999).
330 Lavoie, J. N., L'Allemain, G., Brunet, A., Muller, R. & Pouyssegur, J. Cyclin D1 expression is regulated positively by the p42/p44MAPK and negatively by the p38/HOGMAPK pathway. *J Biol Chem* **271**, 20608-20616 (1996).
331 MacCorkle, R. A. & Tan, T. H. Mitogen-activated protein kinases in cell-cycle control. *Cell Biochem Biophys* **43**, 451-461, doi:10.1385/CBB:43:3:451 (2005).
332 Giono, L. E. & Manfredi, J. J. The p53 tumor suppressor participates in multiple cell cycle checkpoints. *J Cell Physiol* **209**, 13-20, doi:10.1002/jcp.20689 (2006).
333 Shaw, P. H. The role of p53 in cell cycle regulation. *Pathol Res Pract* **192**, 669-675, doi:10.1016/S0344-0338(96)80088-4 (1996).
334 Piette, J., Neel, H. & Marechal, V. Mdm2: keeping p53 under control. *Oncogene* **15**, 1001-1010, doi:10.1038/sj.onc.1201432 (1997).
335 Agarwal, M. L., Agarwal, A., Taylor, W. R. & Stark, G. R. p53 controls both the G2/M and the G1 cell cycle checkpoints and mediates reversible growth arrest in human fibroblasts. *Proc Natl Acad Sci U S A* **92**, 8493-8497 (1995).
336 Guillouf, C., Rosselli, F., Krishnaraju, K., Moustacchi, E., Hoffman, B. & Liebermann, D. A. p53 involvement in control of G2 exit of the cell cycle: role in DNA damage-induced apoptosis. *Oncogene* **10**, 2263-2270 (1995).
337 Stewart, N., Hicks, G. G., Paraskevas, F. & Mowat, M. Evidence for a second cell cycle block at G2/M by p53. *Oncogene* **10**, 109-115 (1995).
338 Kastan, M. B., Onyekwere, O., Sidransky, D., Vogelstein, B. & Craig, R. W. Participation of p53 protein in the cellular response to DNA damage. *Cancer Res* **51**, 6304-6311 (1991).
339 Clarke, A. R., Purdie, C. A., Harrison, D. J., Morris, R. G., Bird, C. C., Hooper, M. L. *et al.* Thymocyte apoptosis induced by p53-dependent and independent pathways. *Nature* **362**, 849-852, doi:10.1038/362849a0 (1993).
340 Lowe, S. W., Ruley, H. E., Jacks, T. & Housman, D. E. p53-dependent apoptosis modulates the cytotoxicity of anticancer agents. *Cell* **74**, 957-967 (1993).
341 Lowe, S. W., Schmitt, E. M., Smith, S. W., Osborne, B. A. & Jacks, T. p53 is required for radiation-induced apoptosis in mouse thymocytes. *Nature* **362**, 847-849, doi:10.1038/362847a0 (1993).
342 Ozaki, T. & Nakagawara, A. Role of p53 in Cell Death and Human Cancers. *Cancers (Basel)* **3**, 994-1013, doi:10.3390/cancers3010994 (2011).
343 Aubrey, B. J., Strasser, A. & Kelly, G. L. Tumor-Suppressor Functions of the TP53 Pathway. *Cold Spring Harb Perspect Med* **6**, doi:10.1101/cshperspect.a026062 (2016).
344 Lisek, K., Campaner, E., Ciani, Y., Walerych, D. & Del Sal, G. Mutant p53 tunes the NRF2-dependent antioxidant response to support survival of cancer cells. *Oncotarget* **9**, 20508-20523, doi:10.18632/oncotarget.24974 (2018).
345 Ham, S. W., Jeon, H. Y., Jin, X., Kim, E. J., Kim, J. K., Shin, Y. J. *et al.* TP53 gain-of-function mutation promotes inflammation in glioblastoma. *Cell Death Differ*, doi:10.1038/s41418-018-0126-3 (2018).
346 Wang, X., Chen, J. X., Liu, J. P., You, C., Liu, Y. H. & Mao, Q. Gain of function of mutant TP53 in glioblastoma: prognosis and response to temozolomide. *Ann Surg Oncol* **21**, 1337-1344, doi:10.1245/s10434-013-3380-0 (2014).
347 Yue, X., Zhao, Y., Xu, Y., Zheng, M., Feng, Z. & Hu, W. Mutant p53 in Cancer: Accumulation, Gain-of-Function, and Therapy. *J Mol Biol* **429**, 1595-1606, doi:10.1016/j.jmb.2017.03.030 (2017).
348 Oren, M. & Rotter, V. Mutant p53 gain-of-function in cancer. *Cold Spring Harb Perspect Biol* **2**, a001107, doi:10.1101/cshperspect.a001107 (2010).
349 Metzger, D., Clifford, J., Chiba, H. & Chambon, P. Conditional site-specific recombination in mammalian cells using a ligand-dependent chimeric Cre recombinase. *Proc Natl Acad Sci U S A* **92**, 6991-6995 (1995).

350 Rohlmann, A., Gotthardt, M., Willnow, T. E., Hammer, R. E. & Herz, J. Sustained somatic gene inactivation by viral transfer of Cre recombinase. *Nat Biotechnol* **14**, 1562-1565, doi:10.1038/nbt1196-1562 (1996).
351 Austin, S., Ziese, M. & Sternberg, N. A novel role for site-specific recombination in maintenance of bacterial replicons. *Cell* **25**, 729-736 (1981).
352 Langer, S. J., Ghafoori, A. P., Byrd, M. & Leinwand, L. A genetic screen identifies novel non-compatible loxP sites. *Nucleic Acids Res* **30**, 3067-3077 (2002).
353 Hoess, R. H. & Abremski, K. Mechanism of strand cleavage and exchange in the Cre-lox site-specific recombination system. *J Mol Biol* **181**, 351-362 (1985).
354 Gaj, T., Sirk, S. J. & Barbas, C. F., 3rd. Expanding the scope of site-specific recombinases for genetic and metabolic engineering. *Biotechnol Bioeng* **111**, 1-15, doi:10.1002/bit.25096 (2014).
355 Lakso, M., Sauer, B., Mosinger, B., Jr., Lee, E. J., Manning, R. W., Yu, S. H. *et al.* Targeted oncogene activation by site-specific recombination in transgenic mice. *Proc Natl Acad Sci U S A* **89**, 6232-6236 (1992).
356 Sauer, B. & Henderson, N. Site-specific DNA recombination in mammalian cells by the Cre recombinase of bacteriophage P1. *Proc Natl Acad Sci U S A* **85**, 5166-5170 (1988).
357 Sauer, B. & Henderson, N. Cre-stimulated recombination at loxP-containing DNA sequences placed into the mammalian genome. *Nucleic Acids Res* **17**, 147-161 (1989).
358 Sternberg, N. & Hamilton, D. Bacteriophage P1 site-specific recombination. I. Recombination between loxP sites. *J Mol Biol* **150**, 467-486 (1981).
359 Sternberg, N., Hamilton, D., Austin, S., Yarmolinsky, M. & Hoess, R. Site-specific recombination and its role in the life cycle of bacteriophage P1. *Cold Spring Harb Symp Quant Biol* **45 Pt 1**, 297-309 (1981).
360 Gierut, J. J., Jacks, T. E. & Haigis, K. M. Strategies to achieve conditional gene mutation in mice. *Cold Spring Harb Protoc* **2014**, 339-349, doi:10.1101/pdb.top069807 (2014).
361 Zhong, Z. A., Sun, W., Chen, H., Zhang, H., Lay, Y. E., Lane, N. E. *et al.* Optimizing tamoxifen-inducible Cre/loxp system to reduce tamoxifen effect on bone turnover in long bones of young mice. *Bone* **81**, 614-619, doi:10.1016/j.bone.2015.07.034 (2015).
362 Sauer, B. Manipulation of transgenes by site-specific recombination: use of Cre recombinase. *Methods Enzymol* **225**, 890-900 (1993).
363 Borgna, J. L. & Rochefort, H. Hydroxylated metabolites of tamoxifen are formed in vivo and bound to estrogen receptor in target tissues. *J Biol Chem* **256**, 859-868 (1981).
364 Jordan, V. C., Collins, M. M., Rowsby, L. & Prestwich, G. A monohydroxylated metabolite of tamoxifen with potent antioestrogenic activity. *J Endocrinol* **75**, 305-316 (1977).
365 Robertson, D. W., Katzenellenbogen, J. A., Long, D. J., Rorke, E. A. & Katzenellenbogen, B. S. Tamoxifen antiestrogens. A comparison of the activity, pharmacokinetics, and metabolic activation of the cis and trans isomers of tamoxifen. *J Steroid Biochem* **16**, 1-13 (1982).
366 Fromson, J. M., Pearson, S. & Bramah, S. The metabolism of tamoxifen (I.C.I. 46,474). I. In laboratory animals. *Xenobiotica* **3**, 693-709, doi:10.3109/00498257309151594 (1973).
367 Harper, M. J. & Walpole, A. L. A new derivative of triphenylethylene: effect on implantation and mode of action in rats. *J Reprod Fertil* **13**, 101-119 (1967).
368 Jordan, V. C. & Allen, K. E. Evaluation of the antitumour activity of the non-steroidal antioestrogen monohydroxytamoxifen in the DMBA-induced rat mammary carcinoma model. *Eur J Cancer* **16**, 239-251 (1980).
369 Jordan, V. C., Allen, K. E. & Dix, C. J. Pharmacology of tamoxifen in laboratory animals. *Cancer Treat Rep* **64**, 745-759 (1980).

370 Jordan, V. C., Fritz, N. F. & Gottardis, M. M. Strategies for breast cancer therapy with antiestrogens. *J Steroid Biochem* **27**, 493-498 (1987).

371 Jordan, V. C., Naylor, K. E., Dix, C. J. & Prestwich, G. Anti-oestrogen action in experimental breast cancer. *Recent Results Cancer Res* **71**, 30-44 (1980).

372 Fabian, C., Tilzer, L. & Sternson, L. Comparative binding affinities of tamoxifen, 4-hydroxytamoxifen, and desmethyltamoxifen for estrogen receptors isolated from human breast carcinoma: correlation with blood levels in patients with metastatic breast cancer. *Biopharm Drug Dispos* **2**, 381-390 (1981).

373 Fisher, B., Costantino, J. P., Redmond, C. K., Fisher, E. R., Wickerham, D. L. & Cronin, W. M. Endometrial cancer in tamoxifen-treated breast cancer patients: findings from the National Surgical Adjuvant Breast and Bowel Project (NSABP) B-14. *J Natl Cancer Inst* **86**, 527-537 (1994).

374 Jankowitz, R. C. & Davidson, N. E. Adjuvant endocrine therapy for breast cancer: how long is long enough? *Oncology (Williston Park)* **27**, 1210-1216, 1224 (2013).

375 Jordan, V. C. Tamoxifen or raloxifene for breast cancer chemoprevention: a tale of two choices--point. *Cancer Epidemiol Biomarkers Prev* **16**, 2207-2209, doi:10.1158/1055-9965.EPI-07-0629 (2007).

376 Jordan, V. C. New insights into the metabolism of tamoxifen and its role in the treatment and prevention of breast cancer. *Steroids* **72**, 829-842, doi:10.1016/j.steroids.2007.07.009 (2007).

377 Jordan, V. C., Fritz, N. F. & Tormey, D. C. Endocrine effects of adjuvant chemotherapy and long-term tamoxifen administration on node-positive patients with breast cancer. *Cancer Res* **47**, 624-630 (1987).

378 Jordan, V. C. Chemoprevention of breast cancer with selective oestrogen-receptor modulators. *Nat Rev Cancer* **7**, 46-53, doi:10.1038/nrc2048 (2007).

379 Jordan, V. C. Tamoxifen as the first targeted long-term adjuvant therapy for breast cancer. *Endocr Relat Cancer* **21**, R235-246, doi:10.1530/ERC-14-0092 (2014).

380 Hughes-Davies, L., Caldas, C. & Wishart, G. C. Tamoxifen: the drug that came in from the cold. *Br J Cancer* **101**, 875-878, doi:10.1038/sj.bjc.6605231 (2009).

381 Jordan, V. C. Chemosuppression of breast cancer with tamoxifen: laboratory evidence and future clinical investigations. *Cancer Invest* **6**, 589-595 (1988).

382 Sutherland, R. L., Green, M. D., Hall, R. E., Reddel, R. R. & Taylor, I. W. Tamoxifen induces accumulation of MCF 7 human mammary carcinoma cells in the G0/G1 phase of the cell cycle. *Eur J Cancer Clin Oncol* **19**, 615-621 (1983).

383 Osborne, C. K., Boldt, D. H., Clark, G. M. & Trent, J. M. Effects of tamoxifen on human breast cancer cell cycle kinetics: accumulation of cells in early G1 phase. *Cancer Res* **43**, 3583-3585 (1983).

384 Kallio, A., Zheng, A., Dahllund, J., Heiskanen, K. M. & Harkonen, P. Role of mitochondria in tamoxifen-induced rapid death of MCF-7 breast cancer cells. *Apoptosis* **10**, 1395-1410, doi:10.1007/s10495-005-2137-z (2005).

385 Caldon, C. E., Daly, R. J., Sutherland, R. L. & Musgrove, E. A. Cell cycle control in breast cancer cells. *J Cell Biochem* **97**, 261-274, doi:10.1002/jcb.20690 (2006).

386 Sutherland, R. L. & Musgrove, E. A. Cyclins and breast cancer. *J Mammary Gland Biol Neoplasia* **9**, 95-104, doi:10.1023/B:JOMG.0000023591.45568.77 (2004).

387 Thiantanawat, A., Long, B. J. & Brodie, A. M. Signaling pathways of apoptosis activated by aromatase inhibitors and antiestrogens. *Cancer Res* **63**, 8037-8050 (2003).

388 Frasor, J., Weaver, A., Pradhan, M., Dai, Y., Miller, L. D., Lin, C. Y. *et al.* Positive cross-talk between estrogen receptor and NF-kappaB in breast cancer. *Cancer Res* **69**, 8918-8925, doi:10.1158/0008-5472.CAN-09-2608 (2009).

389 O'Lone, R., Frith, M. C., Karlsson, E. K. & Hansen, U. Genomic targets of nuclear estrogen receptors. *Mol Endocrinol* **18**, 1859-1875, doi:10.1210/me.2003-0044 (2004).

390 Marino, M., Galluzzo, P. & Ascenzi, P. Estrogen signaling multiple pathways to impact gene transcription. *Curr Genomics* **7**, 497-508 (2006).

391 Ali, S., Rasool, M., Chaoudhry, H., P, N. P., Jha, P., Hafiz, A. *et al.* Molecular mechanisms and mode of tamoxifen resistance in breast cancer. *Bioinformation* **12**, 135-139, doi:10.6026/97320630012135 (2016).

392 Mendez, P., Azcoitia, I. & Garcia-Segura, L. M. Estrogen receptor alpha forms estrogen-dependent multimolecular complexes with insulin-like growth factor receptor and phosphatidylinositol 3-kinase in the adult rat brain. *Brain Res Mol Brain Res* **112**, 170-176 (2003).

393 Cardona-Gomez, G. P., Mendez, P. & Garcia-Segura, L. M. Synergistic interaction of estradiol and insulin-like growth factor-I in the activation of PI3K/Akt signaling in the adult rat hypothalamus. *Brain Res Mol Brain Res* **107**, 80-88 (2002).

394 Park, W. C. & Jordan, V. C. Selective estrogen receptor modulators (SERMS) and their roles in breast cancer prevention. *Trends Mol Med* **8**, 82-88 (2002).

395 Kuiper, G. G., Carlsson, B., Grandien, K., Enmark, E., Haggblad, J., Nilsson, S. *et al.* Comparison of the ligand binding specificity and transcript tissue distribution of estrogen receptors alpha and beta. *Endocrinology* **138**, 863-870, doi:10.1210/endo.138.3.4979 (1997).

396 Katzenellenbogen, B. S., Choi, I., Delage-Mourroux, R., Ediger, T. R., Martini, P. G., Montano, M. *et al.* Molecular mechanisms of estrogen action: selective ligands and receptor pharmacology. *J Steroid Biochem Mol Biol* **74**, 279-285 (2000).

397 Jordan, V. C., Gapstur, S. & Morrow, M. Selective estrogen receptor modulation and reduction in risk of breast cancer, osteoporosis, and coronary heart disease. *J Natl Cancer Inst* **93**, 1449-1457 (2001).

398 An, K. C. Selective Estrogen Receptor Modulators. *Asian Spine J* **10**, 787-791, doi:10.4184/asj.2016.10.4.787 (2016).

399 Jordan, V. C. & O'Malley, B. W. Selective estrogen-receptor modulators and antihormonal resistance in breast cancer. *J Clin Oncol* **25**, 5815-5824, doi:10.1200/JCO.2007.11.3886 (2007).

400 Ferlini, C., Scambia, G., Marone, M., Distefano, M., Gaggini, C., Ferrandina, G. *et al.* Tamoxifen induces oxidative stress and apoptosis in oestrogen receptor-negative human cancer cell lines. *Br J Cancer* **79**, 257-263, doi:10.1038/sj.bjc.6690042 (1999).

401 O'Brian, C. A., Liskamp, R. M., Solomon, D. H. & Weinstein, I. B. Inhibition of protein kinase C by tamoxifen. *Cancer Res* **45**, 2462-2465 (1985).

402 O'Brian, C. A., Ward, N. E. & Anderson, B. W. Role of specific interactions between protein kinase C and triphenylethylenes in inhibition of the enzyme. *J Natl Cancer Inst* **80**, 1628-1633 (1988).

403 O'Brian, C. A., Liskamp, R. M., Solomon, D. H. & Weinstein, I. B. Triphenylethylenes: a new class of protein kinase C inhibitors. *J Natl Cancer Inst* **76**, 1243-1246 (1986).

404 Horgan, K., Cooke, E., Hallett, M. B. & Mansel, R. E. Inhibition of protein kinase C mediated signal transduction by tamoxifen. Importance for antitumour activity. *Biochem Pharmacol* **35**, 4463-4465 (1986).

405 Nakadate, T., Jeng, A. Y. & Blumberg, P. M. Comparison of protein kinase C functional assays to clarify mechanisms of inhibitor action. *Biochem Pharmacol* **37**, 1541-1545 (1988).

406 Mandlekar, S., Yu, R., Tan, T. H. & Kong, A. N. Activation of caspase-3 and c-Jun NH2-terminal kinase-1 signaling pathways in tamoxifen-induced apoptosis of human breast cancer cells. *Cancer Res* **60**, 5995-6000 (2000).

407 Wei, H. Y. & Ma, X. Tamoxifen reduces infiltration of inflammatory cells, apoptosis and inhibits IKK/NF-kB pathway after spinal cord injury in rats. *Neurol Sci* **35**, 1763-1768, doi:10.1007/s10072-014-1828-z (2014).

408 Morad, S. A., Ryan, T. E., Neufer, P. D., Zeczycki, T. N., Davis, T. S., MacDougall, M. R. *et al.* Ceramide-tamoxifen regimen targets bioenergetic elements in acute myelogenous leukemia. *J Lipid Res* **57**, 1231-1242, doi:10.1194/jlr.M067389 (2016).

409 Graham, C. D., Kaza, N., Klocke, B. J., Gillespie, G. Y., Shevde, L. A., Carroll, S. L. *et al.* Tamoxifen Induces Cytotoxic Autophagy in Glioblastoma. *J Neuropathol Exp Neurol* **75**, 946-954, doi:10.1093/jnen/nlw071 (2016).
410 Krakstad, C. & Chekenya, M. Survival signalling and apoptosis resistance in glioblastomas: opportunities for targeted therapeutics. *Mol Cancer* **9**, 135, doi:10.1186/1476-4598-9-135 (2010).
411 Huang, P. H., Xu, A. M. & White, F. M. Oncogenic EGFR signaling networks in glioma. *Sci Signal* **2**, re6, doi:10.1126/scisignal.287re6 (2009).
412 Xu, H., Zong, H., Ma, C., Ming, X., Shang, M., Li, K. *et al.* Epidermal growth factor receptor in glioblastoma. *Oncol Lett* **14**, 512-516, doi:10.3892/ol.2017.6221 (2017).
413 Wilking, N., Appelgren, L. E., Carlstrom, K., Pousette, A. & Theve, N. O. The distribution and metabolism of 14C-labelled tamoxifen in spayed female mice. *Acta Pharmacol Toxicol (Copenh)* **50**, 161-168 (1982).
414 Vertosick, F. T., Jr., Selker, R. G., Randall, M. S., Kristofik, M. P. & Rehn, T. A comparison of the relative chemosensitivity of human gliomas to tamoxifen and n-desmethyltamoxifen in vitro. *J Neurooncol* **19**, 97-103 (1994).
415 Pollack, I. F., Randall, M. S., Kristofik, M. P., Kelly, R. H., Selker, R. G. & Vertosick, F. T., Jr. Effect of tamoxifen on DNA synthesis and proliferation of human malignant glioma lines in vitro. *Cancer Res* **50**, 7134-7138 (1990).
416 Vertosick, F. T., Jr., Selker, R. G., Pollack, I. F. & Arena, V. The treatment of intracranial malignant gliomas using orally administered tamoxifen therapy: preliminary results in a series of "failed" patients. *Neurosurgery* **30**, 897-902; discussion 902-893 (1992).
417 Baltuch, G., Shenouda, G., Langleben, A. & Villemure, J. G. High dose tamoxifen in the treatment of recurrent high grade glioma: a report of clinical stabilization and tumour regression. *Can J Neurol Sci* **20**, 168-170 (1993).
418 Baltuch, G. H., Couldwell, W. T., Villemure, J. G. & Yong, V. W. Protein kinase C inhibitors suppress cell growth in established and low-passage glioma cell lines. A comparison between staurosporine and tamoxifen. *Neurosurgery* **33**, 495-501; discussion 501 (1993).
419 Couldwell, W. T., Weiss, M. H., DeGiorgio, C. M., Weiner, L. P., Hinton, D. R., Ehresmann, G. R. *et al.* Clinical and radiographic response in a minority of patients with recurrent malignant gliomas treated with high-dose tamoxifen. *Neurosurgery* **32**, 485-489; discussion 489-490 (1993).
420 Muanza, T., Shenouda, G., Souhami, L., Leblanc, R., Mohr, G., Corns, R. *et al.* High dose tamoxifen and radiotherapy in patients with glioblastoma multiforme: a phase IB study. *Can J Neurol Sci* **27**, 302-306 (2000).
421 Robins, H. I., Won, M., Seiferheld, W. F., Schultz, C. J., Choucair, A. K., Brachman, D. G. *et al.* Phase 2 trial of radiation plus high-dose tamoxifen for glioblastoma multiforme: RTOG protocol BR-0021. *Neuro Oncol* **8**, 47-52, doi:10.1215/S1522851705000311 (2006).
422 Pearson, J. R. D. & Regad, T. Targeting cellular pathways in glioblastoma multiforme. *Signal Transduct Target Ther* **2**, 17040, doi:10.1038/sigtrans.2017.40 (2017).
423 Hujber, Z., Horvath, G., Petovari, G., Krencz, I., Danko, T., Meszaros, K. *et al.* GABA, glutamine, glutamate oxidation and succinic semialdehyde dehydrogenase expression in human gliomas. *J Exp Clin Cancer Res* **37**, 271, doi:10.1186/s13046-018-0946-5 (2018).
424 Cui, D., Ren, J., Shi, J., Feng, L., Wang, K., Zeng, T. *et al.* R132H mutation in IDH1 gene reduces proliferation, cell survival and invasion of human glioma by downregulating Wnt/beta-catenin signaling. *Int J Biochem Cell Biol* **73**, 72-81, doi:10.1016/j.biocel.2016.02.007 (2016).
425 Izquierdo-Garcia, J. L., Viswanath, P., Eriksson, P., Chaumeil, M. M., Pieper, R. O., Phillips, J. J. *et al.* Metabolic reprogramming in mutant IDH1 glioma cells. *PLoS One* **10**, e0118781, doi:10.1371/journal.pone.0118781 (2015).

426 Leenders, W. Transgenic mouse models of Idh-mutated neural stem cells: an appropriate model for low grade glioma? *Transl Cancer Res* **5**, S1400-S1403, doi:10.21037/tcr.2016.12.31 (2016).
427 Stiles, C. D. & Rowitch, D. H. Glioma stem cells: a midterm exam. *Neuron* **58**, 832-846, doi:10.1016/j.neuron.2008.05.031 (2008).
428 Singh, S. K., Clarke, I. D., Terasaki, M., Bonn, V. E., Hawkins, C., Squire, J. *et al.* Identification of a cancer stem cell in human brain tumors. *Cancer Res* **63**, 5821-5828 (2003).
429 Galli, R., Binda, E., Orfanelli, U., Cipelletti, B., Gritti, A., De Vitis, S. *et al.* Isolation and characterization of tumorigenic, stem-like neural precursors from human glioblastoma. *Cancer Res* **64**, 7011-7021, doi:10.1158/0008-5472.CAN-04-1364 (2004).
430 Luskin, M. B. Restricted proliferation and migration of postnatally generated neurons derived from the forebrain subventricular zone. *Neuron* **11**, 173-189 (1993).
431 Lois, C. & Alvarez-Buylla, A. Long-distance neuronal migration in the adult mammalian brain. *Science* **264**, 1145-1148 (1994).
432 Sanai, N., Tramontin, A. D., Quinones-Hinojosa, A., Barbaro, N. M., Gupta, N., Kunwar, S. *et al.* Unique astrocyte ribbon in adult human brain contains neural stem cells but lacks chain migration. *Nature* **427**, 740-744, doi:10.1038/nature02301 (2004).
433 Calabrese, C., Poppleton, H., Kocak, M., Hogg, T. L., Fuller, C., Hamner, B. *et al.* A perivascular niche for brain tumor stem cells. *Cancer Cell* **11**, 69-82, doi:10.1016/j.ccr.2006.11.020 (2007).
434 Eriksson, P. S., Perfilieva, E., Bjork-Eriksson, T., Alborn, A. M., Nordborg, C., Peterson, D. A. *et al.* Neurogenesis in the adult human hippocampus. *Nat Med* **4**, 1313-1317, doi:10.1038/3305 (1998).
435 Furnari, F. B., Fenton, T., Bachoo, R. M., Mukasa, A., Stommel, J. M., Stegh, A. *et al.* Malignant astrocytic glioma: genetics, biology, and paths to treatment. *Genes Dev* **21**, 2683-2710, doi:10.1101/gad.1596707 (2007).
436 Bachoo, R. M., Maher, E. A., Ligon, K. L., Sharpless, N. E., Chan, S. S., You, M. J. *et al.* Epidermal growth factor receptor and Ink4a/Arf: convergent mechanisms governing terminal differentiation and transformation along the neural stem cell to astrocyte axis. *Cancer Cell* **1**, 269-277 (2002).
437 Uhrbom, L., Dai, C., Celestino, J. C., Rosenblum, M. K., Fuller, G. N. & Holland, E. C. Ink4a-Arf loss cooperates with KRas activation in astrocytes and neural progenitors to generate glioblastomas of various morphologies depending on activated Akt. *Cancer Res* **62**, 5551-5558 (2002).
438 Zhu, Y., Guignard, F., Zhao, D., Liu, L., Burns, D. K., Mason, R. P. *et al.* Early inactivation of p53 tumor suppressor gene cooperating with NF1 loss induces malignant astrocytoma. *Cancer Cell* **8**, 119-130, doi:10.1016/j.ccr.2005.07.004 (2005).
439 Zong, H., Parada, L. F. & Baker, S. J. Cell of origin for malignant gliomas and its implication in therapeutic development. *Cold Spring Harb Perspect Biol* **7**, doi:10.1101/cshperspect.a020610 (2015).
440 Alcantara Llaguno, S. R. & Parada, L. F. Cell of origin of glioma: biological and clinical implications. *Br J Cancer* **115**, 1445-1450, doi:10.1038/bjc.2016.354 (2016).
441 Lee, J., Kotliarova, S., Kotliarov, Y., Li, A., Su, Q., Donin, N. M. *et al.* Tumor stem cells derived from glioblastomas cultured in bFGF and EGF more closely mirror the phenotype and genotype of primary tumors than do serum-cultured cell lines. *Cancer Cell* **9**, 391-403, doi:10.1016/j.ccr.2006.03.030 (2006).
442 Mahesparan, R., Read, T. A., Lund-Johansen, M., Skaftnesmo, K. O., Bjerkvig, R. & Engebraaten, O. Expression of extracellular matrix components in a highly infiltrative in vivo glioma model. *Acta Neuropathol* **105**, 49-57, doi:10.1007/s00401-002-0610-0 (2003).

443 Al-Mayhani, T. M. F., Ball, S. L. R., Zhao, J. W., Fawcett, J., Lchimura, K., Collins, P. V. *et al.* An efficient method for derivation and propagation of glioblastoma cell lines that conserves the molecular profile of their original tumours. *J Neurosci Meth* **176**, 192-199, doi:10.1016/j.jneumeth.2008.07.022 (2009).

444 Pollard, S. M., Yoshikawa, K., Clarke, I. D., Danovi, D., Stricker, S., Russell, R. *et al.* Glioma stem cell lines expanded in adherent culture have tumor-specific phenotypes and are suitable for chemical and genetic screens. *Cell Stem Cell* **4**, 568-580, doi:10.1016/j.stem.2009.03.014 (2009).

445 Joo, K. M., Kim, J., Jin, J., Kim, M., Seol, H. J., Muradov, J. *et al.* Patient-specific orthotopic glioblastoma xenograft models recapitulate the histopathology and biology of human glioblastomas in situ. *Cell Rep* **3**, 260-273, doi:10.1016/j.celrep.2012.12.013 (2013).

446 Xie, Y., Bergstrom, T., Jiang, Y., Johansson, P., Marinescu, V. D., Lindberg, N. *et al.* The Human Glioblastoma Cell Culture Resource: Validated Cell Models Representing All Molecular Subtypes. *EBioMedicine* **2**, 1351-1363, doi:10.1016/j.ebiom.2015.08.026 (2015).

447 Zhang, Y., Li, N. N., Lau, J., Richard-Londt, A., von Deimling, A., Pusch, S. *et al.* Idh1 Mutant Glioma Initiating Cells Are Predisposed to Apoptosis under Endoplasmic Reticulum (Er) Stress. *Neuro-Oncology* **20**, 13-13 (2018).

448 Modrek, A. S., Golub, D., Khan, T., Bready, D., Prado, J., Bowman, C. *et al.* Low-Grade Astrocytoma Mutations in IDH1, P53, and ATRX Cooperate to Block Differentiation of Human Neural Stem Cells via Repression of SOX2. *Cell Rep* **21**, 1267-1280, doi:10.1016/j.celrep.2017.10.009 (2017).

449 Seibler, J., Zevnik, B., Kuter-Luks, B., Andreas, S., Kern, H., Hennek, T. *et al.* Rapid generation of inducible mouse mutants. *Nucleic Acids Res* **31**, e12 (2003).

450 Forget, A., Martignetti, L., Puget, S., Calzone, L., Brabetz, S., Picard, D. *et al.* Aberrant ERBB4-SRC Signaling as a Hallmark of Group 4 Medulloblastoma Revealed by Integrative Phosphoproteomic Profiling. *Cancer Cell* **34**, 379-395 e377, doi:10.1016/j.ccell.2018.08.002 (2018).

451 Bolstad, B. M., Irizarry, R. A., Astrand, M. & Speed, T. P. A comparison of normalization methods for high density oligonucleotide array data based on variance and bias. *Bioinformatics* **19**, 185-193 (2003).

452 Fiehn, O. & Kind, T. Metabolite profiling in blood plasma. *Methods Mol Biol* **358**, 3-17, doi:10.1007/978-1-59745-244-1_1 (2007).

453 Etienne, M. C., Milano, G., Fischel, J. L., Frenay, M., Francois, E., Formento, J. L. *et al.* Tamoxifen metabolism: pharmacokinetic and in vitro study. *Br J Cancer* **60**, 30-35 (1989).

454 Chen, H. Y., Yang, Y. M., Han, R. & Noble, M. MEK1/2 inhibition suppresses tamoxifen toxicity on CNS glial progenitor cells. *J Neurosci* **33**, 15069-15074, doi:10.1523/JNEUROSCI.2729-13.2013 (2013).

455 Yamamoto, A., Tagawa, Y., Yoshimori, T., Moriyama, Y., Masaki, R. & Tashiro, Y. Bafilomycin A1 prevents maturation of autophagic vacuoles by inhibiting fusion between autophagosomes and lysosomes in rat hepatoma cell line, H-4-II-E cells. *Cell Struct Funct* **23**, 33-42 (1998).

456 Seglen, P. O. & Gordon, P. B. 3-Methyladenine: specific inhibitor of autophagic/lysosomal protein degradation in isolated rat hepatocytes. *Proc Natl Acad Sci U S A* **79**, 1889-1892 (1982).

457 Couldwell, W. T., Hinton, D. R., He, S., Chen, T. C., Sebat, I., Weiss, M. H. *et al.* Protein kinase C inhibitors induce apoptosis in human malignant glioma cell lines. *FEBS Lett* **345**, 43-46 (1994).

458 Starr, R., Willson, T. A., Viney, E. M., Murray, L. J., Rayner, J. R., Jenkins, B. J. *et al.* A family of cytokine-inducible inhibitors of signalling. *Nature* **387**, 917-921, doi:10.1038/43206 (1997).

459 Seo, I. A., Lee, H. K., Shin, Y. K., Lee, S. H., Seo, S. Y., Park, J. W. *et al.* Janus Kinase 2 Inhibitor AG490 Inhibits the STAT3 Signaling Pathway by Suppressing

Protein Translation of gp130. *Korean J Physiol Pharmacol* **13**, 131-138, doi:10.4196/kjpp.2009.13.2.131 (2009).

460 Sharfe, N., Dadi, H. K. & Roifman, C. M. JAK3 protein tyrosine kinase mediates interleukin-7-induced activation of phosphatidylinositol-3' kinase. *Blood* **86**, 2077-2085 (1995).

461 Meydan, N., Grunberger, T., Dadi, H., Shahar, M., Arpaia, E., Lapidot, Z. *et al.* Inhibition of acute lymphoblastic leukaemia by a Jak-2 inhibitor. *Nature* **379**, 645-648, doi:10.1038/379645a0 (1996).

462 Waelchli, R., Bollbuck, B., Bruns, C., Buhl, T., Eder, J., Feifel, R. *et al.* Design and preparation of 2-benzamido-pyrimidines as inhibitors of IKK. *Bioorg Med Chem Lett* **16**, 108-112, doi:10.1016/j.bmcl.2005.09.035 (2006).

463 O'Farrell, A. M., Parry, D. A., Zindy, F., Roussel, M. F., Lees, E., Moore, K. W. *et al.* Stat3-dependent induction of p19INK4D by IL-10 contributes to inhibition of macrophage proliferation. *J Immunol* **164**, 4607-4615 (2000).

464 Nichane, M., Ren, X. & Bellefroid, E. J. Self-regulation of Stat3 activity coordinates cell-cycle progression and neural crest specification. *EMBO J* **29**, 55-67, doi:10.1038/emboj.2009.313 (2010).

465 Toedt, G., Barbus, S., Wolter, M., Felsberg, J., Tews, B., Blond, F. *et al.* Molecular signatures classify astrocytic gliomas by IDH1 mutation status. *Int J Cancer* **128**, 1095-1103, doi:10.1002/ijc.25448 (2011).

466 Zhao, H., Kalivendi, S., Zhang, H., Joseph, J., Nithipatikom, K., Vasquez-Vivar, J. *et al.* Superoxide reacts with hydroethidine but forms a fluorescent product that is distinctly different from ethidium: potential implications in intracellular fluorescence detection of superoxide. *Free Radic Biol Med* **34**, 1359-1368 (2003).

467 Burow, S. & Valet, G. Flow-cytometric characterization of stimulation, free radical formation, peroxidase activity and phagocytosis of human granulocytes with 2,7-dichlorofluorescein (DCF). *Eur J Cell Biol* **43**, 128-133 (1987).

468 Potteti, H. R., Tamatam, C. R., Marreddy, R., Reddy, N. M., Noel, S., Rabb, H. *et al.* Nrf2-AKT interactions regulate heme oxygenase 1 expression in kidney epithelia during hypoxia and hypoxia-reoxygenation. *Am J Physiol Renal Physiol* **311**, F1025-F1034, doi:10.1152/ajprenal.00362.2016 (2016).

469 Azar, S., Leventoux, N., Ripoll, C., Rigau, V., Goze, C., Lorcy, F. *et al.* Cellular and molecular characterization of IDH1-mutated diffuse low grade gliomas reveals tumor heterogeneity and absence of EGFR/PDGFRalpha activation. *Glia* **66**, 239-255, doi:10.1002/glia.23240 (2018).

470 Sato, A., Okada, M., Shibuya, K., Watanabe, E., Seino, S., Narita, Y. *et al.* Pivotal role for ROS activation of p38 MAPK in the control of differentiation and tumor-initiating capacity of glioma-initiating cells. *Stem Cell Res* **12**, 119-131, doi:10.1016/j.scr.2013.09.012 (2014).

471 Cullinan, S. B., Zhang, D., Hannink, M., Arvisais, E., Kaufman, R. J. & Diehl, J. A. Nrf2 is a direct PERK substrate and effector of PERK-dependent cell survival. *Mol Cell Biol* **23**, 7198-7209 (2003).

472 Zhang, J., Singh, N., Robinson-Taylor, K. S., Dorsett-Martin, W. A., Morris, M. W., Jr., Earl, T. M. *et al.* Hepatocyte autophagy is linked to C/EBP-homologous protein, Bcl2-interacting mediator of cell death, and BH3-interacting domain death agonist gene expression. *J Surg Res* **195**, 588-595, doi:10.1016/j.jss.2015.01.039 (2015).

473 Pirozzi, C. J., Carpenter, A. B., Waitkus, M. S., Wang, C. Y., Zhu, H., Hansen, L. J. *et al.* Mutant IDH1 Disrupts the Mouse Subventricular Zone and Alters Brain Tumor Progression. *Mol Cancer Res* **15**, 507-520, doi:10.1158/1541-7786.MCR-16-0485 (2017).

474 Liu, L., Wise, D. R., Diehl, J. A. & Simon, M. C. Hypoxic reactive oxygen species regulate the integrated stress response and cell survival. *J Biol Chem* **283**, 31153-31162, doi:10.1074/jbc.M805056200 (2008).

475 Carbonneau, M., L, M. G., Lalonde, M. E., Germain, M. A., Motorina, A., Guiot, M. C. *et al.* The oncometabolite 2-hydroxyglutarate activates the mTOR signalling pathway. *Nat Commun* **7**, 12700, doi:10.1038/ncomms12700 (2016).
476 Janke, R., Iavarone, A. T. & Rine, J. Oncometabolite D-2-Hydroxyglutarate enhances gene silencing through inhibition of specific H3K36 histone demethylases. *Elife* **6**, doi:10.7554/eLife.22451 (2017).
477 Flanagan, S., Lee, M., Li, C. C., Suter, C. M. & Buckland, M. E. Promoter Methylation Analysis of IDH Genes in Human Gliomas. *Front Oncol* **2**, 193, doi:10.3389/fonc.2012.00193 (2012).
478 Piaskowski, S., Bienkowski, M., Stoczynska-Fidelus, E., Stawski, R., Sieruta, M., Szybka, M. *et al.* Glioma cells showing IDH1 mutation cannot be propagated in standard cell culture conditions. *Br J Cancer* **104**, 968-970, doi:10.1038/bjc.2011.27 (2011).
479 Borodovsky, A., Seltzer, M. J. & Riggins, G. J. Altered cancer cell metabolism in gliomas with mutant IDH1 or IDH2. *Curr Opin Oncol* **24**, 83-89, doi:10.1097/CCO.0b013e32834d816a (2012).
480 Verheul, C., Van Der Kaaij, M., Pierson, T., Kers, T., Gao, Y., Struys, E. *et al.* Successful Generation of Five Patient-Derived Endogenous Idh1 Mutant Glioma Cell Lines Provides Opportunities for Development of New Treatment Strategies for Idh Mutant Gliomas. *Neuro-Oncology* **19**, 261-261 (2017).
481 Vallier, L., Alexander, M. & Pedersen, R. Conditional gene expression in human embryonic stem cells. *Stem Cells* **25**, 1490-1497, doi:10.1634/stemcells.2006-0825 (2007).
482 Loonstra, A., Vooijs, M., Beverloo, H. B., Allak, B. A., van Drunen, E., Kanaar, R. *et al.* Growth inhibition and DNA damage induced by Cre recombinase in mammalian cells. *Proc Natl Acad Sci U S A* **98**, 9209-9214, doi:10.1073/pnas.161269798 (2001).
483 Thyagarajan, B., Guimaraes, M. J., Groth, A. C. & Calos, M. P. Mammalian genomes contain active recombinase recognition sites. *Gene* **244**, 47-54 (2000).
484 Paterni, I., Granchi, C., Katzenellenbogen, J. A. & Minutolo, F. Estrogen receptors alpha (ERalpha) and beta (ERbeta): subtype-selective ligands and clinical potential. *Steroids* **90**, 13-29, doi:10.1016/j.steroids.2014.06.012 (2014).
485 Cho, K. S., Yoon, Y. H., Choi, J. A., Lee, S. J. & Koh, J. Y. Induction of autophagy and cell death by tamoxifen in cultured retinal pigment epithelial and photoreceptor cells. *Invest Ophthalmol Vis Sci* **53**, 5344-5353, doi:10.1167/iovs.12-9827 (2012).
486 Kohli, L., Kaza, N., Coric, T., Byer, S. J., Brossier, N. M., Klocke, B. J. *et al.* 4-Hydroxytamoxifen induces autophagic death through K-Ras degradation. *Cancer Res* **73**, 4395-4405, doi:10.1158/0008-5472.CAN-12-3765 (2013).
487 Das, C. K., Mandal, M. & Kogel, D. Pro-survival autophagy and cancer cell resistance to therapy. *Cancer Metastasis Rev*, doi:10.1007/s10555-018-9727-z (2018).
488 Tollet-Egnell, P., Flores-Morales, A., Stavreus-Evers, A., Sahlin, L. & Norstedt, G. Growth hormone regulation of SOCS-2, SOCS-3, and CIS messenger ribonucleic acid expression in the rat. *Endocrinology* **140**, 3693-3704, doi:10.1210/endo.140.8.6878 (1999).
489 Ram, P. A. & Waxman, D. J. SOCS/CIS protein inhibition of growth hormone-stimulated STAT5 signaling by multiple mechanisms. *J Biol Chem* **274**, 35553-35561 (1999).
490 Greenhalgh, C. J., Metcalf, D., Thaus, A. L., Corbin, J. E., Uren, R., Morgan, P. O. *et al.* Biological evidence that SOCS-2 can act either as an enhancer or suppressor of growth hormone signaling. *J Biol Chem* **277**, 40181-40184, doi:10.1074/jbc.C200450200 (2002).
491 Metcalf, D., Greenhalgh, C. J., Viney, E., Willson, T. A., Starr, R., Nicola, N. A. *et al.* Gigantism in mice lacking suppressor of cytokine signalling-2. *Nature* **405**, 1069-1073, doi:10.1038/35016611 (2000).

492 Greenhalgh, C. J., Bertolino, P., Asa, S. L., Metcalf, D., Corbin, J. E., Adams, T. E. *et al.* Growth enhancement in suppressor of cytokine signaling 2 (SOCS-2)-deficient mice is dependent on signal transducer and activator of transcription 5b (STAT5b). *Mol Endocrinol* **16**, 1394-1406, doi:10.1210/mend.16.6.0845 (2002).

493 Endo, T. A., Masuhara, M., Yokouchi, M., Suzuki, R., Sakamoto, H., Mitsui, K. *et al.* A new protein containing an SH2 domain that inhibits JAK kinases. *Nature* **387**, 921-924, doi:10.1038/43213 (1997).

494 Vesterlund, M., Zadjali, F., Persson, T., Nielsen, M. L., Kessler, B. M., Norstedt, G. *et al.* The SOCS2 ubiquitin ligase complex regulates growth hormone receptor levels. *PLoS One* **6**, e25358, doi:10.1371/journal.pone.0025358 (2011).

495 Favre, H., Benhamou, A., Finidori, J., Kelly, P. A. & Edery, M. Dual effects of suppressor of cytokine signaling (SOCS-2) on growth hormone signal transduction. *FEBS Lett* **453**, 63-66 (1999).

496 Bulatov, E., Martin, E. M., Chatterjee, S., Knebel, A., Shimamura, S., Konijnenberg, A. *et al.* Biophysical studies on interactions and assembly of full-size E3 ubiquitin ligase: suppressor of cytokine signaling 2 (SOCS2)-elongin BC-cullin 5-ring box protein 2 (RBX2). *J Biol Chem* **290**, 4178-4191, doi:10.1074/jbc.M114.616664 (2015).

497 Uyttendaele, I., Lemmens, I., Verhee, A., De Smet, A. S., Vandekerckhove, J., Lavens, D. *et al.* Mammalian protein-protein interaction trap (MAPPIT) analysis of STAT5, CIS, and SOCS2 interactions with the growth hormone receptor. *Mol Endocrinol* **21**, 2821-2831, doi:10.1210/me.2006-0541 (2007).

498 Greenhalgh, C. J., Rico-Bautista, E., Lorentzon, M., Thaus, A. L., Morgan, P. O., Willson, T. A. *et al.* SOCS2 negatively regulates growth hormone action in vitro and in vivo. *J Clin Invest* **115**, 397-406, doi:10.1172/JCI22710 (2005).

499 Leung, K. C., Brce, J., Doyle, N., Lee, H. J., Leong, G. M., Sjogren, K. *et al.* Regulation of growth hormone signaling by selective estrogen receptor modulators occurs through suppression of protein tyrosine phosphatases. *Endocrinology* **148**, 2417-2423, doi:10.1210/en.2006-1305 (2007).

500 Leung, K. C., Johannsson, G., Leong, G. M. & Ho, K. K. Estrogen regulation of growth hormone action. *Endocr Rev* **25**, 693-721, doi:10.1210/er.2003-0035 (2004).

501 Hansen, J. A., Lindberg, K., Hilton, D. J., Nielsen, J. H. & Billestrup, N. Mechanism of inhibition of growth hormone receptor signaling by suppressor of cytokine signaling proteins. *Mol Endocrinol* **13**, 1832-1843, doi:10.1210/mend.13.11.0368 (1999).

502 Adams, T. E., Hansen, J. A., Starr, R., Nicola, N. A., Hilton, D. J. & Billestrup, N. Growth hormone preferentially induces the rapid, transient expression of SOCS-3, a novel inhibitor of cytokine receptor signaling. *J Biol Chem* **273**, 1285-1287 (1998).

503 Tannahill, G. M., Elliott, J., Barry, A. C., Hibbert, L., Cacalano, N. A. & Johnston, J. A. SOCS2 can enhance interleukin-2 (IL-2) and IL-3 signaling by accelerating SOCS3 degradation. *Mol Cell Biol* **25**, 9115-9126, doi:10.1128/MCB.25.20.9115-9126.2005 (2005).

504 Letellier, E. & Haan, S. SOCS2: physiological and pathological functions. *Front Biosci (Elite Ed)* **8**, 189-204 (2016).

505 Piessevaux, J., Lavens, D., Montoye, T., Wauman, J., Catteeuw, D., Vandekerckhove, J. *et al.* Functional cross-modulation between SOCS proteins can stimulate cytokine signaling. *J Biol Chem* **281**, 32953-32966, doi:10.1074/jbc.M600776200 (2006).

506 Lee, H., Herrmann, A., Deng, J. H., Kujawski, M., Niu, G., Li, Z. *et al.* Persistently activated Stat3 maintains constitutive NF-kappaB activity in tumors. *Cancer Cell* **15**, 283-293, doi:10.1016/j.ccr.2009.02.015 (2009).

507 Liu, Y., Nirschl, C., Kim, T., Devi, K. & Anandasabapathy, N. Suppressors of cytokine signaling 2 (Socs2) inhibits NF-kB-dependent-signaling during acute

activation of DC. *J Invest Dermatol* **137**, S111-S111, doi:DOI 10.1016/j.jid.2017.02.666 (2017).

508 Park, S. H., Kim, K. E., Hwang, H. Y. & Kim, T. Y. Regulatory effect of SOCS on NF-kappaB activity in murine monocytes/macrophages. *DNA Cell Biol* **22**, 131-139, doi:10.1089/104454903321515931 (2003).

509 Xia, Y., Shen, S. & Verma, I. M. NF-kappaB, an active player in human cancers. *Cancer Immunol Res* **2**, 823-830, doi:10.1158/2326-6066.CIR-14-0112 (2014).

510 Yang, S., Qiang, L., Sample, A., Shah, P. & He, Y. Y. NF-kappaB Signaling Activation Induced by Chloroquine Requires Autophagosome, p62 Protein, and c-Jun N-terminal Kinase (JNK) Signaling and Promotes Tumor Cell Resistance. *J Biol Chem* **292**, 3379-3388, doi:10.1074/jbc.M116.756536 (2017).

511 Salminen, A., Hyttinen, J. M., Kauppinen, A. & Kaarniranta, K. Context-Dependent Regulation of Autophagy by IKK-NF-kappaB Signaling: Impact on the Aging Process. *Int J Cell Biol* **2012**, 849541, doi:10.1155/2012/849541 (2012).

512 Su, Y., Qu, Y., Zhao, F., Li, H., Mu, D. & Li, X. Regulation of autophagy by the nuclear factor kappaB signaling pathway in the hippocampus of rats with sepsis. *J Neuroinflammation* **12**, 116, doi:10.1186/s12974-015-0336-2 (2015).

513 Cilloni, D., Messa, F., Arruga, F., Defilippi, I., Morotti, A., Messa, E. *et al.* The NF-kappaB pathway blockade by the IKK inhibitor PS1145 can overcome imatinib resistance. *Leukemia* **20**, 61-67, doi:10.1038/sj.leu.2403998 (2006).

514 Widera, D., Mikenberg, I., Elvers, M., Kaltschmidt, C. & Kaltschmidt, B. Tumor necrosis factor alpha triggers proliferation of adult neural stem cells via IKK/NF-kappaB signaling. *BMC Neurosci* **7**, 64, doi:10.1186/1471-2202-7-64 (2006).

515 Hinz, M., Krappmann, D., Eichten, A., Heder, A., Scheidereit, C. & Strauss, M. NF-kappaB function in growth control: regulation of cyclin D1 expression and G0/G1-to-S-phase transition. *Mol Cell Biol* **19**, 2690-2698 (1999).

516 Basseres, D. S. & Baldwin, A. S. Nuclear factor-kappaB and inhibitor of kappaB kinase pathways in oncogenic initiation and progression. *Oncogene* **25**, 6817-6830, doi:10.1038/sj.onc.1209942 (2006).

517 Sundberg, M., Savola, S., Hienola, A., Korhonen, L. & Lindholm, D. Glucocorticoid hormones decrease proliferation of embryonic neural stem cells through ubiquitin-mediated degradation of cyclin D1. *J Neurosci* **26**, 5402-5410, doi:10.1523/JNEUROSCI.4906-05.2006 (2006).

518 Barth, S., Glick, D. & Macleod, K. F. Autophagy: assays and artifacts. *J Pathol* **221**, 117-124, doi:10.1002/path.2694 (2010).

519 Langenkamp, E., Zhang, L., Lugano, R., Huang, H., Elhassan, T. E., Georganaki, M. *et al.* Elevated expression of the C-type lectin CD93 in the glioblastoma vasculature regulates cytoskeletal rearrangements that enhance vessel function and reduce host survival. *Cancer Res* **75**, 4504-4516, doi:10.1158/0008-5472.CAN-14-3636 (2015).

520 Uhlen, M., Fagerberg, L., Hallstrom, B. M., Lindskog, C., Oksvold, P., Mardinoglu, A. *et al.* Proteomics. Tissue-based map of the human proteome. *Science* **347**, 1260419, doi:10.1126/science.1260419 (2015).

521 Zhong, Y., Yang, J., Xu, W. W., Wang, Y., Zheng, C. C., Li, B. *et al.* KCTD12 promotes tumorigenesis by facilitating CDC25B/CDK1/Aurora A-dependent G2/M transition. *Oncogene* **36**, 6177-6189, doi:10.1038/onc.2017.287 (2017).

522 Abbaszadegan, M. R., Taghehchian, N., Li, L., Aarabi, A. & Moghbeli, M. Contribution of KCTD12 to esophageal squamous cell carcinoma. *BMC Cancer* **18**, 853, doi:10.1186/s12885-018-4765-z (2018).

523 Li, L., Duan, T., Wang, X., Zhang, R. H., Zhang, M., Wang, S. *et al.* KCTD12 Regulates Colorectal Cancer Cell Stemness through the ERK Pathway. *Sci Rep* **6**, 20460, doi:10.1038/srep20460 (2016).

524 Toledano, M. B. & Leonard, W. J. Modulation of transcription factor NF-kappa B binding activity by oxidation-reduction in vitro. *Proc Natl Acad Sci U S A* **88**, 4328-4332 (1991).

525 Hara, E., Takahashi, K., Tominaga, T., Kumabe, T., Kayama, T., Suzuki, H. *et al.* Expression of heme oxygenase and inducible nitric oxide synthase mRNA in human brain tumors. *Biochem Biophys Res Commun* **224**, 153-158, doi:10.1006/bbrc.1996.0999 (1996).
526 El Andaloussi, A. & Lesniak, M. S. CD4+ CD25+ FoxP3+ T-cell infiltration and heme oxygenase-1 expression correlate with tumor grade in human gliomas. *J Neurooncol* **83**, 145-152, doi:10.1007/s11060-006-9314-y (2007).
527 Tsai, W. C., Hueng, D. Y., Lin, C. R., Yang, T. C. & Gao, H. W. Nrf2 Expressions Correlate with WHO Grades in Gliomas and Meningiomas. *Int J Mol Sci* **17**, doi:10.3390/ijms17050722 (2016).
528 Pan, H., Wang, H., Zhu, L., Wang, X., Cong, Z., Sun, K. *et al.* The involvement of Nrf2-ARE pathway in regulation of apoptosis in human glioblastoma cell U251. *Neurol Res* **35**, 71-78, doi:10.1179/1743132812Y.0000000094 (2013).
529 Kanamori, M., Higa, T., Sonoda, Y., Murakami, S., Dodo, M., Kitamura, H. *et al.* Activation of the NRF2 pathway and its impact on the prognosis of anaplastic glioma patients. *Neuro Oncol* **17**, 555-565, doi:10.1093/neuonc/nou282 (2015).
530 Li, K., Ouyang, L., He, M., Luo, M., Cai, W., Tu, Y. *et al.* IDH1 R132H mutation regulates glioma chemosensitivity through Nrf2 pathway. *Oncotarget* **8**, 28865-28879, doi:10.18632/oncotarget.15868 (2017).
531 Rocha, C. R. R., Kajitani, G. S., Quinet, A., Fortunato, R. S. & Menck, C. F. M. NRF2 and glutathione are key resistance mediators to temozolomide in glioma and melanoma cells. *Oncotarget* **7**, 48081-48092, doi:10.18632/oncotarget.10129 (2016).
532 Huo, L., Li, C. W., Huang, T. H., Lam, Y. C., Xia, W., Tu, C. *et al.* Activation of Keap1/Nrf2 signaling pathway by nuclear epidermal growth factor receptor in cancer cells. *Am J Transl Res* **6**, 649-663 (2014).
533 Yamadori, T., Ishii, Y., Homma, S., Morishima, Y., Kurishima, K., Itoh, K. *et al.* Molecular mechanisms for the regulation of Nrf2-mediated cell proliferation in non-small-cell lung cancers. *Oncogene* **31**, 4768-4777, doi:10.1038/onc.2011.628 (2012).
534 Rojo, A. I., Rada, P., Mendiola, M., Ortega-Molina, A., Wojdyla, K., Rogowska-Wrzesinska, A. *et al.* The PTEN/NRF2 axis promotes human carcinogenesis. *Antioxid Redox Signal* **21**, 2498-2514, doi:10.1089/ars.2014.5843 (2014).
535 Taguchi, K., Hirano, I., Itoh, T., Tanaka, M., Miyajima, A., Suzuki, A. *et al.* Nrf2 enhances cholangiocyte expansion in Pten-deficient livers. *Mol Cell Biol* **34**, 900-913, doi:10.1128/MCB.01384-13 (2014).
536 Haupt, S., Raghu, D. & Haupt, Y. Mutant p53 Drives Cancer by Subverting Multiple Tumor Suppression Pathways. *Front Oncol* **6**, 12, doi:10.3389/fonc.2016.00012 (2016).
537 Chen, W., Sun, Z., Wang, X. J., Jiang, T., Huang, Z., Fang, D. *et al.* Direct interaction between Nrf2 and p21(Cip1/WAF1) upregulates the Nrf2-mediated antioxidant response. *Mol Cell* **34**, 663-673, doi:10.1016/j.molcel.2009.04.029 (2009).
538 Villeneuve, N. F., Sun, Z., Chen, W. & Zhang, D. D. Nrf2 and p21 regulate the fine balance between life and death by controlling ROS levels. *Cell Cycle* **8**, 3255-3256, doi:10.4161/cc.8.20.9565 (2009).
539 Hollinshead, K. E. R., Munford, H., Eales, K. L., Bardella, C., Li, C., Escribano-Gonzalez, C. *et al.* Oncogenic IDH1 Mutations Promote Enhanced Proline Synthesis through PYCR1 to Support the Maintenance of Mitochondrial Redox Homeostasis. *Cell Rep* **22**, 3107-3114, doi:10.1016/j.celrep.2018.02.084 (2018).
540 Thaker, N. G., Zhang, F., McDonald, P. R., Shun, T. Y., Lewen, M. D., Pollack, I. F. *et al.* Identification of Survival Genes in Human Glioblastoma Cells by Small Interfering RNA Screening. *Molecular Pharmacology* **76**, 1246-1255, doi:10.1124/mol.109.058024 (2009).
541 Smith, A. A., Huang, Y. T., Eliot, M., Houseman, E. A., Marsit, C. J., Wiencke, J. K. *et al.* A novel approach to the discovery of survival biomarkers in glioblastoma

using a joint analysis of DNA methylation and gene expression. *Epigenetics-Us* **9**, 873-883, doi:10.4161/epi.28571 (2014).

542 Fack, F., Tardito, S., Hochart, G., Oudin, A., Zheng, L., Fritah, S. *et al.* Altered metabolic landscape in IDH-mutant gliomas affects phospholipid, energy, and oxidative stress pathways. *EMBO Mol Med* **9**, 1681-1695, doi:10.15252/emmm.201707729 (2017).

543 Birner, P., Pusch, S., Christov, C., Mihaylova, S., Toumangelova-Uzeir, K., Natchev, S. *et al.* Mutant IDH1 inhibits PI3K/Akt signaling in human glioma. *Cancer* **120**, 2440-2447, doi:10.1002/cncr.28732 (2014).

544 Singer, E., Judkins, J., Salomonis, N., Matlaf, L., Soteropoulos, P., McAllister, S. *et al.* Reactive oxygen species-mediated therapeutic response and resistance in glioblastoma. *Cell Death Dis* **6**, e1601, doi:10.1038/cddis.2014.566 (2015).

545 Kensler, T. W., Wakabayashi, N. & Biswal, S. Cell survival responses to environmental stresses via the Keap1-Nrf2-ARE pathway. *Annu Rev Pharmacol Toxicol* **47**, 89-116, doi:10.1146/annurev.pharmtox.46.120604.141046 (2007).

546 Motohashi, H. & Yamamoto, M. Nrf2-Keap1 defines a physiologically important stress response mechanism. *Trends Mol Med* **10**, 549-557, doi:10.1016/j.molmed.2004.09.003 (2004).

547 Gilbert, M. R., Liu, Y., Neltner, J., Pu, H., Morris, A., Sunkara, M. *et al.* Autophagy and oxidative stress in gliomas with IDH1 mutations. *Acta Neuropathol* **127**, 221-233, doi:10.1007/s00401-013-1194-6 (2014).

548 Singh, B. & Bhat, H. K. Superoxide dismutase 3 is induced by antioxidants, inhibits oxidative DNA damage and is associated with inhibition of estrogen-induced breast cancer. *Carcinogenesis* **33**, 2601-2610, doi:10.1093/carcin/bgs300 (2012).

549 Reddy, N. M., Potteti, H. R., Vegiraju, S., Chen, H. J., Tamatam, C. M. & Reddy, S. P. PI3K-AKT Signaling via Nrf2 Protects against Hyperoxia-Induced Acute Lung Injury, but Promotes Inflammation Post-Injury Independent of Nrf2 in Mice. *PLoS One* **10**, e0129676, doi:10.1371/journal.pone.0129676 (2015).

550 Ning, W., Song, R., Li, C., Park, E., Mohsenin, A., Choi, A. M. *et al.* TGF-beta1 stimulates HO-1 via the p38 mitogen-activated protein kinase in A549 pulmonary epithelial cells. *Am J Physiol Lung Cell Mol Physiol* **283**, L1094-1102, doi:10.1152/ajplung.00151.2002 (2002).

551 Kietzmann, T., Jungermann, K. & Gorlach, A. Regulation of the hypoxia-dependent plasminogen activator inhibitor 1 expression by MAP kinases. *Thromb Haemost* **89**, 666-673 (2003).

552 Kietzmann, T., Samoylenko, A. & Immenschuh, S. Transcriptional regulation of heme oxygenase-1 gene expression by MAP kinases of the JNK and p38 pathways in primary cultures of rat hepatocytes. *J Biol Chem* **278**, 17927-17936, doi:10.1074/jbc.M203929200 (2003).

553 Demuth, T., Reavie, L. B., Rennert, J. L., Nakada, M., Nakada, S., Hoelzinger, D. B. *et al.* MAP-ing glioma invasion: mitogen-activated protein kinase kinase 3 and p38 drive glioma invasion and progression and predict patient survival. *Mol Cancer Ther* **6**, 1212-1222, doi:10.1158/1535-7163.MCT-06-0711 (2007).

554 Goldsmith, C. S., Kim, S. M., Karunarathna, N., Neuendorff, N., Gerard Toussaint, L., Earnest, D. J. *et al.* Inhibition of p38 MAPK activity leads to cell type-specific effects on the molecular circadian clock and time-dependent reduction of glioma cell invasiveness. *BMC Cancer* **18**, 43, doi:10.1186/s12885-017-3896-y (2018).

555 Son, Y., Kim, S., Chung, H. T. & Pae, H. O. Reactive oxygen species in the activation of MAP kinases. *Methods Enzymol* **528**, 27-48, doi:10.1016/B978-0-12-405881-1.00002-1 (2013).

556 Yang, K., Liu, Y., Liu, Z., Liu, J., Liu, X., Chen, X. *et al.* p38gamma overexpression in gliomas and its role in proliferation and apoptosis. *Sci Rep* **3**, 2089, doi:10.1038/srep02089 (2013).

557 Cullinan, S. B. & Diehl, J. A. PERK-dependent activation of Nrf2 contributes to redox homeostasis and cell survival following endoplasmic reticulum stress. *J Biol Chem* **279**, 20108-20117, doi:10.1074/jbc.M314219200 (2004).

558 Lee, A. S. The ER chaperone and signaling regulator GRP78/BiP as a monitor of endoplasmic reticulum stress. *Methods* **35**, 373-381, doi:10.1016/j.ymeth.2004.10.010 (2005).
559 Suragani, R. N., Zachariah, R. S., Velazquez, J. G., Liu, S., Sun, C. W., Townes, T. M. *et al.* Heme-regulated eIF2alpha kinase activated Atf4 signaling pathway in oxidative stress and erythropoiesis. *Blood* **119**, 5276-5284, doi:10.1182/blood-2011-10-388132 (2012).
560 Hinnebusch, A. G. The scanning mechanism of eukaryotic translation initiation. *Annu Rev Biochem* **83**, 779-812, doi:10.1146/annurev-biochem-060713-035802 (2014).
561 Harding, H. P., Novoa, I., Zhang, Y., Zeng, H., Wek, R., Schapira, M. *et al.* Regulated translation initiation controls stress-induced gene expression in mammalian cells. *Mol Cell* **6**, 1099-1108 (2000).
562 Kearse, M. G. & Wilusz, J. E. Non-AUG translation: a new start for protein synthesis in eukaryotes. *Genes Dev* **31**, 1717-1731, doi:10.1101/gad.305250.117 (2017).
563 Sachs, M. S. & Geballe, A. P. Downstream control of upstream open reading frames. *Genes Dev* **20**, 915-921, doi:10.1101/gad.1427006 (2006).
564 Vattem, K. M. & Wek, R. C. Reinitiation involving upstream ORFs regulates ATF4 mRNA translation in mammalian cells. *P Natl Acad Sci USA* **101**, 11269-11274, doi:10.1073/pnas.0400541101 (2004).
565 Wek, R. C. & Cavener, D. R. Translational control and the unfolded protein response. *Antioxid Redox Signal* **9**, 2357-2371, doi:10.1089/ars.2007.1764 (2007).
566 He, C. H., Gong, P., Hu, B., Stewart, D., Choi, M. E., Choi, A. M. *et al.* Identification of activating transcription factor 4 (ATF4) as an Nrf2-interacting protein. Implication for heme oxygenase-1 gene regulation. *J Biol Chem* **276**, 20858-20865, doi:10.1074/jbc.M101198200 (2001).
567 Doll, S., Urisman, A., Oses-Prieto, J. A., Arnott, D. & Burlingame, A. L. Quantitative Proteomics Reveals Fundamental Regulatory Differences in Oncogenic HRAS and Isocitrate Dehydrogenase (IDH1) Driven Astrocytoma. *Mol Cell Proteomics* **16**, 39-56, doi:10.1074/mcp.M116.063883 (2017).
568 B'chir, W., Maurin, A. C., Carraro, V., Averous, J., Jousse, C., Muranishi, Y. *et al.* The eIF2 alpha/ATF4 pathway is essential for stress-induced autophagy gene expression. *Nucleic Acids Research* **41**, 7683-7699, doi:10.1093/nar/gkt563 (2013).
569 Yamaguchi, S., Ishihara, H., Yamada, T., Tamura, A., Usui, M., Tominaga, R. *et al.* ATF4-mediated induction of 4E-BP1 contributes to pancreatic beta cell survival under endoplasmic reticulum stress. *Cell Metab* **7**, 269-276, doi:10.1016/j.cmet.2008.01.008 (2008).
570 Rouschop, K. M., van den Beucken, T., Dubois, L., Niessen, H., Bussink, J., Savelkouls, K. *et al.* The unfolded protein response protects human tumor cells during hypoxia through regulation of the autophagy genes MAP1LC3B and ATG5. *J Clin Invest* **120**, 127-141, doi:10.1172/JCI40027 (2010).
571 Qin, X., Jiang, B. & Zhang, Y. 4E-BP1, a multifactor regulated multifunctional protein. *Cell Cycle* **15**, 781-786, doi:10.1080/15384101.2016.1151581 (2016).
572 Ma, X. M. & Blenis, J. Molecular mechanisms of mTOR-mediated translational control. *Nat Rev Mol Cell Biol* **10**, 307-318, doi:10.1038/nrm2672 (2009).
573 Yang, L., Miao, L., Liang, F., Huang, H., Teng, X., Li, S. *et al.* The mTORC1 effectors S6K1 and 4E-BP play different roles in CNS axon regeneration. *Nat Commun* **5**, 5416, doi:10.1038/ncomms6416 (2014).
574 Dadey, D. Y., Kapoor, V., Khudanyan, A., Thotala, D. & Hallahan, D. E. PERK Regulates Glioblastoma Sensitivity to ER Stress While Promoting Radiation Resistance. *Mol Cancer Res*, doi:10.1158/1541-7786.MCR-18-0224 (2018).
575 Kouroku, Y., Fujita, E., Tanida, I., Ueno, T., Isoai, A., Kumagai, H. *et al.* ER stress (PERK/eIF2alpha phosphorylation) mediates the polyglutamine-induced LC3

conversion, an essential step for autophagy formation. *Cell Death Differ* **14**, 230-239, doi:10.1038/sj.cdd.4401984 (2007).

576 Yamaguchi, H. & Wang, H. G. CHOP is involved in endoplasmic reticulum stress-induced apoptosis by enhancing DR5 expression in human carcinoma cells. *J Biol Chem* **279**, 45495-45502, doi:10.1074/jbc.M406933200 (2004).

577 Zinszner, H., Kuroda, M., Wang, X., Batchvarova, N., Lightfoot, R. T., Remotti, H. *et al.* CHOP is implicated in programmed cell death in response to impaired function of the endoplasmic reticulum. *Genes Dev* **12**, 982-995 (1998).

578 Li, Z. L., Ueki, K., Kumagai, K., Araki, R. & Otsuki, Y. Regulation of bcl-2 transcription by estrogen receptor-alpha and c-Jun in human endometrium. *Med Mol Morphol* **47**, 43-53, doi:10.1007/s00795-013-0043-y (2014).

579 Marciniak, S. J., Yun, C. Y., Oyadomari, S., Novoa, I., Zhang, Y., Jungreis, R. *et al.* CHOP induces death by promoting protein synthesis and oxidation in the stressed endoplasmic reticulum. *Genes Dev* **18**, 3066-3077, doi:10.1101/gad.1250704 (2004).

580 Miyata, S., Urabe, M., Gomi, A., Nagai, M., Yamaguchi, T., Tsukahara, T. *et al.* An R132H mutation in isocitrate dehydrogenase 1 enhances p21 expression and inhibits phosphorylation of retinoblastoma protein in glioma cells. *Neurol Med Chir (Tokyo)* **53**, 645-654 (2013).

581 Wang, J. B., Dong, D. F., Gao, K. & Wang, M. D. Mechanisms underlying the biological changes induced by isocitrate dehydrogenase-1 mutation in glioma cells. *Oncol Lett* **7**, 651-657, doi:10.3892/ol.2014.1806 (2014).

582 Kavanagh, E. & Joseph, B. The hallmarks of CDKN1C (p57, KIP2) in cancer. *Biochim Biophys Acta* **1816**, 50-56, doi:10.1016/j.bbcan.2011.03.002 (2011).

583 Stampone, E., Caldarelli, I., Zullo, A., Bencivenga, D., Mancini, F. P., Della Ragione, F. *et al.* Genetic and Epigenetic Control of CDKN1C Expression: Importance in Cell Commitment and Differentiation, Tissue Homeostasis and Human Diseases. *Int J Mol Sci* **19**, doi:10.3390/ijms19041055 (2018).

584 Zhang, J., Gong, X., Tian, K., Chen, D., Sun, J., Wang, G. *et al.* miR-25 promotes glioma cell proliferation by targeting CDKN1C. *Biomed Pharmacother* **71**, 7-14, doi:10.1016/j.biopha.2015.02.005 (2015).

585 Crespo, I., Vital, A. L., Gonzalez-Tablas, M., Patino Mdel, C., Otero, A., Lopes, M. C. *et al.* Molecular and Genomic Alterations in Glioblastoma Multiforme. *Am J Pathol* **185**, 1820-1833, doi:10.1016/j.ajpath.2015.02.023 (2015).

586 Solomon, D. A., Kim, J. S., Jenkins, S., Ressom, H., Huang, M., Coppa, N. *et al.* Identification of p18 INK4c as a tumor suppressor gene in glioblastoma multiforme. *Cancer Res* **68**, 2564-2569, doi:10.1158/0008-5472.CAN-07-6388 (2008).

587 Wang, X., Flynn, A., Waskiewicz, A. J., Webb, B. L., Vries, R. G., Baines, I. A. *et al.* The phosphorylation of eukaryotic initiation factor eIF4E in response to phorbol esters, cell stresses, and cytokines is mediated by distinct MAP kinase pathways. *J Biol Chem* **273**, 9373-9377 (1998).

VI. DANKSAGUNG

Mein erster Dank geht an Prof. Dr. Guido Reifenberger für die Möglichkeit meine Promotion am Institut für Neuropathologie an der Heinrich-Heine-Universität Düsseldorf durchführen zu können. Anregende Kritik und Diskussionen in wöchentlichen Laborbesprechungen und beim halbjährlichen Retreat haben mir stets geholfen den Fokus zu bewahren. Danke, dass Sie mir jederzeit Ihr Vertrauen entgegengebracht haben.

Ein weiterer Dank geht an Dr. Christiane B. Knobbe-Thomsen für die Überlassung des interessanten und dringlichen Forschungsthemas, welches mich immer wieder motiviert hat Fehlschläge hinzunehmen und ambitioniert weiterzumachen. An dieser Stelle auch einen herzlichen Dank an die Deutsche Krebshilfe für die Finanzierung des Projektes.

Ich danke weiterhin Prof. Dr. Andreas Weber als Vertreter der Mathematisch-Naturwissenschaftlichen Fakultät der HHU für die Übernahme der Position als Zweitgutachter für die vorliegende Dissertation.

Ich danke René Deenen, Dr. Tabea Mettler-Altmann, David Pauck, Daniel Picard, und Dr. Marc Remke für die experimentelle Zusammenarbeit.

Einen besonderen Dank möchte ich meinem Kollegen und Freund Sascha zukommen lassen, der mich auf dieser abenteuerlichen Reise vom allerersten Tag an begleitet hat und alle Höhen und Tiefen mit durchgemacht hat. Danke für antreibende Kritik, die ich mindestens genauso gebraucht und geschätzt habe wie aufmunternde Gespräche und angeregte Diskussionen. Ich wünsche dir nur das Beste auf deinem weiteren Weg.

Danke außerdem an ausnahmslos alle lieben Kollegen des Instituts für Neuropathologie für nette Gespräche und Hilfestellungen aller Art. Besonderer Dank geht dabei an Bastian und Marietta, die mir so oft mit fachkundiger Meinung zur Seite standen und mich in meiner Arbeit stets bestärkt haben. Danke an Angela, Anne, Ana-Maria, Jana, Micha und Rabia für die ausgelassenen Gespräche und Süßigkeiten-Gelage im Büro. Danke auch an Anna, Marc und Nina – AGH für immer!

Großer Dank gilt auch meiner lieben Familie und meinen Freunden, die nie daran gezweifelt haben, dass ich alles schaffe was ich mir vornehme. Danke für eure Unterstützung, eure aufbauenden Worte und euer Verständnis in stressigen Zeiten. Ich liebe euch!

Das Wichtigste kommt zum Schluss. Danke an mein Herz Marcel. Ich hätte mir niemand Tolleren an meiner Seite wünschen können. Du hast dich mit mir gefreut und aufgeregt, mich runtergebracht und aufgebaut. Du hast mich gestützt und mir Freiraum gegeben. Für mich hast du allein dafür mindestens einen Doktortitel verdient. Du bist Alles ♥ Danke

VII. EIDESSTATTLICHE ERKLÄRUNG

Ich versichere an Eides Statt, dass die Dissertation von mir selbstständig und ohne unzulässige fremde Hilfe unter Beachtung der „Grundsätze zur Sicherung guter wissenschaftlicher Praxis an der Heinrich-Heine-Universität Düsseldorf“ erstellt worden ist.

Ort, Datum

(Miriam Knühmann)